

JAN. - APR. 1997  
Volume III Number I

ISSN 0859 144X

# THE ASEAN JOURNAL OF RADIOLOGY

Published by The Radiological Society and  
the College of Radiologists of Thailand,  
Bangkok, Thailand

Supported through an educational grant from





## *Highest Resolution Available*

The PRISM™ 3000XP from Picker International is, quite simply, the best nuclear brain imaging system. It not only offers three-head sensitivity for increased productivity, but also has the highest practical spatial resolution available. And when it comes to patient comfort, it's ergonomically designed for optimal head, neck, and body positioning.

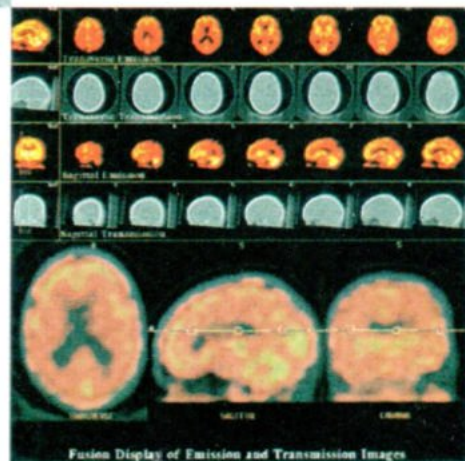
## *Unique Applications to Cost Effectively Manage Patients*

- Stroke Management
- Regional Cerebral Blood Flow Assessment
- Psychiatric Applications



## *Odyssey FX*

And best of all, the Odyssey FX computer represents another gold standard for nuclear image processing and display with the highest performance specs in the industry. The quest for better diagnosis has made 3-D image fusion and DICOM necessary tools, and again the advantages of PRISM 3000XP are evident.



Fusion Display of Emission and Transmission Images

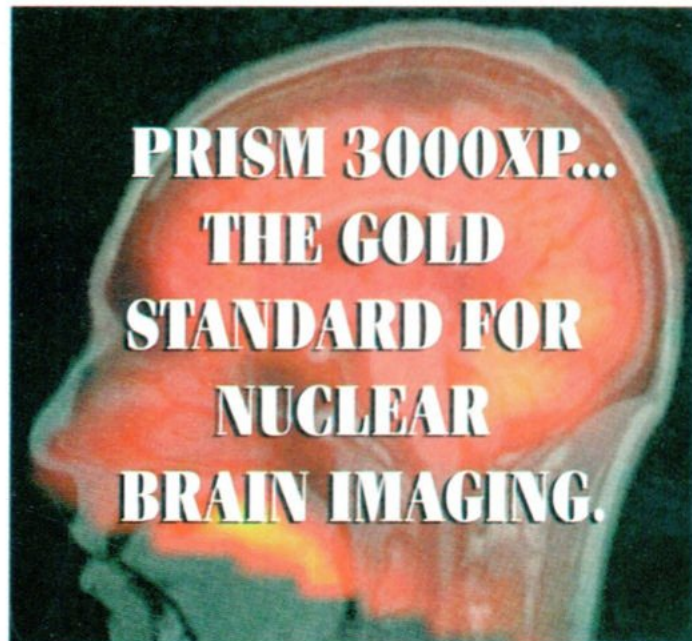
## *Imaging Standards of Tomorrow, Today*

The PRISM 3000XP is compact, affordable, and suitable for both office-based and hospital practices. Unique financing options are available to suit a wide variety of caseloads and clinical practices. Picker and the PRISM 3000XP are bringing you the imaging standards of tomorrow, today.

To find out more about all the PRISM 3000XP can do, call us today at 1-800-323-0550; e-mail us at [info@nm.picker.com](mailto:info@nm.picker.com); or visit us on the Web at the Nuclear Medicine Modality Home Page, <http://www.picker.com/nuclear/nuclear.html>.

## **Picker International**

29 F, 2908 Sun Towers Bldg. B, 123 Vibhavadi-Rangsit Rd., Jatujuk, Bangkok 10900, THAILAND  
Tel. (662) 617-8212-4, FAX : (662) 617-8215



 **PICKER**  
MORE THAN IMAGES. INSIGHT.



JAN. - APR. 1997  
Volume III Number I

ISSN 0859 144X

# THE ASEAN JOURNAL OF RADIOLOGY

Published by The Radiological Society and  
the College of Radiologists of Thailand,  
Bangkok, Thailand

Supported through an educational grant from







EDUCATION

## Asian-Oceanian Seminars on Diagnostic and Interventional Radiology

1 9 9 7

### Imaging and Interventional Radiology of the Hepatobiliary System

**February 19-21**

Khon Kaen, Thailand

Programme Leader:

**B. Sitisara**

### Urogenital Imaging

**April 25-27**

Bombay, India

Programme Leader:

**R. Sukthankar**

### Radiology of Cerebrovascular Disease, including interventional neuroradiology

**October 23-24**

Melbourne, Australia

Programme Leader:

**B. Tress**

### Chest Radiology

**November 1-2**

Kuala Lumpur, Malaysia

Programme Leader:

**Joginder Singh**



For further information please contact:

**Bracco International B.V.**

47 Hill Street

S.C.C.I. Building

#06-05 Singapore 179365

Tel: ++65-337 1880

Fax: ++65- 337 7576



**Editor-in-Chief**

Professor Kawee Tungsubutra

Kaweevej Hospital, 318 Tarksin Road, Dhonburi, Bangkok 10600, Thailand.

**Associate Editors.**

- |                     |  |  |
|---------------------|--|--|
| <b>Indonesia:</b>   | 1. Professor Muhamad Djakaria<br>Dept. of Radiology<br>General Hospital Dr. Cipto<br>Mangunkusumo<br>Jalan Diponegoro 71<br>Jakarta, Indonesia.            | 2. Dr. Cholid Badri<br>Dept. of Radiology<br>General Hospital Dr. Cipto<br>Mangunkusumo<br>Jalan Diponegoro 71<br>Jakarta, Indonesia.      |
| <b>Singapore:</b>   | 1. Dr. Khor Tong Hong.<br>Dept. of Radiotherapy<br>Mt. Elizabeth Hospital<br>Singapore 0922  | 2. Dr. John Hoe.<br>Medi Rad Associates Pte Ltd.<br>300 Orchard Road<br>Singapore 0923   |
| <b>Malaysia:</b>    | 1. Dr. K. Kulaveerasingam<br>Dept. of Radiology<br>Ipoh Specialist Center<br>26 Jalan Tambun,<br>30350 Ipoh, Perak,<br>Malaysia.                           | 2. Dr. Joginder Singh<br>Dept. of Radiology<br>Pantai Medical Center<br>8 Jalan Bukit Pantai<br>59100 Kuala Lumpur,<br>Malaysia.           |
| <b>Philippines:</b> | 1. Dr. Manuel C. Mejia Jr.<br>Santo Tomas University Hospital<br>España, Manila,<br>Philippines.   | 2. Dr. Orestes P. Monson<br>Philippine Heart Center<br>for Asia<br>East Ave., Quezon City,<br>Philippines.                                 |
| <b>Brunei:</b>      | 1. Dr. Mohd Iyaz Mohd Shafi<br>Specialist Radiologist and<br>Head, Radiology Department<br>RIPAS Hospital<br>Bandar Seri Begawan 2680<br>BRUNEI DARUSSALAM | 2. Dr. Shahrin Merican<br>Specialist Radiologis<br>Radiology Department<br>RIPAS Hospital<br>Bandar Seri Begawan 2680<br>BRUNEI DARUSSALAM |
| <b>Thailand:</b>    | 1. Prof. Boontiang Sitisara<br>Dept. of Radiology,<br>Chulalongkorn Hospital<br>Rama IV. Road, Bangkok 10330<br>Thailand.                                  |  |

**Editorial Board:**

- |              |              |  |
|--------------|--------------|--|
| (1) Nitaya   | Suwanwela    | Dept. of Radiology, Chulalongkorn Hospital, Bangkok. |
| (2) Saroj    | Vanaprungs   | Dept. of Radiology, Siriraj Hospital, Bangkok.       |
| (3) Charindr | Euavilaichit | Dept. of Radiology, Ramathibodi Hospital, Bangkok.   |
| (4) Kaesorn  | Vajarapongse | Dept. of Radiology, Chulalongkorn Hospital, Bangkok. |
| (5) Suree    | Titathan     | Dept. of Radiology, Chulalongkorn Hospital, Bangkok. |
| (6) Sutee    | N. Songkla   | Dept. of Radiology, Siriraj Hospital, Bangkok.       |

**Manager:** Permyot Kosolphand.



1. The AAR Journal of Radiology publishes the papers on Radiological Sciences, such as research work, review articles, case reports, innovations in Medical Sciences related to all branches of Radiology, and letters to the editor. The aforementioned materials can be written in English only.

2. The authors have to submit 2 copies of the manuscript and a diskette: **to Prof. Dr. Kawee Tungsubutra**, 318 Kaweevej Hospital, Taksin Road, Dhonburi, Bangkok 10600, Thailand.  
**or to the Associate Editors** at the Radiological Society of Malaysia, Indonesia, Phillippine, Singapore and Brunei. The names and addresses of the Associate Editors in each country were published in the front page of this Journal.

3. The original copy to be submitted must be typed in a double space on one side of the page of 8" x 11" paper.

4. The format of the article must include:

- a. Title page and address of the author (s)
- b. Abstract
- c. Introduction (Background)
- d. Material and Method
- e. Results and discussion (Tables and Illustrations)
- f. Acknowledgement (if any)
- g. References (Follow the Vancouver style developed by ICMJE)

5. We will provide 25 copies of reprints for the author (s) who submit (s) and article for publication in the AAR Journal.

6. The illustrations and tables must be clearly prepared with legends in English as they are the art works to be reproduced.

7. The authors are responsible for the contents of the article as to its facts and findings.

8. Ethics.

Paper reporting studies which might be interpreted as human experimentation (e.g. controlled trials) should conform to the standards of the Declaration of Helsinki (see British Medical Journal 1964;2:177) and should indicate that approval that such studies may proceed has been granted by the local or hospital Ethics Committee.

When reporting experiments on animals indicate whether the institution's or the National Research Council's guide for, or any national law on, the care and use of laboratory animals was followed.



# THE ASEAN JOURNAL OF RADIOLOGY

Volume III Number I JAN. - APR. 1997

---

## CONTENTS

---

	Page
1. CT BRAIN IMAGES IN CANCER PATIENTS WHO HAD NEUROLOGICAL PROBLEMS Patchrin PEKANAN, Tarapong DUANGKAM	1-10
2. BONY ANATOMIC VARIANTS SEEN ON SCREENING SINUS CT Dr Michael LIN, Dr T Y TAN, Dr Cheah Foong KOON, Dr D M KOH, Dr Jeffrey GOH	11-17
3. ABDOMINAL ACTINOMYCOSIS Dr. Y Y Sitoh, Dr. T K Khoo.	19-22
4. SUBCUTANEOUS NODULES ON CT SCAN : A CASE OF METASTATIC MALIGNANT MELANOMA Dr. Y Y Sitoh, Dr. T S G Chee, Dr. C L Chua	23-26
5. RENAL LYMPHOMA IN AN HIV POSITIVE PATIENT Chirote SUCHATO, Patchrin PEKANAN, Udom HARINSUT	27-31
6. AN EARLY GASTRIC CANCER Supraanee NIRAPATHAPONGPORN, Patchrin PEKANAN, Janjira CHATCHAVALA, Jaroen SUWANWILAI	33-36
7. MR IMAGING OF THE BRAIN IN WILSON'S DISEASE. O. CHAWALPARIT, K. DANPUKDEE, S. SUTHIPONGCHAI, P. CHIEWVIT, A. CHUROJANA, W. APICHONKIT	37-41
8. ULTRASONOGRAPHY OF SMALL INTESTINAL INTUSSUSCEPTION IN NEUROFIBROMATOSIS: A CASE REPORT Pannee VISRUTARATNA Pisit WATTANARUANGKOWIT Kanokporn ORANRATANACHAI	43-46
9. ESOPHAGEAL TUBERCULOSIS IN AN HIV-INFECTED CHILD Pannee VISRUTARATNA, Wittanee NA CHIANGMAI	47-49
10. TUBERCULOUS ABSCESS OF THE THIGH MUSCLE IN A PATIENT WITH SYSTEMIC LUPUS ERYTHEMATOSUS MR FEATURES IN AN UNUSUAL PRESENTATION OF TUBERCULOSIS Dr THOO FEI Ling, Dr Thomas CHEE, Dr LEONG KENG Hong	51-55

	Page
11. CONGENITAL CUTIS LAXA: A CASE REPORT Pannee VISRUTARATNA, Kanokporn ORANRATANACHAI, Aurmporn SRESHTHAPUTRA	57-60
12. SMOOTH-MUSCLE TUMORS IN CHILDREN WITH AIDS Pannee VISRUTARATNA, Chusak SIRIVANICHAI, Lumdaun WONGSAWASDI Samreung RANGDAENG	61-65
13. DIAGNOSIS OF HEPATIC CAVERNOUS HEMANGIOMA USING TECHNETIUM-99M RED BLOOD CELL IMAGING Molrudee EKMAHACHAI, Wannee OJARUSPORN, Chusak SIRIVANICHAI, Sakonchai JITRAPITAKKUL, Sombut BOONYAPRAPA	67-74
14. DIPYRIDAMOLE THALLIUM-201 MYOCARDIAL PERFUSION SINGLE PHOTON EMISSION COMPUTED TOMOGRAPHY IN CORONARY ARTERY DISEASE The IAEA supported Co-ordinated Research Project on "Qualitative Nuclear Cardiology in Thailand" 1992-1995 Vacharin RATANAMART, Pawana PUSUWAN, Jiraporn MANGKHARAK, Damras TRISUKOSOL, Sunanta CHIEWVIT, Pachee CHAUDAKSHETRIN, Puangrat BURANAPONG, Nucharee PUTRASRENI, Rujaporn CHANACHAI, Suthee NA SONGKHLA, Supachai CHAITHIRAPHAN, Rudee PLEECHACHINDA	75-86
15. INTEGRATED SOFTWARE TOOLS FOR THE CALCULATION IN RADIOTHERAPY Chonlakiet KHORPRASERT, Kanjana SHOTELERSUK, Chotika JUMPANGERN	87-96
16. LEAD BEADS: THE USE AS THE IRREGULAR FIELD SHIELDING Lalida TUNTIPUMIAMORN, Nuanpen DAMRONGKIJUDOM, Surat VINIJSORN, Prasert ASSAVAPRATHUANGKUL, Yutthapol WICHINIEN	97-103
17. TREATMENT OF COLORECTAL CANCER A MALAYSIAN EXPERIENCE G.C.C. Lim, I. Fuad, K.G. Rampal, A.K.H. Lim	105-112
18. A STUDY OF PREVALENCE RATE AND PREDISPOSING FACTORS OF GALL STONES IN SARABURI HOSPITAL PERSONNEL Panida MUKDEEPROM	113-118
19. HAND-MADE BODY LEAD APRON Atchara SANGCHAI, Patchrin PEKANAN, Preecha TOSKULKAO	119-124
20. "HEPERECHOIC DOTS" AND "SMALL FAT DENSITIES" US AND CT SIGNS OF XANTHOGRANULOMATOUS CHOLECYSTITIS: A CASE REPORT Darunee BOONJUNWETWAT, Onrudi HOJAN	125-129



## CT BRAIN IMAGES IN CANCER PATIENTS WHO HAD NEUROLOGICAL PROBLEMS

Patchrin PEKANAN<sup>1,2</sup>, Tarapong DUANGKAM<sup>1</sup>

### ABSTRACT

A retrospective study of CT images of 154 cancer patients who were sent for CT scanning due to the presence of neurological abnormalities. About 34% of the studied patients had brain metastases. Carcinoma of the lung, the breast and the nasopharynx were the three most common types of cancers in patients who came for the investigations and they represented the three most common types of cancers that had metastases to the brains. Malignant melanoma, malignant mole, chorioCa and Ca lacrimal gland had highest tendency for brain metastases. Facial palsy/hemiparesis, headache, seizure and alteration of consciousness were among the most neurological manifestations. Parenchymal metastases were more common than the dural/leptomeningeal types.

### INTRODUCTION

Metastases to the central nervous system are among the most feared complications of systemic malignant disease. Once metastatic disease in the brain is discovered, the median survival without treatment is only one to two months<sup>7</sup> and only six months with treatment<sup>8</sup>. However, palliative therapy may be beneficial for some patients by controlling the progression of neurological deficits, headaches and dementia. In some patients treatment of brain metastases may result in prolonged periods of useful and relatively comfortable survival. Detection, diagnosis and localization of intracerebral lesions are important roles for these imaging methods, with the intent of determining prognosis as well as planning and assessing the results of treatment. Metastases must be distinguished carefully from benign brain tumors or brain abscesses to avoid critical errors in clinical management<sup>2,13</sup>.

Studies to determine the incidence of brain metastases from different types of cancers by CT

images were considered rare in our country.

### PATIENTS AND METHODS

The retrospective study was performed in the Urupong Medical Center which was the center servicing the CT studies for patients from different parts of the country. The data collection included the CT brain images of cancer patients who had neurological problems, between the year 1984 and 1992. The clinical presentation was only obtained from the request forms and the follow up study was impossible.

The CT machine used were Somatom DRH (Siemens Co., Germany) and GE9800 (GE Co., USA). The standard cuts were parallel to the orbitomeatal line, 5 mm slice thickness at the posterior fossa and 10 mm slice thickness at the rest of the brain. Both noncontrast and intravenous contrast enhancement types of studies were routinely performed in the standard dose (40-80 gram of iodine). The scans were done immediately after the contrast injection. The

<sup>1</sup>Department of Radiology, Ramathibodi Hospital, Rama 6 Street, Bangkok 10400, Thailand.

<sup>2</sup>Urupong Medical Center, BKK.



interpretation was performed by the qualified radiologists.

The purpose of the study was (1) to obtain the incidence of brain metastases in different types of cancers in Thai population who had neurological problems; (2) to define the neurological manifestations in the positive brain metastatic group; (3) to determine the types of brain metastases.

The nodule or nodules with extensive brain edema was considered as parenchymal metastases. Nodule/nodules with less extensive brain edema in the steroid-treating patients was also counted as positive cases. Parenchymal hemorrhage in a high bleeding tendency cancer (chorioCa) in a young patient was classified as having brain metastases and parenchymal hemorrhage in less bleeding tendency cancers was set in a negative group. Dural mass with or without calvarial destruction and abnormally dense leptomeningeal enhancement was considered positive for metastases.

## RESULTS

There were 154 cancer patients, age ranged from 11 to 89 years old; 74 patients were male and 80 cases were female. About 90% of cases belonged to age-group range of 31-80 years old. Twenty-seven varieties of cancers were presented; the three most common cancers were Ca lung, Ca breast and Ca nasopharynx in 36%, 18% and 10% respectively. Twenty-one clinical signs and symptoms were noted and the three most common complaints were facial palsy/hemiparesis, headache and seizure/convulsion in 34%, 22% and 11% respectively. Eleven of 27 types of cancer were responsible for 52 positive brain metastases by CT scan; the three most

common types of cancers were Ca lung, Ca breast and Ca nasopharynx in 50%, 17% and 9% respectively. All cases of melanoma, malignant mole, chorioCa and Ca lacrimal gland and 75% of lymphoma showed positive brain metastases. The three most common age-groups that had positive brain metastases were 51-60 years old, 41-50 years old and 61-70 years old in 33%, 19% and 19% respectively and the patients in age-group 11-20 years old showed 100% metastatic incidence. After the age 50 years old, the incidence of positive brain metastases decreased with the advancing ages. Facial palsy/hemiparesis, headache and seizure/convulsion also represented the three most common signs and symptoms in the metastatic patients in 33%, 25% and 20% respectively.

Those patients who showed no brain metastases, the three most common CT findings were normal, ischemic areas and brain atrophy in 41%, 38% and 13%. The other findings considered negative for metastases but actually metastatic process could not be totally excluded were hydrocephalus, intracerebral hematoma, pituitary mass and thickened pituitary stalk (see discussion). The negative group presented slightly more percentage than the positive group. The brain parenchymal hemorrhage was noted in a case of Ca cervix (53/F), a case of leukemia (30/M) and a case of Ca liver (49/M). The pituitary mass was seen in a case of Ca breast (61/F), mildly thickened pituitary stalk was noted in a case of Ca prostate (85/M).

Positive brain metastases in the case of chorioCa (24/F) was a parenchymal hematoma. Combined leptomeningeal metastases and parenchymal nodules were seen in a case of Ca lung (40/F). A combined dural/calvarial and adjacent parenchymal deposit was noted in a case of Ca breast (62/F).



The history of acute or chronic onset could not be obtained in all patients so that it was not used for the information.

**Table 1.** Numbers of the cancer patients in the study vs age group

Age group	No. of patients (%)	
0-10	0	(0)
11-20	2	(1.3)
21-30	5	(3.3)
31-40	11	(7.1)
41-50	20	(13)
51-60	42	(27.3)
61-70	34	(22)
71-80	32	(20.8)
81-90	8	(5.2)
Total	154	(100)

Male = 74, Female = 80

**Table 2.** Number of studied patients in each type of cancers

Type of Cancers	No. of patients (%)	
Ca lung	56	(36.35)
Ca breast	28	(18.17)
Ca nasopharynx	10	(6.49)
Ca cervix	8	(5.19)
Ca colon	6	(3.9)
Ca prostate	6	(3.9)
Lymphoma	4	(2.6)
Ca stomach	4	(2.6)
Ca thyroid	3	(1.95)
Ca kidney	3	(1.95)
Ca tongue	3	(1.95)
Adenocarcinoma	2	(1.3)
Ca ovary	2	(1.3)
Malignant melanoma	2	(1.3)
CholangioCa	2	(1.3)
Ca pancreas	2	(1.3)
Ca liver	2	(1.3)
Leukemia	2	(1.3)
ChorioCa	1	(0.65)
Ca uterus	1	(0.65)
Ca bladder	1	(0.65)
Ca larynx	1	(0.65)
Leiomyosarcoma	1	(0.65)
Ca rectum	1	(0.65)
Ca mouth	1	(0.65)
Malignant mole	1	(0.65)
Ca lacrimal gland	1	(0.65)
<b>Total</b>	<b>154</b>	<b>(100)</b>

**Table 3.** Clinical signs and symptoms vs number of patients

Signs and symptoms	No. of patients (%)	
Facial palsy and hemiparesis	59	(34.3)
Headache	39	(22.68)
Seizure or convulsion	20	(11.64)
Alteration of consciousness	18	(10.47)
Nausea/ vomiting	6	(3.49)
Vertigo	4	(2.33)
Dizziness	4	(2.33)
Blindness	3	(1.74)
Fainting	3	(1.74)
No history about symptoms	3	(1.74)
Aphasia	2	(1.16)
Ataxia	2	(1.16)
Hallucination	1	(0.58)
Decreased mental status	1	(0.58)
Dementia	1	(0.58)
Dysarthria	1	(0.58)
Dysphagia	1	(0.58)
Hoarseness of voice	1	(0.58)
Stiffneck	1	(0.58)
Fever	1	(0.58)
Leg pain	1	(0.58)
<b>Total</b>	<b>172</b>	<b>(100)</b>

Note; One patient might have more than one sign or symptom  
total studied patients = 154

**Table 4.** Types of cancer vs number of patients with positive brain metastases by CT scan

Types of Cancer	Number of patients (%) who have positive brain metastases by CT scan	
Ca lung	26	(50)
Ca breast	9	(17.30)
Ca nasopharynx	5	(9.62)
Lymphoma	3	(5.77)
Melanoma	2	(3.86)
Ca cervix	1	(1.92)
Ca kidney	1	(1.92)
Malignant mole	1	(1.92)
Ca ovary	1	(1.92)
Ca colon	1	(1.92)
Ca lacrimal gland	1	(1.92)
ChorioCa	1	(1.92)
<b>Total</b>	<b>52</b>	<b>(100)</b>



**Table 4a.** Percentage of types of cancers who had brain metastases by CT scan and number of total patients of the group

Type of Cancer	% of the total group	
Ca lung	26/56	(46.43)
Ca breast	9/28	(32.14)
Ca nasopharynx	5/10	(50)
Lymphoma	3/4	(75)
Melanoma	2/2	(100)
Ca cervix	1/8	(12.5)
Ca kidney	1/3	(33.33)
Malignant mole	1/1	(100)
Ca ovary	1/2	(50)
Ca colon	1/6	(16.67)
Ca lacrimal gland	1/1	(100)
ChorioCa	1/1	(100)
<b>Total</b>	<b>52/122</b>	<b>(42.62)</b>

**Table 5.** Age group of the patients who have positive brain metastases by CT scan vs number of patients in each age group and percentage of the whole studied patients

Age group	Number of patients		% of total patients in the same age group	
0-10	0	(0)	0/0	(0)
11-20	2	(3.92)	2/2	(100)
21-30	2	(3.92)	2/5	(40)
31-40	4	(7.84)	4/11	(36.36)
41-50	10	(19.61)	10/20	(50)
51-60	17	(33.33)	17/42	(40.48)
61-70	10	(19.61)	10/34	(29.41)
71-80	5	(9.8)	5/32	(15.63)
81-90	1	(1.92)	1/8	(12.5)
<b>Total</b>	<b>51</b>	<b>(100)</b>	<b>51/154</b>	<b>(33.12)</b>

**Table 6.** Signs and symptoms in the positive group of brain metastases by CT scan vs number of patients and percentage of the total patients who had that sign and symptom

Signs and symptoms	No. of patients (%) with brain metastases		% of total patients with that sign and symptom	
Facial palsy and hemiparesis	20	(32.78)	20/59	(33.9)
Headache	15	(24.59)	15/39	(38.46)
Seizure or convulsion	12	(19.67)	12/20	(60)
Alteration of consciousness	5	(8.20)	5/18	(27.78)
Nausea/vomiting	2	(3.28)	2/6	(33.33)
Aphasia	2	(3.28)	2/2	(100)
Dizziness	1	(1.64)	1/4	(25)
Blindness	1	(1.64)	1/3	(33.33)
Ataxia	1	(1.64)	1/3	(33.33)
Vertigo	1	(1.64)	1/4	(25)
Fever	1	(1.64)	1/1	(100)
<b>Total</b>	<b>61</b>	<b>(100)</b>	<b>61/172</b>	<b>(35.47)</b>

**Note;**One patient might have more than one sign and symptom

**Table 7.** Findings in the brains in the patients with negative brain metastases by CT scan

CT findings	No. of patients (%)	
No abnormality detected	41	(39.04)
Ischemic areas	38	(36.19)
Brain atrophy	13	(12.38)
Hydrocephalus	5	(6.01)
Intracerebral hematoma	3	(2.86)
Calcified cysticercosis	3	(2.86)
Pituitary mass	1	(0.95)
Thickened pituitary stalk	1	(0.95)
<b>Total</b>	<b>105</b>	<b>(100)</b>

**Table 8.** Number of patients in age group who had negative brain metastases by CT scan

Age group	No. of pts (%)		% of total pts in the same gr.	
0-10	0	(0)	0/0	(0)
11-20	0	(0)	0/2	(0)
21-30	2	(1.97)	2/5	(40)
31-40	7	(6.87)	7/11	(63.64)
41-50	10	(9.80)	10/20	(50)
51-60	25	(24.5)	25/42	(59.52)
61-70	24	(23.53)	24/34	(70.59)
71-80	27	(26.47)	27/32	(84.38)
81-90	7	(6.86)	7/8	(87.5)
<b>Total</b>	<b>102</b>	<b>(100)</b>	<b>102/154</b>	<b>(66.23)</b>



## DISCUSSION

Metastases to the brain are relatively common, occurring in 12% of autopsied cancer patients<sup>1</sup>. Prolonged patient survivals and the increasing prevalence of lung cancer is a factor that increases the incidence of metastatic disease in the brain, in addition to the recent use of computed tomography and magnetic resonance imaging. Lung carcinoma is the most common primary tumor to give rise to clinically evident brain metastases, followed by breast carcinoma and malignant melanoma; together comprise 70%-80% of clinically evident cerebral metastases<sup>9-10</sup>. Approximately 60% for melanoma, 50% for all types of lung cancer, and 30% for breast cancer were found to have brain metastases at autopsy<sup>12</sup>. Next in order of frequency are genitourinary and gastrointestinal cancers<sup>9</sup>. The remaining cases come from a wide variety of primary cancer sites such as bladder, prostate, thyroid, lymph glands, salivary gland, testis, endometrium, and ovary. The primary tumor site for brain metastases may remain undetermined after diagnostic studies in as many as 14% of cases<sup>9</sup>. Most cancer patients who have brain metastases also have metastases to other organs, particularly the lungs. Malignant cells entering the venous blood stream are filtered out first by the lungs; spread to the brain and other organs may then occur as tumor emboli break off into the pulmonary veins from the metastatic lung lesions. Metastases may pass first by way of the portal circulation to the liver and, subsequently, to the lungs and other organs. In accordance with these concepts of tumor spread, it is rare for a cure to be effected in a patient with brain metastases, even if the brain lesions can be controlled. When the primary cancer is in the lung, embolic spread may sometimes occur directly to the brain without involving other organs. This may explain why there seems to be a tendency for lung carcinomas to spread to the brain earlier than they do with other malignancies.

Another route by which cancers are thought to metastasize to the cranial contents is Batson's venous plexus, a network of valveless

paravertebral veins. This route is implicated often in metastases to the intracranial dura. The cranial dura may be involved alone, or there may be concurrent metastases to the brain substance also. In some of these patients there are also metastases to the dural venous sinuses.

The most frequent symptoms of brain metastases are headache, motor weakness, and disordered mentation. Other common symptoms are ataxia, cranial nerve dysfunction, seizures, sensory disturbances, and speech problems. Although the symptoms caused by cerebral metastases tend to evolve progressively over days or weeks, their onset is sometimes sufficiently acute to resemble a stroke. This type of clinical presentation is particularly likely when there has been bleeding into a brain metastases<sup>2</sup>. Approximately 10 to 30% of brain metastases that are evidence on imaging studies or at autopsy may remain neurologically silent for an indefinite period<sup>8</sup>.

Approximately 80% of brain metastases are located supratentorially and involve the cerebrum. Any intracranial structure may harbor a metastatic lesion. Certain carcinomas may be linked with neurological symptoms only as remote (paraneoplastic) manifestations, without direct central nervous system involvement by the tumor. Paraneoplastic neurologic syndromes are most commonly associated with carcinomas of the lung. Some cancer patients have vague neurologic symptoms that may be related to metabolic imbalances. Agitation, irritability, impaired mentation, and somnolence may be associated with low serum sodium, high serum calcium, elevated BUN, or blood ammonia levels; hypoxia, hypercarbia or sepsis (with or without accompanying renal or hepatic disease).

Metastases to the brain are readily detected on CT scans because of the extensive brain edema that metastases cause and because they nearly always enhance strongly after intravenous infusions of contrast medium. Cerebral metastases with diameters of less than 0.5 cm often are shown readily. Using a high-dose contrast infusion technique and waiting an hour after the infusion



to begin CT scanning improve detection rates even further<sup>3</sup>. Because the imaging characteristics of brain metastases can vary so greatly, descriptions of typical appearances on CT scans are hazardous<sup>2</sup>. They are more likely to occur in the territory of the middle cerebral artery than in other regions of the cerebrum. The typical brain metastasis has a distinct enhancing rim on CT scan and a low-density central region. The rim may be thick or thin, irregular or smooth. The smaller ones may have a homogenous solid appearance. It is common to see metastases of different appearances within the same brain. Peritumoral edema may spread along the white matter fiber tracts for considerable distances, but it does not cross the corpus callosum nor does it involve the cortical gray matter. When systemic steroids are administered, cerebral edema may be reduced and the enhancement of metastatic lesions by intravenously administered contrast media may become less obvious on CT scans. In some patients with intracerebral bleeding, the metastatic tumor nodule from which the bleeding originated may be obscured by blood.

On CT scans, differentiating cerebral metastases from other types of brain lesions usually is not difficult because metastases are usually multiple and occur in patients who have known primary tumor elsewhere. However, the diagnosis may be more difficult when a symptomatic brain metastasis is the initial or presenting clinical problem, as it is with 10% of lung carcinoma<sup>12</sup>. Because cerebral abscesses often have smooth, thin margins and low-density centers seen on infusion CT scans, they may be similar in appearance to metastases. The degree of perifocal brain edema also tends to be comparable in both conditions. Early brain abscesses may resemble small tumors. Some patients with brain abscesses may not have systemic signs of infection, and there may be no abnormal CSF

findings. A cerebral biopsy or a follow up study might be helpful, because brain abscesses may change in appearance more rapidly than metastases.<sup>2</sup>

Dural metastases may be missed by CT scans when erosion of the endosteal surface of the cranium is not apparent. Leptomeningeal tumor spread is also difficult to detect on cranial CT scans. The positive CT findings observed with leptomeningeal metastases included contrast enhancement of the subarachnoid space and/or obliteration of the quadrigeminal cistern. Communicating hydrocephalus frequently was present.

In conclusion: (1) The patients with Ca lung and Ca breast were the first two most common groups who were sent for CT scan to rule out brain metastases and were found to be the two most common group that showed positive studies. (2) The third most common type was Ca nasopharynx which was dissimilar to reports from non-Asian patients; melanomas were the third rank in those patients. The reason was that we have much more patients with Ca nasopharynx. Facial palsy/ hemiparesis, headache, seizure/ convulsion and alteration of consciousness were the dominant manifestations of both positive and negative brain metastasis and were agreeable to other reports. (3) Melanoma, malignant mole, chorioCa, Ca lacrimal gland and lymphoma were among the groups that gained high percentage of positive results. (4) The most common age groups that showed brain metastases were between 41-70 years old but the positive percentage decreased with the advancing age, probably due to high incidence of cerebrovascular disease among those patients. (5) Leptomeningeal or dural deposits were found much less than the parenchymal metastases. (6) More negative results for brain metastases indicated that images-investigations were needed to exclude the other possibilities.



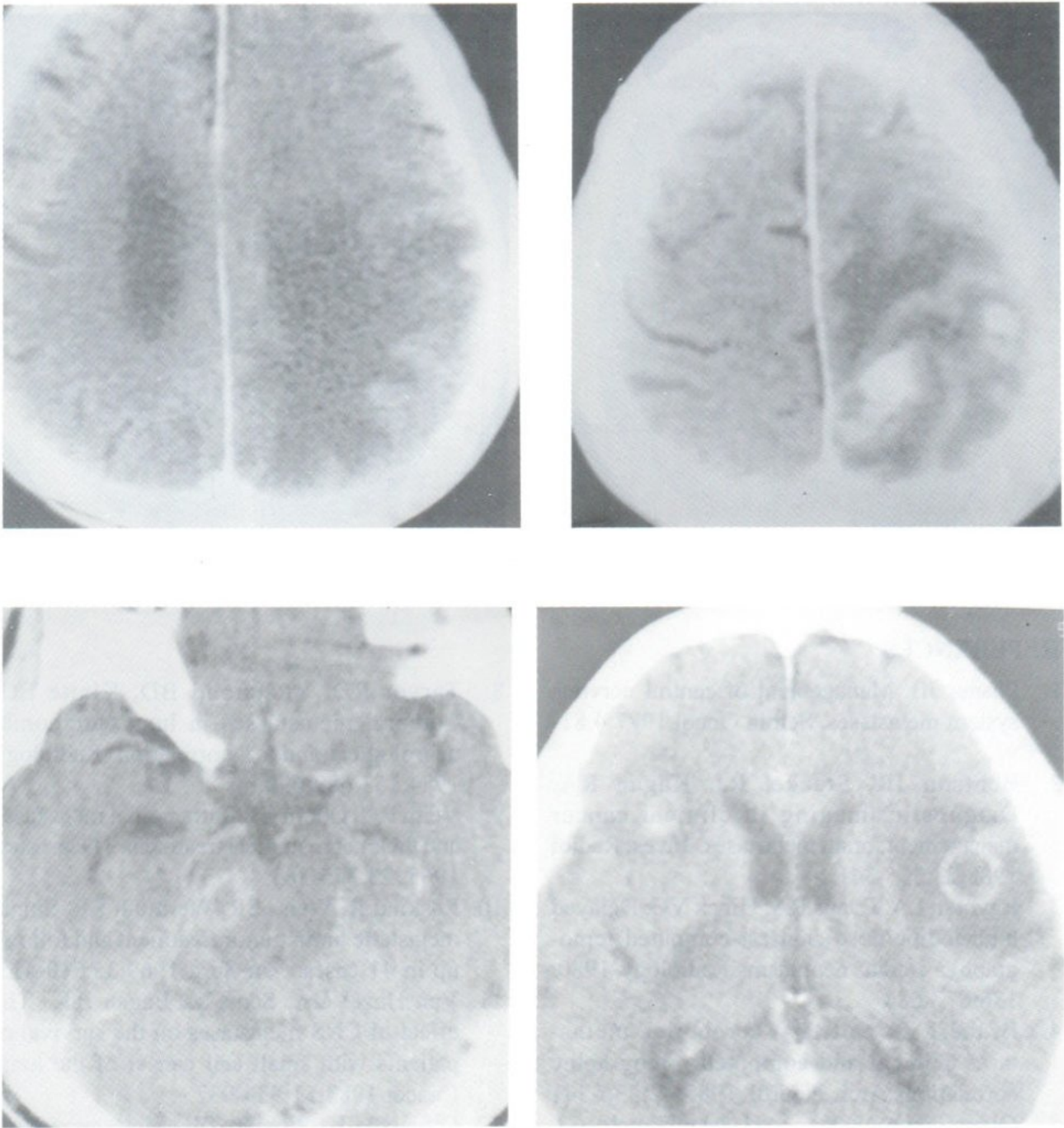


**Fig. 1A**    Parenchymal metastatic lesions

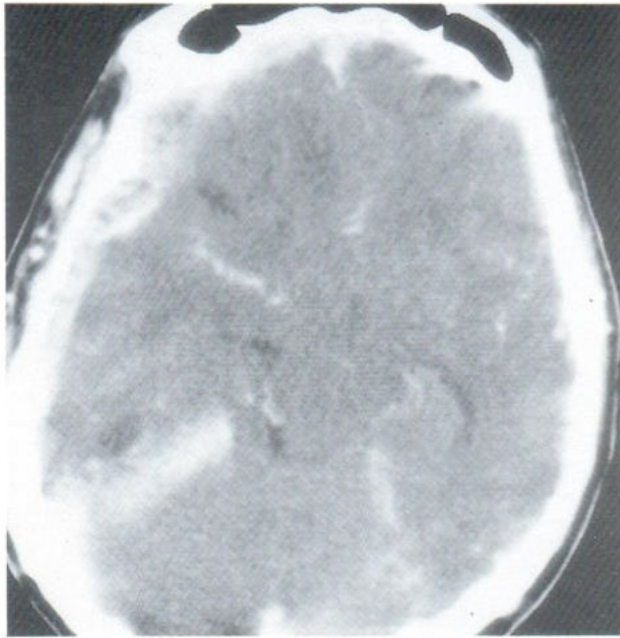


**Fig. 1B** Leptomeningeal/dural metastatic deposits.

## REFERENCES

1. Posner JB. Management of central nervous system metastases. *Semin Oncol* 1977;4:81-91.
2. Bentson JR, Steckel RJ, Kagan RA. Diagnostic imaging in clinical cancer management: brain metastases. *Invest Radiol* 1988;23:335-341.
3. Rayman LA, Evans RA, Hinck VC. Delayed high iodine dose contrast computed tomography: cranial neoplasms. *Radiology* 1980; 136:677-684.
4. Braberg L. Solitary cerebellar metastases. Clinical and computed tomographic correlations. *Arch Neurol* 1985;42:336-341.
5. Oldersleeve N, Koo AH, MacDonald CJ. Metastatic tumor presenting as intracerebral hemorrhage. *Radiology* 1972;124:109-112.
6. Tarmann DR, Krikorian J, Yorke C, et al. Computd tomography in leptomeningeal pread of tumors. *J Comput Assist Tomogr* 1978;2:448-455.
7. DiStefano A, Yap HY, Horobagyi GW, Blumen-schein GR. The natural history of breast cancer patients with brain metastases. *Cancer* 1979;44: 1913-1918.
8. Tarver RD, Richmond BD, Klatte EC. Cerebral metastases in lung carcinoma: neurological and CT correlation. *Radiology* 1984;153:689-692.
9. Veith RG, Odom GL. Intracranial metastases and their neurosurgical treatment. *J Neurosurg* 1965; 23:375-383.
10. Raskind R, Weiss SR, Wermuth RE. Single metastatic brain tumor treatment and follow-up in 41 cases. *Am Surg* 1969;35:510-515.
11. Van Hazel GA, Scott M, Eagan RT. The effect of CNS metastases on the survival of patients with small cell cancer of the lung. *Cancer* 1983;51:933-937.
12. Cifuentes N, Pickren JW. Metastases from carcinoma of mammary gland: an autopsy study. *J Surg Oncol* 1979;11:193-205.
13. Davis JM, Zimmerman RA, Bilaniuk LT. Metastases to the central nervous system. *Radiologic Clinics of North Americ* 1982;20:417-426.



---

## BONY ANATOMIC VARIANTS SEEN ON SCREENING SINUS CT

**Dr Michael LIN, MB,BS, M.Med, FRCR(UK)<sup>1</sup>, Dr T Y TAN, MB,BS, FRCR(UK)<sup>2</sup>,  
Dr Cheah Foong KOON, MB,ChB(Edin), MRCP(UK), FRCR(UK)<sup>3</sup>,  
Dr D M KOH, MB,BS, MRCP(UK), FRCR(UK)<sup>4</sup>, Dr Jeffrey GOH,M.D., MB,BS<sup>5</sup>**

### ABSTRACT

Screening sinus CT (SSCT) has emerged as the standard imaging modality in the investigation of inflammatory disease of the sinuses. Its ability to demonstrate detailed anatomy of the sino-nasal complex makes it an invaluable tool in functional endoscopic sinus surgery (FESS). In addition to exquisite demonstration of the anatomy and pathology of the sinonasal complex, anatomic variants which are identified can be predisposing factors to inflammatory sinus diseases. They are important operative considerations during the planning of FESS. The aim of this study is to document the prevalence of major anatomic variants seen on SSCT in our local population and to illustrate some of these variants as identification of these anomalies may have crucial operative implications. In view of the heterogeneous make up of our study population, an analysis of the prevalences of the variants amongst the different races is also made.

Screening sinus CT of 302 consecutive patients referred for sinonasal symptoms were studied. Anatomic variations were identified and recorded. These included pneumatized middle turbinate (concha bullosa), paradoxical middle turbinate (PMT), Haller's cells, septal deviation and uncinate process pneumatization. Overall bony anatomic variations were seen in 216 (71.5%) patients. A total of 134 (44.4%) patients had concha bullosa, 18 (6.0%) had paradoxical middle turbinate while 24 (7.9%) patients showed the presence of Haller's cells. There was significant lower prevalence of paradoxical middle turbinate noted in the Chinese group when compared with the Non-Chinese. There were only 4 patients (1.3%) with pneumatization of the uncinate process and these were only seen in the Non-Chinese group. Comparison is made between our study population and that of other similar published studies.

### INTRODUCTION

Screening sinus CT (SSCT) has proven to be an important integral preoperative diagnostic tool in the patient with inflammatory disease. The detailed anatomy demonstrated on CT is far superior to that

---

<sup>1</sup> Registrar, Dept of Diagnostic Imaging, Tan Tock Seng Hospital

<sup>2</sup> Senior Registrar, Dept of Diagnostic Imaging, Tan Tock Seng Hospital

<sup>3</sup> Consultant, Dept of Diagnostic Imaging, Tan Tock Seng Hospital

<sup>4</sup> Dept of Diagnostic Imaging, Tan Tock Seng Hospital

<sup>5</sup> Medical Officer (Trainee), Dept of Diagnostic Imaging, Tan Tock Seng Hospital

**Correspondence :** Dr. Michael Lin, c/o Department of Diagnostic Imaging, Tan Tock Seng Hospital, Moulmein Road, Singapore 308433



of plain radiography. In terms of radiation exposure, SSCT has been shown to be well below that associated with cataract formation.<sup>1,2</sup> Hence SSCT has largely replaced the plain radiograph in investigation of sinusitis. Besides confirming the presence or absence of disease, SSCT also demonstrates:

1. Sinonasal anatomy and major mucociliary drainage pathways<sup>3</sup> crucial to the ENT surgeon performing FESS.
2. Normal variants which may predispose to sinus disease and affect the planning of FESS.<sup>3,4,5</sup>
3. Complications of endoscopic sinus surgery.<sup>4,5</sup>
4. Non-inflammatory disease of the sinuses eg tumours.<sup>6</sup>

The purpose of this study is to document the prevalence of major anatomic variants in the local population. Comparison is made with similar published studies.

## METHODS AND MATERIALS

302 consecutive SSCT scans were reviewed over a two and half year period between March 1993 to September 1995. The study group consisted of 120 females and 182 males. Age ranged from 6 to 80 years old with a mean of 37.7 years. The racial breakdown of the study population is as follows in Table 1. Due to the small numbers of Indians, Malays and other races, we have divided the study group into the Chinese and the Non-Chinese for purposes of statistical analysis. There were a total of 88 Non-Chinese (29.1%) and 214 Chinese (70.9%).

All scans were performed at the Department of Diagnostic Imaging at Tock Seng Hospital. All cases were referred from the ENT Department for assessment of sinusitis. The age, sex and race of the patients were recorded. Scans were performed according to a protocol similar to that proposed by Babbal et al.<sup>7</sup> This included use of a sympathomimetic nasal spray (Ko-trin) 15 minutes before the scan, followed by nose blowing. Patients were then placed prone in the gantry with neck extended and the head resting on the chin. The gantry angle was positioned perpendicular to the hard palate and a

lateral scout obtained. The absolute gantry angle is not critical as it has to be adjusted to avoid artefacts from dental amalgam.<sup>7</sup> 5 mm contiguous slices were then performed from the posterior sphenoid wall to the posterior wall of the maxillary sinuses. This was followed by 3mm contiguous scans from the posterior margin of the maxillary sinuses to the anterior wall of the frontal sinuses (see Fig 1). The scans were performed on a Picker 2000 CT machine. No intravenous contrast was used unless there was suspicion of a non inflammatory disease. A bone algorithm was used as part of the imaging protocol. All scans were then filmed at a window level of 250 and width of 2500.

The scans were systematically examined by a head and neck radiologist for evidence of sinus disease and reviewed for the following anatomic variants:

1. Pneumatized middle turbinate. These were further subdivided into three pattern:<sup>8</sup>
  - a. Pneumatization of the lamellar or vertical portion.
  - b. Pneumatization of the inferior or bulbous portion.
  - c. Extensive pneumatization of both the lamellar as well as the inferior portions.
2. Paradoxical middle turbinate : The convexity of the middle turbinate bone is directed laterally.
3. Nasal septum deviation : These were divided into left or right deviation.
4. Haller's cells : These are ethmoidal air cells that project beyond the limits of the ethmoid complex into the floor of the orbit above the maxillary sinuses.
5. Pneumatized Uncinate Process (Uncinate bulla).

## RESULTS

A total of 216 patients (71.5%) were found to have bony variants as described above (see Table 2). The most common normal bony variant was noted to be nasal septum deviation with a total of 144 patients (47.7%) showing either right (21.5%) or left (26.2%) deviation. There was also a large



proportion ( 44.4%) of the study population who had concha bullosa. The vertical lamella was pneumatized in 25.5% while the inferior bulbous portion was pneumatized in 6.3%. Extensive pneumatization of the entire middle turbinate was noted in 12.6%. Haller's cells were seen in 7.9% of our study population. Paradoxical middle turbinate were detected in 6.0%. Only 4 patients (1.3%) had uncinate process pneumatization (uncinate bulla) and these were all Non-Chinese. There was a significant lower prevalence of paradoxical middle turbinate noted in the Chinese group when compared to the Non-Chinese.

## DISCUSSION

Our study of the local population showed 71.5% prevalence of major bony variants. This is higher than the 64.9% reported in a similar study by Bolger et al.<sup>8</sup> This is due to the inclusion of septal deviation in our study which constitutes the largest proportion of the study. A lower prevalence of 52% would be obtained if deviation of septum were omitted from the study.

## CONCHA BULLOSA

This refers to middle turbinate pneumatization ( see Fig 2a and 2b ) and was first described by Santorini in 1739. Depending on the criteria and imaging modality utilized, the reported prevalence ranges widely from 4% to 80%.<sup>9</sup> The highest prevalence being found in patients with chronic sinusitis at the time of ethmoidectomy. The reported prevalence on CT is generally between 33% to 36%.<sup>8,10,11</sup> Our study population showed a higher prevalence of 44.4%. This is likely to be due to our biased study population which were all referred for evaluation of sinusitis. There is generally a higher prevalence of middle turbinate pneumatization in patients with chronic sinusitis.<sup>8,9,12,15</sup> This has been attributed to encroachment of the concha bullosa onto the ostiomeatal unit. The pneumatized concha itself may also be complicated by polyps, cysts, pyoceles or mucocoeles.<sup>9</sup> However, this is not a view shared by all researchers. Zinreich<sup>11</sup> did not find any difference in the inci-

dence of concha bullosa in patients with or without sinusitis. Extensive pneumatization of the entire middle turbinate or a "true" concha bullosa was noted in 12.6% of our patient. This is consistent with the range of 4 to 15.7% quoted by Lane and Smoker.<sup>9</sup> The respective prevalences of pneumatization of the vertical lamellar and inferior bulbous portions were 25.5% and 6.3% in our study. These are lower than the reported respective prevalences of 46.2% and 31.2% in a study by Bolger et al.<sup>8</sup>

## PARADOXICAL MIDDLE TURBINATE

This is a reversal of the normal outward concavity of the middle turbinate ( see fig 3). There were only 6% who demonstrated this bony variant in our study. This is a lower prevalence when compared with similar studies by Bolger et al.<sup>8</sup> and Lloyd<sup>12</sup> who reported 26.1% and 17% respectively. This variation in reported figures may be due the level of the coronal sections.<sup>12</sup> Cases have been noted where a normal curve is seen posteriorly but with a paradoxical curve anteriorly. In our study, we have only included cases which demonstrated the curvature anteriorly, ie at the level of the ostiomeatal unit. Prevalence of this bony variant among the Chinese was 3.3% compared to 12.5% found in the Non-Chinese group. Chi square test confirmed this to be statistically significant (  $p < 0.05$  ).

## HALLER'S CELLS

These are ethmoidal air cells that grow onto the floor of orbit and may narrow the maxillary ostium and infundibulum<sup>4,6</sup> ( see Fig 4). There were 24 patients or a prevalence of 7.9% who demonstrated this bony variant. It can be seen from Table 3 that there is a wide range of reported prevalences of Haller's cells. The reasons include different criteria used in establishing the presence of the variant. Bolger et al.<sup>8</sup> used a broad definition of "any air cells located beneath ethmoid bulla along the maxillary sinus roof and most inferior portion of the lamina papyracea including air cells located within the ethmoid infundibulum". The technique of CT scanning, the use of different



window/level settings and variation in sample size have been implicated<sup>8</sup> as factors in the differing prevalences. In our study, this may be due to real differences in the prevalence of this anatomic variant in our population.

### PNEUMATIZED UNCINATE PROCESS

(See Fig. 2b)

The mechanism causing this anomaly is largely unknown.<sup>10</sup> This is an infrequent entity with only one case noted in 230 patients (or 0.4%) by Kennedy and Zinnreich.<sup>13</sup> Bolger et al<sup>8</sup> describe a 2.5 % prevalence in his study. We had only 4 patients or 1.3% prevalence, confirming the relative infrequency of this variant. All the 4 cases were Non-Chinese with none being found in the Chinese group. Chi square test confirmed significance of this finding at  $p < 0.05$ .

### SEPTAL DEVIATION

This has been noted to occur with a prevalence of approximately 20%.<sup>14</sup> Our study showed a higher prevalence of 44.4% and is in closer agreement with Babbel et al<sup>6</sup> who reported 40% prevalence. This is likely due to the broad criteria we used for assessment. Any form of nasal septum deviation including mild deviations were included in this category. There is slight predominance of left sided deviation which is not statistically significant.

### CONCLUSION

Our study shows that the local prevalence of paradoxical middle turbinate as well as Haller's cells are generally lower than that cited in other studies. The higher prevalence of pneumatized middle turbinate is probably related to the bias selection as our study consisted of symptomatic patients. There is a higher prevalence of septal deviation due to a different criteria used. There was no statistical difference in left or right deviation in this study. Only four patients or 1.3% had pneumatization of the uncinate process. This is in agreement with previous studies and confirms the relative infrequency of this variant. There were significant lower prevalences of paradoxical middle

turbinate and uncinate process pneumatization among the Chinese when compared to the Non-Chinese.

### REFERENCES

1. Michael J Sillers, Frederick A Kuhn, Christopher L Vickery : Radiation exposure in paranasal sinus imaging. *Otolaryngology Head and Neck Surgery* 1995 : 112(2) : 248-251.
2. A.C. MacLennan : Radiation dose to the lens from coronal CT scanning of the sinuses : *Clinical Radiology* 1995: 50 : 265-267.
3. Jerry W. Sonkens, H. Ric Harnsberger, G Marsden Blanch et al: The impact of screening sinus CT on the planning of functional endoscopic sinus surgery. *Otolaryngology-Head and Neck Surgery* 1991: 105(6) : 802-813.
4. Mahmood F Mafee: Preoperative imaging of nasaethmoid complex for functional endoscopic sinus surgery : *Radiologic Clinics of North America* 1993 : 31 (1) : 1-19.
5. Patricia A Hudgins : Complications of endoscopic surgery : The role of the radiologist in prevention : *Radiologic Clinics of North America* 1993 : 31 (1) : 21-32.
6. Robert W. Babbel, H. Ric Harnsberger, Jerry Sonkens et al: Recurring patterns of inflammatory sinonasal disease demonstrated at screening sinus CT : *AJNR* 1992 : 13 : 903-912.
7. Robert Babbel, H. Ric Harnsberger, Brent Nelson et al : Optimization of techniques in screening CT of the sinuses: *American J of Neuroradiology* 1991: 12:849-854.
8. William E. Bolger, Clifford A Butzin, David S Parsons : Paranasal sinus bony anatomic variations and mucosal abnormalities : CT analysis for endoscopic sinus surgery : *Laryngoscope* 1991 : 101 : 56-64.
9. Fred J Laine, Wendy R. K. Smoker : The ostiomeatal unit and endoscopic surgery : anatomy, variations, and imaging findings in inflammatory diseases : *American Journal of Roentology* 1992 : 159 : 849-857.



**Table1 : Race distribution in the study population.**

Race	Number	Proportion of study population
Indian	41	13.6%
Malay	27	8.9%
Others	20	6.6%
Chinese	214	70.9%
<b>Total</b>	<b>302</b>	<b>100%</b>

**Table 2 : Summary of results.**

Race	Pneumatized Middle Turbinate			Paradoxical Middle Turbinate	Haller's Cells	Nasal Deviation		Uncinate Bulla
	Vertical	Inferior	Extensive			Right	Left	
Non-Chinese	18(20.5%)	8(9.1%)	16(18.2%)	11(12.5%)	6(6.8%)	20(22.7%)	31(35.2%)	4(4.5%)
Chinese	59(27.4%)	11(5.1%)	22(10.2%)	7(3.3%)	18(8.4%)	45(20.9%)	48(22.3%)	0(0%)
Total No:	77	19	38	18	24	65	79	4
<b>Prevalence</b>	25.5%	6.3%	12.6%	6.0%	7.9%	21.5%	26.2%	1.3%

**Table 3 : Reported prevalences of Haller's cells.**

Studies	This study	Kennedy & Zinnreich	Bolger(16)
Reported Prevalence	7.9%	10%	45%



**Fig. 1** Lateral scout image of patient undergoing screening sinus CT.

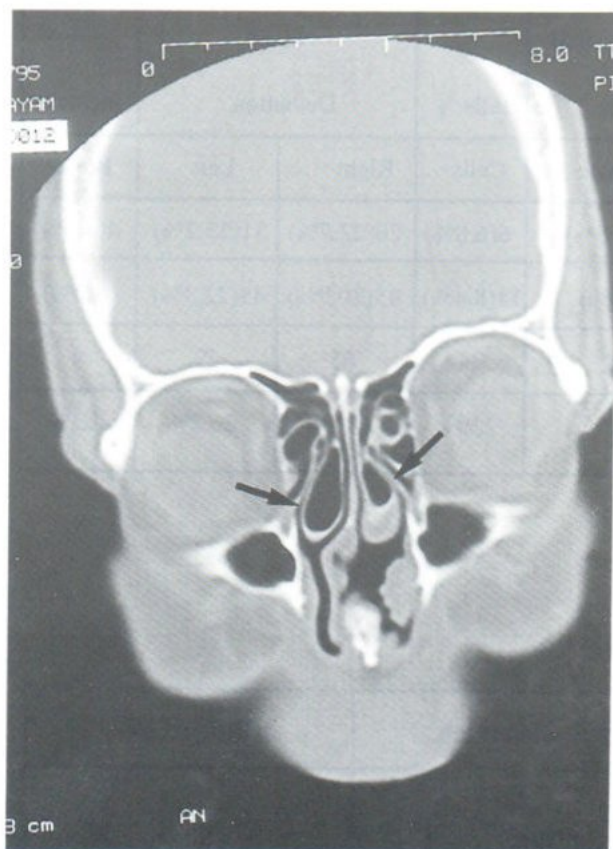


**Fig. 2a** Extensive pneumatization of the middle turbinates - the “true concha bullosa”.

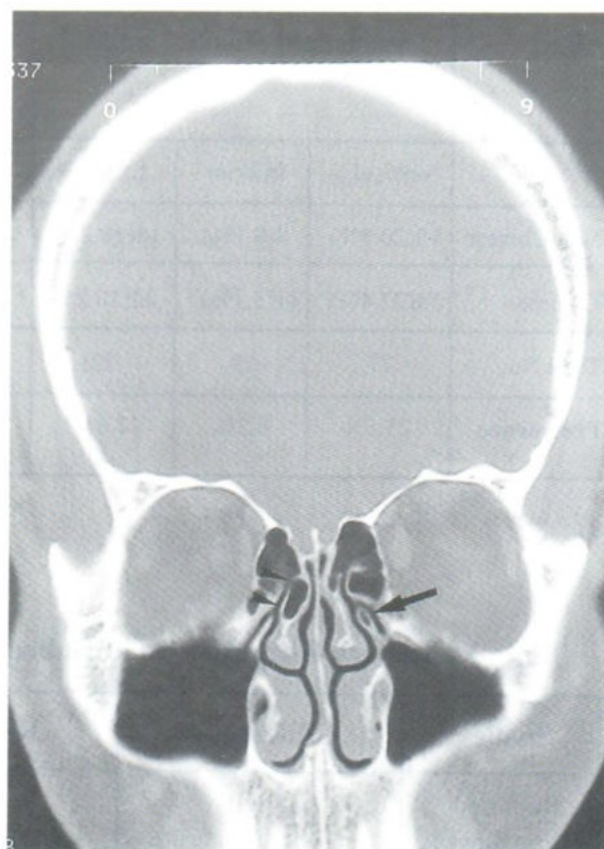


**Fig. 2b** Pneumatization of the vertical lamella of the right middle turbinate (arrow-heads). Pneumatization of the left uncinate process (arrows) is seen as well.



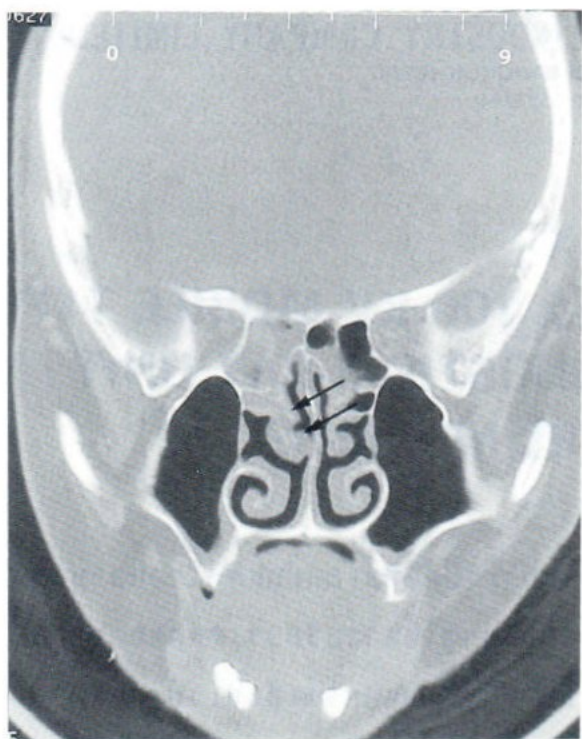


**Fig. 3** Paradoxical middle turbinate seen on the right side (arrows). Disease of the sphenoid and ethmoidal sinuses are noted.

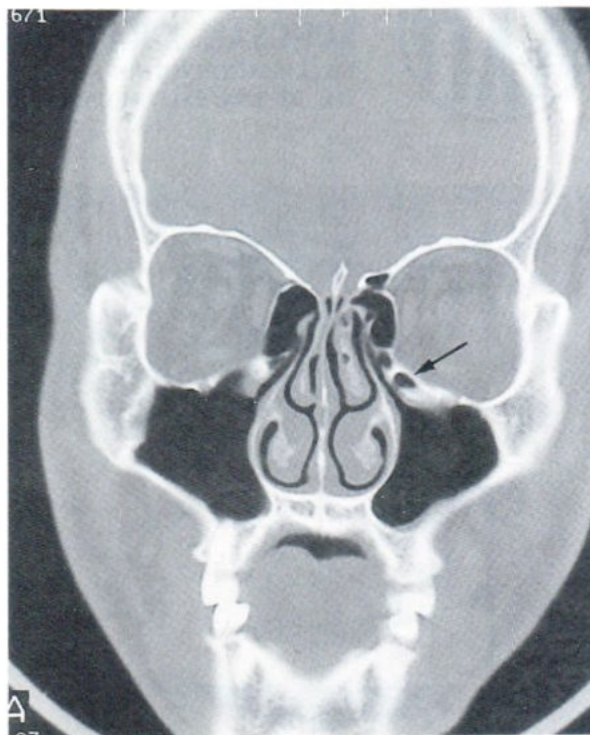


**Fig. 4** Haller's cells demonstrated on the left side (arrows).

10. Jack M Gwaltney, C. Douglas Phillips, R. David Miller et al : Computed tomographic study of the common cold : The New England J of Medicine 1994 : 330 (1) 25-29.
11. S James Zinreich, Douglas E Mattox, David W Kennedy, et al : Concha Bullosa : CT evaluation. J Computed Assisted Tomography 1988: 12(5) : 778-784.
12. G.A.S. Lloyd : CT of the paranasal sinuses: Study of a control series in relation to endoscopic sinus surgery: The J of Laryngology and Otology 1990 : 104 : 477-481.
13. Kennedy D. W., Zinreich SJ : Functional endoscopic approach to inflammatory sinus disease : Current perspective and technique modifications: Am J Rhinology 1988 : 2 : 89-96.
14. Blagaugrund SM : The nasal septum and concha bullosa : Otolaryngologic Clinics of North America 1989 : 22 : 291 -306.
15. Karen H. Calhoun, Gerard A. Waggenspack, Blake Simpson et al : CT evaluation of the paranasal sinuses in symptomatic and asymptomatic populations : Otolaryngology Head and Neck Surgery 1991 : 104 : 480-483.

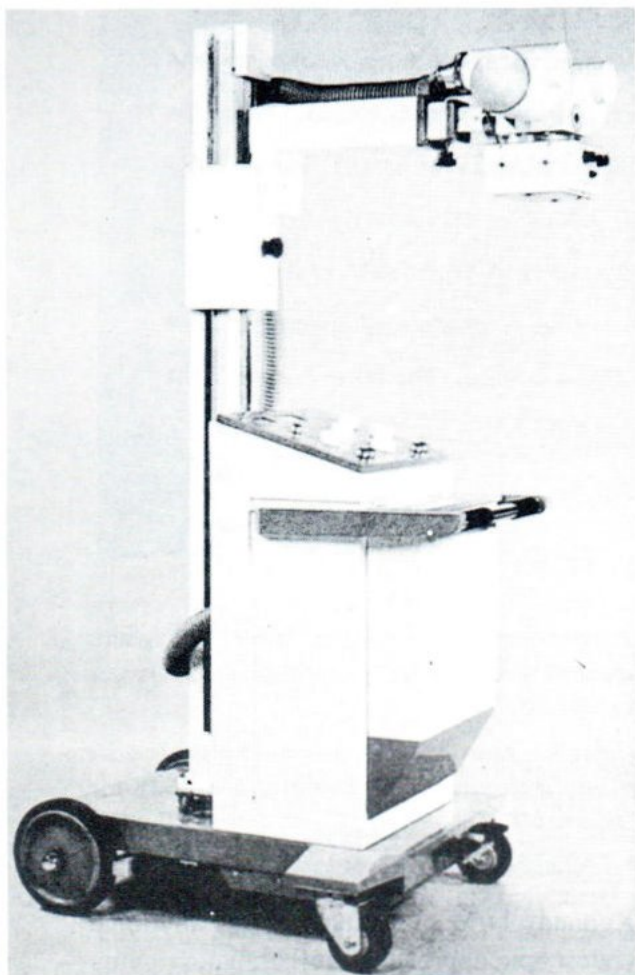


บริษัท คงศักดิ์เอกซเรย์การแพทย์อุตสาหกรรม จำกัด

KONGSAK X-RAY MEDICAL INDUSTRY COMPANY LIMITED

212/1 PHAHONYOTHIN SOI 55 BANGKHEN BANGKOK 10220

TEL. 5213214, 5511794 CABLE: KELEX FAX: 5523744

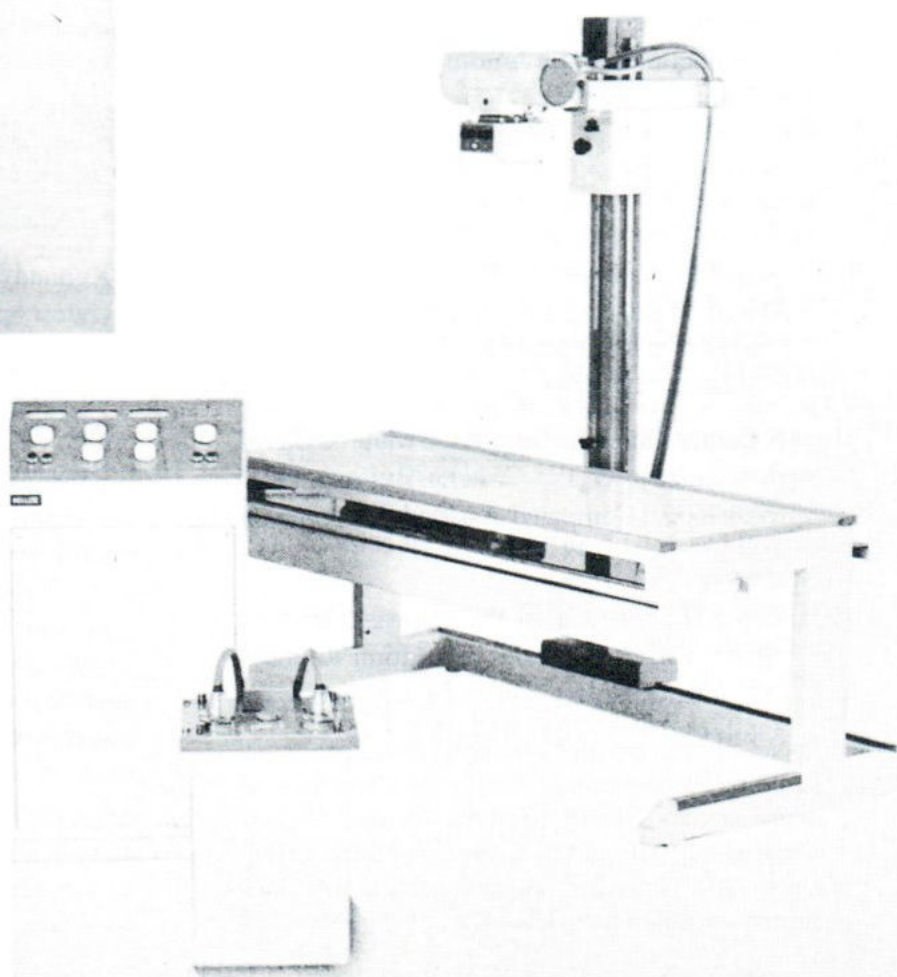


## KELEX

### 50 mA 100 KV MOBILE TYPE DIAGNOSTIC X-RAY UNIT MODEL MD 50-99

- # เหมาะสำหรับคลินิกเอกชนและโรงพยาบาลทั่วไป
- # มีช่างผู้ชำนาญให้การบริการ ตลอดอายุการใช้งาน
- # พร้อมทั้งจำหน่ายอุปกรณ์เอกซเรย์

**KELEX**  
**MD 100-99 X-RAY SYSTEM**  
**FULL WAVE 100 MA 100 KV**





## ABDOMINAL ACTINOMYCOSIS

Dr. Y Y Sitoh<sup>1</sup>, Dr. T K Khoo<sup>2</sup>,

### ABSTRACT

Actinomycosis is an infrequent intra-abdominal infection, mimicking and often mistaken for other diseases. We present a case of lower abdominal actinomycosis presenting as a mass lesion.

### INTRODUCTION

Actinomycosis can affect multiple organs, with local or systemic presentations. While infection is most common in the cervico-facial area, abdominal actinomycosis accounts for about 20% of all cases.<sup>1,2</sup> Though the typical CT features of multiple organ and anatomic compartment involvement with transfascial spread have been described,<sup>3,4</sup> diagnosis remains difficult, especially in the abdomen.<sup>1,2</sup> The correct diagnosis at presentation is obtained in less than 10% of cases.<sup>5,6</sup>

### CASE REPORT

A 25 year old Chinese female presented initially with colicky central abdominal pain and dysuria of one week's duration. Apart from equivocal tenderness at the right iliac fossa, the clinical examination was unremarkable. Urine microscopy was normal.

Clinical review a month later showed a suprapubic mass which appeared related to the uterus. She was otherwise well, urine pregnancy test was negative. Ultrasound showed a right iliac fossa mixed echogenicity mass, possibly related to bowel (Fig. 1); but unrelated to the gynaecological structures which

were normal. The bladder dome showed a fixed plaque of 9 mm thickness (Fig. 2), the nature of which could not be determined then. Some fluid within the pouch of Douglas was noted.

Further investigation with a barium enema revealed an extrinsic lesion in the region of the appendix, caecum and terminal ileum (Fig. 3,4). CT scan before and after intravenous contrast injection confirmed an enhancing soft tissue mass in the lower abdomen infiltrating the bladder dome (Fig. 5), and closely related to intestine. The involved bowel loops showed thickened walls (Fig. 6). There was loss of the normal fat plane between the bladder and uterus. No significant lymphadenopathy but considerable fluid in the pouch of Douglas was noted. The impression was of a malignant mass.

At laparotomy, omental cake of inflammatory tissue with sulphur granules involving intestine, bladder dome and the anterior wall of the uterus were found. Cystoscopy revealed oedema of the bladder wall. Excision of the mass and omentum was performed. The surgical diagnosis of abdominal actinomycosis with appendiceal abscess formation was confirmed histologically. Pathologic examination also showed actinomycosis of the resected bladder dome. Antibiotics were given post operatively. Patient has remained well.

<sup>1</sup> Registrar, Department of Diagnostic Imaging, Tan Tock Seng Hospital Pte. Ltd.

<sup>2</sup> Senior Consultant, Department of Diagnostic Radiology, Toa Payoh Hospital Pte. Ltd.

**Correspondence to :** Dr. Y Y Sitoh, Department of Diagnostic Imaging, Tan Tock Seng Hospital Pte. Ltd., Moulmein Road, Singapore 308433.





**Fig. 1** Sagittal ultrasound shows a mixed echogenicity mass at the right iliac fossa, closely related to a loop of bowel superiorly.



**Fig. 2** Sagittal ultrasound shows a fixed undulating plaque at the bladder dome.

## DISCUSSION

Actinomycosis is a chronic, progressive, suppurative and granulomatous infection. Sulphur granules characterise the colonies formed by this gram positive anaerobic or micro-aerophilic bacteria. The most common aetiologic agent, *Actinomyces israelii*, is a common saprophyte in the oropharynx and gastro-intestinal tract but appears unable to penetrate healthy mucosa. Opportunistic infection can occur with underlying local disease, trauma, surgery or the presence of foreign body.

Abdominal actinomycosis originates from the gastro-intestinal tract, especially the ilio-caecal region.<sup>1,2,7,8</sup> There is a strong association with appendicitis and subsequent appendiceal rupture.<sup>4,9</sup> It may present with multiple abscesses, draining sinuses, granulation and dense fibrosis. The production of proteolytic enzymes enables direct extension across dif-

ferent tissue planes.<sup>10</sup> This pattern of spread and the tumour-like masses from fibrosis<sup>11</sup> imitate neoplastic disease.

CT of abdominal actinomycosis will often show infiltrative enhancing soft tissue masses with foci of decreased attenuation. Cystic masses with enhancing thick walls may also be seen.<sup>4,12</sup> Lymphadenopathy is not a typical feature.<sup>12</sup> Urinary tract involvement is rare. Ultrasound may reveal hydronephrosis consequent to ureteric obstruction by the inflammatory mass.<sup>13</sup> Demonstration of actinomycotic plaque-like bladder wall thickening, as shown in our patient, is distinctly uncommon.

Our case illustrates the difficulties in arriving at a correct diagnosis of actinomycosis. The presentation is often non-specific and the correct diagnosis made only at laparotomy. Though rare, it should be considered in the differential diagnosis in the proper clinical setting.



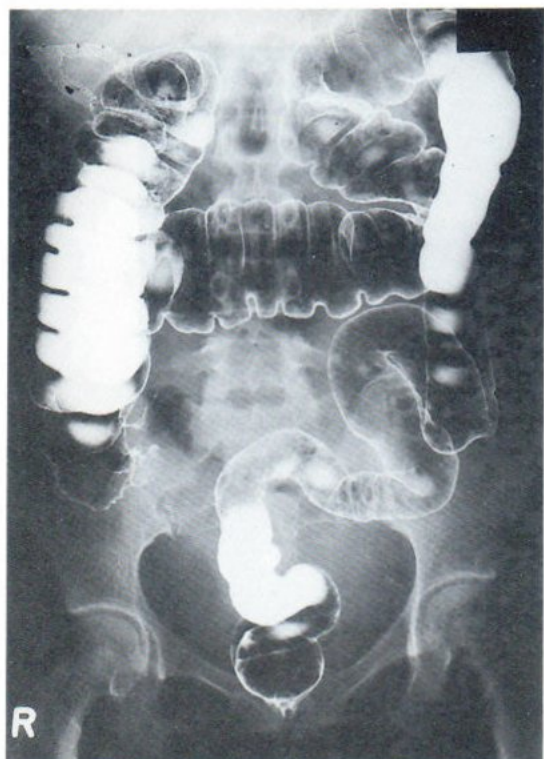


**Fig. 3** Barium enema AP radiograph. Extrinsic lesion at the caecal pole distorts the outline. The rest of the colon is normal.



**Fig. 4** Close up view of the ileo-caecal region. The caecal pole is persistently distorted with thickened, serrated terminal ileal folds.

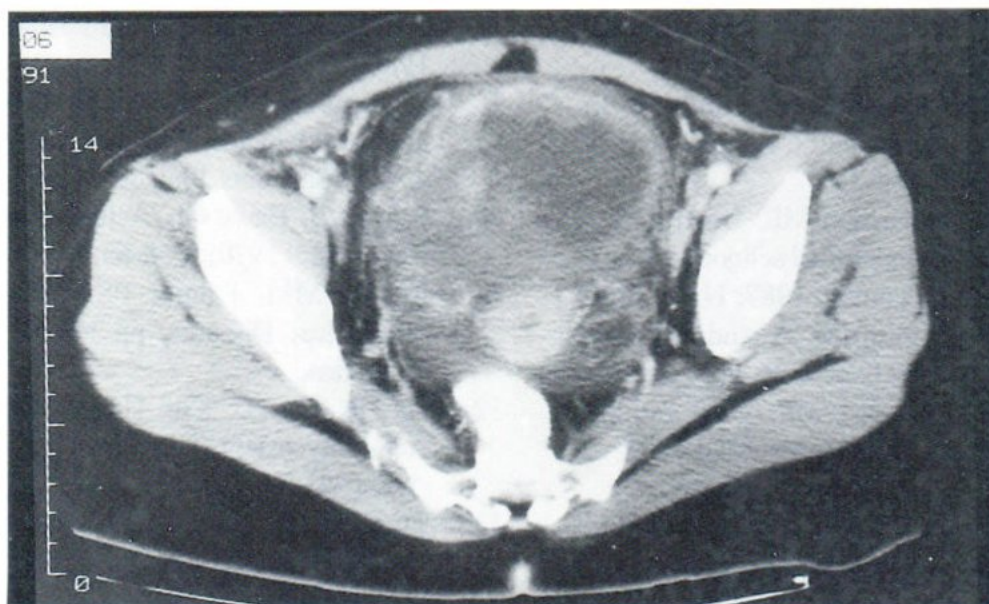


**Fig. 5** Post contrast scan shows infiltration of the bladder dome. There is loss of the normal fat plane between the bladder and uterus. Free fluid is present.



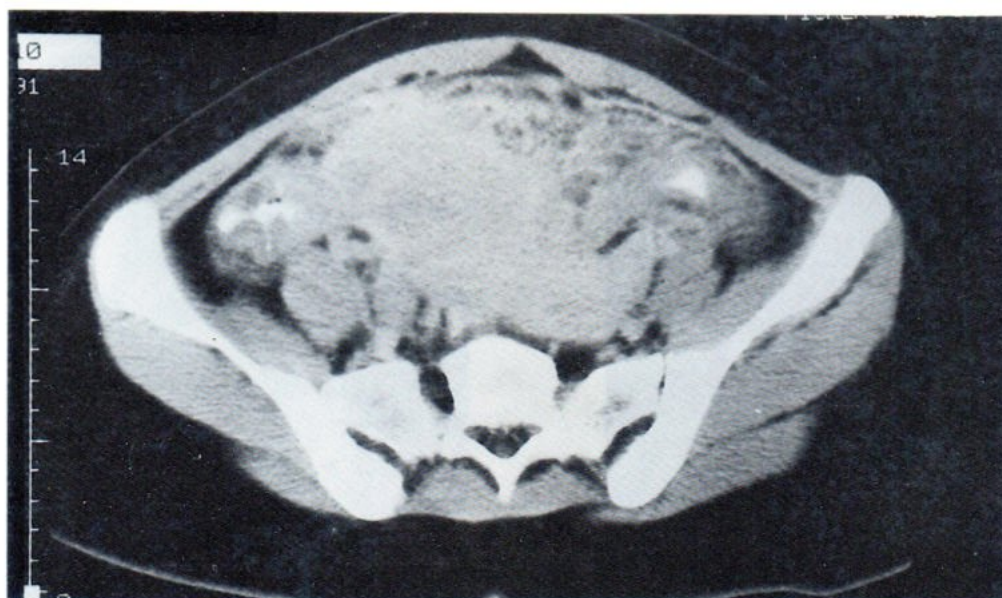


**Fig. 6** Post contrast scan shows an enhancing infiltrative mass involving bowel and the anterior uterus. The bowel wall is thickened.

## REFERENCES

1. Cope VZ. Visceral actinomycosis. *Br Med J* 1949; 2: 1311-6.
2. Davies M, Keddie NC. Abdominal actinomycosis. *Br J Surg* 1973; 60:18-22.
3. Webb WR, Sagel SS. Actinomycosis involving the chest wall: CT findings. *AJR* 1982; 139:1007-9.
4. Shah HR, Williamson MR, Boyd CM et al. CT findings in abdominal actinomycosis. *J Comput Assist Tomogr* 1987; 11(3): 466-9.
5. Weese WC, Smith IM. A study of 57 cases of actinomycosis over a 36 year period. A diagnostic "failure" with good prognosis after treatment. *Arch Intern Med* 1975; 135: 1562-8.
6. Harris LA, DeCosse JJ, Dannenberg A. Abdominal actinomycosis: evaluation by computed tomography. *Am J Gastroenterol* 1989 84: 198-200.
7. Fowler RC, Simpkins KC. Abdominal actinomycosis: a report of three cases. *Clin Rad* 1983;34: 301-7.
8. Deshmukh N, Heaney SJ. Actinomycosis at multiple colonic sites. *Am J Gastroenterol* 1986;81: 1212-4.
9. Wyngaarden JB, Smith LH. *Cecil's Text book of Medicine*, 18th edn., vol. 2, pp.1673-4. W.B. Saunders, Philadelphia.
10. Schwarz J, Baum GL. Actinomycosis. *Semin Roentgenol* 1970; 5: 58-63.
11. Reeder MM, Palmer PS. *The Radiology of Tropical Diseases*, pp 348-51. Williams & Wilkins.
12. Ha HK, Lee HJ, Kim H et al. Abdominal Actinomycosis: CT findings in 10 patients. *AJR* 1993; 161(4): 791-4.
13. Turnbull AE, Cohen MEL. Case report: pelvic actinomycosis with the development and resolution of a recto-sigmoid structure. *Clin Rad* 1991;43: 420-2.



## SUBCUTANEOUS NODULES ON CT SCAN : A CASE OF METASTATIC MALIGNANT MELANOMA

Dr. Y Y Sitoh<sup>1</sup>, Dr. T S G Chee<sup>2</sup>, Dr. C L Chua<sup>3</sup>

### ABSTRACT

The subcutaneous layer is often not scrutinized in the evaluation of CT scans. We present a case of metastatic malignant melanoma where the presence of subcutaneous nodules provided a vital sign toward the correct diagnosis. The relevant clinico-radiological features are reviewed.

### INTRODUCTION

Malignant melanoma is an aggressive neoplasm that can metastasize to all organ systems.<sup>1</sup> The majority of metastases occur within 3-5 years of diagnosis.<sup>2</sup> CT is an important imaging tool for accurate staging of the tumour and for therapy planning.<sup>3,4</sup> The first sign of distant haematogenous spread is often the presence of metastatic subcutaneous nodules.<sup>2,5</sup> CT can detect these small soft tissue nodules within the low density subcutaneous fat.<sup>6</sup>

### CASE REPORT

A 27 year old man with a history of post meningitic mental retardation and congenital giant hairy naevus presented with high fever and abdominal pain for 3 days.

Examination revealed a temperature of 38°C and gross hepatomegaly. There was bilateral lower limb pitting oedema. Giant hairy naevus over the anterior abdomen and back were noted. Apart from jaundice developing from the 4th day of admission, there were no other significant clinical findings.

Laboratory investigations showed leucocytosis of 23,100/dl with raised polymorphonuclear cells (86%). Liver function tests were abnormal :

raised bilirubin 76  $\mu\text{mol/L}$ , alkaline phosphatase 519 U/L, ALT 185 U/L and AST 620 U/L. Hepatitis B surface antigen was negative, serum alpha-fetoprotein was normal. The initial clinical diagnosis was hepatobiliary sepsis.

The abdominal X-ray showed hepatomegaly. Ultrasound confirmed this but no focal intrahepatic lesions nor biliary abnormality were noted. Abdominal CT scan showed diffuse inhomogenous hypodensities in the left hepatic lobe with scattered hypodensities in the right lobe. Small nodular deposits were present on the liver surface (Fig. 1,2). The portal vein and inferior vena cava were patent, but the latter was narrowed at its intrahepatic course. The left hepatic vein was incompletely demonstrated. Some ascitic fluid was present. No lymphadenopathy was discerned but small subcutaneous nodules were noted in the abdominal wall (Fig. 3). Bilateral basal lung consolidation and effusions were associated.

The classic triad of abdominal pain, ascites and hepatomegaly together with the typical CT features indicate the diagnosis of Budd-Chiari syndrome, secondary to metastatic disease. The finding of multiple subcutaneous nodules and the known risk of malignant melanoma in congenital giant

<sup>1</sup> Registrar, Department of Diagnostic Imaging, Tan Tock Seng Hospital Pte. Ltd.

<sup>2</sup> Consultant, Department of Diagnostic Imaging, Tan Tock Seng Hospital Pte. Ltd.

<sup>3</sup> Consultant Surgeon, Gleneagles Hospital Pte. Ltd.



hairy naevus strongly suggest melanoma to be the primary tumour.

At diagnostic laparoscopy, the liver was found to be completely replaced by melanoma deposits (Fig. 4) with a metastatic deposit at the greater omentum. Clear straw coloured ascitic fluid was seen. The patient's condition deteriorated soon after and he succumbed a week after the laparoscopy.

## DISCUSSION

Congenital giant hairy naevus is a rare birthmark, occurring in about one in 500,000 newborn.<sup>7</sup> The risk of developing malignant melanoma in such patients is estimated to be 100 times greater than that of the ordinary acquired naevus.<sup>8</sup>

Malignant melanoma is the most malignant skin cancer and unpredictable in its behaviour.<sup>9</sup> The disease may be localized or widely metastatic at initial clinical presentation. The most common sites of metastases are the lymph nodes, lung, liver and brain.<sup>1</sup> The incidence of skin and subcutaneous metastases ranges from 9 to 11% of cases.<sup>1,4</sup>

In the liver, melanoma metastases are often multiple with nodules ranging in size from 0.5 to 6 cm.<sup>10</sup> In a series of 27 patients by Das Gupta, 25 had multiple hepatic nodules while in one, the entire left lobe was replaced by tumour and in the other, there was marked capsular infiltration with normal parenchyma.<sup>10</sup> Metastatic disease is a known cause of Budd-Chiari syndrome, with either global or segmental obstruction of hepatic venous outflow. Obstruction may be at the level of the inferior vena cava, hepatic veins or small centrilobular veins.<sup>11</sup> In our patient, there was veno-occlusive disease involving obstruction at the small centrilobular veins of the left lobe.

Though malignant melanoma is a hypervascular tumour, its hepatic metastases may appear hypodense on contrast enhanced CT.<sup>12</sup> In patients with hepatic metastases, the incidence of concurrent metastases to the subcutaneous layer and/or musculoskeletal system increases to 47%.<sup>12</sup>

Subcutaneous melanoma metastases are eminently detectable by CT due to the contrast between these soft tissue density nodules and the adjacent lower density subcutaneous fat. However,

they are subtle because of their small size and the peripheral location.<sup>13</sup> Subcutaneous metastases also occur in lung and ovarian cancers.<sup>6</sup> Less commonly, they are associated with carcinomas of the stomach, kidney and breast.<sup>14</sup> Metastatic subcutaneous nodules may arise in locations remote from the site of the primary tumour.<sup>13,14</sup>

Differentiation must be made between these and benign subcutaneous nodules such as sebaceous cysts and injection granulomas. The presence of calcium suggests injection granulomas. Sebaceous cysts are often located just beneath the skin surface as opposed to metastases which may be deeper and distant from the surface. Furthermore, multiplicity of lesions or an increase in size or number on repeat scans are pointers towards malignancy.<sup>13</sup>

## REFERENCES

1. Patel JK, Didolkar MS, Pickren JW et al. Metastatic pattern of malignant melanoma. *Am J Surg* 1978; 135: 807-10.
2. Shirkhoda A, Albin J. Malignant melanoma: correlating abdominal and pelvic CT with clinical staging. *Radiology* 1987; 165: 75-78.
3. Bydder GM, Kreel L. Body computed tomography in the diagnosis of malignant melanoma metastases. *CT* 1981; 5: 21-4.
4. Silverman PM, Heaston DK, Korobkin M et al. Computed tomography in the detection of abdominal metastases from malignant melanoma. *Invest Radiol* 1984; 19: 309-12.
5. Balch CM, Milton GW. Cutaneous melanoma: clinical management and treatment results worldwide, pp. 221-50. Lippincott 1985, Philadelphia.
6. Dunnick NR, Schaner EG, Doppman JL. Detection of subcutaneous metastases by computed tomography. *J Comput Assist Tomogr* 1978; 2: 275-9.
7. Fitzpatrick TB, Johnson RA, Polano MK et al. Colour atlas and synopsis of clinical dermatology, 2nd edn. 1992, pp. 659-63. McGraw-Hill.
8. Lynch PJ. Dermatology for the house officer, 2nd edn. 1987, pp. 165. Williams & Wilkins.



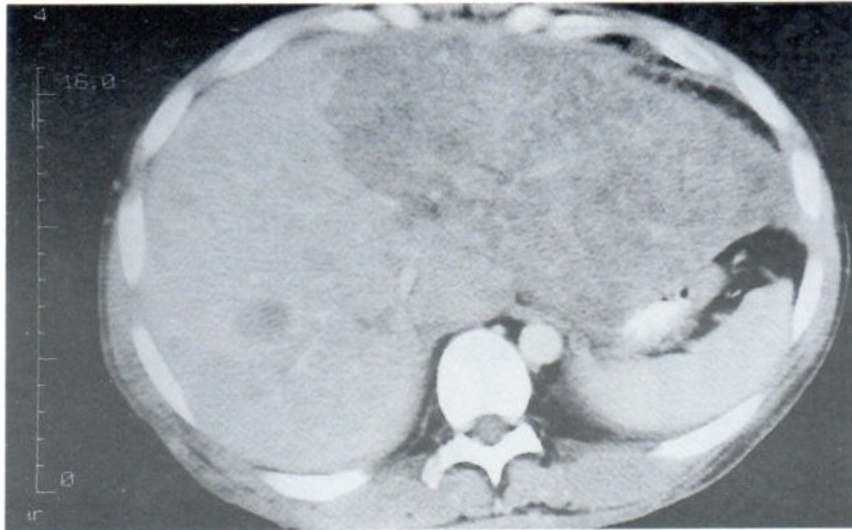


**Fig.1** Post contrast scan shows diffuse inhomogenous hypodensities in the left hepatic lobe and parts of the right lobe. The intra-hepatic inferior vena cava is compressed with incomplete visualisation of the left hepatic vein.



**Fig. 2** Close up view shows nodular deposits on the left hepatic lobe surface. The portal vein is patent.

9. Breslow A. Thickness, cross-sectional areas and depth of invasion in the prognosis of cutaneous melanoma. *Ann Surg* 1970; 172: 902-8.
10. Das Gupta T, Braesfield R. Metastatic melanoma: a clinico-pathological study. *Cancer* 1964; 17: 1323-39.
11. Dahnert W. *Radiology review manual*, 2nd edn. 1992, pp. 428-9. Williams & Wilkins.
12. Chomyn JJ, Stamm ER, Thickman D. CT of melanoma liver metastases: is the examination without contrast media superfluous? *J Comput Assist Tomogr* 1992; 16: 568-71.
13. Patten RM, Shuman WP, Teefey S. Subcutaneous metastases from malignant melanoma: prevalence and findings on CT. *AJR* 1989; 152: 1009-12.
14. Petersdorf RG, Adams RD, Braunwald E et al. *Harrison's Principles of Internal Medicine*, 10th edn. 1983, pp. 829. McGraw-Hill.

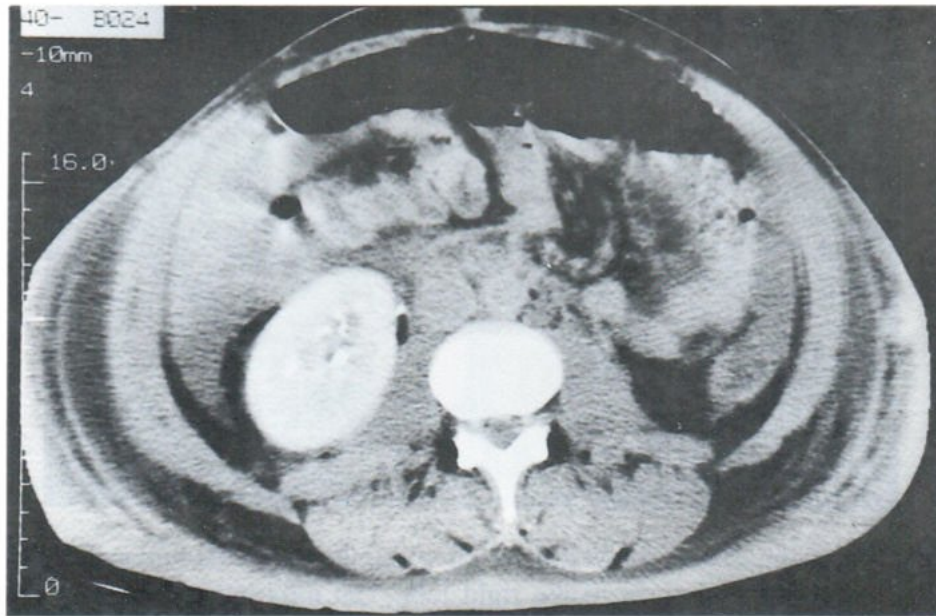


**Fig. 3** Ascitic fluid is present. Subcutaneous melanoma metastases are present at the left lateral abdominal wall.



**Fig. 4** Laparoscopic image showing blackish melanoma deposits on the liver.



## RENAL LYMPHOMA IN AN HIV POSITIVE PATIENT

Chirote SUCHATO<sup>1</sup>, Patchrin PEKANAN<sup>1,2</sup>,  
Udom HARINSUT<sup>3</sup>

### ABSTRACT

Renal lymphoma was presented in an HIV positive patient. The patient was a 52-year-old man with right upper quadrant tenderness. An infiltrative border soft tissue mass was found mainly at right renal hilum. The mass showed lower signal on both T1W and T2W images and created no significant contrast enhancement.

### INTRODUCTION

Primary renal lymphoma is very rare, because kidneys do not contain lymphatic tissue.<sup>1,2</sup> Secondary renal involvement, especially in non-Hodgkin lymphoma is more common and is found in one third of patients with this disease at autopsy.<sup>3,4</sup> Eleven percent of patients with AIDS and lymphoma have renal involvement.<sup>5</sup> The kidney involvement in lymphoma may be caused by hematogenous dissemination, or by direct infiltration originating from neighboring lymph nodes. The clinical symptoms are fairly nonspecific.<sup>1,6</sup>

### CASE REPORT

A 52-year-old man had tenderness at right upper quadrant. Bimanual palpation showed fullness sensation of right side. The patient was a known case of chronic viral B hepatitis and positive anti HIV. Complete blood count and urine examination showed no abnormality. Bulgy and blurred contour of right psoas muscle, lateral deviation of right kidney, pressure effect on distal right renal pelvis and upper ureter was seen at IVP study. I.V. contrast enhancement CT scan revealed an infiltrative border, soft tissue mass, size 5X7X10 cm, between right kidney and right psoas muscle, extending to renal sinus region or

from central sinus to medial perinephric area (Fig. 1). Involvement of the renal parenchyma was probably present at middle-lower pole area. The mass did not enhance significantly (Fig. 2). On T1W, and T2W the signal of the mass was lower than the renal parenchyma; the mass is slightly brighter on T2WI and showed no significant contrast enhancement with Magnevist (Fig. 3).

Malignant lymphoma involving medial and lower aspect of right kidney, perinephric and peripelvic fatty tissue, and the wall of renal vein was found at surgery and pathology. There was no lymph nodes involvement.

### DISCUSSION

On CT, renal lymphoma may manifest in various ways, with bilateral renal involvement in about 75% of cases. Various patterns of involvement are detected only after i.v. contrast medium is administered.<sup>1,4,7-15</sup> The following types of renal involvement may be seen: (1) multinodular changes (45%-mild to moderate enhancement after i.v. contrast administration is seen in the mostly 1-5 cm large, mainly cortical nodules, (2) Circumscribed intrarenal lesions (15%) (3) diffuse bilateral involvement without circumscri-

<sup>1</sup> Department of Radiology, Samitivej Hospital, Sukhumvit 49, Bkk. Thailand.

<sup>2</sup> Department of Radiology, Ramathibodi Hospital.

<sup>3</sup> Department of Medicine, Samitivej Hospital.



bed tumors (10%), with pronounced kidney enlargement and unilaterally or bilaterally decreased or absent contrast excretion (4) infiltration of the kidney originating from other retroperitoneal lymphoma localization (25%): soft tissue tumor extending into the kidney, often without changes in renal function, but with obstruction (depending on the site of the involvement), (5) renal sinus lymphoma: soft tissue infiltration surrounding the renal pelvis and the proximal ureter, infiltrating the pyramids.

Samelka<sup>16</sup> studied non-Hodkin's lymphoma of the kidneys in twelve patients by MRI, observed three types of renal involvement: (1) large paraaortic retroperitoneal masses with extension into the renal hilum, the subcapsular space, or both (2) unilateral diffuse infiltration of the renal parenchyma (3) focal rounded intraparenchymal masses. Untreated lymphoma was slightly hypointense relative to the renal cortex on T1-weighted images and was heterogenous and slightly hypointense or isointense on T2-weighted images. Enhancement of lymphomatous tissue was mildly

heterogenous and was minimal on early images after gadolinium enhancement and remained minimal on late contrast enhanced images in most tumor masses. No central necrosis of tumor was identified, and no renal vein thrombus was present. The patients who presented as a large paraortic mass showed diminished renal cortical perfusion of the involved kidney. All of these patients also had tumor extension into the renal hilum.

Lymphoma is characterized by conglomerate masses of monotonous cellularity that usually contain few small blood vessels.<sup>16,17</sup> Hypovascular solid tissues have long T1 values and are generally low in signal intensity of T1-weighted images. Such tissue enhances minimally with contrast agents, particularly on early enhanced images.<sup>18</sup> Untreated tumors that were hypointense to isointense in signal intensity relative to the renal cortex on T2-weighted images also reflected the hypovascular nature of those untreated tumors.

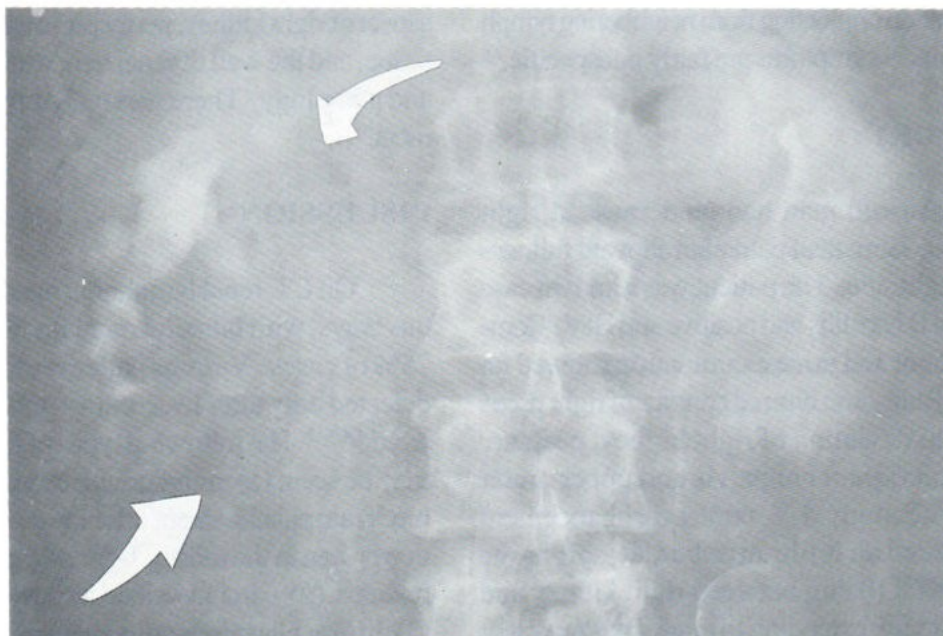


**Fig. 1** IVP showed evidence of mass lesion in the region of right renal hilum with mild obstructive hydronephrosis.



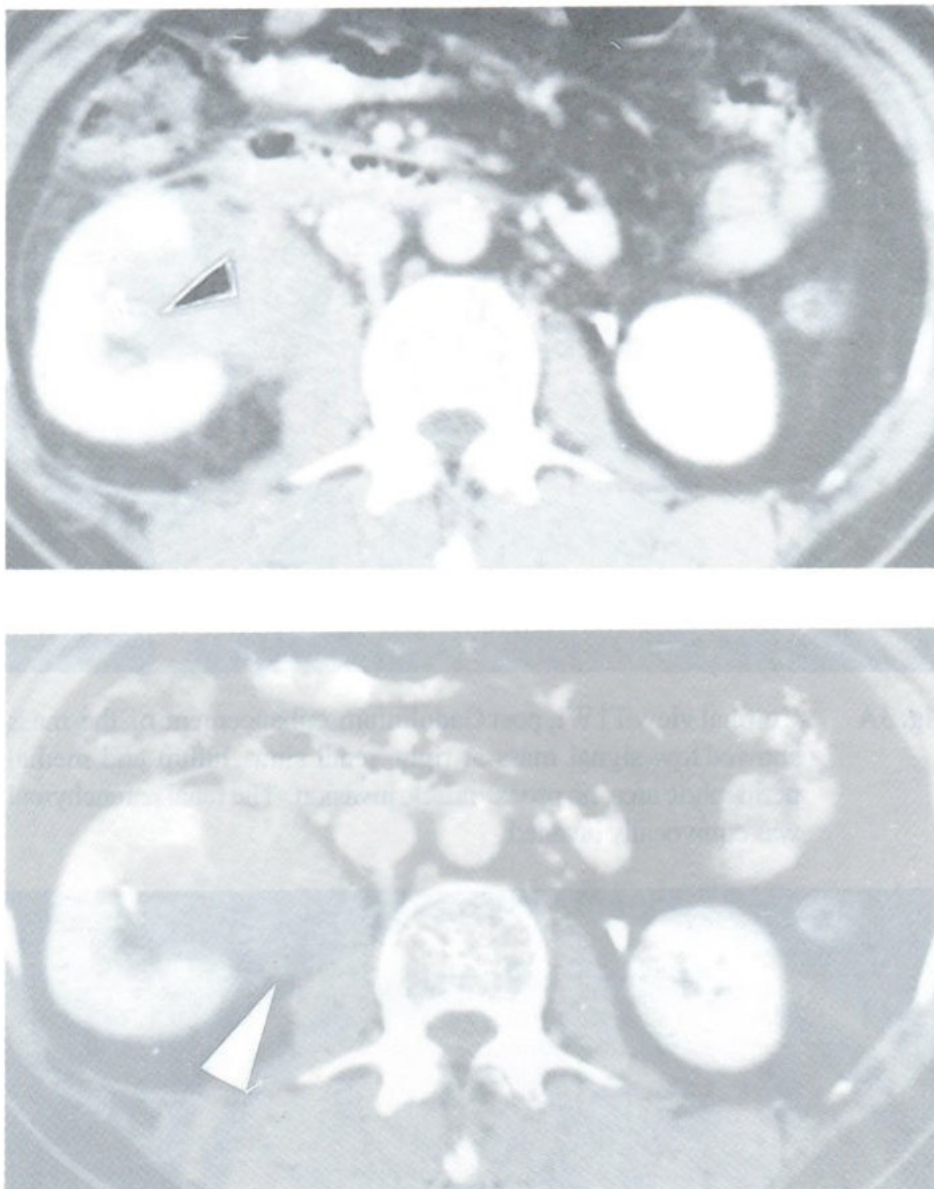


**Fig. 2** I.V. contrast enhanced CT scan revealed an infiltrative border solid mass at right renal hilum, extending to renal sinus and medial perinephric tissue.



**Fig. 3A** Coronal view T1WI, post Gadolinium enhancement of the mass showed low signal mass at right renal sinus, hilum and medial perinephric area, no psoas muscle invasion. The renal parenchymal was equivocally invaded.

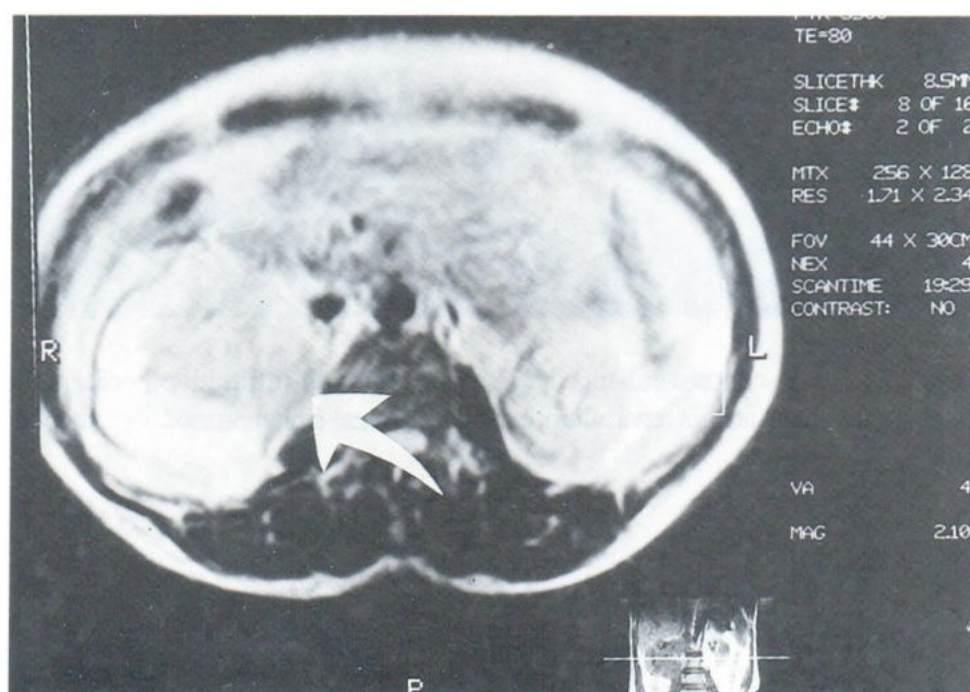


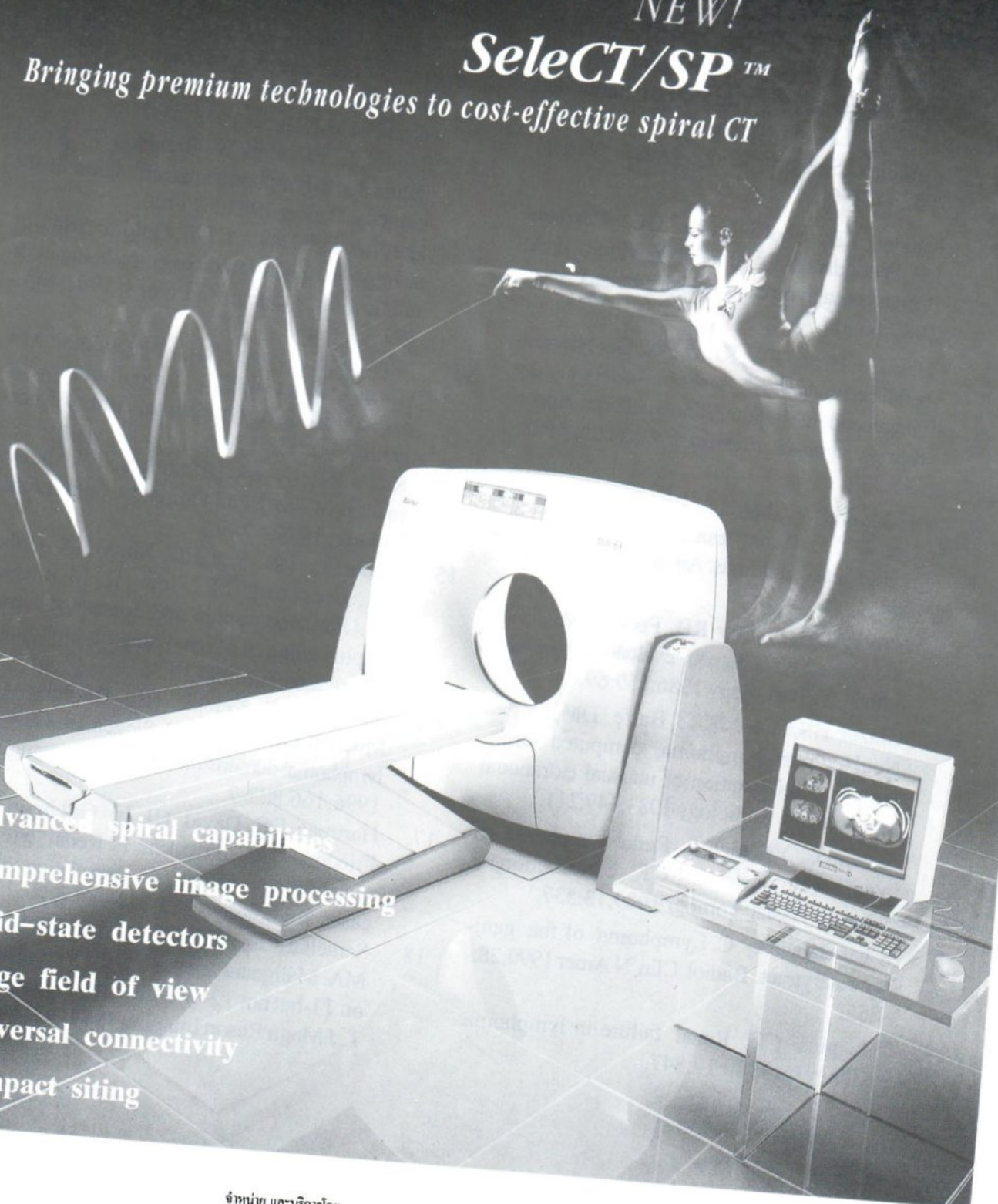
**Fig. 3B** T2WI axial view of the lesion showed slightly increased signal in the mass, but the signal was still lowered than the kidney



## REFERENCES

1. Schweden FJ, Schild HH, Riedmiller H. Renal tumors In adults. in Schild HH, Schweden FJ, Lang EK, ed. Computed tomography in urology. Stuttgart: Georg Thieme Verlag, 1992:-154-6.
2. Kandel LB, McCullough DL, Harrison LH, Woodruff RD, Ahl ET Jr, Munitz HA. Primary renal lymphoma: does it exist. Cancer 1987;60:386.
3. Hess CF, Busch FW, Kurtz FW. Der Nierrenbefall bei malignem Lymphom: bedeutung der bildgebenden Verfahren innerhalb der Ausbreitungsdiagnostik. Fortschr. Roentgenstr. 1988;-148:374.
4. Richmond J, Sherman RS, Diamond HD, Craver LF. Renal lesions associated with malignant lymphomas. Amer J Med 1962;32:-184.
5. Nyberg DA, Jeffrey RB, Federle MP, et al. Aidsrelated lymphomas: evaluation by abdominal CT. Radiology 1986;159:69.
6. Glazer HS, Lee JKT, Balfe DM, et al. NonHodgkin lymphoma, computed tomographic demonstration of unusual extranodal involvement. Radiology 1983;149:211.
7. Levine C, Vrlenich L. Renal lymphoma in ataxia-telangiectasia: CT contribution. J Comput Assist Tomogr 1989;13:537.
8. Charnsangavej C. Lymphoma of the genitourinarytract. Radiol Clin N Amer 1990;28:-865.
9. Coggins CH. Renal failure in lymphoma. Kidney Int 1980;17:847.
10. Kanfer A, Vandewalle A, Morel-Maroger L et al. Acute renal insufficiency due to lymphomatous infiltration of the kidneys: report of six cases. Cancer 1976;38:2588.
11. Randolph VL, Hall W, Bramson W. Renal failure due to lymphomatous infiltration of the kidneys. Cancer 1983;52:1120.
12. Hartman DS, Davis CJ Jr, Goldman SM, et al. Renal lymphoma: radiologic-pathologic correlation of 21 cases. Radiology 1982;144:-759.
13. Jafri SZH, Bree RL, Amendola MA, Glazer GM et al. CT of renal and perirenal Non-Hodgkin lymphoma. Amer J Roentgenol 1982;138:1101.
14. Rubin BE. Computed tomography in the evaluation of renal lymphoma. J Comput Assist Tomogr 1979;3:759.
15. Ruchman RB, Yeh HC, Mitty HA, Cohen BA, Greenberg M, Plous R, Mendelson DS. Ultrasonographic and computed tomographic features of renal sinus lymphoma. J Clin ultrasound 1988;16:35.
16. Semelka RC, Kelekis NL, Burdeny DA, Mitchell DG, Brown JJ, Siegelman ES. Renal lymphoma: demonstration by MR imaging. AJR 1996;166:823-7.
17. Hartman DS, David CJ Jr. Goldman SM, Friedman AC, Fritzsche P. Renal lymphoma: radiologic-pathologic correlation of 21 cases. Radiology 1982;144:759-66.
18. Samelka RC, Bagley As, Brown ED, Kroeker MA. Malignant lesions of the liver identified on T1-but not T2-Weighted MR images at 1.5 T. J Magn Reson Imaging 1994;4:315-6.

NEW!  
**SeleCT/SP™**  
*Bringing premium technologies to cost-effective spiral CT*



Advanced spiral capabilities  
Comprehensive image processing  
Solid-state detectors  
Large field of view  
Universal connectivity  
Compact siting

จำหน่าย และบริการโดย

**supreme**  
PRODUCTS CO., LTD.  
**บริษัท สุปรีม โปรดักส์ จำกัด**

163/81-82 ถ.พระปิ่นเกล้า แขวงบางยี่ขัน เขตบางพลัด กรุงเทพฯ 10700 แผนกขาย 434-0040, 434-0050 แผนกบริการ 434-0060 โทรสาร 433-3971



## AN EARLY GASTRIC CANCER

Supranee NIRAPATHAPONGPORN<sup>1,2</sup>, Patchrin PEKANAN<sup>1,2</sup>,  
Janjira CHATCHAVALA<sup>1,2</sup>, Jaroen SUWANWILAF<sup>3</sup>

### ABSTRACT

An early gastric carcinoma was presented in a 55-year-old woman who suffered from chronic neutropenia and indigestion. Upper GI series were performed twice and the lesion at both examinations was similar. It appeared as a plaque like elevation, small ulcer craters surrounding by nodular mucosa and was interpreted as erosive antral gastritis. Biopsy of the lesion revealed mucosal spread of cancer. Biopsy should be performed in such lesion.

### INTRODUCTION

During the past decade, attention has been focused on the role of double contrast barium studies and endoscopy for the early diagnosis of gastric cancer. The Japanese have had tremendous success in detecting early gastric cancer by mass screening of the adult population with these techniques.

Most adenocarcinomas of the stomach are diagnosed at an advanced stage. By definition, advanced lesions have invaded the muscularis propria, and they are usually associated with metastases to regional lymph nodes or other local or distant structures. In contrast, early gastric cancers are defined histologically as cancers in which malignant invasion is limited to the mucosa or submucosa, regardless of the presence of lymph node metastases.<sup>1,2</sup> Early gastric cancers are curable lesions with 5-year survival rates of more than 90%. So the detection of an early cancer lesion of the stomach is an important task for radiologists.

### CASE REPORT

This 55-year-old lady, has been followed up

for mild chronic neutropenia for the past 9 years; her CBC revealed WBC running between 3000-5000 cu/mm. Due to only having mild degree of periodic neutropenia and she has never have any problem causing by the low WBC, the bone marrow study was not done. She has been given Folic acid 1 tab/day and has been doing fine. One year ago, she developed indigestion, the UGI revealed mild erosive gastritis at the distal gastric body and at antrum (Fig. 1). She was consulted for a gastroscope but the patient was unable to swallow the gastroscope. She was instructed by the gastro-enterologist to continue Zantac and re-X-ray of the UGI tract in the next 3 weeks if the lesion was still present. She became well after the medication and did not return to see the gastroenterologist. Another year later, she appeared for a general physical check up. UGI series was again performed due to her complaint of abdominal discomfort. The UGI series revealed erosive antral gastritis (Fig.2). Gastroscope was performed under general anesthesia. Few shallow ulcers was found at the incisura angularis and ulcer with edema and bleeding was noted at the ridge of incisura. The biopsy was performed from the ulcerative lesions. Histology revealed fragments of diffuse type of infiltrative adeno-carcinoma. The

<sup>1</sup> Department of Radiology, Ramathibodi Hospital, Rama 6 Street, Bangkok 10400, Thailand.

<sup>2</sup> Department of Radiology, Samitivej Hospital

<sup>3</sup> Department of Pathology, Samitivej Hospital



metastatic work up showed no evidence of metastases. Radical subtotal gastrectomy was performed. Histology revealed signet ring type gastric carcinoma involving lesser curvature of the antrum. The tumor was present in the mucosa as multiple isolated islands and small sheets. No lymphatic or vascular invasion was seen. The lines of excision and omentum was not involved. There was no metastases to the available regional lymph nodes. The uninvolved mucosa showed moderate chronic gastritis and mild intestinal metaplasia.

## DISCUSSION

The double contrast upper gastrointestinal examination has been widely recognized as the best radiologic technique for diagnosing early gastric cancer.<sup>1,3-6</sup> The Japanese Endoscopic Society has divided these lesions into three basic types.<sup>7</sup>

Type I early gastric cancers typically appear as small, elevated lesions in the stomach.<sup>4,5</sup> Because

adenomatous polyps may undergo malignant degeneration, the possibility of early gastric cancer should be suspected for any sessile or pedunculated polyps greater than 1 cm. in size. Other type I lesions may protrude considerably into the lumen and still be classified histologically as early gastric cancers.<sup>5</sup> Thus, polypoid carcinomas cannot be definitively diagnosed as early or advanced lesions on the basis of the radiographic findings.

Type II early gastric cancers are superficial lesions with elevated (IIa), flat (IIb), or depressed (IIc) components. These lesions may be manifested by plaque like elevations, mucosal nodularity, shallow areas of ulceration, or some combination of these findings.<sup>3-6</sup> Occasionally type II lesions may be quite extensive and involve a considerable surface area of the stomach.

Type III early gastric cancers are typically characterized by shallow, irregular ulcer craters with nodularity of the adjacent mucosa and clubbing, fusion, or amputation of radiating folds.<sup>1,4,5</sup>

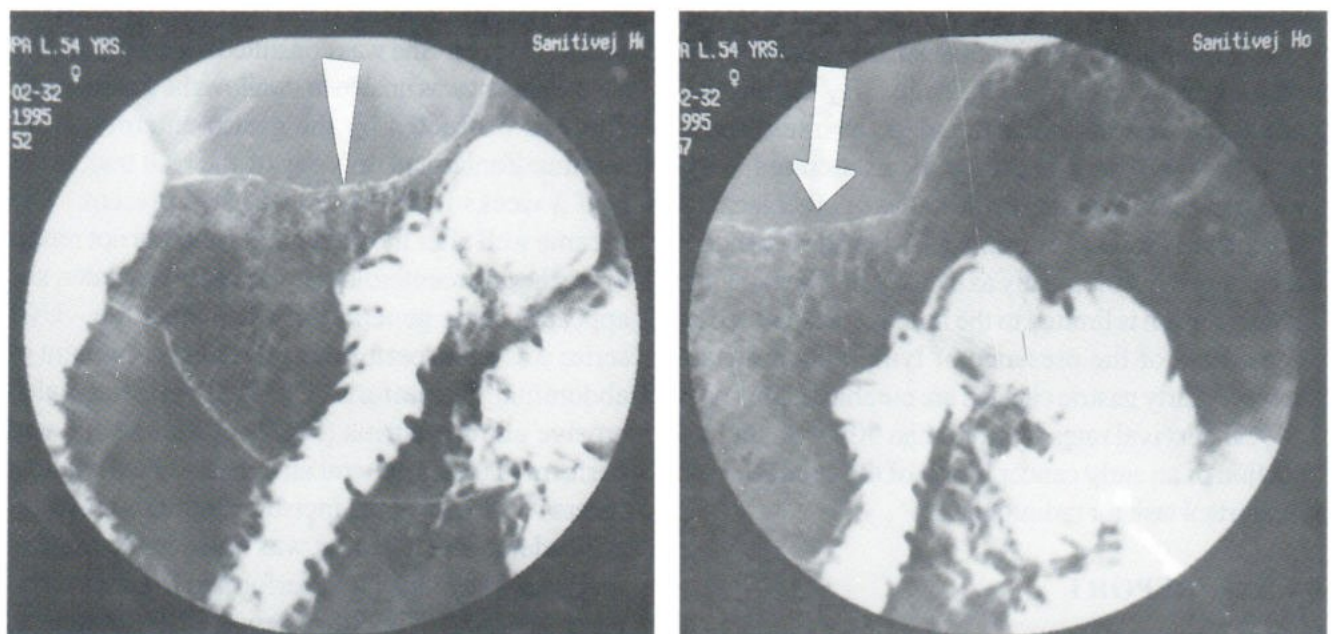


**Fig. 1** UGI series in March 1995, the lesion was seen at the gastric antrum as mixed plaque like elevations, mucosal nodularity and shallow ulcerations. Irregularity of the mucosa at the lesser curvature of the gastric antrum was presented. These lesions appeared somewhat similar to the erosive gastritis.



Although some lesions with an equivocal or suspicious appearance are found to be benign ulcers, endoscopy and biopsy should be performed for all lesions with suspicious radiographic findings to avoid missing early cancers.

About 70% of the ulcers in type IIc or III early gastric cancers are reported to undergo significant healing on medical treatment.<sup>8</sup> It has been postulated that these cancers are characterized by a cycle of ulceration, healing, and recurrent ulceration. Rarely, complete healing of malignant ulcers has also been described.<sup>8</sup> However, malignancy may still be suspected on follow-up barium studies if mucosal nodularity or other abnormalities are detected at the site of the previous ulcer.

Early gastric cancers may appear radiographically as depressed (ulcerated), elevated (polypoid), or superficial lesions. Ulcerated cancers must be distinguished from benign gastric ulcers. Occasion-

ally, early gastric lymphomas may also appear as ulcerated lesions. Polypoid cancers must be distinguished from adenomatous or hyperplastic polyps or other benign or malignant tumors in the stomach. Finally, superficial cancers must be distinguished from a focal area of gastritis or intestinal metaplasia. When early gastric cancer is suspected on the basis of barium studies, endoscopy and biopsy are required for a definitive diagnosis.

Patients with advanced gastric carcinoma have a dismal prognosis, with 5-year survival rates of only 3 to 21%.<sup>9-14</sup> In contrast, patients with early gastric cancer have 5-year survival rates of 85 to 100%.<sup>15-18</sup> Early detection of these lesions is therefore essential for improving survival of patients. Because it is frequently not possible to distinguish early gastric cancer from advanced carcinoma on preoperative studies, an aggressive surgical approach is justified for all patients with resectable lesions.

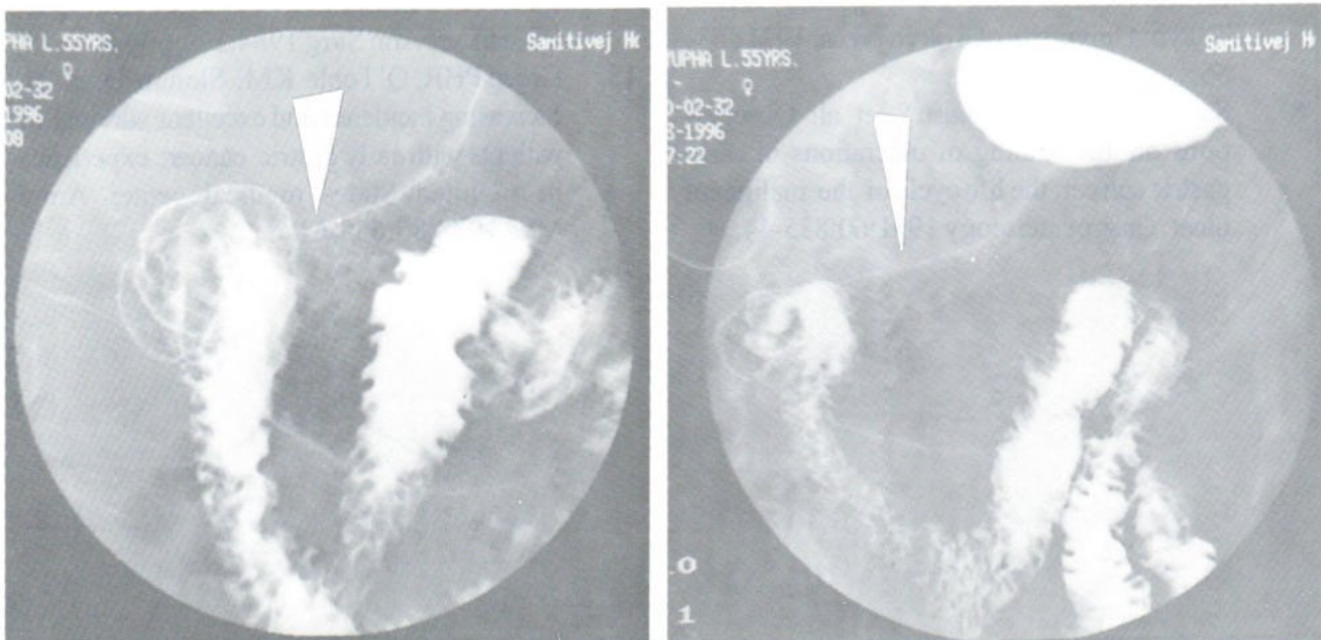


**Fig.2** UGI series in March 1996, the lesion noted at the gastric antrum was seen similar to that in 1995.

## REFERENCES

1. Levine MC, Megibow AJ. Carcinoma. In: Gore, Levine, Laufer, ed. Textbook of gastrointestinal radiology. Philadelphia: W.B. Saunders Company, 1994:660-63.
2. Shirakabe H, Nishizawa M, Maruyama M, et al: Atlas of X-ray Diagnosis of early gastric cancer. New York: Igaku-Shoin, 1982 : 1-18.
3. Koga M, Nakata H, Kiyonari H, et al. Roentgen features of the superficial depressed type of early gastric carcinoma. Radiology 1975;15:289-92.
4. Montesi A, Graziani L, Pesaresi A, et al. Radiologic diagnosis of early gastric cancer by routine double-contrast examination. Gastrointes Radiol 1982;7:205-15.
5. Gold RP, Green PH, O'Toole KM, et al. Early gastric cancer: radiographic experience. Radiology 1984;152:283-90.
6. White RM, Levine MS, Enterline HT, et al. Early gastric cancer: recent experience. Radiology 1985;155:25-7.
7. Murakami T. Pathomorphological diagnosis. In Murakami T (ed): Early gastric cancer. Tokyo: University of Tokyo press, 1971 : 53-55.
8. Sakita T, Ogura Y, Takasu S, et al: Observations on the healing of ulcerations in early gastric cancer: the life cycle of the malignant ulcer. Gastroenterology 1971;60:835-44.
9. Dupont JB, Lee JR, Burtoon GR, et al. Adenocarcinoma of the stomach: review of 1497 cases. Cancer 1978;41:941-47.
10. Ochsner A, Weed TE, Nuessle WR. Cancer of the stomach. Am J Surg 1981;141:10-4.
11. Faivre J, Justrabo E, Hilton P, et al. Gastric carcinoma in Cote d'Or (France): a population based study. Gastroenterology 1985;88:1874-79.
12. Moore JR. Gastric carcinoma: 30-year review. Can J Surg 1986;29:25-8.
13. McBride CM, Boddie AW. Adenocarcinoma of the stomach: are we making any progress? South Med J 1987;80:283-6.
14. Cady B, Rossi RL, Silverman ML, et al. Gastric adenocarcinoma: a disease in transition. Arch Surg 1989;124:303-8.
15. Kaneko E, nakamura T, Umeda N, et al. Outcome of gastric carcinoma detected by gastric mass survey in Japan. Gut 1977;18:626-30.
16. Okui K, Tejima H. Evaluation of gastric mass survey. Acta Chir Scand 1980;146:185-7.
17. Carter KJ, Schaffer HA, Ritchie WP. Early gastric cancer. Ann Surg 1984;199:604-9.
18. Green PHR, Q'Toole KM, Slonim D, et al. Increasing incidence and excellent survival of patients with early gastric cancer: experience in a United States medical center. Am J Med 1988;85:658-61.



## MR IMAGING OF THE BRAIN IN WILSON'S DISEASE.

O. CHAWALPARIT, K. DANPUKDEE, S. SUTHIPONGCHAI,  
P. CHIEWVIT, A. CHUROJANA, W. APICHONKIT

### ABSTRACT

Four cases of proven Wilson's disease underwent MRI studies of brain. The characteristic appearance of the putaminal lesion with high and low intensity spots centrally and high intensity "frame" peripherally was shown on T2WI-TSE in three neurologically symptomatic patients. We also found that the gradient echo imaging showed low signal intensity not more pronouncedly than the spin echo imaging. The mid brain, brain stem and cerebellar lesions were also seen in symptomatic patients. Some good correlation of the neurological examinations and MRI findings were found.

**Key Words:** Wilson's disease, MR Imaging.

Wilson's disease or hepatolenticular degeneration is an uncommon autosomally recessive inherited disorder of copper metabolism characterized by abnormal deposition of copper in various tissues, most notable in brain and liver. Although it is rare, early diagnosis and prompt treatment can prevent the devastating neurologic sequelae of the untreated illness. In this report, we described the magnetic resonance (MR) findings in various pulse sequences and some clinical correlation of the patients.

### MATERIALS AND METHODS

We have studied four male patients with clinically and biochemically proven of Wilson's disease. The age of the patients are between 11 and 24 years. The magnetic resonance images (MRI) of the brain were done with 1.5 Tesla magnet (Philips Gyroscan). In all patients, axial scan was done in T1WI and dual T2WI-TSE (Turbo-spin echo) (TR/TE = 450/15; 2000/25, 120). The TSE is the fast spin echo technique in this machine. The sagittal T1WI-TSE and coronal T2WI-TSE were also obtained. The axial fast field echo (FFE) was also done in three of the four patients (TR/TE/FA = 600/15/25). The FFE is the gradient echo imaging in this machine.

### RESULTS

Three of the four patients have neurological symptoms and signs as shown in Table 1. The fourth patient came to the hospital with liver disease and abnormal liver function test but no abnormal neurological symptom and sign.

The MRI findings are also summarized in the table. All patients who have neurological deficits show abnormalities on MRI. The common finding is the abnormality of both basal ganglia especially the lentiform nucleus. In the center of the putamen, there is spots of hypointensity on both T1WI and T2WI interspersed with spots of high intensity on T2WI. The periphery shows a band of high intensity surrounding the putamen appeared to "frame" the putamen (Fig. 1A). Only one case shows abnormal high intensity in the globus pallidus on T2WI (Fig. 2). The caudate nucleus was involved in varying degree in all three patients.

In gradient echo imaging of the two symptomatic patients, the abnormal low signal intensity in the putamen appears not more pronouncedly than that as shown on T2WI-TSE (Fig. 1B). In the asymptomatic patient, the GEI reveals no abnormality as well as T2WI-TSE (Fig. 3).

All symptomatic patients have abnormal



high intensity in the mid brain or lower brain stem, but no good correlated symptoms can be done. The patient who has rigidity and bradykinesia (Case #2) has abnormal high intensity in the dentate nucleus as well as the red nucleus and periaqueductal gray matter, while the patient who has lesion in mid brain (Case #1) shows no other neurological symptoms except dysarthria.

## DISCUSSION

Wilson's disease was first described by Kinear Wilson in 1912. The pathological changes in the central nervous system are always associated with increased tissue copper content. The toxic copper substances interfere with enzymatic activity or damage cellular structure.

Many articles have dealt with computed

tomography and MRI findings in the brain in Wilson's disease. The most common described abnormality is the lesion in basal ganglion. In the earlier studies of MRI using low field magnet, only high intensity was noted in the affected parts of the brain.<sup>1</sup> In the later articles, high field MRI have also shown low intensity in the lesion.<sup>4,5,6,9</sup> The typical findings on MRI are high intensity in the putamen, caudate nucleus and globus pallidus bilaterally.<sup>1,3,4,5,6,7,8</sup> In the putamen, low intensity of the lesion seen on T2WI but high intensity band in the periphery, mainly lateral, appeared to frame the the putamen have been described.<sup>4,7</sup> In our cases, there is also spots of high intensity interspersed with low intensity in the center of the putamen. The possible pathologic explanation is the cavitating degeneration of the neuronal tissue with deposition of iron and/or copper.<sup>5,6</sup>

The susceptibility effect is more pronounced

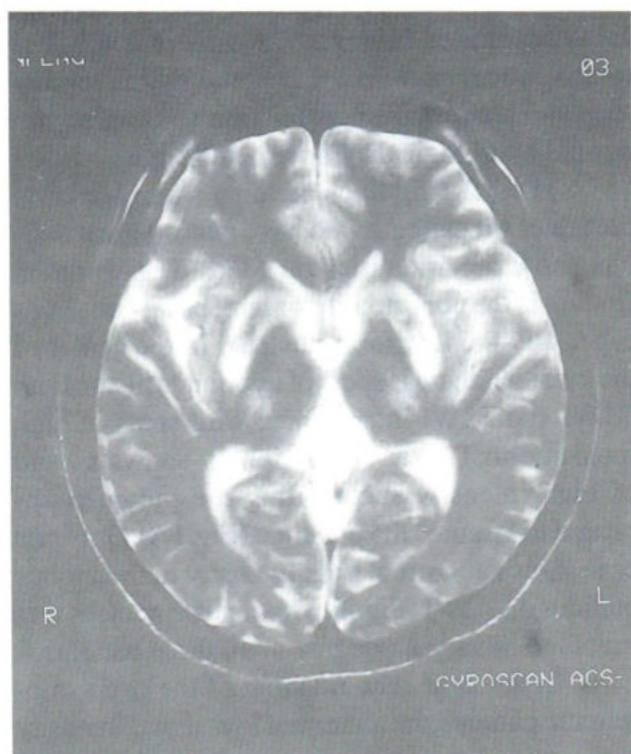


**Fig.1A** Axial T2WI of the patient No.1 shows characteristic hypointensity and hyperintensity lesion in the putamen and caudate nucleus. Note the "frame" appearance of the putamen.

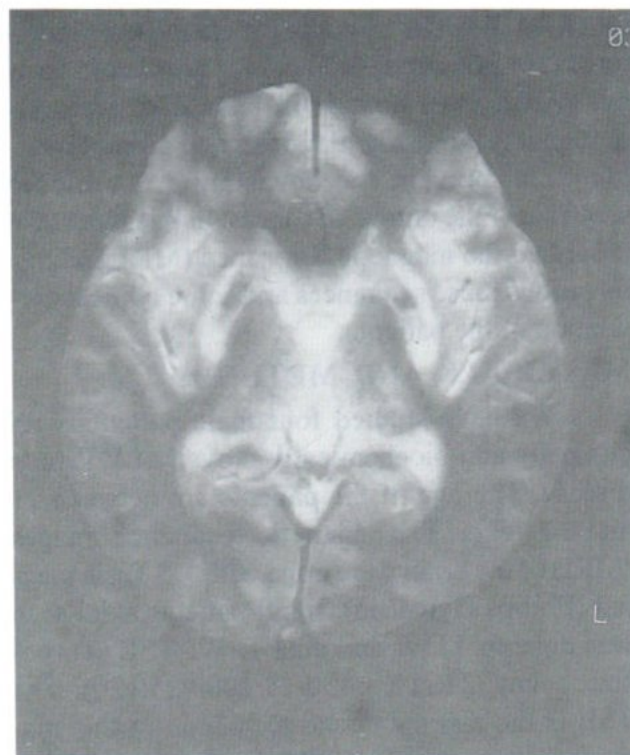


**Fig. 1B** Axial GEI of the same level shows the same changes of the basal ganglia.



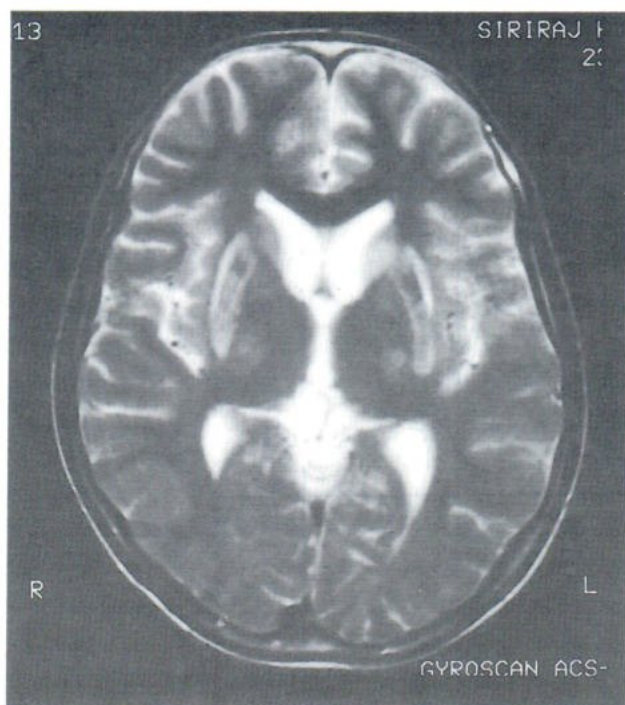
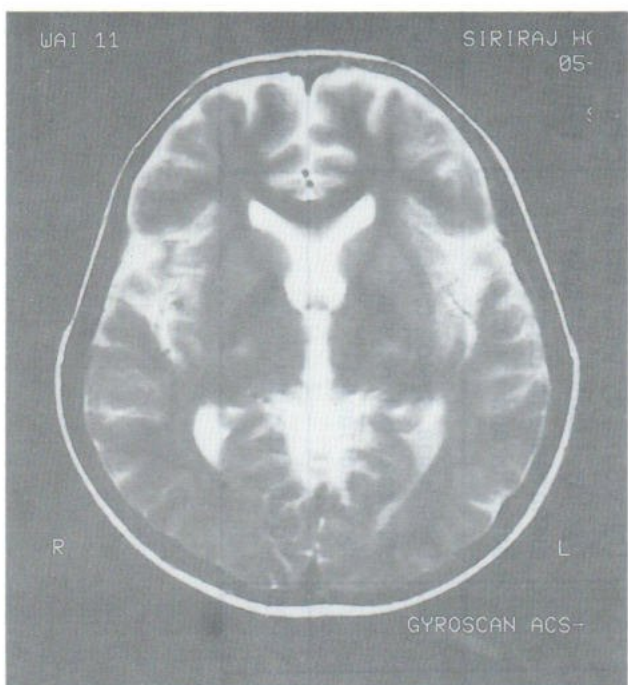
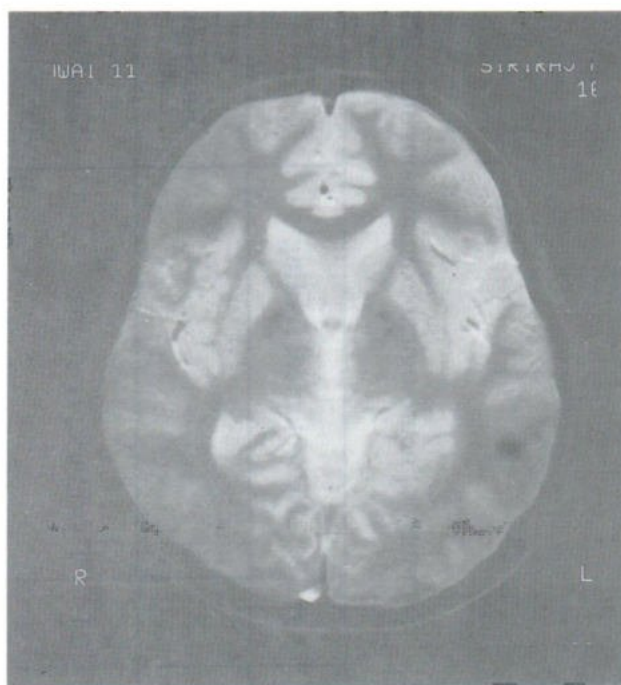


**Fig. 2** Axial T2WI of the patient No.2 shows abnormal signal intensity in the basal ganglia. Note the high intensity in the globus pallidus.



**A**



**B**

**Fig.3 (A,B)** : Axial T2WI and GEI of the patient No.4 shows no abnormal intensity in the basal ganglion.

in increasing magnetic field, compartmentalization of the paramagnetic substances, prolonged TE, and gradient echo pulse sequences. The blooming appearance in the paramagnetic deposition area is the suggestive evidence. In our cases, we noticed no blooming effect on gradient echo images. The explanation of low intensity may be not simply intracellular accumulation of the paramagnetics. Even though there are many reports about the low intensity on T2WI, no report has been done on gradient echo images to detect the deposition of paramagnetics in the basal ganglia of the Wilson's disease. We think that more cases are needed to evaluate the benefit of the gradient echo imaging in detecting very early copper or iron deposition in the brain before seen by spin-echo imaging. However, in our study it seems to be likely that the gradient echo images will not be more sensitive in this matter.

Aisen et al<sup>1</sup> studied 23 patients with Wilson's disease and found good correlation between the neurological examination and the MRI findings. Many articles were also reported the same result.<sup>3,4,7</sup> In our study we found some

**Table 1** Summary of neurological examinations and MRI findings.

Patient	Age	Neurological finding	Abnormal MRI			
			Basal ganglion	Mid brain	Cerebellum	Ventricular and subarachnoid
1	24	Dysarthria, Dystonia	Putamen, Caudate nucleus	Red nucleus, Substantia nigra, Periaqueductal gray	Normal	Mild dilatation
2	13	Dysarthria, dystonia, tremor, rigidity, bradykinesia, gait disturbance, change of behavior and abnormal mood.	Putamen, Globus pallidus, Caudate n.	Red n., Periaqueductal gray	Dentate n.	Normal
3	12	Dysarthria, dystonic, rigidity, change of behavior and abnormal mood	Putamen, Caudate n.	Normal	Cerebellar peduncle	Mild to moderate dilatation
4	11	No abnormality	Normal	Normal	Normal	Mild dilatation



correlation of the clinical and MRI findings. We also found abnormality in the mid brain, lower pons and cerebellum. The severity of the neurological examination cannot be explained by the only findings of the lesion in the brain stem, suggestive of the significant cooperative function of the supratentorial, brain stem and infratentorial neural tissue.

## REFERENCES

1. Aisen AM., Martel W., Gabrielsen TO., et al (1985) Wilson's disease of the brain: MR Imaging. *Radiology* 157:137-141.
2. Imiya M., Ichikawa K., Matsushima H., et al (1992) MR of the base of the pons in Wilson disease. *AJNR* 13:1009-1012
3. Oder W., Prayer L., Grimm G., et al (1993) Wilson's disease: evidence of subgroups derived from clinical findings and brain lesion. *Neurology* 43:120-124.
4. Magalhaes ACA., Caramelli P., Menezes JR., et al (1994) Wilson's disease: MRI with clinical correlation. *Neuroradiology* 36:97-100.
5. Sener RN. (1993) Wilson's disease: MRI demonstration of cavitations in basal ganglion and thalami. *Pediatr. Radiol.* 23:157.
6. Brugieres P., Combes C., Ricolfi F., et al (1992) Atypical MR presentation of Wilson disease: possible consequence of paramagnetic effect of copper? *Neuroradiology* 34:222-224.
7. Prayer L., Wimberger D., Krammer G., et al (1990) Cranial MRI in Wilson's disease. *Neuroradiology* 32:211-214.
8. Hitoshi S., Iwata M., Yoshikawa K. (1991) Midbrain pathology of Wilson's disease: - MRI analysis of the three cases. *J. of Neurosurg., Psych.* 54(7):624-6.
9. Yuh WT., Flickinger FW. (1988) Unusual MR findings in CNS Wilson disease (letter). *AJR* 151:834.

SHIMADZU

INVERTERTYPE Mobile X-ray system

SCT-4800T WHOLE BODY CT SCANNER



MAGNETIC  
RESONANCE  
IMAGING

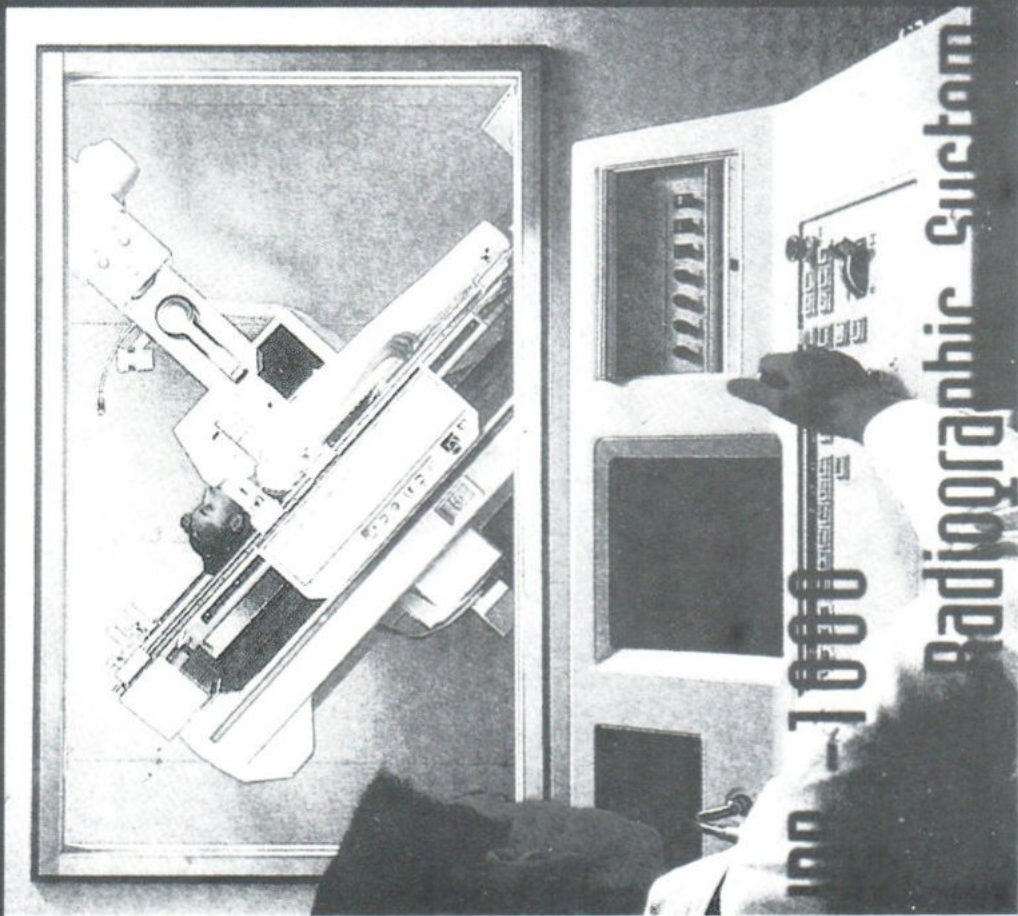
บริษัท รังสีภัณฑ์ จำกัด

RADIOLOGICAL EQUIPMENT CO.,LTD.

170-172/1 (ชั้น 2-3) ถนนบริพัตร ป้อมปราบ กรุงเทพฯ 10100

170-172/1 (Floor 2-3) BORIPHAT ROAD BANGKOK 10100 THAILAND

TEL: 2212386, 2237954, 2239791, 2243402 TELEFAX: (02) 2251657



100-10000

Radiographic Suctom



## ULTRASONOGRAPHY OF SMALL INTESTINAL INTUSSUSCEPTION IN NEUROFIBROMATOSIS: A CASE REPORT

Pannee VISRUTARATNA  
Pisit WATTANARUANGKOWIT  
Kanokporn ORANRATANACHAI

### ABSTRACT

Ultrasonographic diagnosis of intussusception is now a part of standard clinical practice. There are reports in the literature in which ultrasonography enabled the identification of their underlying causes; however, there has been no report of ultrasonographic features of intussusception caused by a neurofibroma.

We report a case of small intestinal intussusception caused by a neurofibroma. Ultrasound of the abdomen revealed concentric rings with the lead point formed a complex mass in the center of the intussusception. This was proven on operative and pathological findings.

### INTRODUCTION

Intussusception is the leading cause of intestinal obstruction in children, however, in adults it is rare and accounting for 5%-16% of all intussusceptions.<sup>1</sup> About 90% of adult intussusceptions occur in the small or large bowel, and over 90% have a demonstrable causes. Of the small-bowel intussusception, 17% were due to malignant tumors and 40% to benign tumors.<sup>2</sup> Ultrasonography is considered positive for intussusception if a "target sign" or "concentric rings" is seen in transverse section and a "pseudokidney" or "sandwich" sign is seen in longitudinal section. Ultrasound of intussusception with lead points due to various causes were reported,<sup>3,4</sup> however as far as we know, there is no publication of the ultrasonographic findings of intussusception due to a neurofibroma.

### CASE REPORT

A 41-year old woman presented with a history of intermittent abdominal pain for 2 months. On physical examination, there was a 10 cm diameter soft tissue mass at mid abdomen. The mass was movable and there was no tenderness on palpation. Multiple cutaneous neurofibromas occurring predominantly over the trunk and the forearms were noted. Multiple cafe' au lait spots were also present. The vital signs were normal. Ultrasonography was performed and showed a "sandwich" sign in longitudinal section in the left side abdomen. Transverse section through the apex of the intussusception showed a complex mass, about 2.6X4.3 cm in dimensions causing pressure effect on the compressed echogenic mucosa [Fig 1]. Eleven days later barium enema was



done and revealed a soft tissue mass in the right side of pelvic cavity causing pressure effect on the cecum, appendix, and terminal ileum [Fig 2]. There was also a soft tissue mass causing crescent shadow on the distal ileum in the right iliac fossa. Repeated ultrasonography showed a "concentric rings" with a complex mass at the center in the right lower abdomen [Fig 3]. There was no mass in the left side abdomen. Explore laparotomy was performed 6 days later. Intussusception of proximal ileum into

distal jejunum and numerous palpable polypoid masses along jejunum and ileum (about 1.5 feet from ligament of Trietz to 3.5 feet from ileocecal valve) were seen. Small bowel resection at 1.5 feet from ligament of Trietz and at 3.5 feet from ileocecal valve and end to end anastomosis were performed. Pathological findings showed 40 neurofibromas in the submucosa of resected jejunum and ileum. The largest lesion was about 5 cm in diameter and thought to cause intussusception.

## DISCUSSION

Neurofibromatosis is a mesodermal and ectodermal dysplasia with a broad spectrum of clinical



**Fig 1** Transverse section through the apex of the intussusception shows a "concentric rings" typical for intussusception. A complex mass is seen in the center of the lesion and causes pressure effect on the echogenic mucosa.



**Fig. 2** Barium enema (post-evacuation film) shows extrinsic pressure effect on the cecum, appendix and terminal ileum. A soft tissue mass causing a crescent shadow on the distal ileum is seen in the right iliac fossa.





**Fig 3.** Repeated ultrasound reveals “concentric rings” with a complex mass at the center of the lesion.

and radiological findings. The disease is characterized by multiple, soft, sessile or pedunculated skin nodules of varying sizes and areas of cutaneous pigmentation (café au lait spot). The gastrointestinal tract is involved in 25% of patients with neurofibromatosis.<sup>5</sup> The ileum is most frequently involved. They usually arise from subserosal nerves, Auerbach plexus, or less often from the submucosal plexus. The submucosal lesions are more likely to cause symptoms of recurrent melena or obstruction from intussusception.

The ultrasonographic findings of intussusception is widely recognized. The intussusceptum contained within the intussuscepti has been described as a “target” image with double concentric rings in the transverse section. The echogenic center of the lesion is

formed by the compressed mucosa. The center of the simple intussusception is always a round echogenic area in the transverse section. When a lead point is present, the uniform echogenic center of the intussusception is replaced by a complex mass lesion. The echo pattern of this complex mass depends on the nature of the lead point. When a bowel loop, such as an inverted Meckel’s diverticulum or appendix is present, a complex mass formed by convoluted bowel loops. When a polyp or tumor is present, a polypoid mass arising from the intussusceptum is seen.<sup>3</sup> Eustace S, et al.<sup>4</sup> reported a patient with colonic lipoma-induced intussusception who had increase both in size and echogenicity of the inner core of the leading edge of intussusception.

Although the ultrasonographic findings of a complex mass seen in this patient can be seen in intussusception from other causes, when one encountered a patient with the characteristic skin lesions of neurofibromatosis with a complex mass causing intussusception, the diagnosis of a neurofibroma causing intussusception should be the first consideration.

#### ACKNOWLEDGEMENT

We would like to express our thanks to Professor Dr.Sanan Simarak for reviewing the manuscript.

#### REFERENCES

1. Agha FP. Intussusception in adults. *AJR* 1986;146:527-531.
2. Felix EL, Cohen MH, Bernstein AD, Schwartz JH. Adult intussusception: case report of recurrent intussusception and review of the literature. *Am J Surg* 1976; 131:758-761.
3. Lam AH, Firman K. Ultrasound of intussusception with lead points. *Australas Radiol* 1991;35: 343-345.
4. Eustace S, Murray JG, O'Connell D. Sonographic diagnosis of colonic lipoma-induced intussusception. *J Clin Ultrasound* 1993; 21:472-474.
5. Davis G, Berk RN. Intestinal neurofibromas in von Recklinghausen's disease. *Am J Gastroenterol* 1973;60:410-414.



## ESOPHAGEAL TUBERCULOSIS IN AN HIV-INFECTED CHILD

Panee VISRUTARATNA, MD, Wittanee NA CHIANGMAI, MD

### ABSTRACT

We describe an unusual case, a young girl with perinatal infection of HIV who presented with chronic dry cough. Mediastinal lymphadenopathy and left pleural effusion were noted on her chest film. Esophagography revealed a fistula between the esophagus and the left main bronchus. Barium in the left thoracostomy tube was also seen after esophagography. Gastric washings were positive for acid fast bacilli. Treatment with antituberculous drugs was successful, and a follow-up chest film showed smaller mediastinal lymph nodes and no left pleural effusion.

### INTRODUCTION

Around the world, tuberculosis (TB) has emerged as the most common opportunistic infection in patients with human immunodeficiency virus (HIV). Not only are increasing instances of TB seen in these patients but the disease is more virulent. TB of the esophagus has been reported in patients with advanced pulmonary TB, patients with miliary TB, and also in children with primary TB infection.<sup>1</sup> Since the advent of drugs to combat TB effectively, esophageal involvement with TB has been rare. However, with the acquired immunodeficiency syndrome (AIDS) epidemic, an increase in the incidence of thoracic and extrathoracic mycobacterial disease has been observed. We describe an HIV-infected child with an esophago-bronchial fistula and a bronchopleural fistula resulting from TB.

### CASE REPORT

A 1-year-9-month-old girl presented with a dry cough which had persisted for 1 month. She had received antibiotics, antitussives and a bronchodilator from another hospital. However, she still had a severe cough and dyspnea. She had contacted HIV perinatally. On physical examination she had subcostal

retraction. Respirations were 58/min, pulse was 140/min, and her temperature was 38 degrees Celsius. She was cachectic. Oral thrush and pale conjunctiva were noted. Breathing sounds were not as loud as usual and rhonchi were heard in the left lower lung. The liver was palpable 3 cm below the right costal margin.

A chest film on admission (Fig 1) showed widening of the mediastinum because of enlarged lymph nodes and left pleural effusion. Left pleurocentesis produced milky fluid, which contained 1057 mg/dl of triglycerides, 4.7 g/dl of proteins, 112 g/dl of sugar and 343 units/L of LDH. There were 3250 cells/cu.mm.. 90% of these were lymphocytes and 10% were neutrophils. Gram stain was negative. A smear for acid-fast bacilli was negative. Turbidity remained after addition of a few drops of 10% KOH, which indicated that the fluid had no chyle. Intercostal drainage (ICD) was performed on the left chest. A sample of the type of milk she usually drank was analyzed. Its chemical composition was similar to that of the pleural fluid. A green syrup was dripped into her nasogastric (NG) tube; a green fluid was seen in the ICD tube. Esophagography was done by injecting barium into the NG tube with its tip at the mid thoracic esophagus. This showed a fistula



between the esophagus and the left main bronchus (Fig 2). We could not demonstrate a fistula between the left main bronchus and pleural cavity, although barium sulfate was seen in the ICD tube.

Gastric washings for acid-fast bacilli were positive. The patient received antituberculous drugs and underwent gastrostomy for feeding. After 2 months the ICD tube was removed because there was no more pleural fluid. She was finally discharged after a 2 1/2 month stay. A follow-up chest film (Fig 3) showed smaller mediastinal lymph nodes and no left pleural effusion.

## DISCUSSION

Esophageal TB is rare and has been found in only 1% of cases presenting with TB.<sup>1</sup> Most esophageal TB patients present with dysphagia. Rubinstein et al,<sup>2</sup> proposed four mechanisms for the spread of mycobacteria to the esophagus:<sup>1</sup> Infection

of a pre-existing esophageal mucosal lesion by swallowed tuberculous sputum;<sup>2</sup> Extension from pharyngeal or laryngeal TB;<sup>3</sup> Extension from caseating mediastinal or hilar nodes or a TB spine;<sup>4</sup> Involvement in the course of miliary tuberculosis. The most likely mechanism for our patient is that mycobacteria invaded her esophagus from adjacent mediastinal lymph nodes. Mycobacteria can spread to the esophagus by transmural inflammation from infected and often necrotic mediastinal lymph nodes, with associated fistulas and formation of sinuses.

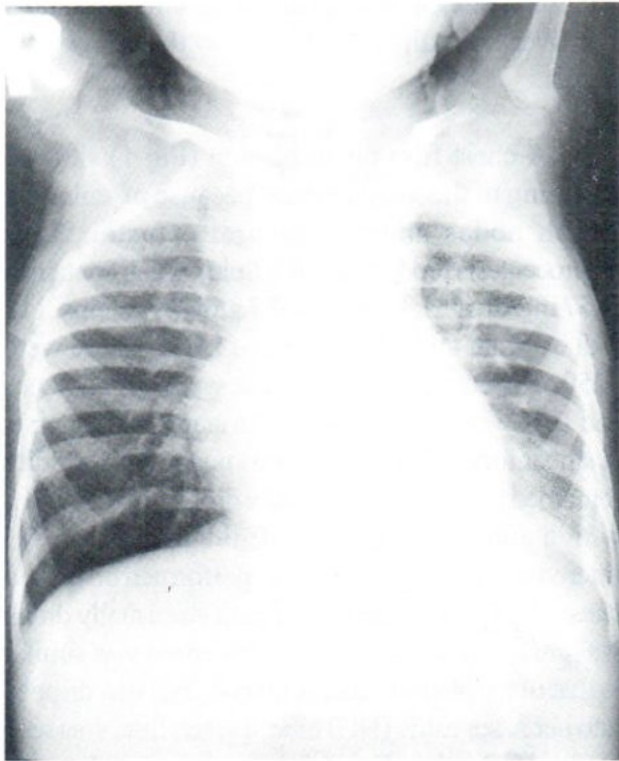


**Fig. 1** Chest film shows widening of the mediastinum from enlarged lymph nodes, left pleural effusion, and infiltration of the left lower lobe.

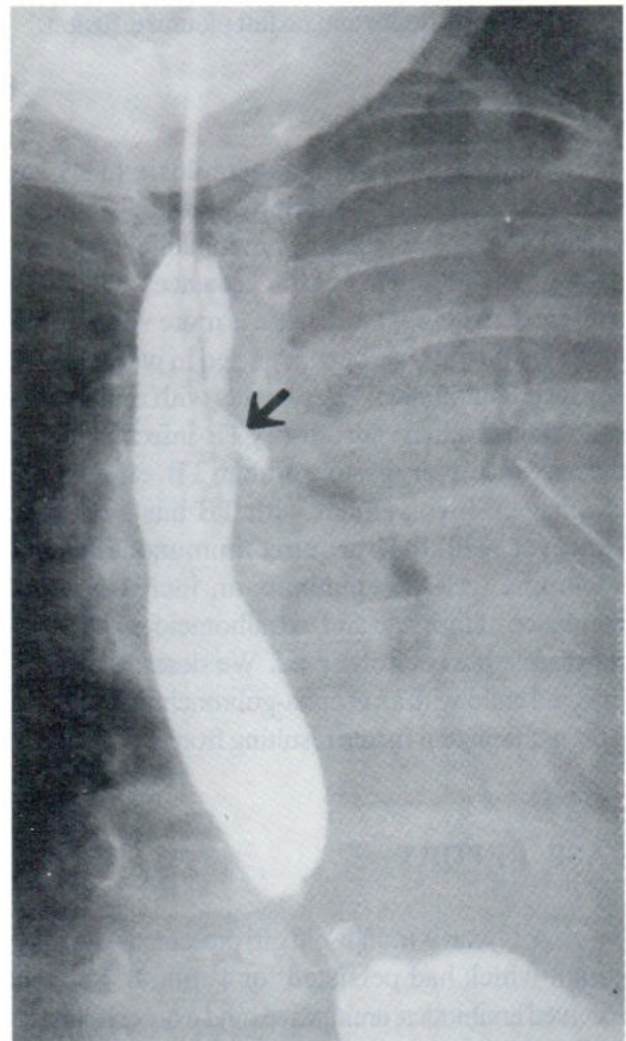


**Fig. 2** Esophagogram shows a fistula (arrow) between the esophagus and the left main bronchus, ICD tube in the left chest, and opacification of the left hemithorax.



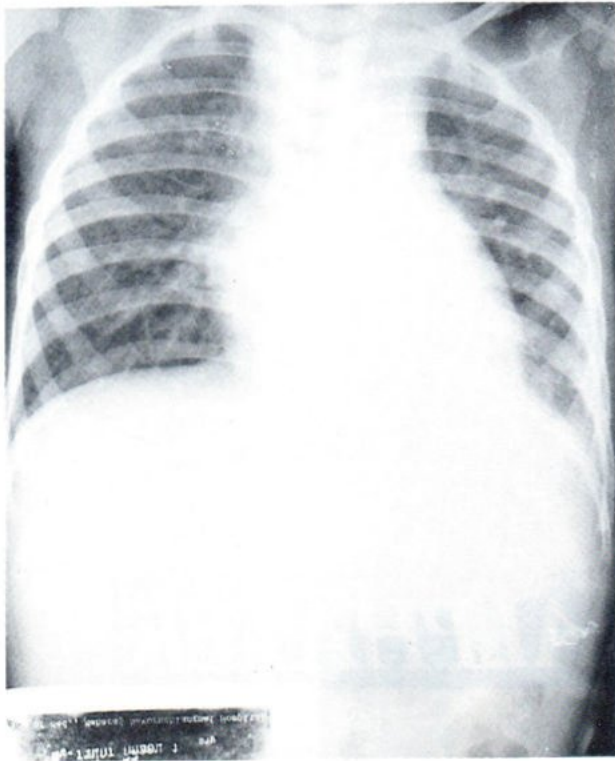


**Fig. 3** A follow-up chest film shows smaller mediastinal lymph nodes, with no left pleural effusion or infiltration of the left lower lobe.

Fistulas between the tracheobronchial tree and the esophagus caused by tuberculosis are rare; usually they are associated with extensive pulmonary and/or mediastinal infection.<sup>3</sup> They usually involve the right main bronchus.

Mycobacterial esophagitis in patients with AIDS has been reported.<sup>4,5</sup> Almost all the reported cases were infected by *M. tuberculosis*. Only one patient was infected by *M. avium* and this infection was disseminated.<sup>4</sup> An esophagogram of patients with mycobacterial esophagitis may show deviation of the esophagus by enlarged lymph nodes, narrowing of the lumen, ulceration through the esophageal wall, or a fistula into the trachea or the mediastinum.

Most cases of *M. avium-intracellulare* infection are disseminated with normal chest films.<sup>6</sup> Occasionally a case may have hilar and mediastinal lymphadenopathy, parenchymal opacities, nodules, or even diffuse fine nodular infiltrations. However, most infection is largely extrapulmonary. Although our patient's gastric washings were not cultured for TB, we believe that she was infected with *M. tuberculosis* because TB is endemic to northern Thailand and she responded to antituberculous drugs.

Although a tracheoesophageal fistula is an unusual complication of TB, if there is an HIV-infected patient with tracheoesophageal fistula and enlarged mediastinal lymph nodes, a diagnosis of esophageal TB should be considered. If diagnosed early, TB infection and the complicating fistula may be treated effectively with antituberculous drugs. Most importantly, spread of the disease to other patients and health care personnel should be prevented.

## REFERENCES

1. Dow CJ. Oesophageal tuberculosis: four cases. *Gut* 1981;22:234-236.
2. Rubinstein BM, Pastrana T, Jacobson HG. Tuberculosis of the esophagus. *Radiology* 1958; 70:401-403.
3. Wingley FM, Murray HW, Mann RB, et al. Unusual manifestation of tuberculosis: TE fistula. *Am J Med* 1976;60:310-314.
4. De Silva R, Stoopack PM, Raufman JP. Esophageal fistulas associated with mycobacterial infection in patients at risk for AIDS. *Radiology* 1990;175:449-453.
5. Goodman P, Pinero SS, Rance RM, et al. Mycobacterial esophagitis in AIDS. *Gastrointest Radiol* 1989;14:103-105.
6. Grattan-Smith D, Harrison LF, Singleton EB. Radiology of AIDS in the pediatric patient. *Curr Probl Diagn Radiol* 1992;21:79-109.



# Continental X-Ray Corporation

*Microprocessor Controlled*

*High Frequency Isowatt Output*

*Automatic Exposure Control*

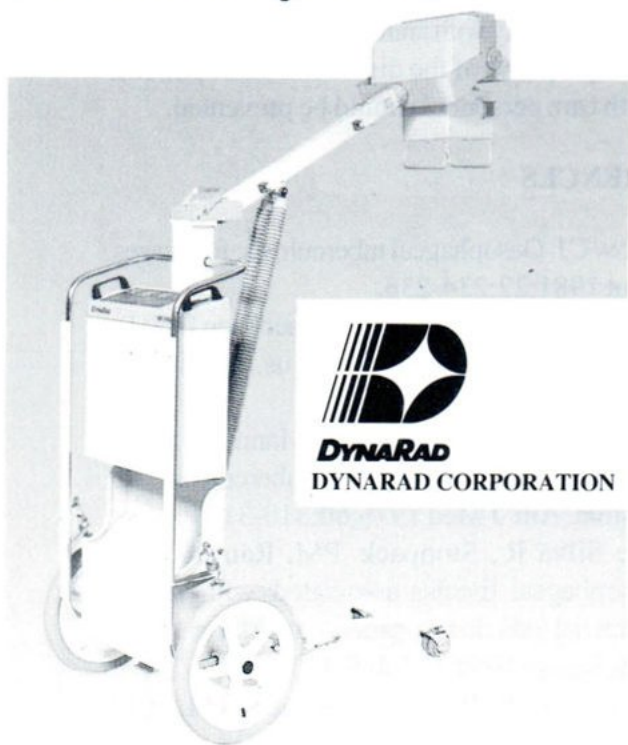


**CONTINENTAL X-RAY CORPORATION**

2000 South 25th Avenue  
Broadview, IL 60153

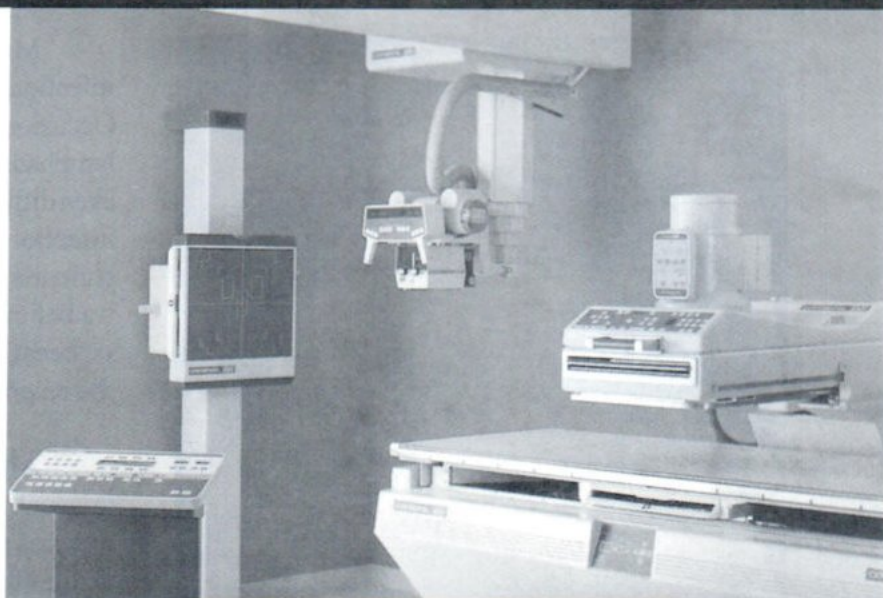
PHONE: 708/345-3050  
FAX: 708/345-1227

**DynaRad  
HF-110A System,**



**DYNARAD**  
DYNARAD CORPORATION

- ▶ SUPERIOR IMAGE QUALITY
- ▶ HIGH FREQUENCY OUTPUT
- ▶ MICROPROCESSOR CONTROL
- ▶ ELECTRONIC REGULATION OF kVp AND mAs
- ▶ CONVENIENT OPERATION



**ALPHATEK**



**ALPHATEK**  
CORPORATION

**45 Second Processing**

บริษัท อุดม เมดิคอล อีควิปเมนต์ จำกัด  
**Udom Medical Equipment Co., Ltd.**

29/26 หมู่ 1 ซอยอ่อนนุช 62 ถนนสุขุมวิท 77 แขวงสวนหลวง เขตประเวศ กรุงเทพฯ 10250  
29/26 MOO 1 SOI ONNUCH 62, SUKHUMVIT 77 ROAD, SUANGLUANG DISTRICT, PRAWET, BANGKOK 10250  
TEL. 320-1232-5 FAX: 322-7124



## TUBERCULOUS ABSCESS OF THE THIGH MUSCLE IN A PATIENT WITH SYSTEMIC LUPUS ERYTHEMATOSUS MR FEATURES IN AN UNUSUAL PRESENTATION OF TUBERCULOSIS

Dr THOO FEI Ling,<sup>1</sup> Dr Thomas CHEE,<sup>2</sup> Dr LEONG KENG Hong,<sup>3</sup>

### ABSTRACT

Infections are a major cause of morbidity and mortality in systemic lupus erythematosus patients. Although these patients are susceptible to infection, soft tissue infections are rare. We report a case of tuberculous abscess and myositis involving the left vastus lateralis muscle but with no pulmonary manifestation of tuberculosis. The rare localization of tuberculosis to skeletal muscle in this case is likely to be related to immunosuppression from chronic steroid therapy and the underlying autoimmune disease.

### CASE REPORT

A 59 year old lady with a history of systemic lupus nephritis, on long term (more than 18 years) low dose steroids, presented with left thigh swelling and pain of 1 year's duration. She was on prednisolone 7.5 mg om prior to her presentation. There was no history of fever, chills, sweats or antecedent trauma during the previous year. Clinically, the patient was afebrile. A fluctuant swelling was seen on the lateral aspect of the left thigh. No skin erythema was present. The white blood cell (WBC) count was  $4.8 \times 10^9/l$  with an essentially normal differential count. No infective change was seen on the chest radiograph. Radiograph of the left femur did not show significant abnormality.

Magnetic resonance imaging (ME 1.5 T) images showed a large cystic collection in the left vastus lateralis muscle; the lesion is hypointense on T1 weighted [Fig. 1(a) and 2(a)] and hyperintense on T2 weighted images [Fig. 1(b) and 2(b)]. T1-weighted image also shows a subtle high signal inten-

sity surrounding a large cystic hypointense collection in the left vastus lateralis muscle. The lesion measured approximately 7 cm by 5 cm by 19 cm in size. There was adjacent inflammatory change in the left vastus lateralis muscle, seen as infiltrative areas of hyperintensity seen on T2 weighted images [Fig. 1(b)]. Following intravenous Gadolinium, there was intense peripheral rim and adjacent muscle enhancement [Fig. 1(c) and 2(c)]. The adjacent muscle enhancement corresponded to the areas of hyperintensity noted on the T2 weighted images [Fig. 2(c)]. The overlying skin or subcutaneous tissue was not involved. No osteomyelitis was seen in the left femur.

During open biopsy, the left vastus lateralis muscle appeared pale and oedematous. The cyst in the left vastus lateralis muscle was thick walled. Biopsy and drainage of the cystic structure was performed. Histopathological examination of the cyst wall showed fibrous tissue with multiple epithelioid granulomas with many Langhans type multinucleate giant cells. Caseation necrosis was seen. The adja-

om = every morning

<sup>1</sup> Registrar, Dept of Diagnostic Imaging, Tan Tock Seng Hospital.

<sup>2</sup> Consultant, Dept of Diagnostic Imaging, Tan Tock Seng Hospital.

<sup>3</sup> Consultant, Dept of Rheumatology, Tan Tock Seng Hospital.

Tan Tock Seng Hospital Moulmein Road Singapore 1130 Telephone: 3595452 Facsimile: 2553618

Correspondence to : Dr F L Thoo, Department of Diagnostic Imaging, Tan Tock Seng Hospital Pte Ltd, Moulmein Road, Singapore 1130.



cent muscle was also involved. Acid fast bacilli (AFB) and fungus were not seen. The pathological diagnosis was of necrotising granulomatous inflammation suggestive of tuberculosis.

on follow-up, the patient was found to be Mantoux positive (24mm). The AFB culture from the biopsy specimen of the left vastus lateralis grew Myco Tuberculosis Complex sensitive to Streptomycin, Rifampicin, Isoniazid and Ethambutol. The findings were conclusive that this systemic lupus patient had tuberculous abscess in the left vastus lateralis muscle with adjacent myositis. She was started on anti-tuberculosis treatment post-operatively.

## DISCUSSION

The common presentation of tuberculous abscesses is with localized pain and swelling, in the involved muscle. There may be accompanying fever, malaise, leucocytosis and elevated erythrocyte sedimentation rate. Serum muscle enzymes may be raised but are frequently normal in infective myositis despite extensive myonecrosis.<sup>1</sup> A negative chest radiograph in an adult patient, like in this case, does not exclude the possibility of musculoskeletal tuberculosis.<sup>2</sup>

The differential diagnosis of the inflammatory cystic lesion in the thigh muscle include pyogenic abscess and granulomatous abscess. Staphylococcus aureus is the most common causative organism in pyogenic abscesses,<sup>1</sup> others include streptococci and gram negative organism. Granulomatous tuberculous abscess of the muscle is more often reported in psoas abscesses, seen in 5% of case of tuberculous spondylitis.<sup>2</sup> Rarely, such abscesses develop in the absence of bone abnormalities.<sup>2</sup> The isolated localization of tuberculosis in the skeletal muscle of the thigh in this patient is unusual.

The predisposing factor to tuberculous infection in this patient with underlying systemic lupus erythematosus is postulated to be chronic steroid therapy. Corticosteroid therapy is known to reactivate latent tuberculous infection. Postulated mechanisms include suppression of microbiocidal activity, macrophage and monocyte response to lymphokines and lymphopenia.<sup>3</sup> The mechanisms of musculoskeletal spread include hematogenous spread and

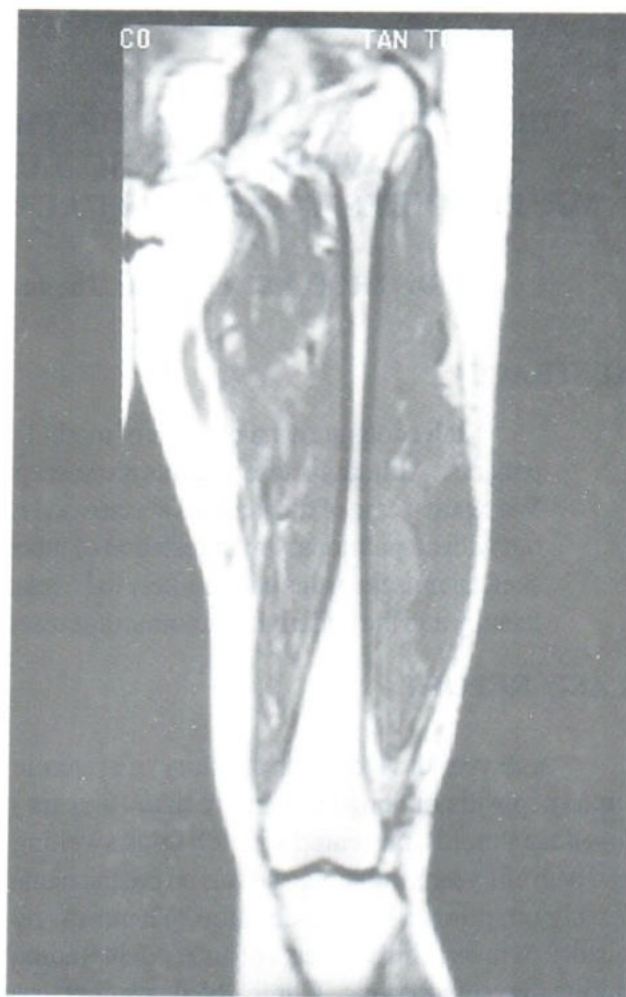


**Fig.1** Coronal MR images of the thigh of the patient. (a) T1-weighted image illustrates the subtle high signal intensity surrounding a large cystic hypointense collection in the left vastus lateralis muscle

contamination after local injury. As skeletal muscle generally is highly resistant to metastatic infections, the pathogenesis of tuberculous localization in muscle with the development of abscesses is not clear, although it is suggested that an initial muscular insult is required to allow such localization. Concurrent diseases including diabetes, HIV (human immunodeficiency virus), connective tissue disorders and varied haematologic disorders further predispose individuals to the development of a muscle infection.<sup>4</sup> It is hypothesized that these systemic processes, which result in varying degrees of immunosuppression, like local muscle trauma, make the muscle more suscep-



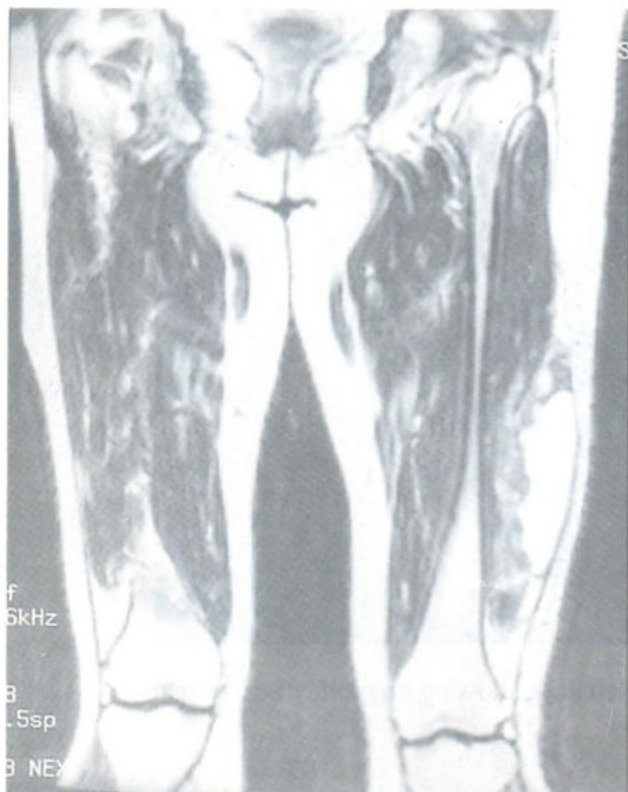


**Fig.1(b)** Coronal T2-weighted images demonstrate a high signal intensity fluid collection in the left vastus lateralis. Adjacent inflammatory change in the left vastus lateralis muscle, seen as infiltrative areas of hyperintensity.

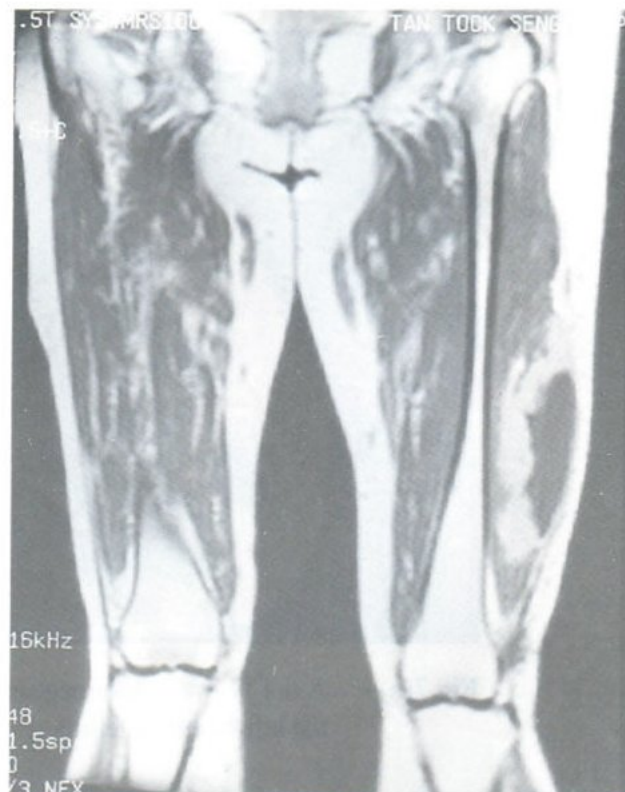


**Fig.1(c)** Gadolinium enhanced coronal T2-weighted image shows enhancement of the wall of the abscess.

tible to infection especially in the setting of transient bacteremia.

As plain radiography provides little clinical information regarding the proper diagnosis or the ideal site of tissue aspiration, attention has been directed towards other imaging techniques. ultrasound, computerized tomography (CT) and MRI have proved helpful in the diagnosis of pyomyositis. discrete abscess collection may be seen on ultrasound; their internal echoes and through transmission varying with the extent of debris.<sup>5</sup> Sonographically or CT guided percutaneous drainage may be helpful in the diagnosis and management of muscular abscesses. CT findings indicative of muscular abscess include enlargement of the muscle(s), effacement of intramuscular

and intermuscular fat planes, fluid or gas collections within the involved musculature and a 'rim' sign (consisting of a rim of increased tissue attenuation that enhances after intravenous contrast administration).<sup>6</sup> MR imaging findings include muscle enlargement. abscesses characterized by a peripheral rim of increased signal intensity on T1-weighted spin echo MR images and a central region, representing fluid, of intense signal on T2-weighted spin echo MR images and by peripheral enhancement after intravenous Gadolinium, and associated abnormalities of subcutaneous edema in some cases.<sup>7</sup> The imaging findings of pyomyositis is not specific for the causative organism and aspiration or surgical drainage is often required to diagnose the causative organism.

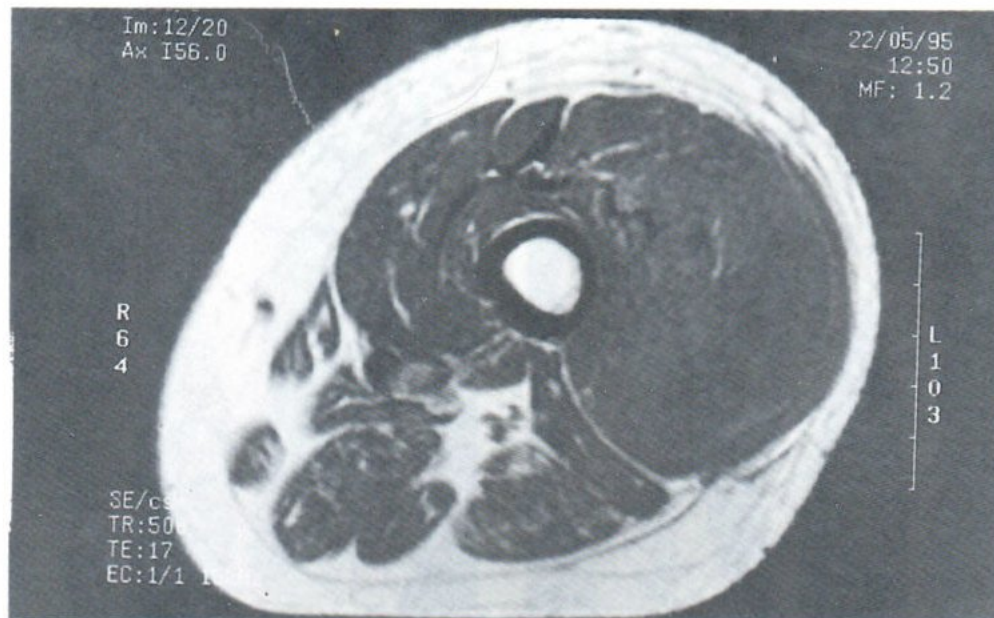


**Fig.2(a)** Axial T1-weighted image of the left thigh showing a hypointense lesion in the left vastus lateralis

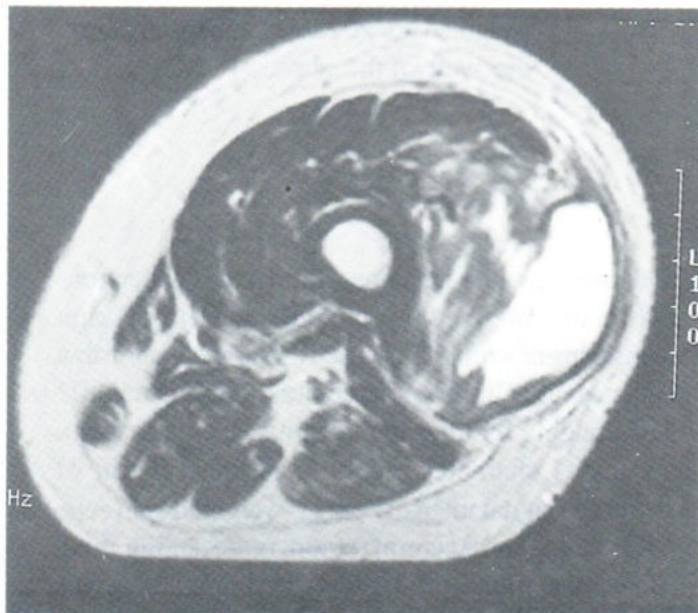


**Fig.2(b)** Axial MR image of the left thigh demonstrates a high signal intensity fluid collection in the muscle and increase signal intensity in the adjacent muscle.

Radionuclide studies with gallium<sup>8</sup> or indium<sup>9</sup> are helpful in defining additional nearby or distant abscesses.

Surgical procedures including myotomy and abscess drainage, when combined with antimicrobial therapy, usually ensure resolution.<sup>10</sup>

## CONCLUSION

This case illustrates that tuberculosis abscess and myositis, though uncommon, needs to be considered in the differential diagnosis of localised limb swelling, especially in immunocompromised patients. MRI is a sensitive diagnostic aid, enabling precise identification of the tissues affected and the extent of the involvement.



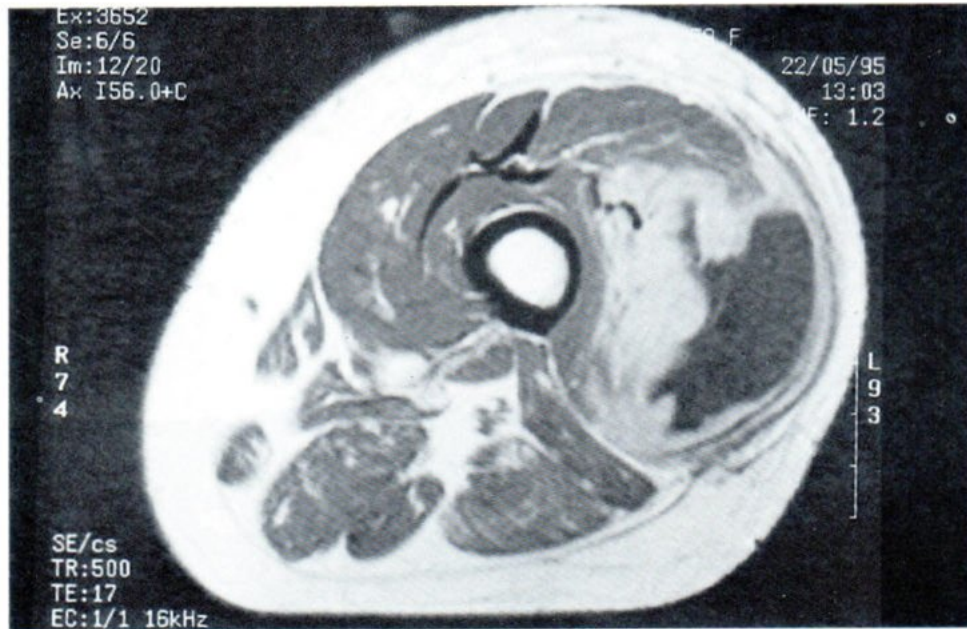


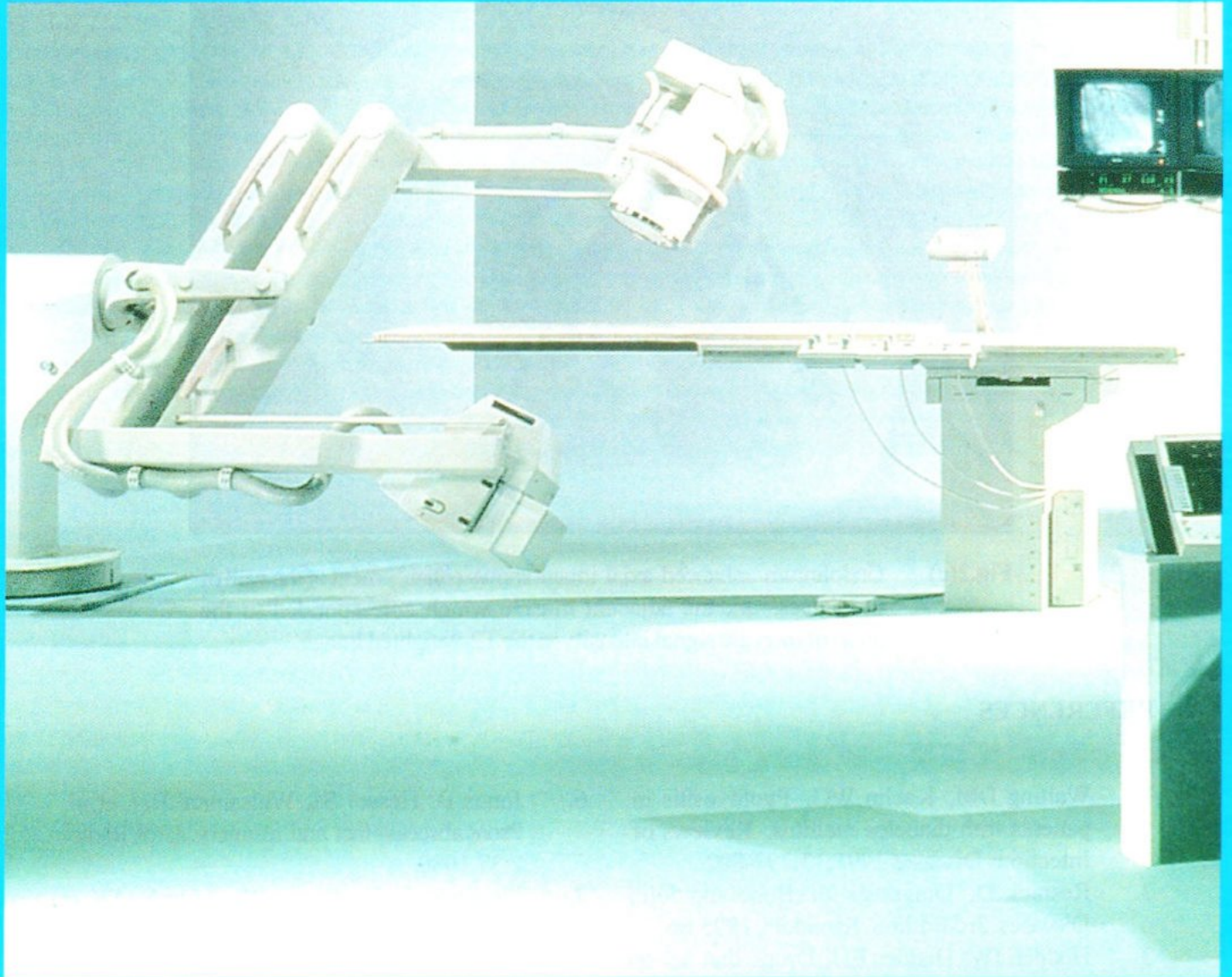
**Fig.2(c)** Gadolinium enhanced axial image shows enhancement of the wall of the abscess and the adjacent muscle which corresponded to the areas of increase signal intensity in the T2-weighted image.

## REFERENCES

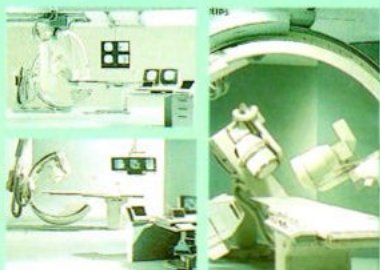
1. Walling DM, Kaelin WG. Pyomyositis in patients with diabetes mellitus. *Reviews of Infectious Diseases* 1991;13:797-802.
2. Resnick D, *Diagnosis of Bone and Joint Diseases*, 3rd Edition. Saunders, 1995:66
3. Hadden JW, Hadden EH. Drugs that act on the immune system: Immunopharmacology and immunotherapy. From: Munson PL, Mueller RA, Breese GR, eds. *Principles of Pharmacology; Basic Concepts & Clinical Applications*. Chapman and Hall, 1995:11
4. Brigid AG, Salutaris M, Andrew JC Pyomyositis: Characteristics at CT and MR Imaging. *Radiology* 1995;197:279-286
5. Holseeck MV, Introcaso JH. *Musculoskeletal Ultrasound*. Mosby Year Book, 1991:39
6. Jones B, Hessel SJ, Weissman BN et al. Psoas abscess - fact and mimicry. *Urol Radiol* 2:37,1980
7. Fleckenstein JL, Burns DK, Murphy FK et al: Differential diagnosis of bacterial myositis in AIDS: Evaluation with MR imaging. *Radiology* 179:653, 1991.
8. Yousefzadeh DK, Schumann EM, Mulligan GM et al: The role of imaging modalities in diagnosis and management of pyomyositis, *Skeletal Radiology* 8:285, 1992.
9. Applegate GR, Cohen AJ: Pyomyositis: Early detection utilizing multiple imaging modalities. *Magnetic Resonance Imaging* 9:187, 1991.
10. Clementsen P, Hansen M, Conrad C et al: Percutaneous drainage of tuberculous abscess of the psoas muscle. *Tubercle*, 69:1, 1988 Mar, 63-5



# INTEGRIS H SERIES



*Let's make things better.*  
สร้างนวัตกรรม สู่อนาคต



FOR MORE INFORMATION  
PLEASE CONTACT

**PHILIPS MEDICAL SYSTEMS**

- TEL. 745-4090 Ext. 3332
- FAX. 398-0792

Imported by  
**Philips Electronics (Thailand) Ltd.**  
209/2 Sanpavuth Road, Prakanong,  
Bangkok 10260



# PHILIPS



## CONGENITAL CUTIS LAXA: A CASE REPORT

Pannee VISRUTARATNA,<sup>1</sup> MD, Kanokporn ORANRATANACHAI,<sup>1</sup> MD,  
Aurmporn SRESHTHAPUTRA,<sup>2</sup> MD.

### ABSTRACT

An infant with congenital cutis laxa, a rare generalized disorder of connective tissue, is described. Radiographic manifestations were multiple diverticula of the urinary bladder, and a hiatal hernia involving the entire stomach, the right side of the colon and a distal portion of the small bowel.

### INTRODUCTION

Congenital cutis laxa is an inherited disorder of connective tissue. At birth, there is a striking laxity of the skin, which hangs in pendulous folds all over the entire body. This may be especially pronounced on the face, giving an appearance of premature aging. While it is the changes in the skin which give cutis laxa its name, other manifestations of the disorder involve the pulmonary, cardiovascular, gastrointestinal, and genitourinary systems. This report describes an infant with cutis laxa, hiatal hernia and bladder diverticula.

### CASE REPORT

A 6-month old boy appeared with congenitally lax skin. He was the second child, born by cesarean section at another hospital. His birth weight was 4100 grams. After birth, he had neonatal jaundice, which disappeared after 2 days of phototherapy. When he was 3 months old, he went to a private clinic because of abdominal pain, where he was advised to have a chromosome study because of his bizarre face. His older sibling looked normal. His growth and development were normal. On physical examination, the patient had generalized lax skin (Figs. 1 and 2). He also had a fever; his body temperature was 40.2 degrees Celsius. Everything else was normal. His chest film (Fig. 3) showed an air-fluid level in the right

lower hemithorax and abnormal air density superimposed on the mediastinum, causing deviation of the mediastinum to the left. A barium study was done because diaphragmatic hernia was suspected. It showed herniation of the stomach into the right lower hemithorax and herniation of a loop of the large bowel into the thoracic cavity (Figs. 4 and 5). His urine had 7-8 white blood cells per high power field. *Klebsiella Pneumoniae* grew in a urine culture. After this he was given Bactrim for urinary tract infection. Then a voiding cystourethrography was done which showed multiple bladder diverticula (Fig. 6). Next the patient underwent an explore laparotomy, which showed a hiatal defect about 3 cm in diameter with paraesophageal hernia. The whole stomach, the right side of the colon, and a distal portion of the small bowel had herniated into the thorax. The surgeon reduced the visceral organs back into the abdominal cavity and closed the hiatal defect. Five days after surgery, the patient underwent an explore laparotomy again because of a recurrent hernia. At this time, the surgeon reduced the stomach back into the abdominal cavity and performed an anterior gastropexy, suturing the stomach to the diaphragm and abdominal wall. The patient has been well since.

### DISCUSSION

Cutis laxa is a rare disorder of connective tissue in which there is reduction in the amount and size

<sup>1</sup> Department of Radiology, Faculty of Medicine, Chiang Mai University, Chiang Mai 50200, THAILAND.

<sup>2</sup> Department of Pediatrics, Faculty of Medicine, Chiang Mai University, Chiang Mai 50200, THAILAND.



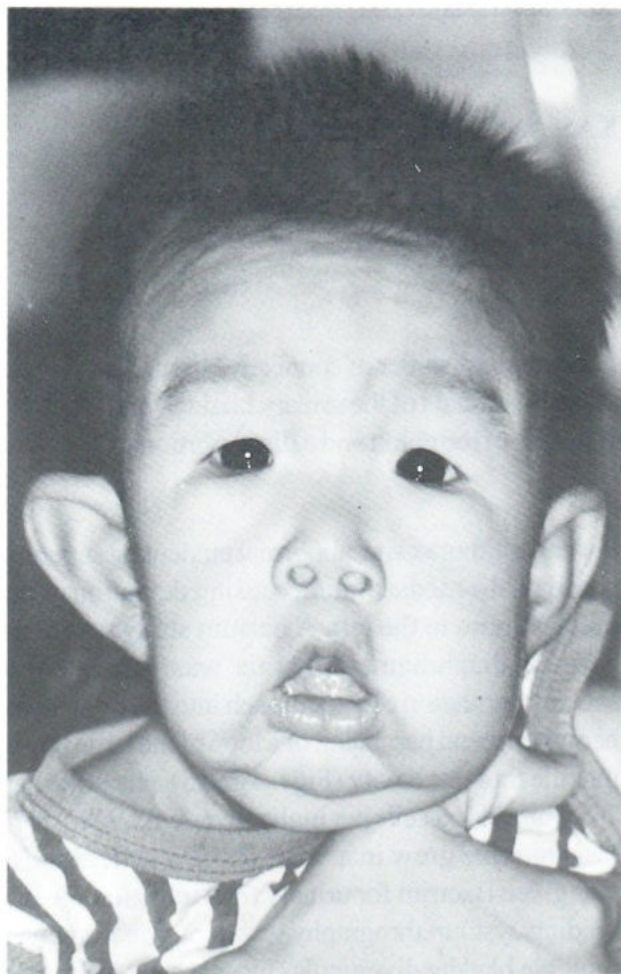


**Fig.1** Strikingly elderly looking face and huge ears.

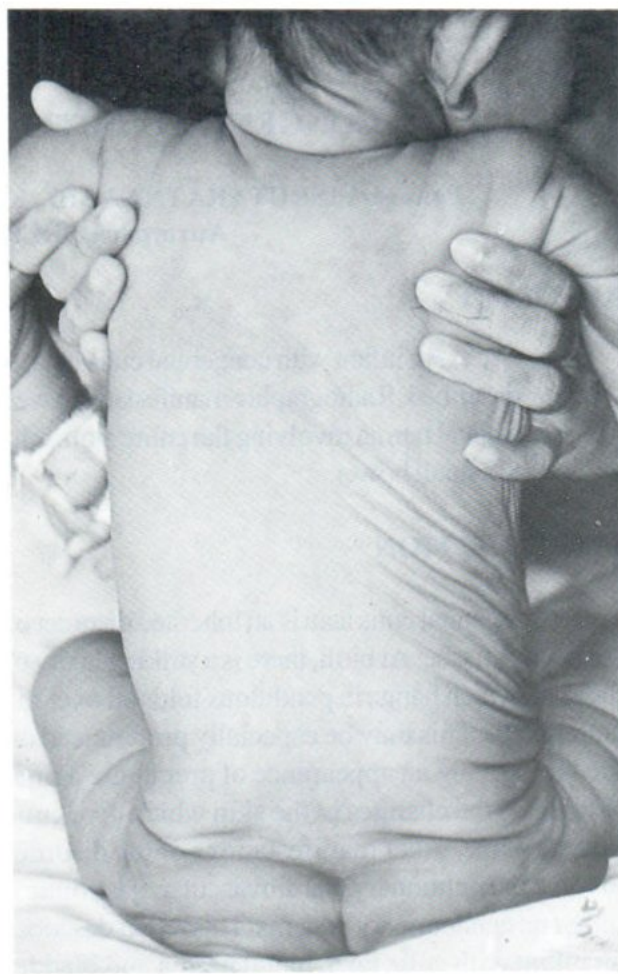


**Fig.2** Generalized lax skin is evident in many loose folds over back, buttocks, and thighs.

of the elastic fibers.<sup>1</sup> The etiology is unknown. Both congenital and acquired forms have been described.<sup>2,3,4</sup> Modes of inheritance include autosomal dominance with variable penetrance, autosomal recessiveness present at birth or shortly after birth and X-linked recessiveness.<sup>1</sup> Though time of onset of symptoms and clinical presentation may vary in these patients, this syndrome is always characterized by loose, pendulous, inelastic folds of skin.

The reported radiologic manifestations include pulmonary emphysema,<sup>2</sup> hernia,<sup>3,5</sup> dilatation and tortuosity of blood vessels,<sup>5</sup> and diverticula of the gastrointestinal and urogenital tracts.<sup>4,5</sup>

In this case, the hiatal hernia which recurred after the first surgery, the multiple bladder diverticula;

and the generalized lax skin were the results of abnormality of elastic fibers. The roentgenographic findings of hiatal hernia and multiple bladder diverticula described in this patient can also be seen in patients with Ehlers-Danlos syndrome; however, hyperelasticity of the skin, hyperextensible joints, bleeding diathesis and soft-tissue calcifications characteristic of Ehlers-Danlos syndrome<sup>6</sup> were lacking in this patient.

## REFERENCES

1. Taybi H. Syndromes. In: Taybi H, Lachman RS (eds.): *Radiology of Syndromes, metabolic disorders and skeletal dysplasias*. 4th ed. St. Louis: Mosby; 1996. p 115-117.



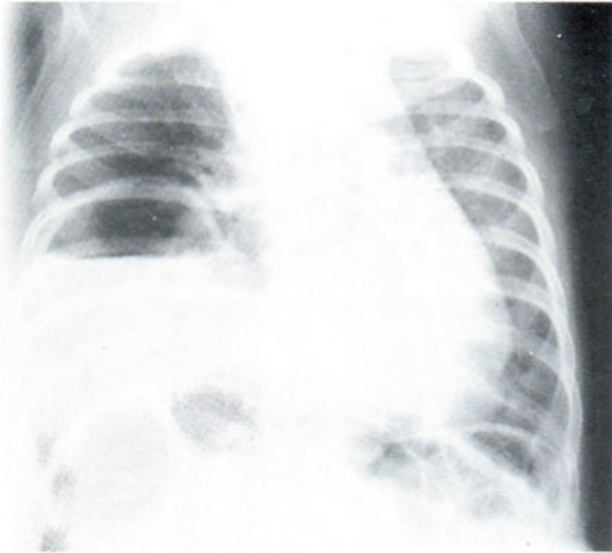


**Fig.3** Chest film shows an air-fluid level in the right lower hemithorax. Abnormal air density is also seen superimposed on the mediastinum, and causing it to deviate to the left.

2. Merten DF, Rooney R. Progressive pulmonary emphysema associated with congenital generalized elastolysis (cutis laxa). *Radiology* 1974;-113:691-692.
3. Agha A, Sakati NO, Higginbottom MC, et al. Two forms of cutis laxa presenting in the newborn period. *Acta Paediatr Scand* 1978;-67:775-780.
4. Lally JF, Gohel VK, Dalinka MK, Coren GS. The roentgenographic manifestations of cutis laxa (gen-eralized elastolysis). *Radiology* 1974;113:605-606.
5. Meine F, Grossman H, Forman W, Jackson D. The radiographic findings in congenital cutis laxa. *Radiology* 1974;113:687-690.
6. Beighton P, Thomas ML. The radiology of the Ehlers-Danlos syndrome. *Clin Radiol* 1969;20:354-361.

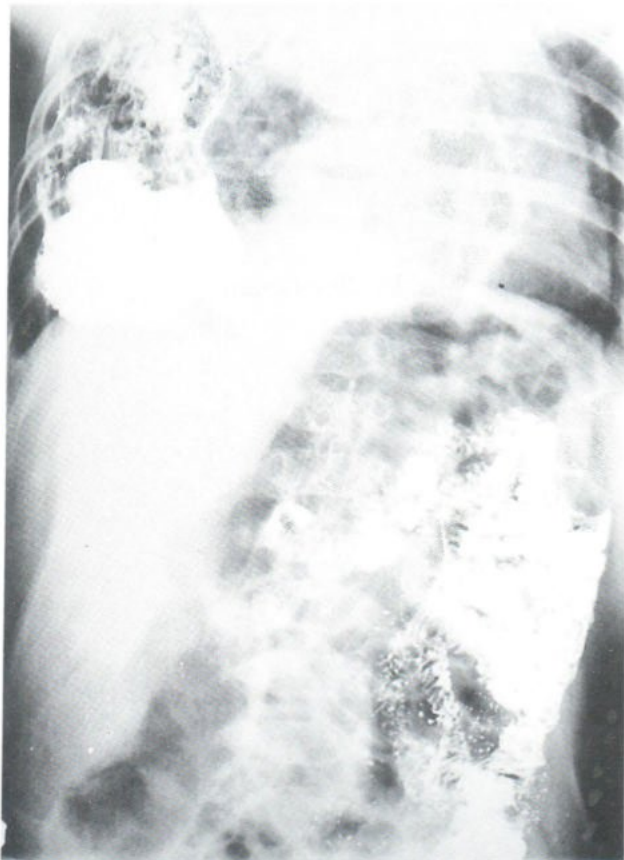


**Fig.4** Barium study shows herniation of the stomach into the right lower hemithorax.

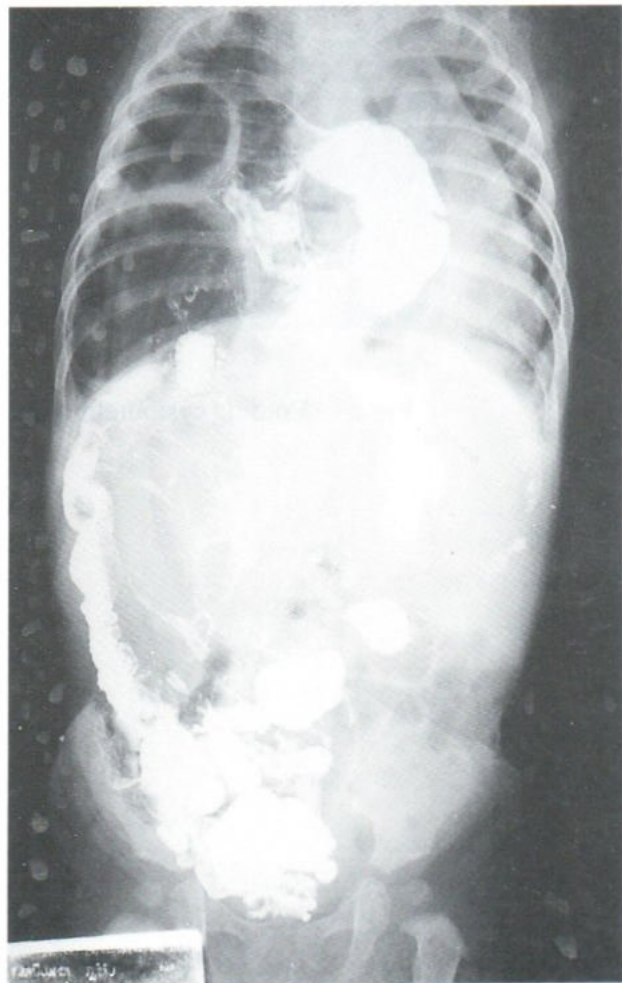


**Fig.5** Barium study at 10 hours shows herniation of a portion of large bowel into the thorax.

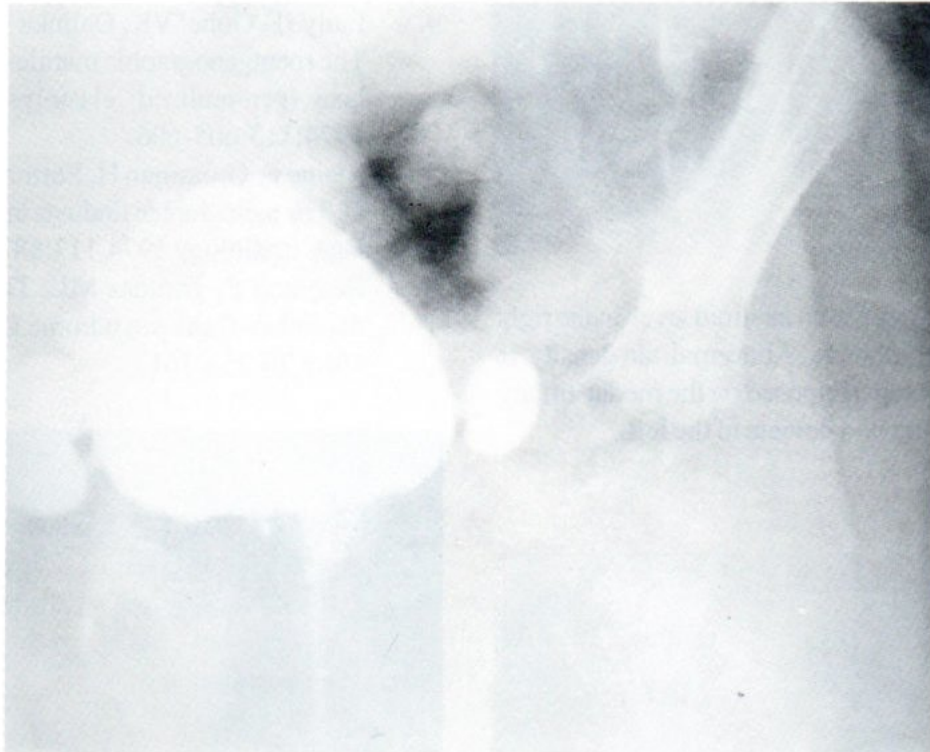


**Fig.6** Voiding cystourethrogram shows multiple bladder diverticula.



## SMOOTH-MUSCLE TUMORS IN CHILDREN WITH AIDS

Panee VISRUTARATNA<sup>1</sup>, MD., Chusak SIRIVANICHAI<sup>1</sup>, MD.,  
Lumdaun WONGSAWASDI<sup>2</sup>, MD., and Samreung RANGDAENG<sup>3</sup>, MD.

### ABSTRACT

Images of multiple hepatic smooth-muscle tumors in a 42-month-old girl and of multiple smooth-muscle tumors of the gastrointestinal tract in a 34-month-old boy are described. Both children were perinatally human immunodeficiency virus (HIV) positive.

### INTRODUCTION

Gastrointestinal manifestations of the acquired immunodeficiency syndrome (AIDS) in children are seen when they have opportunistic infections, lymphoproliferative disease, or cancer.<sup>1</sup> In children with AIDS and cancer, cases of lymphoma outnumber cases of Kaposi's sarcoma. Since 1990 smooth-muscle tumors (leiomyomas and leiomyosarcomas) have been reported in children with AIDS.<sup>2-4</sup> We describe images of two children with smooth-muscle tumors and HIV infection.

### CASE REPORT

**CASE 1.** - A 42-month-old girl perinatally HIV positive was referred for a CT examination of the chest because of persistent infiltrates in her right lung. She had had frequent episodes of otitis media, diarrhea, oral candidiasis, herpetic stomatitis, *Salmonella* bacteremia, and pneumonia. Physical examination revealed generalized lymphadenopathy and hepatosplenomegaly. The CT scan showed patchy infiltration in both lungs. A hypodense mass about 3 cm in diameter was noted in her left liver lobe (Fig. 1). Abdominal ultrasonography showed two hypoechoic masses with hyperechoic centers ("target" lesions) in the liver (Figs. 2 and 3). Enlarged periportal lymph

nodes and peripancreatic lymph nodes were also seen. A fine needle aspiration biopsy was performed to check for liver abscesses. The specimen had spindle cells.

Follow-up CT examination at 5 months showed that the two hepatic masses had increased and had hypodense centers, which might have been necrotic tissue (Figs. 4 and 5). Two additional masses were also seen in the left liver lobe (Fig. 6). At this time, a fine needle aspiration biopsy of the right chest revealed acute suppurative inflammation. No organisms were found.

One month later, she developed scalp infection from *Staphylococcal aureus*, which subsided after an antibiotic. She has not returned to the hospital since then.

**CASE 2.** - A 34-month-old boy was admitted because of intermittent abdominal pain and hematochezia. His father had died from AIDS. He had been tested to have HIV-positive at another hospital one year before. Physical examination revealed multiple cervical lymphadenopathy. On palpation, there was no tenderness of the abdomen. He had mild hepatosplenomegaly. A barium enema showed multiple polypoid filling defects mostly about 5 mm in diameter in the rectum, sigmoid and colon (Fig. 7). There was a lesion about 3 cm in diameter in the ascending colon.

<sup>1</sup> Department of Radiology,

<sup>2</sup> Department of Pediatrics, and

<sup>3</sup> Department of Pathology, Faculty of Medicine, Chiang Mai University, Chiang Mai 50200, THAILAND.



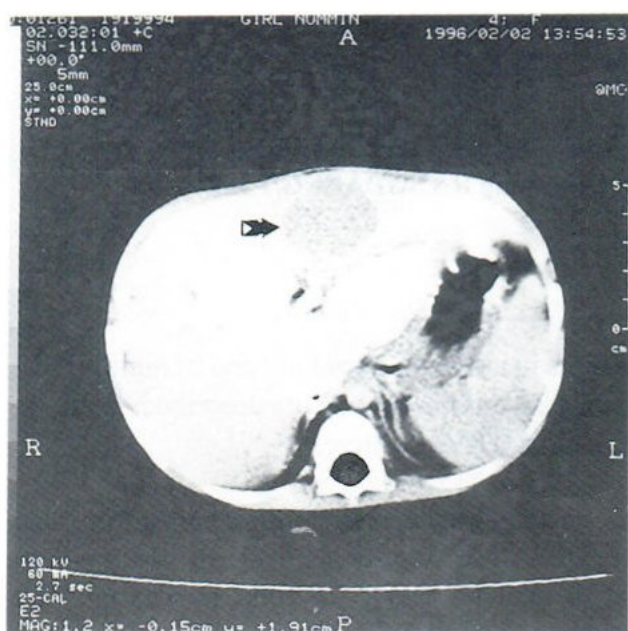


**Fig 1.** Contrast-enhanced CT scan shows a hypodense mass (arrow) in left liver lobe.

Malignant change of this one was suspected. Colonoscopy was done and showed to have multiple polypoid lesions, about 3-5 mm in diameter, scattered throughout the colon. The largest was in the ascending colon. A colonoscopic biopsy of this lesion showed to be a leiomyosarcoma. An upper GI study showed a few polypoid filling defects in the stomach and multiple lesions in the duodenum. The patient did not undergo surgery because the lesions were scattered throughout his gastrointestinal tract. He has not returned to the hospital since then.

## DISCUSSION

Smooth-muscle tumors can arise in any tissue that contains smooth muscle. They are rare in pediatric patients.<sup>5</sup> In the gastrointestinal tract frequent symptoms are abdominal pain, gastrointestinal bleeding, and intestinal obstruction.<sup>6</sup> All the reported cases in

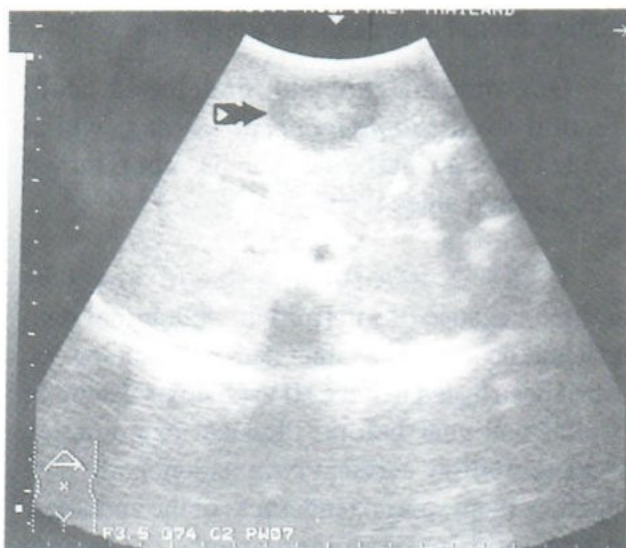


**Fig 2.** Transverse sonogram shows a "target" lesion (arrow) in left liver lobe.



**Fig 3.** Transverse sonogram shows a "target" lesion (arrow) in caudate lobe of liver. Note enlarged lymph node (N) adjacent to the head of pancreas.



immunocompetent patients have had only one lesion.<sup>7</sup>

In children with AIDS smooth-muscle tumors have been reported in the gastrointestinal tract,<sup>2-4</sup> tracheobronchial tree,<sup>2</sup> lungs,<sup>2</sup> and liver.<sup>4,8</sup> Most patients, particularly those with tumors in the gastrointestinal tract, have had multiple lesions.

Smooth-muscle tumors in adults with AIDS have also been reported. One patient had multiple smooth-muscle tumors of the colon and a smooth-muscle tumor of the right adrenal gland.<sup>9</sup> Another patient had two leiomyomas of the liver.<sup>10</sup>

Multiple factors are likely to predispose patients with AIDS to develop cancer, such as defective immunosurveillance, the presence of multiple coinfecting organisms, chronic antigenic stimulation with unregulated polyclonal B-cell expansion, abnormal regulation of various growth

factors and cytokines, and oncogenesis by the HIV itself.<sup>2</sup> Recently it has been reported that Epstein-Barr virus may contribute to the development of leiomyomas and leiomyosarcomas in patients with AIDS.<sup>11</sup>

The ultrasonography of hepatic smooth-muscle tumors has been well-circumscribed hypoechoic masses in patients with AIDS.<sup>8,10</sup> Some of these masses have had circumferential halos.<sup>10</sup> CT scans of hepatic smooth-muscle tumors in patients with AIDS have shown a hypodensity mass,<sup>8</sup> a homogeneously enhanced mass surrounded by an enhancing halo on a delayed scan,<sup>10</sup> and for a large tumor inhomogeneous enhancement with a hypodense center.<sup>8</sup> The ultrasonograms of our first case were different; the tumors had "target" lesions. The differential diagnosis of "target" lesions in the liver includes lymphoma, metastatic tumor, and abscess. The CT scans of our case were similar to

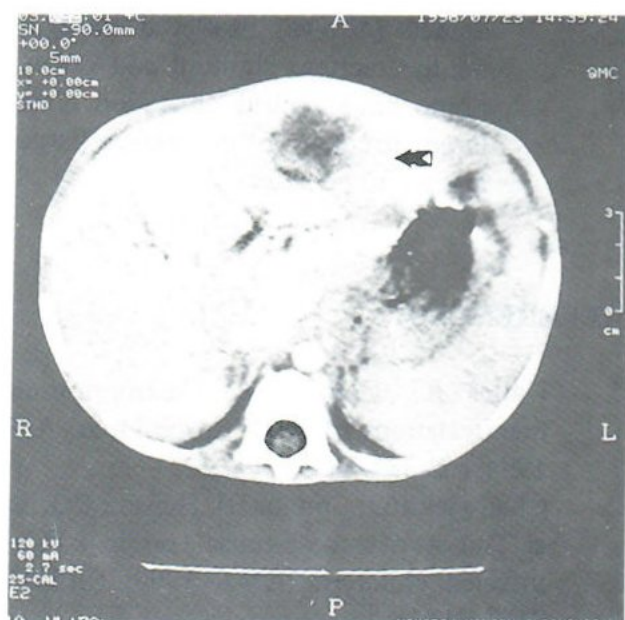


**Fig 4.** Follow-up CT scan with larger mass in left liver lobe (arrow). Note hypodense center.

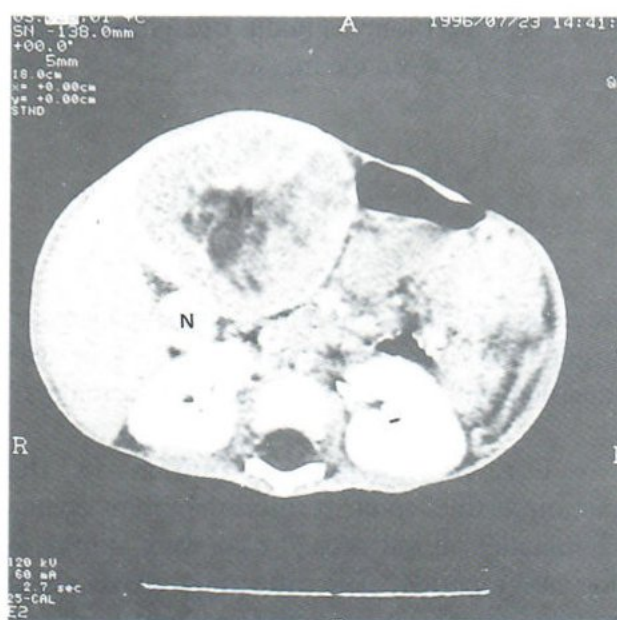


**Fig 5.** Follow-up CT scan shows a 6-cm mass (M) in caudate lobe. Note rim enhancement, hypodense center, and enlarged lymph node (N).



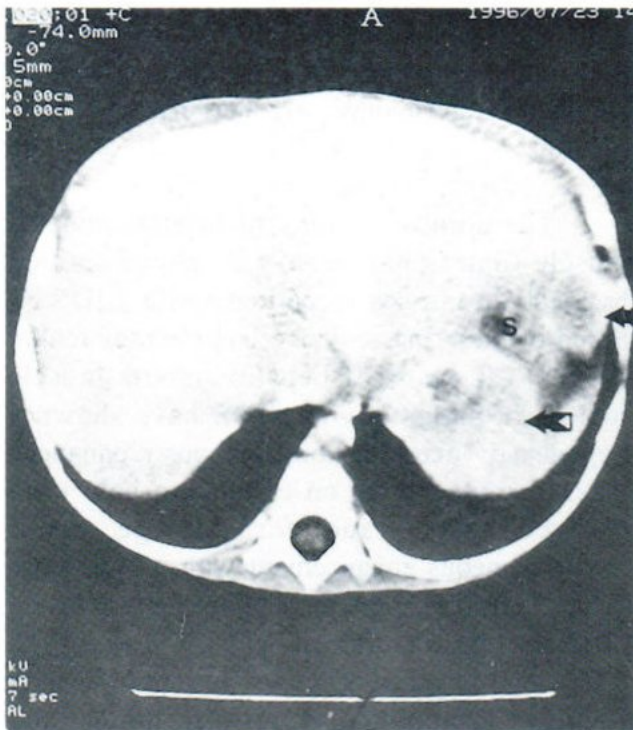


**Fig 6.** Contrast-enhanced CT scan shows two additional masses (arrows) in left liver lobe. Fundus of stomach (s) is between the masses.

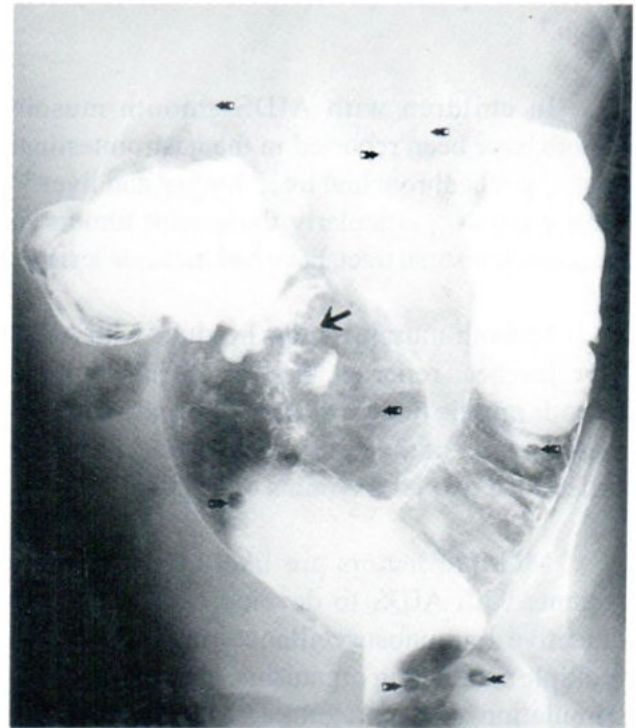


**Fig 7.** Barium enema (RPO projection) shows multiple polypoid filling defects (arrows). Scattered throughout the rectum, sigmoid and colon. Some have central ulceration. Note large irregular filling defect (large arrow) in ascending colon.

previous reports. Small tumors had hypodensity; larger tumors had central necrosis. This was consistent with the gross pathology of the tumors.<sup>5</sup>

For smooth-muscle tumors in the gastrointestinal tract, results of barium enema examination in our second case were similar to one case reported.<sup>9</sup> The differential diagnosis of multiple colonic polyps with or without ulceration in a patient with HIV infection includes Kaposi's sarcoma and lymphoma.

Smooth-muscle tumors have been seen with increasing frequency in HIV positive children. They should be suspected when a mass or, especially, multiple masses are seen.

## REFERENCES

1. Haller JO, Cohen HL. Gastrointestinal manifestations of AIDS in children. *AJR* 1994;162:387-393.
2. Chadwick EG, Connor EJ, Hanson CG, et al. Tumors of smooth-muscle origin in HIV-infected children. *JAMA* 1990;263(23):3182-3184.
3. McLoughlin LC, Nord KS, Joshi VV, DiCarlo FJ, Kane MJ. Disseminated leiomyosarcoma in a child with acquired immune deficiency syndrome. *Cancer* 1991;67:2618-2621.

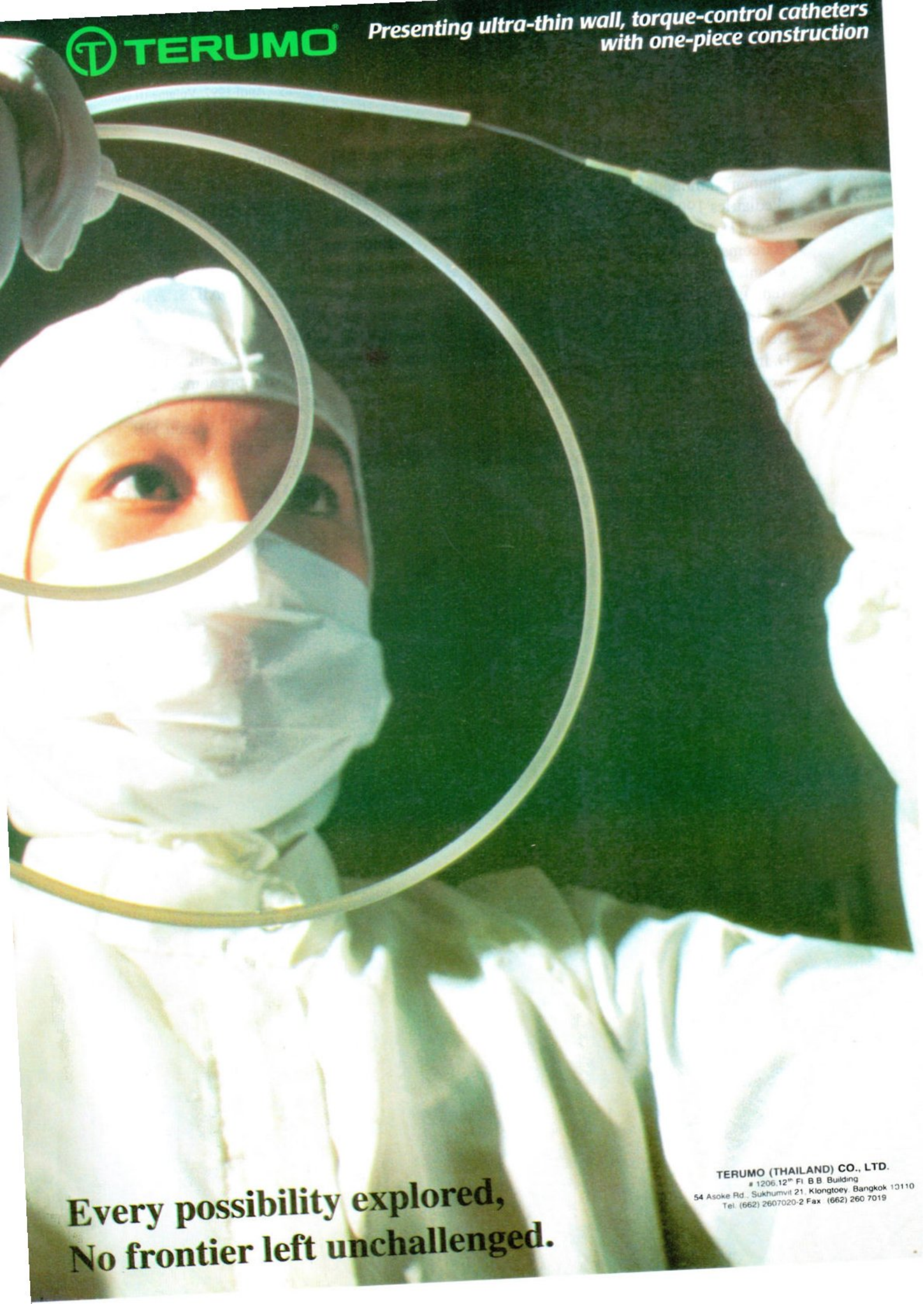


4. Mueller BU, Butler KM, Higham MC, et al. Smooth muscle tumors in children with human immunodeficiency virus infection. *Pediatrics* 1992;90:460-462.
5. Kim TH, Bell BA, Maurer HM, Ragab AH. Sarcomas of the soft tissues and their benign counterparts. In: Fernbach DJ, Vietti TJ (eds.): *Clinical Pediatric Oncology*, 4th ed. St. Louis: Mosby. 1991. p 530-533.
6. Delucchi MA, Latorre JJ, Guiraldes E, Oddo D. Intestinal leiomyosarcoma in childhood: report of two cases. *J Pediatr Surg* 1988;-23(4):377-379.
7. Angerpointer ThA, Weitz H, Haas RJ, Hecker WCh. Intestinal leiomyosarcoma in childhood-case report and review of the literature. *J Pediatr Surg* 1981;16(4):491-495.
8. Levin TL, Adam HM, van Hoeven KH, Goldman HS. Hepatic spindle cell tumors in HIV positive children. *Pediatr Radiol* 1994;24:78-79.
9. Radin DR, Kiyabu M. Multiple smooth-muscle tumors of the colon and adrenal gland in an adult with AIDS. *AJR* 1992;-159:545-546.
10. Wachsberg RH, Cho KC, Adekoso A. Two leiomyomas of the liver in an adult with AIDS: CT and MR appearance. *J Comput Assist Tomogr* 1994;18(1):156-157.
11. McClain KL, Leach CT, Jenson HB, et al. Association of Epstein-Barr virus with leiomyosarcomas in young people with AIDS. *N Engl J Med* 1995;332:12-18.





*Presenting ultra-thin wall, torque-control catheters  
with one-piece construction*



**Every possibility explored,  
No frontier left unchallenged.**

TERUMO (THAILAND) CO., LTD.  
# 1206, 12<sup>th</sup> Fl. B.B. Building  
54 Asoke Rd., Sukhumvit 21, Klongtoey, Bangkok 10110  
Tel. (662) 2607020-2 Fax (662) 260 7019



## DIAGNOSIS OF HEPATIC CAVERNOUS HEMANGIOMA USING TECHNETIUM-99M RED BLOOD CELL IMAGING

Molrudee EKMAHACHAI, M.D., Wannee OJARUSPORN, M.D.  
Chusak SIRIVANICHAI, M.D., Sakonchai JITRAPITAKKUL, Cert.in Rad.Tech.  
Sombut BOONYAPRAPA, M.D.

### ABSTRACT

Thirty-one patients with various focal hepatic lesions suspected of hepatic cavernous hemangiomas (HCHs) on liver ultrasonography (US) and/or computed tomography (CT) were evaluated by Technetium-99m red blood cell imaging. All patients were studied with blood-flow and sequential planar blood-pool images. Additional single-photon emission CT (SPECT) images were also performed in 19 patients. Twenty-five patients with scintigraphic characteristic of HCH were diagnosed as HCH, 5 proven by angiography and 20 proven by maintaining a stable clinical course ranging from 6 to 24 months with the absence of any signs and symptoms of a liver malignancy, either primary or metastatic disease. All except 3 patients with a history of hepatitis B or C virus carrier had completely normal liver function tests. Six of 25 hemangioma patients had multiple lesions. Twenty-two cases of HCHs were clearly diagnosed by planar imaging and the other 3 patients needed SPECT imaging for diagnosis of HCHs. The remaining 6 patients, 4 had a final diagnosis as hepatoma proven by angiography and liver biopsy, and the other 2 patients were diagnosed as liver metastases proven by follow-up clinical course and liver US study.

### INTRODUCTION

Hepatic cavernous hemangioma (HCH) is the most common benign tumor of the liver. It is the second most common hepatic tumor following hepatic metastases. It is usually an incidental finding during examination of the liver.<sup>1</sup> When they are found, they may make troublesome in the differential diagnosis, especially in patients with known primary malignancy outside the liver or high risk for developing hepatic malignancy.

HCH is more common in females and can be occurred in any age group, but it is most frequently found in older patients. Most of these tumors are small, discrete and usually solitary, but multiple le-

sions are also found in about 10% of cases.<sup>1</sup> Most HCHs are typically less than 3 cm in diameter, however they may grow slowly to large size with increasing age, which are classified as giant hemangiomas when they are larger than 4 cm.<sup>2</sup> The lesions are frequently found in a subcapsular location and more commonly in the right hepatic lobe, especially the posterior segment.<sup>1,3</sup> HCHs are usually asymptomatic, but larger tumors may result in liver enlargement and abdominal discomfort secondary to pressure effect on adjacent organs.<sup>1</sup>

Although HCHs are usually asymptomatic and require no treatment, the differentiation from other hepatic lesions is still important. Several noninvasive imaging techniques such as ultrasono-



graphy (US),<sup>4-10</sup> computed tomography (CT),<sup>4,8-11</sup> magnetic resonance imaging (MRI)<sup>8-10,12-14</sup> and liver scintigraphy with Technetium-99m labeled red blood cells (Tc-99m RBC)<sup>3,6,7,13-22</sup> have been used for differential diagnosis of HCH from other focal hepatic lesions. Among these modalities, blood-flow and sequential planar blood-pool (BP) imaging with/without single-photon emission CT (SPECT) images of the liver with Tc-99m RBC are well recognized as a sensitive and specific procedure for the diagnosis of HCH. Definitive diagnosis of a HCH will eliminate the need for further workup, because most of them require no treatment.<sup>23</sup>

The purpose of this article is to reiterate the usefulness and effectiveness of noninvasive Tc-99m RBC liver imaging for the differential diagnosis of HCH from other focal hepatic lesions.

## MATERIALS AND METHODS

Thirty-one patients with various focal hepatic lesions suspected of HCHs on liver US and/or CT images, were referred for further evaluation with Tc-99m RBC imaging. There were 20 women and 11 men, ranging in age from 36 to 68 years (mean, 50.3). Of the 31 patients, 6 had a known primary malignancy in another site and the focal hepatic lesions were found during metastatic workup. The remaining patients had no prior evidence of malignancy, 18 of these presented with right upper abdominal discomfort, 2 were known cases of hepatitis B virus carrier, one was carrier of hepatitis C virus, and the last 4 patients, focal hepatic lesions were found as an incidental finding during examination of the liver.

All patients had Tc-99m RBC imaging performed with 20 mCi (740 MBq) of Tc-99m labeled red blood cells using a modified *in vivo* technique as described by Callahan et al.<sup>24</sup> The patients were positioned under a large-field-of-view gamma camera, equipped with a low-energy all-purpose parallel hole collimator in the projection that best demonstrated the lesion as seen on the US and/or CT imaging. Blood-flow images of the liver were obtained at 2 sec per frame for 1 min after a bolus injection. Then, sequential planar BP imaging was acquired for 1000 Kcounts for each image in the same position at 1, 5,

15, 30 min, 1 hr and 2 hr after injection. Additional projections such as right lateral or oblique views were also obtained in some cases. Additional SPECT imaging was also performed in 19 patients at 30 min after injection, by a rotating single-headed gamma camera (Apex-SP4 Elscint) equipped with a low-energy, all-purpose collimator. SPECT imaging was acquired in 128 x 128 matrix, using a 360 degree rotation with 60 angular projectional images for 25 seconds per frame (continuous-shoot technique). The total time for SPECT imaging was approximately 25 minutes. Computerized reconstructions were processed at 1-2 pixel width per slice in the transaxial, sagittal and coronal planes. Three dimensional imaging was also performed in all patients.

## RESULTS

Of the 31 patients with various focal hepatic lesions evaluated with Tc-99m RBC imaging, 25 patients had the scintigraphic characteristic of hemangiomas and were diagnosed as HCH, 4 had a final diagnosis as hepatoma and the last 2 patients were diagnosed as liver metastases. Of the 25 hemangioma patients, 5 proven by angiography and 20 proven by maintaining a stable clinical course ranging from 6 to 24 months with no definite signs and symptoms of a liver malignancy, either primary or secondary disease. All except 3 patients with a history of hepatitis B or C virus carrier also had completely normal liver function tests, and had no change in size and appearance of the lesions on follow-up US and/or CT images. Twenty-two hemangioma patients were diagnosed by planar Tc-99m RBC imaging and they all demonstrated definite focal increased BP activity on serial BP imaging, with persistent uptake up to 2 hr after injection. The remaining 3 patients had negative planar BP images and needed SPECT imaging for the diagnosis of HCHs.

The 4 patients with a final diagnosis as hepatoma were proved by selective angiography and liver biopsy. The last 2 patients with liver metastases were proved by clinical course and follow-up liver imaging with US and liver colloid scan, which revealed increased size of the previous lesion with multiple new focal lesions seen in the liver. None of



these 6 patients demonstrated definite focal increased BP activity on either delayed planar or SPECT images.

Of the 25 patients with HCHs, 11 had no symptoms, and 14 complained of symptoms attributable to the lesions discovered such as right upper abdominal discomfort and/or pain. All of these patients had liver US studies, 15 had CT examination of the liver and 5 had selective angiography for the final diagnosis.

The 25 patients had a total of 37 hemangiomas. Nineteen patients had solitary HCH and 6 patients had multiple lesions. Of the 6 patients with multiple HCHs, 3 had 2 lesions and the other 3 had 4 lesions. These lesions ranged in size from 1.0-12.0 cm in diameter (average, 3.8 cm), as measured on US and/or CT. Seven of these were smaller than 2 cm, 20 were between 2-4 cm, and 10 were larger than 4 cm. Of these HCHs, 31 lesions were located in the right hepatic lobe and 6 in the left lobe.

Twenty-five of the 37 HCHs (67.6%) were identified on planar Tc-99m RBC imagings and 32 lesions (86.5%) were identified with the adjunctive SPECT images. The sensitivity of Tc-99m RBC imagings was 100% (30 of 30 lesions) for HCHs larger than or equal to 2 cm in diameter, and for lesions less than 2 cm in size, the sensitivity was 28.6% (2 of 7 lesions).

Twenty-five of the 37 hemangiomas were demonstrated on planar imagings as a focal increased BP activity within the liver parenchyma. Seven additional lesions were found on SPECT imagings and these lesions were 1.5-3.5 cm in diameter, average 2.1 cm. Twelve HCHs that could not be demonstrated by planar BP images, were 1.0-3.5 cm in size (mean 1.9 cm), the 3.5 cm lesion was located deep inside the liver parenchyma and adjacent to the inferior vena cava. Five HCHs that could not be identified on SPECT, were 1.0-1.8 cm in size, average 1.2 cm. The smallest HCH identified with SPECT image was 1.5 cm and this lesion was located at subcapsular region of the left hepatic lobe, whereas 2.0 cm was the smallest lesion detected with planar BP imaging.

Of the 32 HCHs found on Tc-99m RBC images, 14 revealed normal perfusion, 15 had focal

decreased perfusion, and 3 had some areas of increased perfusion during the blood-flow studies. However, all hemangiomas demonstrated definite focal increased BP activity on delayed planar and/or SPECT imagings, with persistent uptake upto 2 hrs after injection, which were characteristic of hemangiomas. In our study, only hemangiomas revealed evidence of focal increased BP activity on either delayed planar BP or SPECT images.

## DISCUSSION

Most of HCHs are asymptomatic and usually found as an incidental finding during examination of the liver.<sup>1</sup> It is important to differentiate HCH from other focal hepatic lesions, in order to avoid inadvertent needle biopsy of a hemangioma, which can result in an extensive bleeding. Noninvasive diagnosis of HCH can be made easily using sequential Tc-99m RBC imaging, which is reported to be highly sensitive and specific in distinguishing HCH from other focal hepatic lesions.<sup>3,17-19,25</sup>

HCHs, particularly if they are larger than 2 cm in diameter, can be visualized with high accuracy by Tc-99m RBC imaging.<sup>7,25</sup> Like in our study, all HCHs equal to or larger than 2 cm in size were identified on the Tc-99m RBC images.

Front et al<sup>18</sup> had described the characteristic scintigraphic findings of HCH on Tc-99m RBC imaging as a perfusion/BP mismatch, which revealed decreased blood-flow activity on dynamic images and increased BP activity on delayed imagings. This perfusion/ BP mismatch is the key to the scintigraphic diagnosis of HCH, which is observed only in the HCH and has not been reported in any other type of focal hepatic lesions,<sup>16-18</sup> except for a rare case of hepatic angiosarcoma.<sup>26</sup> The perfusion/BP mismatch is highly specific for HCH and usually can be used to diagnose most hemangiomas 3 cm or larger on planar BP imagings.<sup>17</sup> However, in smaller lesions, they usually reveal normal perfusion during the blood-flow imagings with typically focal increased activity on delayed BP images. In our series, only 15 HCHs demonstrated this characteristic of perfusion/BP mismatch and all of them were equal to or larger than 3.5 cm in size (range 3.5-12.0 cm, mean 6.2 cm).



Pathologically, HCH consists of various sized blood-filled vascular spaces lined by a single layer of flat endothelial cells, which are separated by fibrous septae.<sup>1</sup> Therefore, sluggish blood-flow through these large vascular spaces produces a pattern of perfusion/BP mismatch on Tc-99m RBC imaging, which reveals hypoperfusion on dynamic images with gradually increasing BP activity on sequential delayed imagings.<sup>22</sup> Since Tc-99m labeled RBC is an excellent intravascular marker, it can directly fill-in the vascular spaces of HCH and permit the typical scintigraphic finding of HCH.

While some hypervascular hepatic tumors such as hepatomas, hepatic adenomas, focal nodular hyperplasia or metastatic disease may reveal increased BP activity on delayed imagings like HCH, these lesions would be expected to demonstrate increased activity on early blood flow images. Thus, HCH and these tumors can be differentiated on the basis of the flow pattern during the dynamic imagings. HCHs usually demonstrate normal or hypoperfusion, whereas hepatomas and other hypervascular lesions typically reveal increased perfusion during the early dynamic images.<sup>8,16,25</sup>

Despite its highly sensitive for diagnosis of HCH, planar Tc-99m RBC imaging usually fails to detect HCH equal to or smaller than 2 cm in size and/or deep-seated lesion within the liver parenchyma.<sup>3,25</sup> Therefore, SPECT image plays an important role as an adjunctive imaging, in order to enhance the image contrast and increase the sensitivity for detection of small or deep-seated lesions that beyonds the resolution of the planar imaging. Many reports have documented that additional SPECT image has significantly increased the sensitivity and specificity of the Tc-99m RBC imaging in the detection of small or deep-seated HCHs, due to improve the image contrast.<sup>16,20,25,27,28</sup> The use of SPECT imagings help to demonstrate the lesions equal to or smaller than 2 cm in size or deep-seated lesions, especially lesions adjacent to normal vascular structures, which can not be detected on conventional planar BP images. However, detection of HCH on SPECT imaging is primarily dependent on the size and location of the lesion. Therefore, the limitations of SPECT imaging for identifying small HCH are also described,

particularly for lesions less than or equal to 1 cm in size or lesions located near major vascular structures, due to the limits of the resolution of conventional gamma camera.<sup>20,25,27</sup> However, higher resolution multi-headed SPECT system has shown to improve the performance for identifying as small as 0.5 cm HCH, as demonstrated by Ziessman et al.<sup>29</sup>

False negative and false positive studies on Tc-99m RBC imagings may also be encountered. False negative study may be found in cases of HCH with extensive thrombosis and/or fibrosis<sup>16,17</sup> and false positive study may be found in case of hepatic angiosarcoma, which is extremely rare in contrast to HCH.<sup>26</sup>

In our study, only HCHs revealed definite focal increased BP activity more than normal liver parenchyma on delayed BP imagings, with persistent up to 2 hr after injection. In 2 patients with metastatic disease and 4 cases with hepatoma showed focal increased perfusion during the blood-flow images with isoactive or slightly decreased BP activity on delayed images. Thus, isoactive or hypoactive lesions on delayed BP imagings are unlikely to be HCH and indicate a need for further investigations.<sup>19</sup>

Selective angiography is well accepted as the most sensitive and specific method for diagnosis of HCH, but its technically invasive, expensive and several complications make the procedure unsuitable for a routine investigation in these patients. Therefore, angiography should be reserved only for patients who can not be confidently diagnosed by other noninvasive diagnostic methods, including Tc-99m RBC imaging.<sup>9</sup>

Although US is very sensitive for detecting small HCH, its appearance of HCH is variable and nonspecific, especially in large lesions. HCH may appear as hyperechoic, mixed-echoic or hypoechoic lesion within the liver parenchyma.<sup>4-10</sup> Thus, this modality does not permit a definitive diagnosis of HCH.<sup>8,9</sup>

CT and MRI demonstrate superior sensitivity in the detection of lesions smaller than 2 cm, especially the deep-seated lesion adjacent to normal vascular structures. Although Tc-99m RBC imaging with SPECT has a lower sensitivity for small lesions less than 2 cm, as compared with the US, CT or MRI,



its specificity and positive predictive value for diagnosing HCH are reported to be very high and approach 100% in many series.<sup>16,19,25</sup>

As compared with dynamic CT, MRI or selective angiography, Tc-99m RBC imaging with either planar or SPECT image is noninvasive, economical, low-risk, easily performed and relatively specific method for diagnosing HCH. Therefore, Tc-99m RBC imaging of the liver has recently been recommended as a procedure of choice for the differential diagnosis of HCH from other focal hepatic lesions. Because of its high sensitivity and high specificity, focal hepatic lesions that demonstrate the classic scintigraphic findings of HCH on Tc-99m RBC imaging usually require no further diagnostic workup.<sup>14,19,25</sup>

In conclusion, Tc-99m RBC imaging is highly recommended as a further noninvasive investigation of choice to confirm the suspected diagnosis of HCHs found on US and/or CT images, especially in patients with a history of known primary malignancy or high-risk for developing hepatocellular carcinoma. Furthermore, additional SPECT imaging should be routinely performed as an adjunctive method in the evaluation of suspected hemangioma patients. We also consider that Tc-99m RBC imaging of the liver is probably the best noninvasive imaging modality available for confirming the suspected diagnosis of HCH found on other noninvasive diagnostic images.

## ACKNOWLEDGMENTS

The authors gratefully thank Professor Dr. Snan Simarak for his valuable suggestion and reviewing of this manuscript.

## REFERENCES

1. Ishak KG, Rabin L. Benign tumors of the liver. *Med Clin North Am* 1975; 59: 995-1013.
2. Adam YG, Huvos AG, Fortner JG. Giant hemangiomas of the liver. *Ann Surg* 1970; 172: 239-245.
3. Moinuddin M, Allison JR, Montgomery JH, et al. Scintigraphic diagnosis of hepatic hemangioma: Its role in the management of hepatic mass lesions. *AJR* 1985; 145:223-228.
4. Itai Y, Ohtomo K, Araki T, et al. Computed tomography and sonography of cavernous hemangioma of the liver. *AJR* 1983; 141: 315-320.
5. Gibney RG, Hendin AP, Cooperberg PL. Sonographically detected hepatic hemangiomas: absence of change over time. *AJR* 1987; 149: 953-957.
6. Lisbona R, Derbekyan V, Novales-Diaz JA, et al. Scintigraphic and ultrasound features of giant hemangiomas of the liver. *J Nucl Med* 1989; 30: 181-186.
7. Jacobson AF, Teefey SA. Cavernous hemangiomas of the liver: association of sonographic appearance and results of Tc-99m labeled red blood cell SPECT. *Clin Nucl Med* 1994; 19: 96-99.
8. Nelson RC, Chezmar JL. Diagnostic approach to hepatic hemangiomas. *Radiology* 1990; 176: 11-13.
9. Brant WE, Floyd JL, Jackson DE, et al. The radiological evaluation of hepatic cavernous hemangioma. *JAMA* 1987; 257: 2471-2474.
10. Bree RL, Schwab RE, Glazer GM, et al. The varied appearances of hepatic cavernous hemangiomas with sonography, computed tomography, magnetic resonance imaging and scintigraphy. *Radio Graphics* 1987; 7: 1153-1174.
11. Freeny PC, Marks WM. Hepatic hemangioma: dynamic bolus CT. *AJR* 1986; 147:711-719.
12. Itoh K, Saini S, Hahn PF, et al. Differentiation between small hepatic hemangiomas and metastases on MR images: importance of size-specific quantitative criteria. *AJR* 1990; 155: 61-66.
13. Birnbaum BA, Weinreb JC, Megibow AJ, et al. Definitive diagnosis of hepatic hemangiomas: MR imaging versus Tc-99m-labeled red blood cell SPECT. *Radiology* 1990; 176: 95-101.
14. Brown RKJ, Gomes A, King W, et al. Hepatic hemangiomas: Evaluation by magnetic resonance imaging and technetium-99m red blood cell scintigraphy. *J Nucl Med* 1987; 28: 1683-1687.



15. Larcos G, Farlow DC, Gruenewald SM, et al. A typical appearance of a hepatic hemangioma with technetium-99m-red blood cell scintigraphy. *J Nucl Med* 1989; 30:1885-1888.
16. Intenzo C, Kim S, Madsen M, et al. Planar and SPECT Tc-99m red blood cell imaging in hepatic cavernous hemangiomas and other hepatic lesions. *Clin Nucl Med* 1988; 13:237-240.
17. Rabinowitz SA, McKusick KA, Strauss HW. <sup>99m</sup>Tc-red blood cell scintigraphy in evaluating focal liver lesions. *AJR* 1984; 143: 63-68.
18. Front D, Royal HD, Israel O, et al. Scintigraphy of hepatic hemangiomas: The value of Tc-99m-labeled red blood cells: Concise communication. *J Nucl Med* 1981; 22:684-687.
19. Engel MA, Marks DS, Sandler MA, et al. Differentiation of focal intrahepatic lesions with <sup>99m</sup>Tc-red blood cell imaging. *Radiology* 1983; 146: 777-782.
20. Brodsky RI, Friedman AC, Maurer AH, et al. Hepatic cavernous hemangioma: Diagnosis with <sup>99m</sup>Tc-labeled red cells and single photon emission CT. *AJR* 1987; 148: 125-129.
21. Kim SM, Park CH, Yang SL, et al. Pathognomonic scintigraphic finding of hepatic cavernous hemangioma. *Clin Nucl Med* 1987; 12: 53-54.
22. Alavi A, Rubin RA, Lichtenstein GR. Scintigraphic evaluation of liver masses: cavernous hepatic hemangioma. *J Nucl Med* 1993; 34: 849-852.
23. Trastek VF, Van Heerden JA, Sheedy PF, et al. Cavernous hemangiomas of the liver: Resect or observed ?. *Amer J Surg* 1983; 145: 49-53.
24. Callahan RJ, Froelich JW, McKusick KA, et al. A modified method for the in vivo labeling of red blood cells with Tc-99m: concise communication. *J Nucl Med* 1982; 23: 315-318.
25. Kudo M, Ikekubo K, Yamamoto K, et al. Distinction between hemangioma of the liver and hepatocellular carcinoma: Value of labeled RBC-SPECT scanning. *AJR* 1989; 152: 977-983.
26. Ginsberg F, Slavin JD, Spencer RP. Hepatic angiosarcoma: mimicking of angioma on three-phase technetium-99m-red blood cell scintigraphy. *J Nucl Med* 1986; 27: 1861-1863.
27. Guze BH, Hawkins RA. Utility of the SPECT Tc-99m labeled RBC blood pool scan in the detection of hepatic hemangiomas. *Clin Nucl Med* 1989; 14: 817-818.
28. Malik MH. Blood-pool SPECT and planar imaging in hepatic hemangioma. *Clin Nucl Med* 1987; 12: 543-547.
29. Ziessman HA, Silverman PM, Patterson J, et al. Improved detection of small cavernous hemangiomas of the liver with high-resolution three-headed SPECT. *J Nucl Med* 1991; 32: 2086-2091.

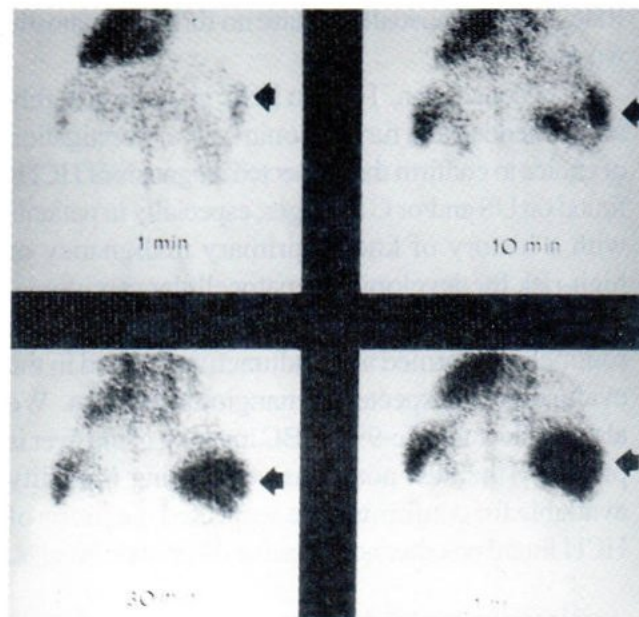


**Fig.1** A 36-year-old man in whom the US shows a large 8 x 10 cm mixed hyperechoic lesion at the posterior of right hepatic lobe. Tc-99m RBC blood-flow study shows decreased perfusion to the lesion. Serial planar BP imagings on the posterior view demonstrate peripheral enhancement with subsequent central enhancement and complete fill-in of BP activity (arrows) at 1 hr after injection, which is typical for a large HCH.

BP = Blood Pool



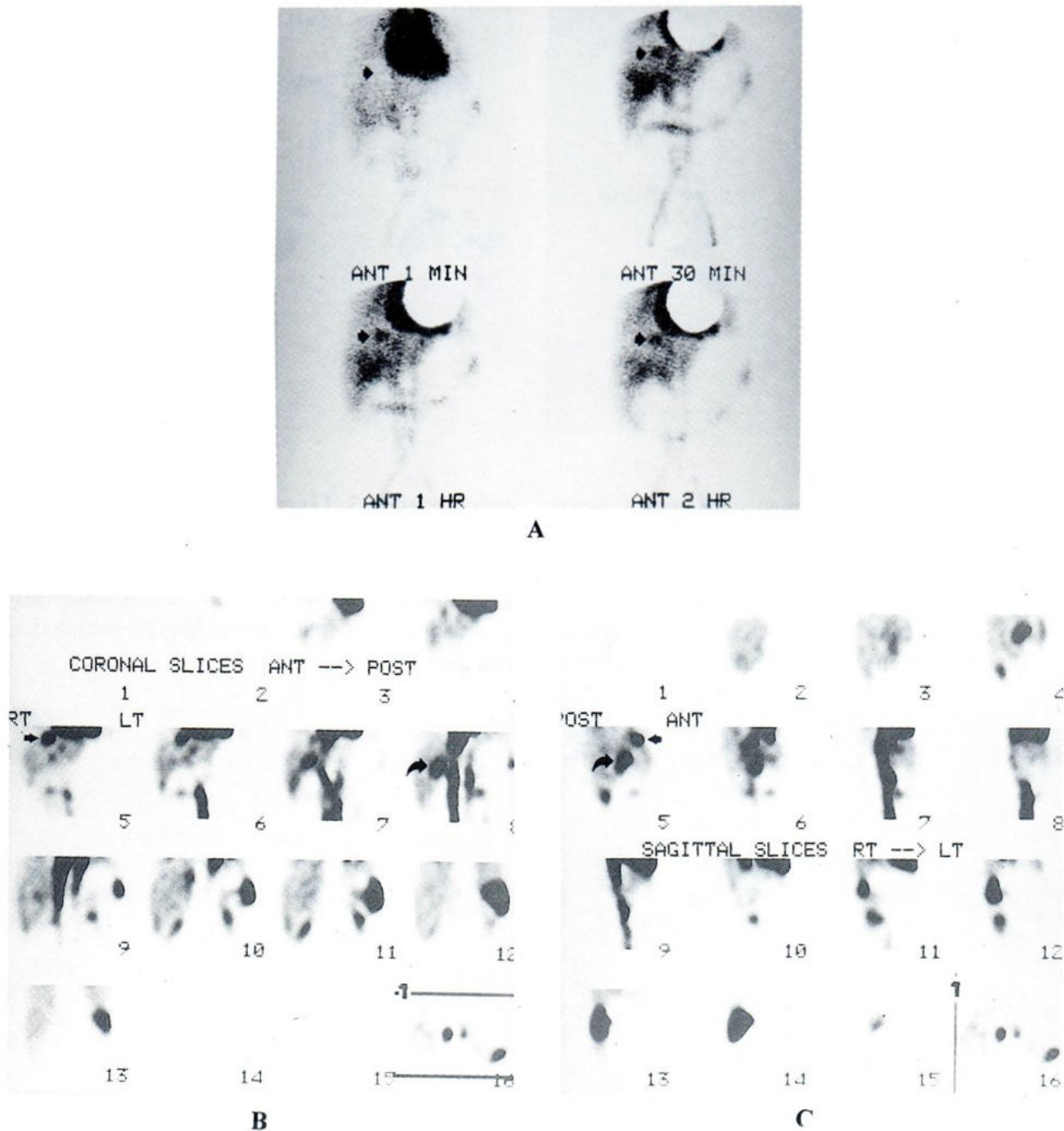


**Fig.2** Multiple HCHs in a 54-year-old man with right upper quadrant discomfort. LiverUS shows two hyperechoic lesions, one is 3 x 3 cm at dome of right hepatic lobe and another is 3 x 3.5 cm adjacent to IVC. Serial planar BP images(A) are positive only in the lesion at dome of right lobe(arrows). Coronal(B) and sagittal (C) SPECT images clearly demonstrate these two HCHs, which reveal discrete areas of intensely increased BP activity corresponding to the US findings.(Straight arrow shows lesion at dome of right lobe and curve arrow shows another lesion deepseated within the liver parenchyma adjacent to IVC.)

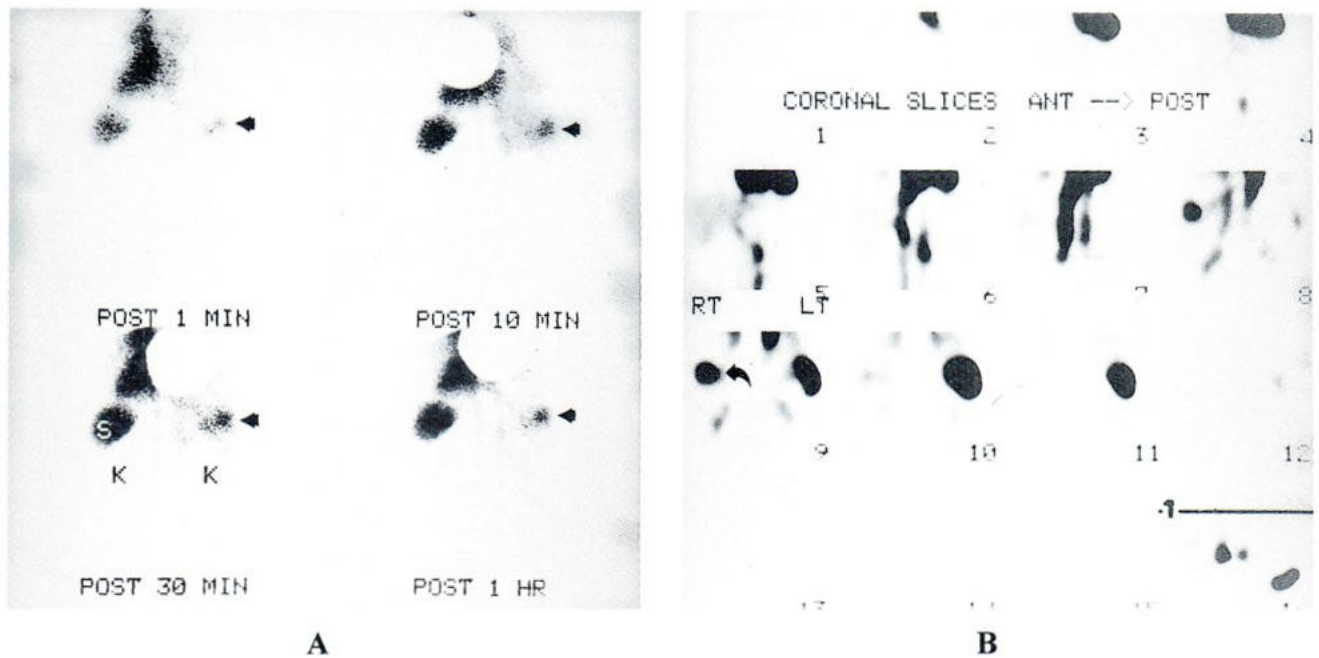


**Fig.3** A 52-year-old woman with known ovarian carcinoma stage 3. Liver US shows a 2.6 x 2.7 cm hyperechoic lesion at right hepatic lobe. Tc-99m RBC blood-flow images reveal normal perfusion to the lesion. Serial BP images(A) show gradually increased BP activity within the right hepatic lesion (arrows), which is persisted up to 2 hr after injection. Coronal SPECT images(B) clearly demonstrate a focal increased BP activity within the lesion (arrow) much greater than the surrounding liver paren chyma, compatible with a hemangioma. (S = spleen, K = kidney)

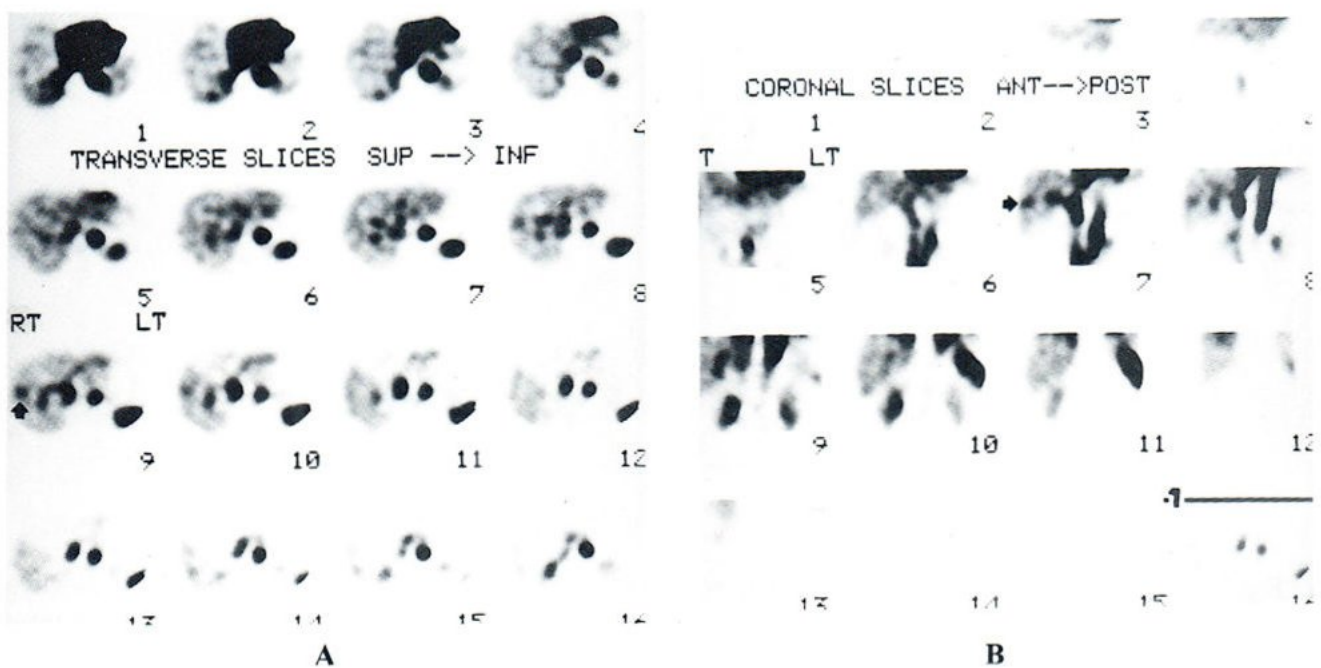


**Fig.4** A 51-year-old woman with a history of hepatitis B virus carrier, in whom the US shows a 2 cm hyperechoic lesion at anterior segment of right hepatic lobe. Blood-flow and serial planar Tc-99m RBC images do not show any abnormality. Transverse(A) and coronal(B) SPECT images clearly demonstrate a focal increased BP activity within the right hepatic lesion(arrow), consistent with a small hemangioma.



## **DIPYRIDAMOLE THALLIUM-201 MYOCARDIAL PERFUSION SINGLE PHOTON EMISSION COMPUTED TOMOGRAPHY IN CORONARY ARTERY DISEASE**

The IAEA supported Co-ordinated Research Project on "Qualitative Nuclear Cardiology in Thailand" 1992-1995

**Vacharin RATANAMART, M.D.<sup>1</sup> Pawana PUSUWAN, M.D.<sup>1</sup>  
Jiraporn MANGKHARAK, M.D.<sup>1</sup> Damras TRISUKOSOL, M.D.<sup>2</sup>  
Sunanta CHIEWVIT, M.D.<sup>1</sup> Pachee CHAUDAKSHETRIN, B.Sc., M.Eng.<sup>1</sup>  
Puangrat BURANAPONG, M.Sc.<sup>1</sup>  
Nucharee PUTRASRENI, M.Sc. ( Medical Audio-Visual Communicaton )<sup>1</sup>  
Rujaporn CHANACHAI, Ph.D.<sup>1</sup> Suthee NA SONGKHLA, M.D.<sup>1</sup>  
Supachai CHAITHIRAPHAN, M.D.<sup>2</sup> Rudee PLEEHACHINDA, M.D.<sup>1</sup>**

### **ABSTRACT**

We performed dipyridamole Tl-201 myocardial perfusion tomographic studies imaging in 38 patients with suspected or known coronary artery disease to determine the sensitivity, specificity, and accuracy of the procedure in the detection of coronary artery disease and in localization of individual stenosed vessel. The overall sensitivity, specificity, accuracy, positive predictive value, and negative predictive value of the test were 96.8%, 42.9%, 86.8%, 88.2%, and 75.0%, respectively. And those for the detection of stenosed vessels were 75.8%, 46.4%, 66.7%, 75.8%, and 43.3%, respectively. The sensitivity in the detection of individual stenosed vessel was significantly higher in vessels with severe than with moderate stenosis (54.5% vs. 87.5%). Fixed defects usually indicate very severe and complete occlusion of coronary arteries. Reversible defects generally indicate significant but nonocclusive coronary artery stenosis. We conclude that dipyridamole thallium-201 myocardial perfusion tomography is a useful noninvasive test for coronary artery disease.

### **INTRODUCTION**

Exercise thallium-201 myocardial perfusion tomographic study has been widely used in the detection of coronary artery disease, assessment of myocardial viability, and evaluation of prognosis.<sup>1-6</sup> However, there are many patients who cannot exercise adequately for the test due to noncardiac causes. The pharmacologic stress test has been introduced as an alternative to exercise stress test.<sup>7</sup> Many investigators had reported very good results with dipyridamole Tl-201 myocardial perfusion tomographic study.<sup>8-12</sup> Pharmacologic stressors are useful for patients who cannot exercise for various reasons including physical

limitations, peripheral vascular disease, limiting orthopedic disorders and aortic aneurysm. The purpose of administration of dipyridamole is to create a disparity in coronary blood flow between normal and stenosed arteries by vasodilatory effects of dipyridamole.

This study was performed to evaluate the sensitivity, specificity, accuracy, positive predictive value, and negative predictive value for the detection of coronary artery disease and for the localization of individual abnormal vessel. The ability of the test to evaluate severity of coronary artery disease was also examined.

<sup>1</sup> Division of Nuclear Medicine, Department of Radiology, Faculty of Medicine Siriraj Hospital, Mahidol University.

<sup>2</sup> Her Majesty's Cardiac Center, Faculty of Medicine Siriraj Hospital, Mahidol University.



## MATERIALS AND METHODS

**Patient population.** The study group consisted with 38 patients suspected of coronary artery disease referred to our department for dipyridamole Tl-201 myocardial perfusion tomographic study. The clinical data and the hemodynamic parameters of the patient population are cited in Table 1. Thirteen patients had previous myocardial infarction diagnosed by electrocardiography (ECG) and clinical history. In all patients beta-blockers and anti-anginal medications ( long acting nitrates and calcium antagonists) were discontinued at least 48 hours before radionuclide studies.

**Study protocol.** The patients were asked to fast overnight and remain fast until the redistribution images were finished. Dipyridamole was administered in an intravenous infusion with a total dose of 0.56 mg/kg over a period of 4 minutes. Two minutes after the infusion was completed, thallium-201 was injected rapidly via the infusion line. Imaging was begun at 10 minutes after thallium-201 injection. Two sets of tomographic images were acquired after single injection. The stress images taken within 10 minutes after the thallium-201 injection and the redistribution images were obtained 3 hours later .

**Coronary angiography .** Coronary angiography was performed by Sheldinger technique. Angiographic results were reported in consensus by two experienced observers. Angiographic demonstration of 50% or more narrowing of anyone of the epicardial coronary arteries was considered abnormal. A luminal stenosis of 50 to 75% was considered moderate, while a luminal stenosis more than 75% was considered severe.

**Thallium-201 imaging.** SPECT imaging was performed using a large field of view gamma camera ( Toshiba ,GCA 901A) equipped with a low-energy , high resolution , parallel hole collimator and connected with a dedicated computer system ( TOSBAC GHS 901a). Thirty-

six projections ( 35 second/projection) were obtained over a semicircular 180 degrees arch which extended from the 45 degrees right anterior oblique to the 45 degrees left posterior oblique position .Two 20% symmetrical window centered on the 69-80 keV. and 135 keV. peaks were used. The projection images were stored in 64x64 matrix. Filtered backprojection was performed with a Butter-worth filter with a cut-off frequency of 0.15 cycle/pixel, order 5 , to reconstruct transverse axial tomograms Sagittal and oblique tomograms parallel to the long axis and short axis of the left ventricle were then extracted from the filtered transaxial tomograms by performing coordinate transformation with the appropriate interpolation. No attenuation or scatter correction was applied.

**Data analysis.** In each patient, corresponding dipyridamole and redistribution tomographic images were evaluated for direct comparison. For each study, tomograms were divided into 29 myocardial segments, as shown in Figure 1. Each segment was assigned to one of the major vascular territories. The anterior descending artery ( LAD ) territory included the anterior wall (segments 1,7,13,-19,20), septum (segments 2,3,8,9,14,15,-25,26), and apical wall ( segments 21,22,27). The lateral wall ( segments 5,6,11,12,17,-18,28,29,) was assigned to the left circumflex artery ( LCX ). The inferior wall (segments 4,10,16,23,24 ) was assigned to the right coronary artery (RCA ) if coronary angiography showed right dominant circulation, and was assigned to the LCX if coronary angiography revealed left dominant circulation.

Regional thallium-201 activity was visually analyzed on the three short- axis ( one apical, one mid-ventricular and one basal ) tomograms and on one horizontal and one vertical long-axis tomograms. The Tl-201 myocardial perfusion stress and rest images were reviewed and marked, 'N' for normal thallium-201 uptake , 'R' for reversible thallium-201 defects and 'F' for fixed or irreversible thallium-201 defects,



independently by two experienced observers, the studies with discordant readings were reviewed by the third observer and agreement of two out of three observers was considered.

**Statistical analysis.** Data are expressed as mean  $\pm$  1 SD. Differences of the mean value were assessed by Student's *t* test for paired or unpaired data, as appropriate. Chi square analysis was used to assess differences between proportions. A probability ( *P* ) value  $< 0.05$  was considered statistically significant. Sensitivity was defined as the number of true-positives divided by the sum of true-positives and false-negatives  $\times 100$ . Specificity was defined as the number of true-negatives divided by the sum of true-negatives and false-negatives  $\times 100$ . Diagnostic accuracy was defined as the sum of true-positives and true-negatives divided by the total. Positive predictive value (PPV) was defined as true-positives divided by the sum of true- and false-positives. Negative predictive value (NPV) was defined as true-negatives divided by the sum of true- and false-negatives.

## RESULTS

### *Coronary angiography*

The results of coronary angiography are summarized in Table 2. Of the 38 patients, 31 (81.6%) had at least one major coronary artery stenosis of 50% or more of luminal diameter. There were 10 patients with single-vessel disease, 10 with double-vessel disease and 11 with triple-vessel disease. Six patients had normal coronary arteries and one had angiographically insignificant stenosis (40,40,45% stenosis of LAD, RCA and LCX, respectively), thus, constituted seven patients with negative angiographic findings. Individual vessel analysis showed 22 coronary arteries with moderate ( 50 % to 75% ) luminal stenosis and 40 coronary arteries with severe ( more than 75% ) luminal stenosis.

### *Dipyridamole test results*

Hemodynamic parameters recorded at rest and at peak exercise and dipyridamole-induced ECG changes are presented in Table 1.

### *Tl-201 myocardial perfusion imaging*

At visual analysis, 30 of 31 patients with significant stenosis of at least one coronary artery showed abnormal Tl-201 myocardial perfusion images ( sensitivity 96.8% ) (Table 3). On the otherhand, 3 of 7 patients without significant coronary narrowing showed normal findings (specificity 42.9% ) Fig. 2 and 3 show two representative examples of dipyridamole stress / redistribution Tl-201 myocardial perfusion images in a patient with normal study and a patient with coronary artery disease documented at angiography.

The overall sensitivity, specificity and diagnostic accuracy of dipyridamole Tl-201 myocardial perfusion tomography in the detection of individual stenosed vessels were 75.8%, 46.4%, and 66.7% ,respectively (Table 4). Sensitivity, specificity, and diagnostic accuracy in each of the individual vascular territories were not significantly different. The overall sensitivity, specificity and diagnostic accuracy in the identification of individual stenosed coronary artery in patients with single-vessel disease were 66.7%, 38.9%, and 48.1% respectively (Table 5). In multivessel disease the overall sensitivity, specificity, and accuracy were 77.4%, 60.0%, and 74.6% respectively. Sensitivity of dipyridamole Tl-201 myocardial perfusion tomography in the detection of LAD and accuracy of LAD and LCX were significantly ( $P < 0.05$ ) higher in patients with multivessel disease than with single-vessel disease. There was otherwise no significant difference of sensitivity, specificity, and accuracy in the detection of other individual stenosed vessels between the two groups (  $P > 0.05$  ).



***Comparison between patients with and without previous myocardial infarction.*** There were 13 patients (41.9% of CAD patients) with history and ECG diagnosis of previous myocardial infarction (Table 6). Overall sensitivity in the detection of coronary artery disease was not different between the patients with and without prior myocardial infarction.

***Effects of the severity of coronary artery stenosis on diagnostic accuracy.*** Individual vessel analysis showed 22 coronary arteries (35.5%) with moderate (50-75%) luminal stenosis and 40 coronary arteries (64.5%) with severe (>75%) luminal stenosis. The effect of stenosis severity on detection of lesions is shown in Table 7. The overall sensitivity in the identification of individual diseased vessels with severe luminal stenosis (87.5%) was significantly ( $P < 0.05$ ) higher compared to those with moderate luminal stenosis (54.5%).

***The distribution of 'fixed' and 'reversible' perfusion defects*** The distribution of 'fixed' and 'reversible' perfusion defects in relation to severity of coronary artery stenosis was shown in Table 8. Of 84 abnormal segments, 43 were 'fixed' and 41 were 'reversible'. Fifteen (34.9%) of fixed and 3 (7.3%) of reversible defects were in the territories of vessels with 100% luminal stenosis. The remaining 28 (65.1%) fixed and 38 (92.7%) reversible defects were in the territories of nonocclusive vessels.

## DISCUSSION

The principle of vasodilator stress myocardial perfusion imaging was first introduced by Strauss and Pitt<sup>7</sup> who showed that dimethyladenosine increased coronary blood flow and Tl-201 uptake to normal area of myocardium, while regions of myocardium perfused by coronary artery with a haemodynamically significant coronary stenosis had reduced flow reserve and, thus less thallium-201 uptake. Dipyridamole is a complex pyrimidine derivatives with a molecular

weight of 504. It is lipophilic and is metabolized by hepatic biotransformation with subsequent biliary and fecal excretion.<sup>13</sup> In human, intravenous dipyridamole infusion results in a mild decreased in blood pressure, a slight reflex increase in heart rate, a slight increase in cardiac output but no change in myocardial oxygen demand. Coronary vascular resistance significantly decreases and coronary sinus flow increases, with a small increase in pulmonary artery pressure.<sup>14,15</sup> The vasodilator effect of dipyridamole is up to 20 to 40 minutes.<sup>16</sup> The initial myocardial distribution of intravenously administration of Tl-201 is proportional to blood flow when the tracer is administered following dipyridamole infusion. Under condition of myocardial ischemia, dipyridamole-induced vasodilatation results in diminished Tl-201 myocardial uptake and delayed redistribution similar to that observed with exercise scintigraphy.<sup>17,18,19</sup> Redistribution perfusion defects are seen with comparable frequency on serial myocardial scintigrams acquired with vasodilators stress or exercise stress in patients with CAD who underwent both tests at different time.

We studied the clinical utility of dipyridamole Tl-201 myocardial perfusion tomographic images in patients with known or suspected coronary artery disease who underwent coronary arteriography. Very good overall sensitivity, accuracy, positive predictive value, and negative predictive value in the detection of coronary artery disease was observed. The specificity was rather low, probably due to referral bias. The results in this study is corresponded to the results reported by other investigators.<sup>8-12</sup> The sensitivity in the identification of coronary artery disease in patients with and without previous myocardial infarction was not different (Table 3).

The overall sensitivity, specificity, accuracy, and NPV in the identification of individual stenosed vessels were moderate (Table 4). Only the sensitivity in the detection of LAD was high. The



low accuracy could be due to many factors, for example, false positive due to technical factors and soft tissue attenuation, the assignment of myocardial regions to the coronary arteries, the degree of coronary stenosis, the effects of collateral circulations, and also the possibility of coronary spasm. Similar results were reported by many investigators.<sup>8-12</sup>

We found that the overall diagnostic accuracy in the detection of individual stenosis vessels were significantly higher ( $P < 0.05$ ) in patients with multivessel disease than those with single-vessel disease (Table 5). There were low specificity of LAD in both groups and LCX in the single-vessel disease patients.

We analyzed the effects of severity of coronary artery stenosis (Table 7) and observed that the overall sensitivity in the detection of individual diseased vessel was significantly ( $P < 0.05$ ) higher in coronary arteries with severe luminal stenosis (87.5%) than those with moderate luminal stenosis (53.6%). This could be due to the fact that coronary blood flow is significantly decreased in more severe coronary artery stenosis and thallium-201 uptake, over a wide range of physiologic blood flow, is proportional to coronary blood flow.<sup>20-22</sup> The more severe luminal stenosis the more severe diminished coronary blood flow and thallium-201 uptake. So the severely ischemic lesions appears more prominent than areas with less ischemia.

By visual analysis of the Tl-201 myocardial perfusion images, there were 84 abnormal segments of which 43 were fixed perfusion defects and 41 were reversible perfusion defects. Of 18 segments of perfusion defects in the areas perfused by vessels with total occlusion (100% stenosis), 15 segments (83.3%) were fixed and 3 segments (16.7%) were reversible defects. The reason why not all of the areas perfused by totally occluded vessels were infarcted may be the collateral circulations.<sup>23</sup> On the other hand, of 43 fixed defects, only 15 segments (34.9%) were in the territories of coronary arteries with 100% luminal

stenosis and 28 fixed defects (65.1%) were in the territories of nonocclusive coronary arteries. Cuocolo et al<sup>24</sup> reported that with thallium-201 'reinjection' 47% of 122 myocardial regions with irreversible defects on standard stress-redistribution thallium-201 imaging demonstrated enhance uptake of thallium-201. Contrariwise, there is growing consensus that about 90% of transmural acute myocardial infarctions are caused by an occlusive intracoronary thrombus overlying an ulcerated or fissured stenotic atheroma.<sup>25</sup> Platelet aggregation and activation and vasospasm may contribute to the development of myocardial infarction even in the absence of fixed critical stenoses.<sup>26</sup> Although not all of the fixed defects were in the areas supplied by complete stenosis, 'fixed defects' still denoted very severe coronary artery stenosis. However, in this study, about two third (61.0%) of reversible defects were in the areas perfused by coronary arteries with severe but incomplete occlusion (76-99% luminal stenosis). This is suggestive that reversible defects represent areas of high-risk of cardiac events and indicate catheterization and revascularization. Brown et al<sup>27</sup> showed that the number of Tl-201 redistribution defects was the best predictor of future cardiac events as determined by logistic regression analysis in CAD patients without prior myocardial infarction.

**Study limitations** There were some limitations to the study that should be considered. The first limitation might be the lack of computer quantitation of coronary angiography and SPECT quantitation was not applied. The second was the assignment of myocardial segments which might not really be confined to the assigned coronary artery. There was variation in size of the myocardial wall in diseased heart as seen in thallium-201 images. The soft tissue attenuation of anterior wall by breast tissue and the inferior wall by the diaphragm. Referral bias was another factor. Because at present, Tl-201 myocardial perfusion study is generally accepted as a clinical tool in the diagnosis of coronary artery, patients with normal thallium-201 studies were usually not



referred to coronary angiography but patients with abnormal thallium-201 studies were more likely to proceed to the procedure. So the number of patients with normal angiogram was disproportionately low.

## CONCLUSIONS

Dipyridamole Tl-201 myocardial perfusion single photon emission computed tomography is a useful noninvasive means to evaluate patients suspected of coronary artery disease. It provides very good sensitivity, accuracy, PPV, and NPV in the detection of coronary artery disease. Although specificity is low, probably due to referral bias and technical factors. The accuracy of detection of individual coronary artery stenosis is higher in patients with multivessel than in

patients with single-vessel disease. The sensitivity of detection of individual coronary artery stenosis is better in severe (>75%) stenosis than in moderate (50-75%) stenosis. The fixed defects usually indicate very severe, critical and often complete occlusion of coronary arteries. The reversible defects, on the other hand, generally indicate significant but nonocclusive coronary artery stenosis. We conclude that dipyridamole thallium-201 myocardial perfusion study is safe and useful for the evaluation of coronary artery disease.

## ACKNOWLEDGEMENTS

Supported by the International Atomic Energy Agency (IAEA), Research Contract No. 6910/R1/RB.

**Table 1** Clinical data and haemodynamic parameters recorded at rest and at dipyridamole stress test in the patient population (n = 38 cases)

Clinical data and haemodynamic parameters	
age (years)	59 ± 9 (range 40-77 years)
Sex (men/women)	21/17 age 58 ± 8 / 60 ± 8
History of myocardial infarction	13 cases
Dipyridamole dose	44.0 ± 13.5 mg.
Rest	
Heart rate (bpm)	71.0 ± 14.2
Systolic blood pressure (mmHg)	139.2 ± 23.2
Diastolic blood pressure (mmHg)	85.3 ± 13.8
Dipyridamole test	
Heart rate (bpm)	91.0 ± 13.0
Systolic blood pressure (mmHg)	130.7 ± 24.2
Diastolic blood pressure (mmHg)	78.3 ± 13.2
% of maximal predicted heart rate	56.5 ± 8
Dipyridamole stress ECG	
Positive	15 cases
Negative	23 cases



**Table 2** Coronary arteriographic results in 31 patients

coronary artery disease	cases	LAD	LCX	RCA	Lt.mian
Single-vessel	10	6	2	1	1
Double-vessel	10	8	5	7	0
Tripple-vessel	11	11	11	11	0
Total	31	25	18	19	0
Severity of stenosis vessels (n)					
Moderate stenosis	22	6	10	6	1
Severe stenosis	40	19	8	13	-

**Table 3** Sensitivity , specificity , accuracy , positive predictive value (PPV) , negative predictive value (NPV). in the detection of coronary artery disease in 38 patients.

	no. of patients	%	patients with previous MI	No previous MI
Sensitivity	30/31	96.8	100%(13/13 )	94.4% (17/18)
Specificity	3/7	42.9	—	42.9% (3/7)
Accuracy	33/38	86.8	—	80.0% (20/25)
PPV	30/34	88.2	—	80.9% (17/21)
NPV	3/4	75.0	—	75.0% (3/4)

**Table 4** Sensitivity , specificity , diagnostic accuracy, and predictive values in the detection of individual stenosed vessels in 31 patients with coronary artery disease

	LAD	LCX	RCA	Overall
Sensitivity	92.0% (23/25)	66.7% (12/18 )	63.2% (12/19)	75.8% (47/62)
Specificity	20.0% (1/5)	50.0% (6/12)	54.5% (6/1)	46.4% (13/28)
Accuracy	80.0% (24/30)	60.0% (18/30)	60.0% (18/30)	66.7% (60/90)
PPV	85.2% (23/27 )	66.7% (12/18)	70.6% (12/17)	75.8% (47/62)
NPV	33.3% (1/3 )	50.0% (6/12)	50.0% (6/12)	43.3% (13/30)
$P > 0.05$				

LAD = left anterior descending artery, LCX = left circumflex artery,

RCA = right coronary artery

PPV = positive predictive value, NPV = negative predictive value



**Table 5** Sensitivity, specificity, and accuracy in the detection of stenosed vessels in patients with single-vessel and multivessel disease

	Single-vessel disease			Multivessel disease		
	Sensitivity	Specificity	Accuracy	Sensitivity	Specificity	Accuracy
LAD	66.7%	33.3%	55.6%	100.0%	0.0%	90.5%
LCX	50.0%	28.6%	33.3%	68.8%	80.0%	71.4%
RCA	100.0%	50.0%	55.6%	61.1%	66.7%	61.9%
All vessels	66.7%	38.9%	48.1%	77.4%	60.0%	74.6%

**Table 6** Sensitivity of dipyridamole Tl-201 myocardial perfusion SPECT in the detection of CAD in patients with and without previous myocardial infarction

Coronary artery disease	Previous MI	Sensitivity (%)	No previous MI	Sensitivity(%)
Single-vessel	3	100.0%	7	85.7%
Double-vessel	5	100.0%	5	100.0%
Tripple-vessel	5	100.0%	6	100.0%
Total	13	100.0%	18	94.4%

**Table 7** Sensitivity in the detection of stenosed vessels in territories supplied by arteries with moderate ( 50- 75% ) and severe ( 76-100 % ) stenosis in 31 patients

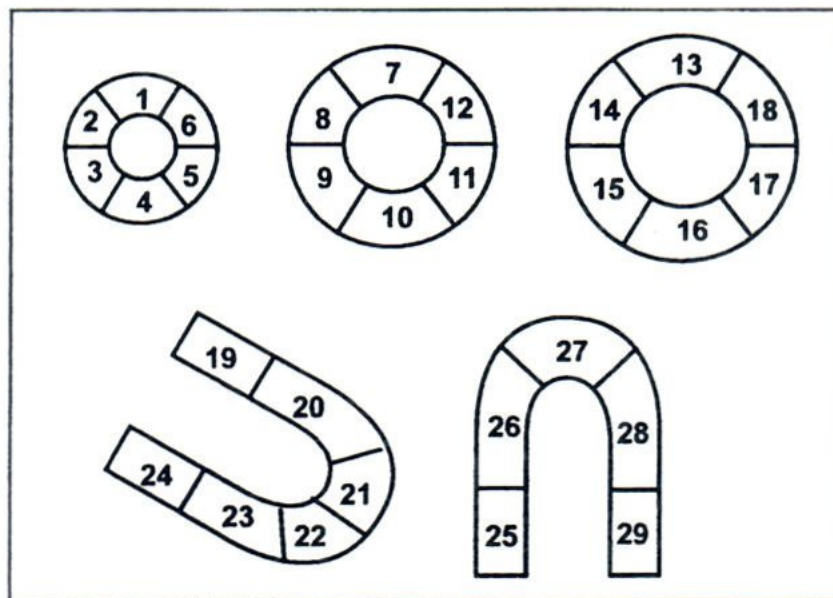
no. stenosed vessels		Moderate stenosis ( 50 - 75 % )	Severe stenosis ( 76-100 % )
LAD	25	83.3% (5/6 )	94.7% (18/19)
LCX	18	60.0% (6/10 )	75.0% (6/8 )
RCA	19	16.7% (1/6 )	84.6% (11/13)
All vessels	63	54.5% (12/22 )	87.5% (35/40 )

LAD = Left anterior descending artery, LCX= left circumflex artery,  
RCA = right coronary artery



**Table 8** Number of fixed and reversible perfusion defects in the areas supplied by coronary arteries with varying degree of luminal stenosis

Perfusion defects (n=112)	% of luminal stenosis			
	100%	90-99%	76-89%	50-75%
Fixed (43segments)	15 (34.9%)	17 (39.5%)	5 (11.6%)	6 (14.0%)
Reversible(41segments)	3 (7.3%)	17 (41.5%)	8 (19.5%)	13 (31.7%)

**Fig.1** The perfusion images were divided into 29 segments as illustrated, represent the anterior wall (segments 1, 7, 13, 19, 20), the anteroseptal wall (segments 2, 8, 14), the inferoseptal wall (segments 3, 9, 15), the septum (segments 25, 26), the anterolateral wall (segments 6, 12, 18), the inferolateral wall (segments 5, 11, 17), the lateral wall (segments 28, 29), the inferior wall (segments 4, 10, 16, 23, 24), and the apical wall (segments 21, 22, 27).



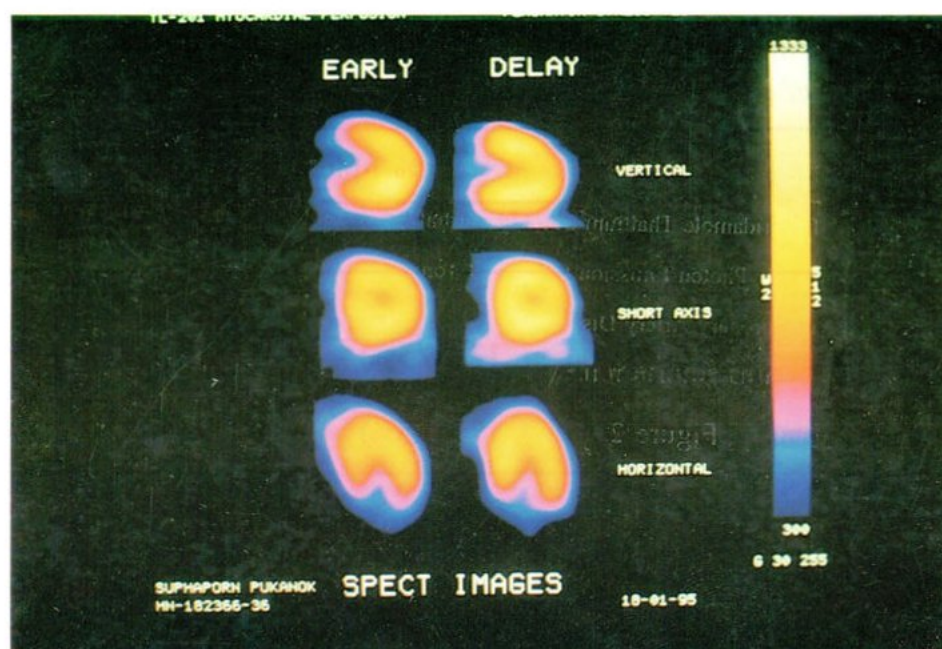


**Fig.2** Dipyridamole stress and redistribution images of thallium-201 myocardial perfusion SPECT study in a patient with normal coronary arteriogram. There is homogeneous distribution of radioactivity in all of the myocardial walls.

## REFERENCES

1. Lebowitz E, Green MW, Fairchild R, Bradley-Moore PR, Atkins HL, Ansari AN, Richards P, Belgrave E. TI-201 for medical use. *J Nucl Med* 1975; 16:151-155.
2. Steinberg EP, Klag MJ, Bakal CW, Strauss HW, Boucher CA, Guiney TE. Exercise thallium scan: Patterns of use and impact on management of patients with known or suspected coronary artery disease. *Am J Cardiol* 1987;59:50-55.
3. Bonow RO, Dilsizian V. Assessing viable myocardium with thallium-201. *Am J Cardiol* 1992; 70: 10E-17E.
4. Iskandrian AS, Hakki AH, Kane-Marsch S. Prognostic implication of exercise thallium-201 scintigraphy in patients with suspected or known coronary artery disease. *Am Heart J* 1985;110 : 135-143.
5. Iskandrian AS, Heo J, Decoskey D, Askenase A, and Segal BL. Use of exercise thallium-201 imaging for risk stratification of elderly patients with coronary artery disease. *Am J Cardiol* 1988;61:269-272.
6. Maddahi J, Garcia EV, Berman DS, Waxman A, Swan HJC, Forester J. Improved noninvasive assessment of coronary artery disease by quantitative analysis of regional stress myocardial distribution and washout of thallium-201. *Circulation* 1981; 64: 924-935.
7. Strauss HW, Pitt B. Noninvasive detection of subcritical coronary arterial narrowings with a coronary vasodilator and myocardial perfusion imaging. *Am J Cardiol* 1977;-39: 403-406.
8. Leppo JA. Dipyridamole-thallium imaging: the lazy man's stress test. *J Nucl Med* 1989; 30: 281-287.



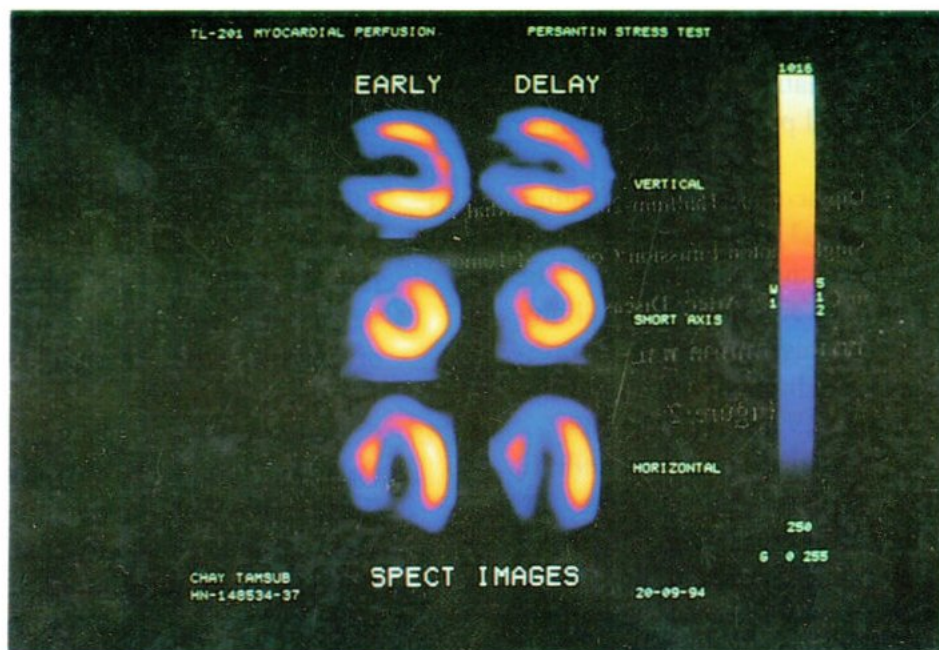


**Fig.3** Dipyridamole stress and redistribution images of thallium-201 myocardial perfusion SPECT study in a patient with coronary artery disease. Coronary arteriography showed 80% stenosis of the left main coronary artery, 70% stenosis of LAD, 65% stenosis of RCA and normal LCX. TI-201 myocardial perfusion images show fixed defects of apex, anterior wall and septum. The inferior and lateral walls look normal.

LAD = left anterior descending artery  
 RCA = right coronary artery  
 LCX = left circumflex artery

9. Leppo J, Bourcher CA, Okada RD, Newell JB, Strauss HW, Pohost GM. Serial thallium-201 myocardial imaging after dipyridamole infusion : diagnostic utility in detecting coronary stenoses and relationship to regional wall motion. *Circulation* 1982; 66 : 649-657.
10. Schmoliner R, Dudczak R, Kronik G, Hutterer B, Kletter K, Mosslacher H, Frischauf H. Thallium-201 imaging after dipyridamole in patients with coronary multivessel disease. *Cardiology* 1983; 70: 145-151.
11. Francisco DA, Collins SM, Go RT, Ehrhardt JC, Van Kirk OC, Marcus ML. Tomographic thallium-201 myocardial perfusion scintigrams after maximal coronary artery vasodilation with intravenous dipyridamole. Comparison of qualitative and quantitative approaches. *Circulation* 1982; 66 : 370-379.
12. Laarman GJ, Verzijbergen JF, Ascoop CA. Ischemic ST-segment changes after dipyridamole infusion. *Int J cardiol* 1987; 14: 384-386.



13. Strauss HW, Harrison K, Langan JK, Lebowitz E, Pitt B. Thallium-201 for myocardial imaging. Relation of thallium-201 to regional myocardial perfusion. *Circulation* 1975; 51: 641-645.
14. Beller GA. Pharmacologic stress imaging. *JAMA* 1991; 265: 633-638.
15. Ranhosky A, Kempthorne-Rawson J. The safety of intravenous dipyridamole thallium-201 myocardial perfusion imaging. Intravenous dipyridamole thallium imaging study group. *Circulation* 1990; 81: 1205-1209.
16. Granato JE, Watson DD, Belardinelli L, Cannon JM, Beller GA. Effects of dipyridamole and aminophylline on hemodynamics, regional myocardial blood flow and thallium-201 washout in the setting of a critical coronary stenosis. *J Am Coll Cardiol* 1990; 16: 1760-1770.
17. Beller GA, Holzgrefe HH, Watson DD. Effects of dipyridamole-induced vasodilation on myocardial uptake and clearance kinetics of thallium-201. *Circulation* 1983; 68: 1328-1338.
18. Beller GA, Holzgrefe HH, Watson DD. Intrinsic washout rates of thallium-201 in normal and ischemic myocardium after dipyridamole-induced vasodilation. *Circulation* 1985; 71: 378-386.
19. Okada RD, Leppo JA, Boucher CA, Pohost GM. Myocardial kinetics of thallium-201 after dipyridamole infusion in normal canine myocardium and in myocardium distal to a stenosis. *J Clin Invest* 1982; 69: 199-209.
20. Weich HF, Strauss HW, Pitt B. The extraction of thallium-201 by the myocardium. *Circulation* 1977; 56: 188-191.
21. Dahlberg ST, Leppo JA. Myocardial kinetics of radiolabeled perfusion agents: Basis for perfusion imaging. *J Nucl Cardiol* 1994; 1: 189-197.
22. Grunwald AM, Watson DD, Holzgrefe HH Jr, Irving JF, Beller GA. Myocardial thallium-201 kinetics in normal man and ischemic myocardium. *Circulation* 1981; 64: 610-618.
23. Rigo P, Becker LC, Griffith LS, Alderson PO, Bailey IK, Pitt B, Burow RD, Wagner HN Jr. Influence of coronary collateral vessels on the results of thallium-201 myocardial stress imaging. *Am J Cardiol* 1979; 44: 452-458.
24. Cuocolo A, Pace L, Ricciardelli B, Chiariello M, Trimarco B, Salvatore M. Identification of viable myocardium in patients with chronic coronary artery disease: Comparison of thallium-201 scintigraphy with reinjection and technetium-99m-methoxyisobutyl isonitrile. *J Nucl Med* 1992; 33: 505-511.
25. Willerson JT, Campbell WB, Winniford MD, Schmitz J, Apprill P, Firth BG, Ashton J, Smitherman T, Bush L, Buja LM. Conversion from chronic to acute coronary artery disease: Speculation regarding mechanism. *Am J Cardiol* 1984; 54: 1349-1354.
26. Feldman RL. Coronary thrombosis, coronary spasm, and coronary atherosclerosis and speculation on the link between unstable angina and acute myocardial infarction. *Am J Cardiol* 1987; 59: 1187 - 1190.
27. Brown KA, Osbakken M, Boucher CA, Strauss HW, Pohost GM, Okada RD. Positive exercise thallium-201 test responses in patients with less than 50% coronary stenosis: Angiographic and clinical predictors. *Am J Cardiol* 1985; 55: 54-57.



## INTEGRATED SOFTWARE TOOLS FOR THE CALCULATION IN RADIOTHERAPY

Chonlakiet KHORPRASERT M.D. Kanjana SHOTELERSUK M.D.  
Chotika JUMPANGERN Msc.

### ABSTRACT

To enhance quality and readiness of treatment with radiation at division of radiation oncology, Chulalongkorn Hospital, we have invented the integrated software tools for various calculation in radiotherapy. The program was written on personal computer and Microsoft Access was chosen as a programming environment because of its powerful database management, calculation and graphic capabilities. There are several separated modules for each calculation. The modules consist of the radiation isoeffect dose module for radiobiological dose calculation, the monitor unit module for double-checking of monitor unit for a linear accelerator, the percentage depth dose module for quick finding of percentage depth dose of single field radiation treatment, the craniospinal technique calculation module, the gap between adjacent fields module, the body surface area module for quick calculation of body surface area, the activity of radioisotope module for calculation of residual activity of radioisotope after known time interval and tangential breast technique module for calculation in simulation of breast irradiation.

### INTRODUCTION

Computer can be used in the field of radiation oncology in many ways. Radiotherapy treatment planning, information storage, interactive tutorial and clerical functions are frequently mentioned and sold by commercial company. Those systems are costly, inflexible, not widely used and typically based on mainframe or minicomputers. Because Powerful and relatively inexpensive microcomputers have been available for many years. With the development of icon-based windowing operating systems and hardware optimized for graphics, they have enable us to write a very complex program but easily to used. There have been prior published reports of microcomputer used for calculation in radiotherapy, a text-based system with limited scope, such as spreadsheets for dosimetric calculations.<sup>6</sup> So the graphical user interface calculation program has been developed at Chulalongkorn Hospital since August 1995.

### METHODS AND MATERIALS

#### Hardware

The minimum requirements for hardware are :

1. A personal computer based upon the Intel 80486 or Intel Pentium processor series.
2. Hard disk which has at least 40 megabytes of free disk space.
3. RAM (Random Access Memory) which has at least 8 megabytes.
4. Color graphic display and color monitor.
5. Mouse and keyboard.

These hardwares are relatively inexpensive and widely available in Thailand.

#### Programming environment

We chose Microsoft Access version 7 that needs Microsoft Window 95 to run as a programming environment. Microsoft Window 95 is operating system that is widely used in the world and consists of many powerful tools. Microsoft Access version 7 was chosen as the programming environment because of its powerful database management, calculation and graphic capabilities. The written program has many tables, forms, macros and codes. Tables are collections of data about physic parameters for monitor unit and percentage depth dose calculation such as field size factors, tray factors, wedge factors,



tissue maximum ratios (TMRs), equivalent areas of rectangular fields and percentage depth doses. Forms are used as data entry tools or switchboards. They contain text fields, calculation fields, graphics and various controls ("buttons, list box, combo box"). Macros are sets of actions and codes are sets of Visual Basic Programming Codes that do some tasks such as opening a form or printing a report. The macros or codes may be associated with any fields, forms or controls, and their actions will be activated so that a specific event is detected such as clicking left mouse button or double clicking left mouse button.

## Data

Data for the program were obtained from both private and published sources. Raw data for monitor unit calculation such as field size factors, tray factors, wedge factors, TMRs, percentage depth doses measured by physicists during the installation of the linear accelerator are kept in spreadsheet format. They were changed to the database format for easy retrieve. Most of the equations in the program were abstracted from published sources.

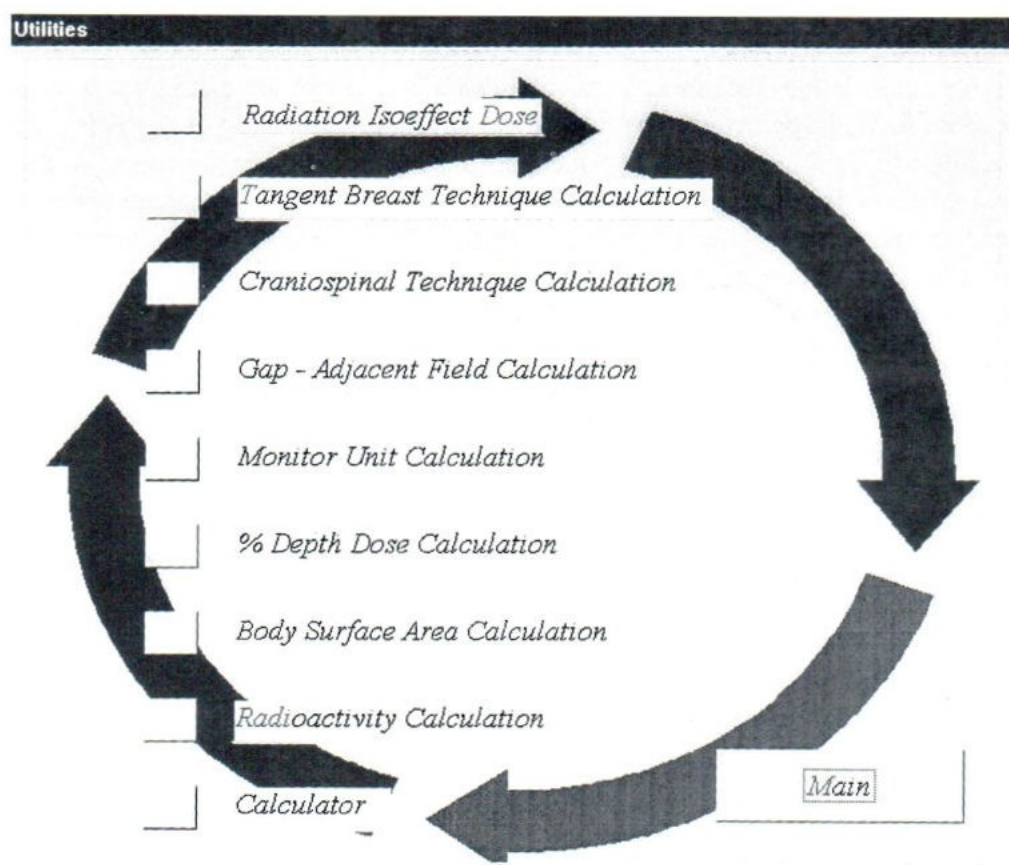


**Fig. 1** Main menu screen.

## RESULT

The modules, created to date, include the radiation isoeffect dose module, the monitor unit module, the percentage depth dose module, the craniospinal technique calculation module, gap between adjacent fields module, body surface area module, activity of radioisotope module and tangential breast technique module. Details of all modules are described below.

Because of graphic user interface of the operating system, the user just move the mouse over various areas of the screen and click the left mouse button that indicate the chosen module to be activated (Figure 1). This main menu is the form that include all the modules in the program. After finishing each module, it always goes back to the main menu automatically.

### Radiation isoeffect dose module

Despite the increasing accumulation of radio-biological data, radiotherapy planning does not take into account the biologically effective dose of irradiated tissues. Altered fractionation regimens is a challenging treatment in modern radiotherapy. The radiation isoeffect dose module is designed for calculation of biologically effective dose in radiation treatment. The module can compute the different fractionation schemes based upon the same biologically effective dose. The module contains three equations as followings :

#### 1. Linear-quadratic module (Fig. 2)

The calculation is based upon the extrapolated response dose model, as proposed by Barendsen (1982) and developed by Dale (1985).<sup>1,2</sup> This model is based on the linear-quadratic relationship between dose and bioeffect which is found on cell survival and microdosimetric theories. The ERD\* equations for fractionated for high dose rate fractionated treatment and low dose rate continuous treatments are shown in equation 1 and equation 2 respectively.

#### Equation 1

$$ERD = Nd \left[ 1 + \frac{d}{\alpha / \beta} \right]$$

ERD = Extrapolated response dose (Gy)

N = Number of fractions

d = Dose per fraction (Gy)

$\alpha/\beta$  Tissue - specific parameter (Gy)

#### Equation 2

$$ERD = RT \left\{ 1 + \frac{2R[1 - 1/(\mu T)]}{\mu(\alpha / \beta)} \right\}$$

ERD = Extrapolated response dose (Gy)

R = Dose - rate (Gy/h)

T = Implant time : T > 10 h

$\mu$  = Tissue specific parameter ( $h^{-1}$ )

\* ERD = Extrapolated response dose (Gy)

LQ HDR

LQ Formula for HDR
Close

Standard Fractionations

Dose per fraction (Gy):

Number of fraction:

alpha/beta

ERD results

ERD ( alpha/beta)

ERD3

ERD10

Changing of Dose/fraction

If New dose per fraction(Gy):

Therefore New No. of fraction(alpha/beta):

Therefore New No. of fraction(ERD3):

Therefore New No. of fraction(ERD10):

Changing of No. of fraction

If New No. of fraction:

Therefore New dose per fraction:

Therefore New dose per fraction(ERD3):

Therefore New dose per fraction(ERD10):

**Fig. 2** LQ formula for HDR screen. This screen based on equation 1. After entering the standard fractionation, the user can change dose per fraction or number of fraction, and the program will calculate the new number of fractions or the new dose per fraction correspondingly.



**Nominal Standard Dose**

<i>Nominal Standard Dose</i>		<i>Close</i>
<div style="text-align: center; border-bottom: 1px solid black; margin-bottom: 10px;"><i>Standard Fractionations</i></div> <div style="margin-bottom: 5px;">Total Dose (cGy): <input style="width: 50px;" type="text" value="7000"/></div> <div style="margin-bottom: 5px;">Total Time (day) <input style="width: 50px;" type="text" value="45"/></div> <div style="margin-bottom: 5px;">Number of fraction: <input style="width: 50px;" type="text" value="35"/></div>	<div style="text-align: center; border-bottom: 1px solid black; margin-bottom: 10px;"><i>NSD results</i></div> <div style="margin-bottom: 5px;">NSD skin: (T=0.11,N=0.24) <input style="width: 80px;" type="text" value="1961.86"/></div> <div style="margin-bottom: 5px;">NSD spinal cord: (T=0.377,N=0.058) <input style="width: 80px;" type="text" value="1469.25"/></div>	
<div style="border: 1px solid black; display: inline-block; padding: 5px 20px;"><i>Changing Number of fraction and total time</i></div>		
<div style="margin-bottom: 5px;">If New Number of Fraction: <input style="width: 50px;" type="text" value="1"/></div> <div style="margin-bottom: 5px;">If New Total Treatment time (day): <input style="width: 50px;" type="text" value="1"/></div>	<div style="margin-bottom: 5px;">Total Dose skin(cGy): (T=0.11,N=0.24) <input style="width: 80px;" type="text" value="1961.86"/></div> <div style="margin-bottom: 5px;">Total Dose brain(cGy): (T=0.44,N=0.06) <input style="width: 80px;" type="text" value="1165.50"/></div> <div style="margin-bottom: 5px;">Total Dose spine(cGy): (T=0.377,N=0.058) <input style="width: 80px;" type="text" value="1469.25"/></div>	

**Fig.3** Nominal standard dose screen. After input the fractionation data, the NSDs are shown, and the user can change number of fractions or total treatment time that base upon the previous NSD.

## 2. Nominal Standard Dose Module (Fig.3)

The calculations are based upon the Ellis nominal standard dose (NSD).<sup>3</sup> The constant parameters for overall treatment time of days and number of fractions were changed according to specified tissues such as skin in equation 3.

Equation 3

$$D = (NSD) T^{0.11} N^{0.24}$$

$D$  = Total treatment dose (Gy)

$T$  = Overall time (day)

$N$  = Number of fractions

## Tangent Breast Technique Module

This is a graphic illustration one of methods of calculating the location of isocenter of tangential irradiating technique for breast carcinoma. The calculations based upon trigonometric functions as shown below.

$$D = \frac{1}{2} (s \cos(d)) - W(\sin(d))$$

$$S = \frac{1}{2} (s \sin(d)) - W(\cos(d))$$

$D$  = Depth of Isocenter (cm.)

$S$  = Shift of Isocenter (cm.)

$s$  = Separation of Tangent Field (cm.)

$d$  = Degree of Tangent Field

$W$  = Width of Tangent Field

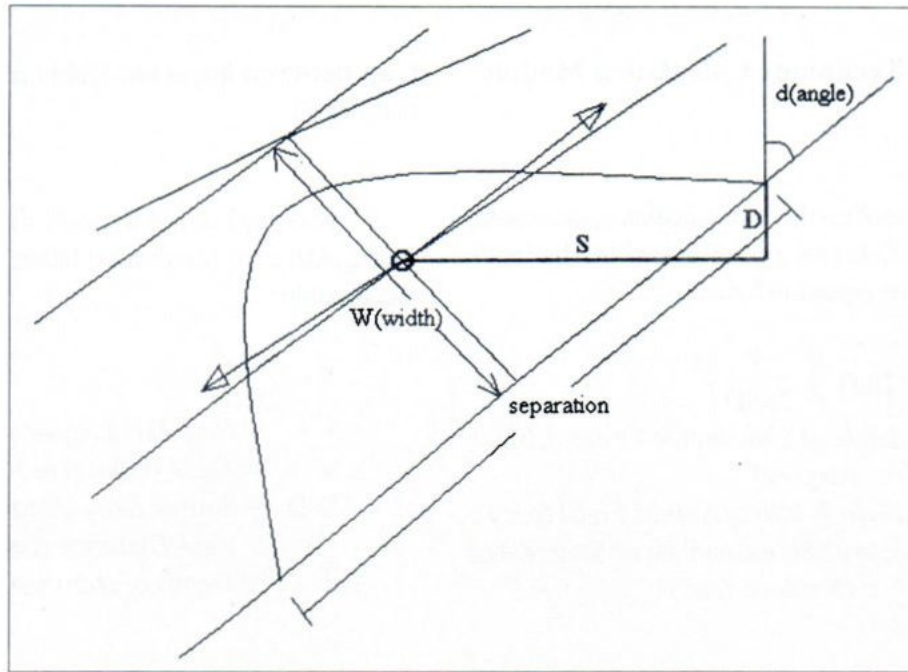


**Fig.4** Illustration of tangent breast technique calculation.

To find the location of the isocenter, the user must enter the parameters that can be measured by our special designed ruler, field width, separation of field and bridge angle of field (Figure 4). With this technique, it takes few minutes to simulate tangential field technique for breast irradiation.

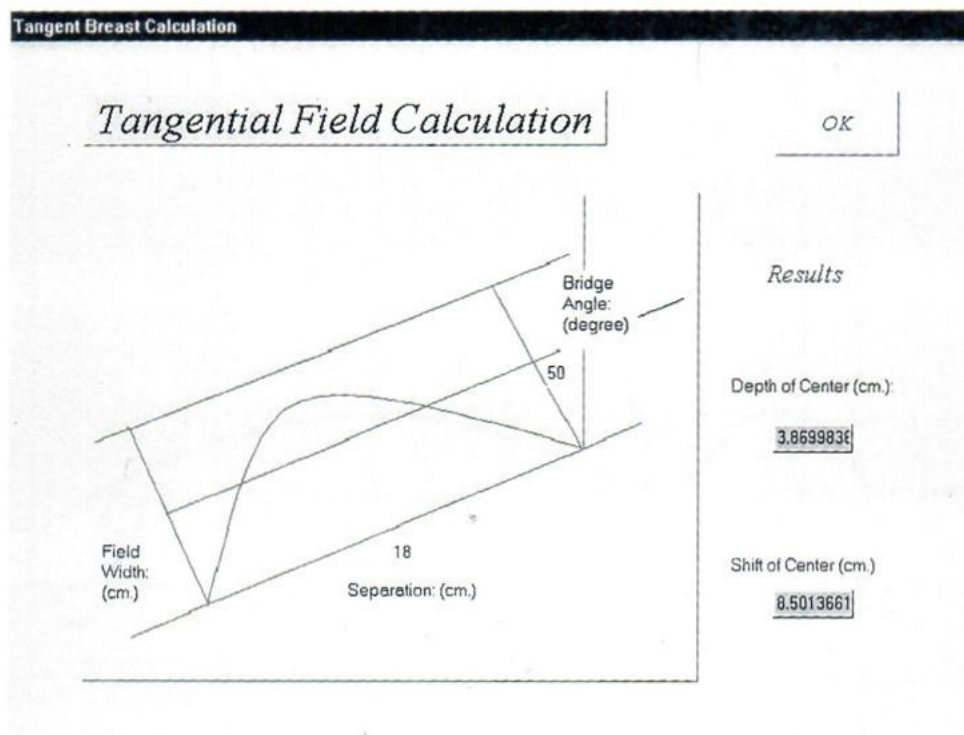


**Fig.5** Tangential field calculation screen. After input three parameters, field width, separation and bridge angle, the program will show the location of the treatment isocenter. Depth of isocenter is the depth of isocenter at midline of patient, and shift of isocenter is the distance from midline of the patient to isocenter.



### Craniospinal Technique Calculation Module (Figure 6)

This is one of methods of calculating collimator angle of cranial field in the craniospinal irradiation. It is based upon the equation below.

$$\text{Angle} = \tan^{-1} \left( \frac{w}{2SSD} \right)$$

Angle = Angle of Collimator Cranial Field  
(degree)

w = Field Width of Spinal Field (cm.)

SSD = Source Skin Distance or Source Axis  
Distance (cm.)

### Gap between adjacent fields module (Figure 7)

This module has a simple illustration of calculating skin gaps for abutted fields. The equation for this module is:

$$S = \frac{w \times d}{2SSD}$$

S = Half Field Separation (cm.)

w = Field Width (cm.)

SSD = Source Skin Distance or Source  
Axis Distance (cm.)

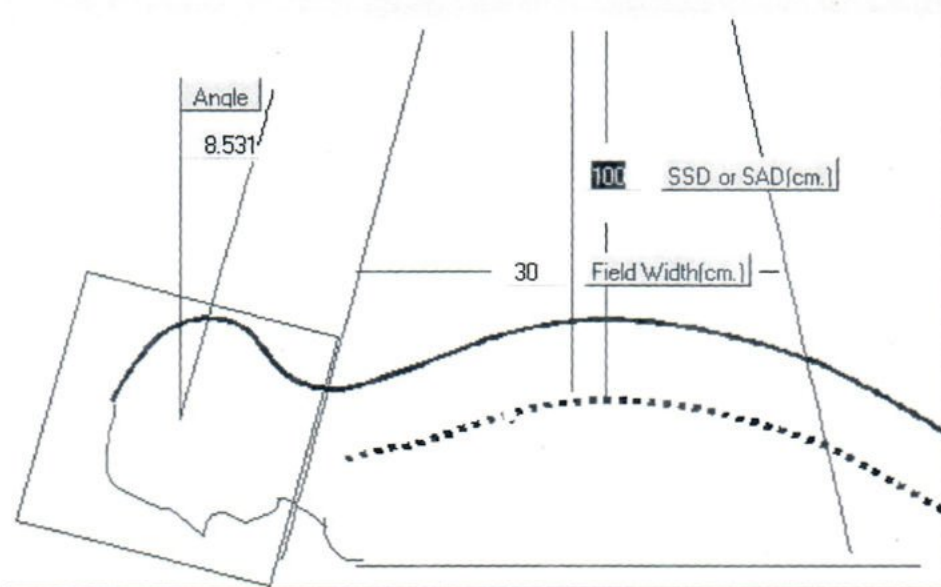
d = Depth of treatment (cm.)

#### Craniospinal Irradiation

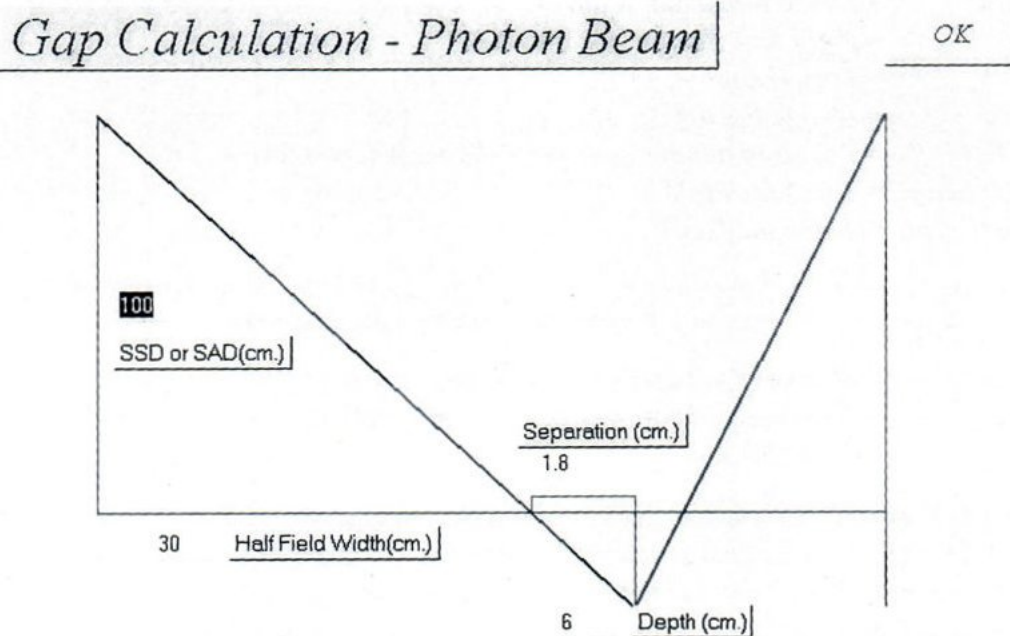
*Craniospinal Irradiation*

*Collimator Angle of Cranial Field*

OK



**Fig.6** Craniospinal irradiation screen. After the user enters the SSD or SAD of the spinal field and the width of the spinal field, the collimator angle will be shown.

**Craniospinal Irradiation**

**Fig.7** Gap calculation screen. To find out the half field separation, three parameters, SSD or SAD, half field width and depth of treatment.

### Monitor unit module

This module is a sophisticated module, and can be used as an independent check for the consistency of radiation therapy dose calculations. It verifies the calculated monitor units (MU) required to deliver a prescribed dose to a certain point on an isodose line to the monitor units calculated manually by the technologist or by any commercial treatment planning system. There are many tables that contain numerous data about physics parameters for monitor unit and percentage depth dose calculation such as field size factors, tray factors, wedge factors, TMRs (Tissue Maximum Ratios), equivalent areas of rectangular

fields and percentage depth doses. For photon monitor unit calculation, 6 and 10 MV modules are available. For electron monitor unit calculation, 6, 9, 12, 16, 20 MeV modules are available. The user can move the mouse over different areas of the form and click to indicate which of the input data items are to be changed. After the user specifies treatment parameters by easy clicking left mouse button within the list box of specific item or by entering number in some fields, the number of monitor unit will be shown immediately. The equation used in this module is:<sup>4</sup>



$$MU = \frac{TD}{TMR \times Fs \times Tf \times Wf \times SSDfactor}$$

$MU$  = Monitor Unit  
 $TMR$  = Tissue Maximum Ratio  
 $Fs$  = Field Size Factor  
 $Tf$  = Tray Factor  
 $Wf$  = Wedge Factor  
 $TD$  = Required tumour dose per field per fraction (cGy)  
 $SSDfactor$  = 1.030 for 6MV  
 $SSDfactor$  = 1.051 for 10MV

For photon monitor unit calculation

$$MU = \frac{TD}{0.8 \times CF}$$

$MU$  = Monitor Unit at 80% isodose line  
 $TD$  = Required tumour dose per field per fraction (cGy)  
 $CF$  = Cone Factor

For electron monitor unit calculation

In the calculation of one treatment field, the user first enters the tumour dose in centigray and then selects type of tray and wedge. After the area is selected, the program will find out the field size factor for that area and display only various TMRs of the specified area according to depth of tumour. Finally, the user just selects depth of tumour and the program will show the monitor unit of the treatment in less than one second. It also has automatic recalculation feature updates the monitor units as each parameter is changed. (Fig. 8)

6MV : Form

**The Monitor Units**

**Tumor Dose**  
 cGy

**Tray**  
 No Tray 1  
 Tray .972

**Wedge**  
 15 .78  
 30 .636  
 45 .485  
 60 .419  
 No 1

**Area** 16 ▲ .935  
 20  
 25  
 30  
 36  
 40  
 45  
 49  
 55  
 60  
 64  
 70  
 75  
 81  
 85  
 90  
 100  
 105  
 110  
 115  
 121  
 125  
 130  
 135  
 140  
 144 ▼

**TMR**  
 1.5 1  
 2 .993  
 2.5 .986  
 3 .979  
 3.5 .965  
 4 .949  
 4.5 .935  
 5 .917  
 5.5 .901  
 6 .885  
 6.5 .868  
 7 .851  
 7.5 .837  
 8 .82  
 8.5 .804  
 9 .789  
 9.5 .772  
 10 .756  
 11 .723  
 12 .693  
 13 .665  
 14 .638  
 15 .613  
 16 .587  
 18 .54  
 20 .496

**Equivalent Areas**  
 5 5 25  
 6 5 30.3  
 6 6 36  
 7 5 33.6  
 7 6 42.3  
 7 7 49  
 8 5 38.4  
 8 6 47.6  
 8 7 56.3  
 8 8 64  
 9 5 42.3  
 9 6 51.8  
 9 7 62.4  
 9 8 72.3  
 9 9 81  
 10 5 44.9  
 10 6 56.3  
 10 7 67.2  
 10 8 79.2  
 10 9 90.3  
 10 10 100  
 11 5 47.6  
 11 6 60.8  
 11 7 74  
 11 8 86.5  
 11 9 98  
 11 10 110 ▼

**Monitor Unit** 394.7555271

Close

Fig. 8 Monitor unit screen for 6MV.

### Body surface area module

Most of the radiation oncologists in Thailand treat their patients not only by radiation but also combined with chemotherapeutic drugs, so this module should be useful for our staffs. Two parameters, weight and height of a patient, have to be involved. The equation is shown below.

$$BSA = \sqrt{\frac{w \times h}{3600}}$$

$$\begin{aligned} BSA &= \text{Body Surface Area} \\ w &= \text{Weight (kg.)} \\ h &= \text{Height (cm.)} \end{aligned}$$

### Activity of radioisotope module

This module shows the decay activity of radioactive material frequently used in radiotherapy. The equation for this module is:

$$A = A_0 e^{-\lambda t}$$

$$\begin{aligned} A &= \text{Activity at time } t \text{ (Ci.)} \\ A_0 &= \text{Original Activity (Ci.)} \\ \lambda &= \text{Transformation Constant} \\ t &= \text{time (day)} \end{aligned}$$

## DISCUSSION

At the division of radiation oncology, Chulalongkorn Hospital, we need tools for calculation to help us in our routine work because of the overloaded number of patients. These tools should be easy to handle and should have quick calculation results and good database management. With windowing operating system, the users can use various programs without hard effort. Our program can be useful not only for radiation oncologist, but also for physicists and technologists. Fractionations of radiation treatment can be changed quickly based on the linear-quadratic relationship or Ellis nominal standard dose equation by using the radiation isoeffect module. During the simulation, the radiation oncologists can calculate various parameters by the

tangent breast technique module, the craniospinal technique calculation module and the gap between adjacent fields module. Monitor unit calculation is very important in radiation treatment. Precise doses of radiation delivered to treat the patients come from the correct monitor unit calculation. In manual calculation, the physicist has to search for many parameters for the equation mentioned above from a big bunch of data file, and make calculation by calculator. With the monitor unit calculation module, the physicist just only enters number or click to select the parameters and rapidly get the answer. The body surface area module and the activity of radioisotope module are also used frequently as the others.



**REFERENCE**

1. Barendsen GW, Dose fractionation, dose rate and iso-effect relationships for normal tissue responses, *Int. J. Radiat. Oncol. Biol. Phys.* 8: 1981-1997, 1982
2. Dale RG, The application of the linear-quadratic dose effect equation to fractionated and protracted radiotherapy, *Brit. J. Radiology* 58: 515-528; 1985
3. Eric J. Hall : The concept of Nominal Standard Dose. In : *Radiobiology for The Radiologist* 1st ed. USA : Harper & Row, Publishers, 1973 : 261-266
4. Faiz M. Khan : A System of Dosimetric Calculations. In : *The Physics of Radiation Therapy* 2nd ed. USA : Williams & Wilkins, 1994 : 200-225
5. Faiz M. Khan : Nuclear Transformations. In : *The Physics of Radiation Therapy* 2nd ed. USA : Williams & Wilkins, 1994 : 12-31
6. Starkschall, G.; Riggs, J.D. Use of a personal computer and spreadsheet software for treatment machine time calculations. *Int. J. Radiat. Oncol. Biol. Phys.* 11: 1896-1872; 1985.

## LEAD BEADS: THE USE AS THE IRREGULAR FIELD SHIELDING

Lalida TUNTIPUMIAMORN, M.Sc<sup>1</sup>  
Nuanpen DAMRONGKIJUDOM, B.Sc<sup>1</sup>  
Surat VINIJSORN, M.Eng<sup>1</sup>  
Prasert ASSAVAPRATHUANGKUL, B.Sc<sup>2</sup>  
Yutthapol WICHINEN, B.Sc<sup>3</sup>

### ABSTRACT

The use of lead beads in the irregular field shielding to replace the normal custom block is presented. By studying the shielding efficiency of two bead sizes ( $3.52 \pm 0.37$  mm and  $5.13 \pm 0.43$  mm in diameter) with two packing methods, pressure and unpressure packing. From the study, it revealed that the small beads with pressure packing method (HVL = 1.6 cm) has a little higher shielding efficiency depending on the dense of the beads. To provide the convenience in a practical use, the two perspex trays were designed to mounted with the collimator beam shaping rails (MURT 37/1) and table mounted beam shaping tray (MURT 37/2) to fit to the treatment couch of the Cobalt-60 machine for the larger field size. Test of accuracy and reproducibility in shielding position were accomplished by radiographic film. Comparison of shielding effect between the shielding blocks made by alloy and lead beads are also presented. Advantages in the use of lead beads are the ease and rapidity construction. Moreover, it is economical and no need of melting in the re-used. The only problem is that much care has to be taken for the correct position of the shielding block. It can be concluded from the study that the lead bead is practical for shielding irregular shaped field, especially in an urgent situation in megavoltage therapy.

### INTRODUCTION

The shaping of treatment fields is primarily dictated by tumour volume. Not only the critical organs but also the normal tissue surrounding should be spared. From this reason, the treatment fields sometimes are complex and irregular in shape that required the use of shielding block. Most common the shielding blocks are made of lead. But in 1973, Power et al.<sup>1</sup> suggested the use of alloy (or Lipowitz metal or brand name cerrobend). The alloy is a combination of bismuth 50%, lead 26.7%, tin 13.3% and cadmium 10%. The advantage of alloy to lead is its lower melting point (70°C) than lead's (327°C).<sup>2</sup> Thus it can be easily made into any shape. However,

some problems encountered in the use of alloy. Primarily, in Thailand, alloy was introduced from abroad, so the cost is very high (approx 800 baht/kg). Secondly, in the process of making alloy, without attention, sometimes there are air bubbles inside that they can minimize the shielding efficiency.<sup>2</sup> Finally, it takes 1-2 days before alloy shielding block can be introduced to the patients. Therefore the use of lead beads to replace the alloy in the irregular field shielding has been developed. Since it is economical (20 baht/kg) and no need of melting in the re-used process. This study will investigate the shielding efficiency, the procedure of construction and the convenience in the use of lead beads compared with alloy.

<sup>1</sup> Division of Radiation Oncology, Faculty of Medicine, Siriraj Hospital, Mahidol University

<sup>2</sup> Division of Radiation Oncology, Faculty of Medicine, Ramathibodi Hospital, Mahidol University

<sup>3</sup> Department of Radiological Technology, Faculty of Medical Technology, Mahidol University



## MATERIALS AND METHODS

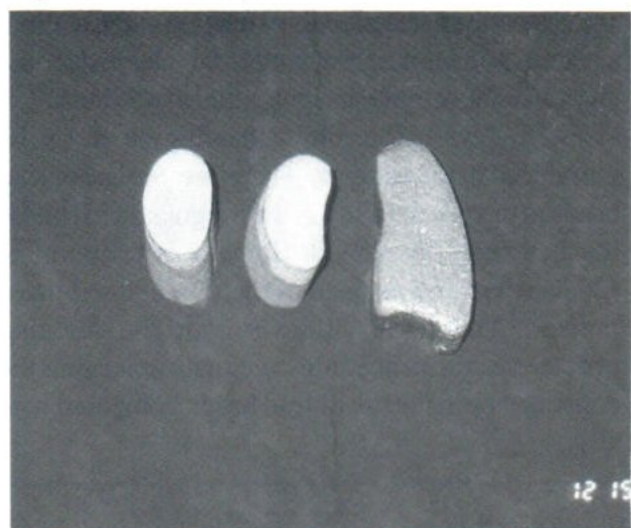
1. Cobalt-60 Teletherapy machine
2. Farmer Dosemeter type 2570/A/B
3. Water phantom 30 x 30 x 20 cm<sup>3</sup>.
4. Styrofoam cutter
5. Densitometer
6. Two lead bead sizes ( $3.52 \pm 0.37$  mm and  $5.13 \pm 0.43$  mm diameter)
7. Perspex sheets

The investigation in shielding efficiency between the two sizes of lead beads and the methods of packing them into the styrofoam block mold was done by measuring the transmitted radiation in water phantom compared between the same thickness of lead beads and the two packing methods. In the first packing method, lead beads were packed randomly by filling in the mold cavity. The second method is the same as in the first one but only this time the pressure was added at the bead front surface until they were packed and lied dense firmly together. After this packing processes, the transmitted radiation at various points of lead beads in the block mold will also be measured to find the uniformity of shielding efficiency.

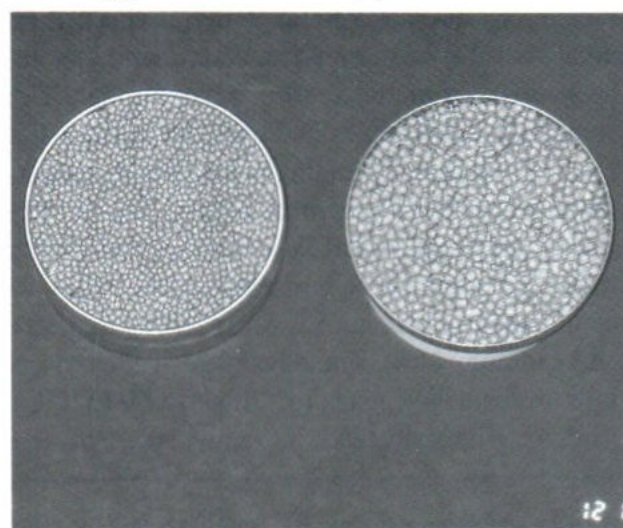
After the first measurement, the size of lead beads and the packing method will be chosen to carry on the HVL findings. Then the two perspex trays were designed to hold the styrofoam block mold with the lead bead inside for at least 5 HVL in depth. The first tray will be fit with the collimator beam shaping rail of the Cobalt-60 machine. Because of the thick-

ness of the styrofoam block, there is no room between the shaping tray and the outer surface of the collimator so the maximum treatment field feasible to this tray was only 26x26 cm<sup>2</sup>. This tray was called MURT 37/1. (Fig 3) To overcome such a problem another tray was designed to fit with the treatment couch for the large treatment field, like Mantle or inverted-Y, the maximum field setting was enlarged to 35x35 cm<sup>2</sup> as shown in Fig 4.

In order to study the shielding efficiency of leads beads compared to alloy, both materials were constructed at the same thickness (5 HVL). By the shielding tray MURT 37/1 and MURT 37/2 the shielding blocks were made for inverted-Y and mantle field treatment respectively. Exposed these two different materials shielding blocks with radiographic film and measured the transmitted radiation in term of the optical density by densitometer. Time consuming in each step of construction was also recorded to compare between alloy and lead beads. Test of accuracy and reproducibility in the shielding position was done by port film.

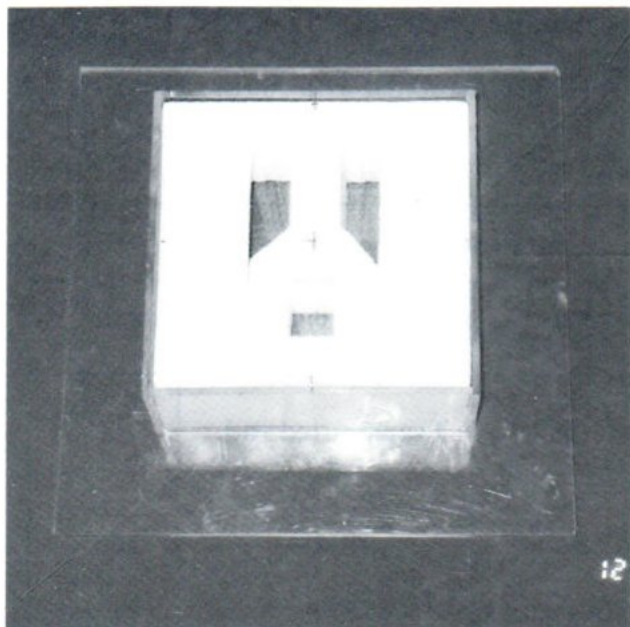
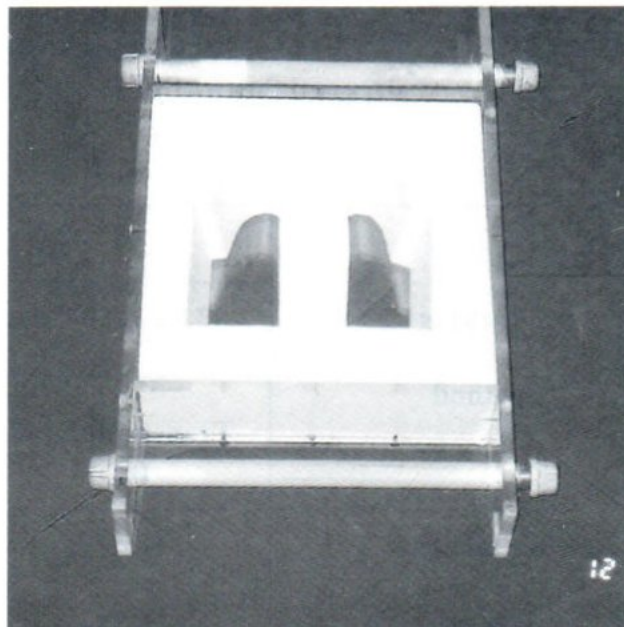
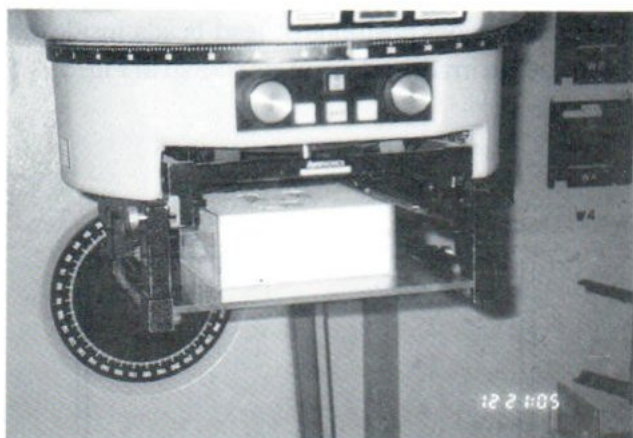


**Fig.1A** Alloy custom blocks



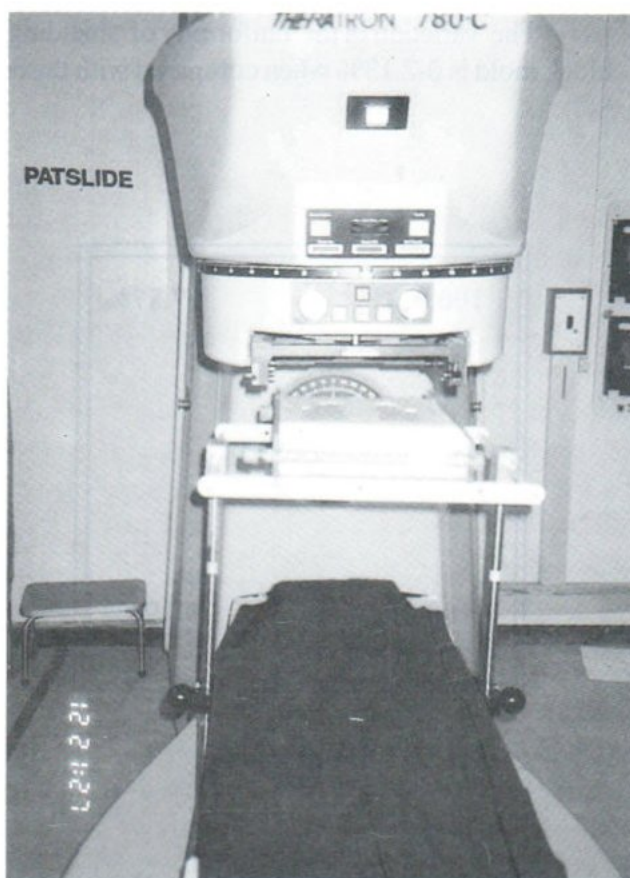
**B.** Lead bead in different sizes



**MURT 37/1****MURT 37/2****Fig.2** The perspex trays MURT (37/1) and MURT (37/2)**Fig.3** The collimator shielding tray (MURT 37/1) that available for maximum field size 26x26 cm<sup>2</sup>

## RESULTS

The shielding efficiency was performed by measuring the transmitted radiation in water phantom by NE dosimeter type 2570 A/B to study the shielding efficiency. The data showed that the shielding effect was not significantly difference in both sizes of the bead and packing methods. But it is obviously seen that the small bead size with the pressure packing gives a little higher shielding efficiency than the others as shown in table 1.

**Fig.4** The table mounted beam shaping tray MURT 37/2 available for the maximum field size 35x35 cm<sup>2</sup>



**TABLE 1**      **The transmitted radiation (nanocoulombs, nC) measured between the two bead sizes and the two different packing methods irradiated with 10 cm x 10 cm Cobalt-60 beam.**

Packing method	Lead beads			
	3.52 + 0.37 mm diameter		5.13 + 0.43 mm diameter	
	Transmitted rad. (nC)	%	Transmitted rad. (nC)	%
-No lead bead	44.4	100	44.4	100
-Unpressure	5.35	12.5	5.25	11.82
-Pressure	4.70	10.58	5.10	11.48

The variation in the uniformity of shielding efficiency in various positions of lead beads inside the block mold is 0-2.13% when compared with the central axis of the irradiated beam as shown in Fig. 5

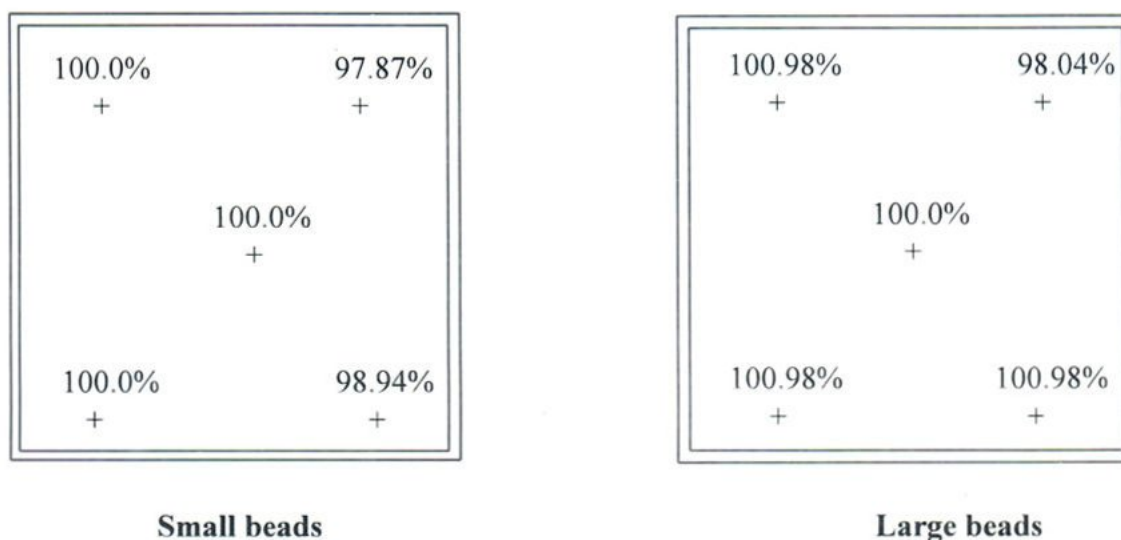


**Fig.5**      The shielding efficiency uniformity of lead beads.

For the shielding efficiency of the small lead beads with the pressure packing method, the HVL measurement was done for three times in the plastic phantom to prove that there is no human error in the packing process. From the measurement, the HVL is

1.6 cm. Then the styrofoam mold with the thickness of 5 HVL were made to fit in the MURT 37/1 and MURT 37/2. The comparison of shielding efficiency between lead bead and alloy was shown in Fig.6 and Fig 7.

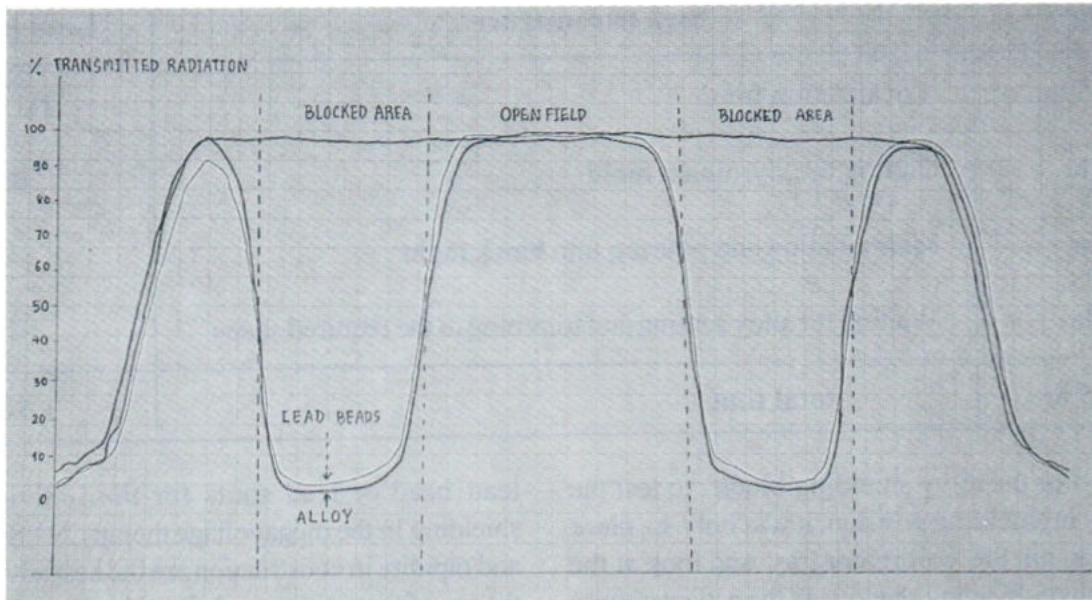


**Fig. 6** The comparison of shielding efficiency between alloy and lead beads in inverted-Y treatment field for collimator shielding tray. (MURT 37/1)

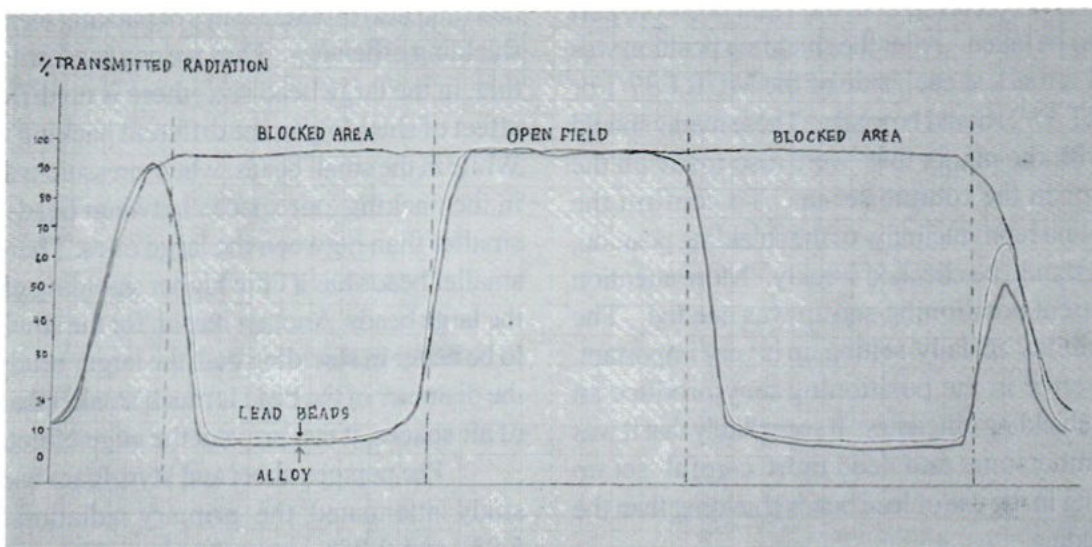


**Fig. 7** The comparison of shielding efficiency between alloy and lead beads in mantle treatment field for table mounted beam shaping tray. (MURT 37/2)



The time-consuming in the construction processes of the alloy and the lead beads shielding block were shown in Table II. The data show that it

takes only 1.5-2 hours to construct the lead beads shielding block compared with 5.5-7.5 hours in the case of an alloy shield.

**TABLE II Time-consuming in each step of construction processes between alloy and lead beads shielding block.**

Alloy	Step to construct	Lead beads
0.5-1.5 hr.	Localization film	1-1.5 hr.
0.5 hr.	Cutting the styrofoam mold	0.5 hr.
0.5 hr.	Melting alloy and pouring into block mold	-
4-5 hr.	Waiting for alloy settling and trimming to the required shape	-
5.5-7.5 hr.	<b>total time</b>	1.5-2 hr.

For the alloy shielding block, to test the accuracy in shielding position, it was only to place the block on the collimator tray and look at the projection of shielding shadow on the patient surface whether it matched with the area we want to block or not. This procedure cannot be done using the lead beads shield. It is the collimator tray that hold the styrofoam mold and the lead beads inside which blocked the light field. The only way to ensure that the lead beads shielding is in the right position, port film has to be taken. After the shielding position was satisfied, a mark at each side of the MURT 37/1 or the MURT 37/2 should be made. These marks should match with the marks that were also made on the collimator in the routine set-up. To confirm the accuracy and reproducibility of the shielding position, port film should be checked weekly. More attention in the patient positioning set-up was needed. The reproducibility in daily setting up is very important. A small error in the positioning may produce an incorrect shielding efficiency. It seems likely that it was more cumbersome and need more careful set up positioning in the use of lead beads shielding than the alloy shielding.

## DISCUSSION

There are some studies in the introduction of

lead bead or lead shots for the individualized shielding in the megavoltage therapy.<sup>4,5,6</sup> Simplicity and rapidity in construction are the best advantage in the use of them. The size of lead beads and the packing method should be determined before bringing them into the routine use. But the study of Abraham W<sup>5</sup> suggested that any size of lead beads with the ideal packing would have the same shielding effect. In this study we have investigated using both sizes of lead bead and also different ways of packing them on their shielding efficiency. Thus we can see from the result that, in the large bead size, there is no difference in effect of shielding in the different packing methods. While in the small beads, when pressure was applied in the packing, air spaces between beads become smaller than between the large ones. Therefore the smaller beads have a little higher shielding effect than the large beads. Another reason for the smaller beads to be better in shielding than the larger beads is that if the diameter of the bead is much smaller than the size of air spaces, it can prevent the edge effect.<sup>5</sup>

The perspex sheet and styrofoam used in this study attenuated the primary radiation beam by 5.9% and 0.85% respectively. This attenuation effect should be accounted for in the dosage calculation.

The limitation in the use of MURT 37/1 and



MURT 37/2 in this study is that it can be used only in the anterior port only. Improvement of shielding tray to provide for any direction of the beam port should be developed.

MURT 37/1 in this study is now put in practical use. Most treatment area of the external beam teletherapy are not greater than 26cmx26cm except for the mantle technique which required the bigger treatment field but the MURT 37/2 can solve this problem.

## CONCLUSION

In the study of introducing the lead beads to be used as an irregular field shielding, we found that.

1. The small size of the lead beads ( $3.52 \pm 0.37$  mm) and the packing method using pressure packing gave the best shielding efficiency.
2. There is a good uniformity of shielding effect in both sizes of lead beads, the small or the large.
3. The HVL of the small lead beads in this study is 1.6 cm
4. The MURT 37/1 tray designed to use with collimator beam shaping rail was applicable for most treatment techniques with the field not greater than  $26 \times 26$  cm<sup>2</sup>. For larger treatment field, MURT 37/2 tray, attached with table mounted beam shaping tray will serve that purpose.
5. MURT 37/1 and MURT 37/2 can be used only for anterior port.
6. The comparison between alloy and lead bead shielding block:

6.1 Considering for the shielding efficiency, alloy and lead beads shield have the same shielding efficiency.

6.2 The time consuming to build the block, lead beads shield can be made easily and rapidly (1.5-2 hr). While for the alloy shield it consume more time to make (5.5-7.5 hr). Moreover, there are some other advantages for the use of lead beads, such as

- no toxicity of evaporation from melting process.
- can be re-used immediately.
- economical price (20 baht/kg) while the alloy cost 800 baht/kg.

6.3 For shielding accuracy, lead beads shield needs more careful and complicated work to setup shielding position than to setup an alloy shield.

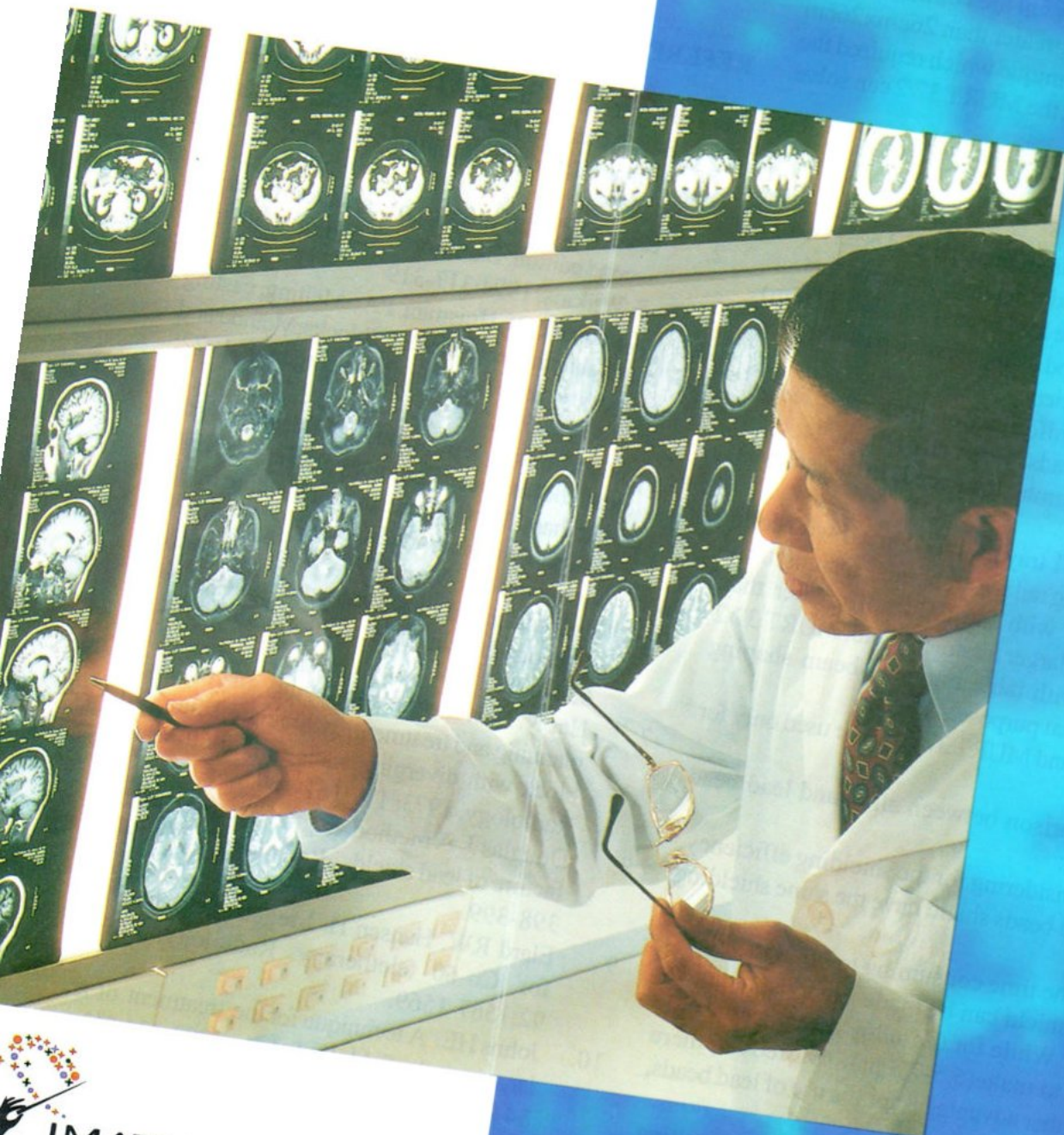
## REFERENCES

1. Power WE, Kinzie JJ, Demidecki AJ et al. A new system for field shaping for external beam radiation therapy. *Radiology*, 1973; 108:407-411.
2. Khan FM. The physics of radiation therapy. second edition. Baltimore / London: Williams & Wilkins, 1994:317-319
3. Kavzmark CJ, Huisman PA. Melting, casting and shaping lead shielding blocks: Method and toxicity aspects. *Am J Roentgenol*, 1972; 114:636-638.
4. Maruyama Y. Comments on shielding by the lead shot method. *Radiology*, 1972; 445: 1972.
5. Abraham W. Comments on shielding by the lead shot method. *Radiology*, 1971; 98:190.
6. Maruyama Y, Moore VC, Burns D. Individualized lung shields constructed from lead shot embedded in plastic. *Radiology*, 1969; 92: 634-635.
7. Has K. New methods to facility radiotherapy planning and treatment, including a solid lead block with diverging walls for Co-60 beam. *Radiology*, 1973; 117:161-167.
8. Douglas J. A method for the accurate manufacture of lead shields. *Radiology*, 1971; 44: 398-399.
9. Elard RW, Hansen H. Irregular field shaping for Co-60 teletherapy. *Radiology*, 1969; 92:1567-1569.
10. Johns HE. A technique for the treatment of a large irregular field. *Radiology*, 1980; 134:543-544.
11. Huen A, Findley Do, Skov DD. Attenuation in Lipowitz's metal of x-ray produced at 2, 4, 10, and 18 MeV and gamma rays from Cobalt-60. *Med Phys*, 1979; 6: 147-148.



## Important developments since we were last 3M.

You knew us as 3M. You counted on us for truly innovative medical imaging solutions and superb service. Now, we're Imation. And we're determined to surpass even your highest expectations with our *Customer First* commitment and broad base of medical imaging solutions that make your organization more effective. More efficient. And more committed.



Imation Singapore Pte. Ltd. (Thailand Representative Office)  
Floor Na-Nakorn Building, 99/349 Chengwatana Rd.,  
Bangkok, Bangkok 10210 Thailand.  
Tel. 662-576-0064, 576-0067-9 Fax. 662-576-0065  
Telex 661-624-9625



## TREATMENT OF COLORECTAL CANCER A MALAYSIAN EXPERIENCE

G.C.C.Lim, FRCR<sup>1</sup>, I. Fuad, MD<sup>2</sup>,  
K.G. Rampal, MPH<sup>3</sup>, A.K.H. Lim, FRCR<sup>4</sup>

### ABSTRACT

Three hundred and twenty patients with colorectal cancer who had undergone treatment in the Institute of Radiotherapy and Oncology, Hospital Kuala Lumpur between 1986 and 1994 were analysed. Patients with tumours of the rectum or rectosigmoid colon made up the largest group (62.5%). Dukes' A disease (1.9%) appeared to be underrepresented while the proportion of patients (11.6%) under the age of 40 years was higher than other studies. The largest racial group in this series was Chinese (61.9%).

Treatment with surgery, radiotherapy and chemotherapy together with the difficulties involved was discussed. The highlights were the lack of serious toxicity of chemotherapy even when used in combination with radiotherapy. The patterns of treatment have been influenced largely by the late stage at presentation, the practical considerations in the population as well as the available resources.

**Keywords:** colorectal cancer, epidemiology, radiotherapy, chemotherapy, recurrence, crude survival

### INTRODUCTION

Rectal cancer was among the four most frequently reported cancers in Penang among Malays, Chinese males and Indian males.<sup>1</sup> Colorectal cancer comprised 7% of the diagnoses of new patients seen in the Institute of Radiotherapy and Oncology, Hospital Kuala Lumpur<sup>2</sup> which is the national referral centre for cancer in Malaysia.

Modest improvements in overall survival and disease-free survival have been demonstrated in trials on adjuvant chemotherapy and adjuvant radiotherapy.<sup>3,4,5,6,7,8,9</sup> On the other hand, the role of palliative radiotherapy and palliative chemotherapy have been established in other studies.<sup>10</sup>

The objectives of this study are to review treatment of colorectal cancer in this centre, the morbidity associated with chemotherapy and radiotherapy, the problems encountered, and the patterns of recurrence and survival of these patients.

### MATERIALS AND METHODS

A retrospective study of patients with colorectal cancer treated at the Institute of Radiotherapy and Oncology, Hospital Kuala Lumpur was conducted. The study population were patients presenting as new cases of colorectal cancer and who had undergone treatment in this Institute between 1986 and 1994.

The sample included all patients who met the following inclusion criteria: any primary malignant tumour arising for the colon or rectum (between the ileo-caecal junction and the anorectal junction), and histologically verified by a pathologist. The exclusion criteria applied in this study were: patients with primary anal cancers, metastatic cancers with unknown primary sites of disease, no histological verification, and patients whose records could not be traced.

Data was collected using a check-list ques-

<sup>1,2,4</sup> Institute of Radiotherapy and Oncology, Hospital Kuala Lumpur

<sup>3</sup> Department of Community Health, Faculty of Medicine, Universiti Kebangsaan, Malaysia, Kuala Lumpur



tionnaire. Case notes, referral letters, histopathology reports, laboratory tests, operation findings, radiotherapy records, simulator films and other relevant investigations were reviewed. The records were retrieved manually. Information on chemotherapy, radiotherapy treatment and complications of treatment was retrieved from the case notes. Staging of colorectal cancer was based on the Dukes' Classification.<sup>11</sup> Chemotherapy toxicities were graded according to recommendations by the World Health Organization.<sup>12</sup> Marrow suppression that was recorded in this study reflected the most severe of the various haematological toxicities. Performance status of patients on presentation to the Radiotherapy Clinic was based on Zubrod Scale.<sup>13</sup>

Crude survival time was calculated from the date of primary surgery to the date of last follow-up or to the date of death due to any cause. Relapse-free interval was calculated from the date of Primary Surgery to the date of first relapse. Patients who had macroscopic residual disease post-operatively were considered to have no disease-free interval. The dates of notification of death of patients who were lost to follow-up were provided by the Malaysian National Registration Department. The status of 16 patients are still unknown as their identification card numbers were not traceable from our records or they were from areas other than Peninsular Malaysia. Data was entered into a database management programme (DBASE IV) and analysed using EPID INFO Version 5.

## RESULTS

Data from a total of 320 patients' records were analysed. The median age of the study population was 56 years with the age distribution ranging from 13 years to 87 years. The male:female ratio was 1.3:1. The majority of the patients were Chinese. Patients with tumours involving the rectum or rectosigmoid regions made up the largest group (62.5%). Only a fifth of the tumours were well-differentiated in grade. Patients who had tumours that were limited to the bowel wall formed a distinct minority. At least half of the patients had metastatic disease at presentation [Table 1]. The commonest

presenting symptoms in this study were alteration in bowel habits (53.8%), rectal bleeding (44.1%) and abdominal pain (37.2%).

Concurrent diseases were: villous adenoma (2 cases), ulcerative colitis/inflammatory bowel disease (1 case), Familial Polyposis Coli (2 cases). The majority of the patients had a Zubrod status of 0 to 2 (83.8%). Performance status was poor in 15.6% while it was unknown in 0.6%.

Forty per cent of patients are known to have died [Table 2]. Recurrences occurred in nearly 60% of patients. Sole recurrences at the local site was the commonest form of relapse [Table 3]. Dukes' C patients had the highest local relapse rate (29.2%) compared to Dukes' A and B (16.5%).

Some sites of disease spread were: forehead (1 patient), parametrium (1 patient), vagina (2 patients), Fallopian tube (1 patient) and anterior abdominal wall (2 patients) and one patient experienced recurrence in the bladder eight years later. Other sites of spread included the anus, scrotum, para-aortic and inguinal lymph nodes. Spread to the supraclavicular fossa lymph nodes was not a prominent feature.

Three hundred and eight patients (96.2%) had records of having surgery, 222 patients (69.4%) had chemotherapy while 168 patients (52.5%) had radiotherapy. Treatment was multimodal in most of the patients.

Abdomino-perineal resections, anterior resections and Hartman's procedures together accounted for 53.7% of the operations. Palliative surgery such as defunctioning colostomy was possible in 9.4% while no surgery was performed in 3.7%. Bulky disease was a feature in at least a third of patients presenting to our department.

Chemotherapy was given in 222 patients (69.4% of the study population). Palliative chemotherapy was given in 123 while adjuvant chemotherapy was used in 98. The intent of chemotherapy for one patient was not ascertainable as it was received at another hospital.

A regime containing 5-fluorouracil was used in all chemotherapy patients except in one patient. 5-Fluorouracil alone was the most frequently used regime (64%). Levamisole was used together with 5-fluorouracil in both adjuvant and palliative settings



in 16%. Leucovorin factor plus 5-fluorouracil was given palliatively in only 2% of patients. Fluorouracil was most frequently prescribed via the oral route (48%); a continuous infusion over 5 days once every three weeks was employed in 23%.

The chemotherapy used was generally well tolerated. This was reflected in the toxicity profile of the patients [Table 4]; the majority of the patients experienced minimal diarrhoea, nausea and vomiting, mucositis, alopecia and marrow suppression. The single patient who had grade 3 marrow toxicity had advanced liver metastases. One patient with thalassaemic trait developed grade 2 anaemia. The other side effects encountered were thrombophlebitis due to a direct irritant effect of the drug on the vein used in chemotherapy, hyperpigmentation of the skin and nails and a generalised pruritic skin rash. Toxicity was an uncommon reason for stopping chemotherapy (2.7%). The most frequent reasons for stopping chemotherapy were progressive disease (29.7%) and defaulting of treatment (18.0%) [Table 5].

In the 8 patients who had palliative chemotherapy without preceding definitive surgery, the overall crude survival ranged from 1 to 52 months.

Radiotherapy was prescribed in 168 patients. Palliative radiotherapy was given in 103 while adjuvant pelvic radiotherapy was given in 64 patients. The intent of treatment was not known in one patient as it was given at another centre.

In the group of patients who received palliative radiotherapy, 8 patients did not undergo prior definitive surgery. The patient and treatment characteristics of these eight patients and a further 13 patients with only colostomy as the sole surgical procedure are summarized in Table 6. The total dose delivered in a palliative setting varied between 2 Gy and 60 Gy, with a median of 45 Gy. The most commonly used number of fractions were 20 to 25 fractions (50%). The *two* field technique was the most frequently used (76%).

Adjuvant pelvic radiotherapy was given to 64 patients. The delay after primary definitive surgery ranged from less than one month to nine months, with a median of two months. The total dose delivered in the adjuvant setting ranged between 10 Gy and 60 Gy, the most frequently used doses being 50 Gy

(54.7%) and 45 Gy (31.3%). The number of fractions used most frequently were 20 to 25 fractions (78.1%). The most frequently used radiotherapy technique was again the *two* field technique (84.4%), followed by the *three*-field technique (9.4%) and the *four*-field technique (6.3%). The perineal boost was used in 14.1% of the patients. The upper border of the radiotherapy field was at the junction between the fifth lumbar and first sacral vertebrae (L5/S1 junction) in 78.1%. Preoperative radiotherapy was given in the adjuvant setting in only two patients.

## DISCUSSION

Our patients appear to present at an earlier age in contrast with other series in which the proportion of patients less than 40 years old was only 4.5%.<sup>14</sup> Sex distribution for rectal cancer was less extreme than in published literature<sup>15</sup> where the male to female ratio is reported to be approximately 2:1. The distribution by site is similar to published data<sup>16</sup> in which three quarters of all tumours within the large bowel are found in the rectum, rectosigmoid and sigmoid colon. Although the proportion of patients with Dukes' A disease may be lower than in other series,<sup>17,18</sup> it has to be noted that one fifth of our data on stage could not be determined. Moreover, many patients who were in Dukes' Stage A may not be referred to our Institute. The proportion of the tumours that were recorded as adenocarcinoma is similar to published figures of 90% to 95%.<sup>19</sup> While the proportion of our tumours that are poorly differentiated or undifferentiated is compatible with the data from Singapore,<sup>18</sup> it is lower when compared to other published series from the West where the figures are around 20% of the cases.<sup>17</sup>

Only a minority of patients in this series were found to have a predisposing factor to colorectal cancer. This finding contrasts with Western populations in which approximately a third of cancer cases have associated polyps.

Although adjuvant therapy has been shown to have the greatest impact on patients with Dukes' C disease,<sup>9</sup> the practice of this institute has been the use of adjuvant treatment for Dukes' B as well as Dukes' C colorectal cancer. This is partly due to the



fact that the incidence of morbidity in our centre appears to be lower than that reported in other centres. Although serious toxicity was seen in 35% of patients in the combined chemo/radiotherapy arm of the Gastrointestinal Tumor Study Group (GITSG) trial,<sup>3</sup> the addition of 5-fluorouracil to radiotherapy did not add significantly to morbidity in our experience. This could be related to the route and method of administration of 5-fluorouracil which was often given orally or via a continuous intravenous infusion. Moreover, the upper border of the pelvic radiotherapy field was not extended higher than the junction between the fifth lumbar and first sacral vertebrae in the majority of patients, thus further minimising morbidity.

Fluorouracil has remained the mainstay of palliative chemotherapy despite a general response rate of approximately 20% and a median duration of response of 5 months in patients with advanced colorectal cancer.<sup>16</sup> The toxicity of a combination of folinic acid with 5-fluorouracil is greater than with 5-fluorouracil alone and thus only a minority of our patients were given this combination.

The survival in the eight patients with rectal cancers in this study who received only radiotherapy and the thirteen patients who had only defunctioning colostomy and radiotherapy highlights the role of primary radiotherapy and palliative surgery in such cases. Although the quality of life could not be clearly demonstrated in this retrospective study, the crude survival of patients receiving radiotherapy as the primary modality of treatment has been demonstrated to be at least 3 years in half of these patients.

In conclusion, the epidemiological characteristics of the patients with colorectal cancer were similar to other published series except for a younger age at presentation and an underrepresentation of localized (Dukes' A) disease. The patterns of treatment have been influenced by the late stage at presentation, the practical considerations in the population as well as the resources that were available. As the toxicities of therapy experienced by our patients appeared to be less than in other centres, the use of adjuvant treatment in Dukes' B patients was not unjustified. A limitation in this study

was the lack of details on the quality of life, especially in the group of patients who had been given palliative treatment.

**TABLE 1 Patient characteristics**

<b>Total number of patients</b>	320
<b>Age</b>	
Mean	55.4 years
s.d.	12.7 years
Less than 40 years	11.6 %
<b>Sex</b>	
Male	183 (57.2%)
Female	137 (42.8%)
<b>Race</b>	
Malay	94 (29.4%)
Chinese	198 (61.9%)
Indian	23 (7.2%)
Other	5 (1.5%)
<b>Site of Primary tumour</b>	
Rectum	163 (50.9%)
Recto-sigmoid colon	37 (11.6%)
Sigmoid colon	48 (15.0%)
Ascending colon	21 (6.6%)
Transverse colon	16 (5.0%)
Descending colon	17 (5.3%)
Caecum	14 (4.4%)
Unrecorded	4 (1.2%)
<b>Dukes' Stage</b>	
A	6 (1.9%)
B	85 (26.6%)
C	106 (33.1%)
Disseminated	57 (17.8%)
Unrecorded	66 (20.6%)
<b>Histological Type</b>	
Adenocarcinoma	286 (89.4%)
Unrecorded	34 (10.6%)
<b>Grade</b>	
Well differentiated	62 (19.4%)
Moderately well differentiated	157 (49.1%)
Poorly or Undifferentiated	30 (9.4%)
Unrecorded	71 (22.2%)

**TABLE 2 SURVIVAL STATUS**

Alive	169 (52.8%)
Dead	134 (41.9%)
Unknown	17 (5.3%)
<b>Total</b>	<b>320 (100%)</b>
<b>Crude survival</b>	
Mean	27.2 mths
(s.d.)	(24.4 mths)
Median	19.0 mths
Range	1 - 112 mths
<b>Disease free survival</b>	
Mean	12.4 mths
(s.d.)	(17.2 mths)
Median	7.0 mths
Range	0 - 125 mths

**TABLE 3 Recurrence Pattern**

<b>ALL PATIENTS (n=320)</b>		
No recurrence	133	41.6%
Local recurrence only	82	25.6%
Local recurrence + Distant recurrence	30	9.4%
Distant recurrence only	73	22.8%
Unrecorded	2	0.6%
<b>Total</b>	<b>320</b>	<b>100.0%</b>

N.B. The liver was involved in 61 patients (18.9%).



**TABLE 4 Toxicity of chemotherapy**

	<b>Grade 0 No. (%)</b>	<b>Grade 1 No. (%)</b>	<b>Grade 2 No. (%)</b>	<b>Grade 3 No. (%)</b>	<b>Grade Unrecorded No. (%)</b>
<b>Diarrhoea</b>	159 (71.6)	9 (4.1)	9 (4.1)	1 (0.4)	44 (19.8)
<b>Nausea / vomitting</b>	167 (15.3)	6 (2.7)	4 (1.8)	1 (0.4)	44 (19.8)
<b>Mucositis</b>	172 (77.5)	3 (1.3)	2 (0.9)	0 (0)	45 (20.3)
<b>Marrow suppression</b>	158 (71.1)	11 (5.0)	9 (4.1)	1 (0.4)	43 (19.4)
<b>Alopecia</b>	168 (75.7)	4 (1.8)	4 (1.8)	0 (0)	46 (20.7)

**TABLE 5 Reasons for stopping chemotherapy**

<b>REASONS FOR STOPPING CHEMOTHERAPY</b>	<b>Number</b>	<b>Percentage</b>
<b>PROGRESSIVE DISEASE</b>	66	29.7
<b>DEFAULTED TREATMENT</b>	40	18.0
<b>COMPLETED TREATMENT</b>	38	17.1
<b>TOXICITY</b>	6	2.7
<b>PATIENT'S CHOICE</b>	2	0.9
<b>UNKNOWN</b>	18	8.1
<b>TOTAL</b>	<b>170 #</b>	<b>76.6</b>

# Fifty two patients (23.4%) were still undergoing chemotherapy.

**TABLE 6. Patients receiving palliative radiotherapy without preceding surgery or with only colostomy****Patients who had undergone only radiotherapy without any preceding surgery**

age (yrs)	Duke	zubro status	status	survive (mths)	dose (Gy)	no. frac.	no. fields
49	unk.	2	alive	73	50	25	2
59	unk.	3	alive	47	30	15	2
45	unk.	2	alive	36	50	25	2
65	unk.	1	alive	36	50	25	2
87	unk.	1	alive	21	59	20	4
67	unk.	1	dead	11	30	10	1
62	unk.	1	dead	7	60	20	2
61	D	5	dead	5	30	10	1

**Patients who had undergone only colostomy and palliative radiotherapy**

age (yrs)	Duke	zubro status	status	survive(mths)	dose (Gy)	no. frac.	no. fields
32	C	2	dead	4	10	4	2
38	unk.	3	alive	15	30	10	2
41	unk.	2	alive	48	60	30	2
43	C	2	dead	4	30	10	2
43	unk.	3	alive	1	30	10	2
54	unk.	3	dead	13	50	20	2
58	unk.	3	dead	12	45	20	2
60	C	1	dead	7	50	25	2
63	D	2	dead	10	45	20	2
65	unk.	2	dead	3	30	10	2
67	D	4	dead	3	40	18	2
67	unk.	2	alive	24	50	25	2
70	D	2	dead	18	45	15	2

unk = unknown

Those patients being treated with only one field were treated with a single perineal field.



## ACKNOWLEDGEMENTS

The authors would like to acknowledge the assistance provided by: the staff of the Radiotherapy Clinic and the Radiotherapy Records Office, especially Encik Arshad, and the staff of Identity Card Division, Malaysian National Registration Department. We would like to thank the Director General of Health, Malaysia for permission to publish these results.

## BIBLIOGRAPHY

1. Chan CK, Singh J, Rasid BK, Devaraj T. Penang cancer cases reported to the National Cancer Registry of Malaysia, 1987 - 1990: An epidemiological analysis. *Med J of Malaysia*. 1994;49(2):122-131.
2. Lim AKH, Lim GCC. Burden of advanced cancer in Malaysia. *Proceedings of the National Hospice Conference, Penang*. 1993;13-18.
3. Gastrointestinal Tumor Study Group. Prolongation of the disease-free interval in surgically treated rectal carcinoma. *N Engl J Med*. 1985;312:1465-1472.
4. Gastrointestinal Tumor Study Group. Survival after postoperative combination treatment of rectal cancer. *N Engl J Med*. 1986;315:1294-1295.
5. Krook JE, Moertel CG, Gunderson LL. Effective surgical adjuvant therapy for high-risk rectal carcinoma. *N Engl J Med*. 1991;324:709-715.
6. Gerard A, Buyse M, Nordlinger B. Preoperative radiotherapy as adjuvant treatment in rectal cancer: Final results of a randomized study of the European Organization on Research and Treatment of Cancer Gastrointestinal Tract Cancer Co-operative Group. *Ann Surg*. 1988;208:606-614.
7. Moertel CG, Fleming TH, Macdonald JS. Levamisole and fluorouracil for adjuvant therapy of resected colon carcinoma. *N Engl J Med*. 1990;322:352-358.
8. O'Connell M, Maillard J, Macdonald J. An Intergroup trial of intensive course 5-FU and low dose leucovorin as surgical adjuvant therapy for high risk colon cancer [abstract]. *Proc ASCO*. 1993;12:552.
9. Moertel C, Fleming T, Macdonald J, Haller D, Laurie J. The Intergroup study of fluorouracil plus levamisole and levamisole alone as adjuvant therapy for stage C colon cancer: A final report [abstract]. *Proc Am Soc Clin Oncol*. 1992;11:161.
10. Gunderson LL, Martin KJ, O'Connell MJ, Beart RW, Kvols LK, Nagorney DM. Residual, recurrent or unresectable gastrointestinal cancer. Role of radiation in single or combined modality treatment. *Cancer*. 1985;55:2250-2258.
11. Dukes CE. The classification of cancer of the rectum. *J Pathol. Bacteriol*. 1932;35:323-332.
12. Miller AB, Hoogstraten B, Staquet M, Winkler A. Reporting results of cancer treatment. *Cancer*. 1981;47:207-214.
13. Zubrod CG, Schneiderman M, Frei E, et al. Appraisal of methods for the study of chemotherapy of cancer in man: comparative therapeutic trial of nitrogen mustard and triethylene thiophosphoramide. *J Chronic Dis*. 1960;11:7-33.
14. Ohman U. Colorectal carcinoma in patients less than 40 years of age. *Dis Colon Rectum*. 1982;25:209-214.
15. Dayal Y, DeLellis RA. The gastrointestinal tract. In: Cotran RS, Kumar V, Robbins SL (eds). *Robbins Pathologic Basis of Disease*. 4th edition. Philadelphia: WB Saunders, 1989;18:898.
16. Arnott S. Gastrointestinal tract. In: Sikora K, Halnan KE (eds). *Treatment of cancer*. London: Chapman and Hall, 1990:485.
17. Lockhart-Mummery HE, Ritchie JK, Hawley PR. The results of treatment for cancer of the rectum at St. Mark's Hospital from 1948-1972. *Br J Surg*. 1976;63:673-677.
18. Goh HS, Ti TK, Rauff A, Foong WC, Lee YS. Colorectal cancer in Singapore: Preliminary report of the colorectal cancer project from the University Department of Surgery, NUS. *Singapore Med J*. 1985;26(1):65-72.
19. Cohen AM, Minsky BD, Schilsky RL. Colon cancer. In: De Vita VT Jr, Hellman S, Rosenberg SA (eds). *Cancer: Principles and practice of oncology*. Philadelphia: JB Lippincott, 1993;30:937.



## A STUDY OF PREVALENCE RATE AND PREDISPOSING FACTORS OF GALL STONES IN SARABURI HOSPITAL PERSONNEL

Panida MUKDEEPROM<sup>1</sup>

### ABSTRACT

This paper reports the prevalence rate and possible risk factors of gall stone in Saraburi hospital personnel. 400 Cases were randomly selected for ultrasonographic examination of the abdomen. There were 64 men (16%) and 336 women (84%). Gall stones were found in 18 cases (4.5%). The prevalence is 1.6% in men (1 in 64 cases) and 5.1% in women (17 in 336 cases). The predisposing factors for gall stones are aging and increasing number of parity. Although there is more tendency for women and obese person to have gall stones according to this study but there is no statistical significant increased prevalence of gall stones in these two groups.

### INTRODUCTION

Gall stone is one of common diseases of western countries. Autopsy series in USA report at least a prevalence rate about 20% in women and 8% in men over 40 years of age. In eastern countries, gall stones are less common but there is a tendency to increase in prevalence of this disease due to dietary change. There are three types of gall stone: cholesterol stone, pigmented stone and mixed. The causes of cholesterol stones, which are mainly composed of cholesterol, are bile supersaturation, nucleation of cholesterol monohydrate and abnormality of gall bladder contraction or gall bladder stasis. Pigmented stones are mainly composed of calcium bilirubinate. This type of stone is common in Asian countries. They are caused by unconjugated insoluble bilirubin in bile which precipitated and became pigmented stones or nidus for cholesterol stones. There are many risk factors associated with formation of the gall stones such as aging, obesity, female sex, race, hereditary, parity, rapid weight loss, medication, ileal disease or resection, cystic fibrosis, cirrhosis, hemolysis and intravenous hyperalimentation. The pathophysiology of which is variably understood. For example, obesity increases cholesterol saturation of bile and the risk of stones formation. On the contrary, the pathophysi-

ological change that occur during aging that leads to increased risk of gall stone formation is not well understood. Most of the identified risk factors commonly said are fat, forty (aging), female and fertile (4F)

The clinical symptoms of gall stones are vary, there may be no any symptom at all for 'silent gall stone' or biliary pain which is fairly typical in most patients. Although this pain has many variations, the overall theme is similar for each patient. The pain is often in right upper quadrant or epigastrium. It may be referred to right shoulder. The hall mark of true biliary pain is episodicity. The pain may be accompanied by nausea and vomiting or diaphoresis and tachycardia, depend on the severity of the attack. Patients with milder symptom may describe as a pressure or heavy feeling, or a localized bloating. Cholecystectomy is the treatment of choice for symptomatic gall stone which includes both traditional open and laparoscopic approaches. Oral bile salt therapy, extracorporeal shock wave lithotripsy (ESWL) and percutaneous radiological extraction of the stones from the gall bladder are another alternatives but are less popular or still under investigation. The purpose of this study is to determine prevalence rate and risk factors of gall stones in Saraburi hospital personnel.

<sup>1</sup> Department of radiology, Saraburi hospital, Saraburi



## MATERIAL AND METHOD

The population was obtained by calculating the formula:  $n = 400N/399+N$ , with 5% deviation. The calculated samples were 400 cases. Ultrasonography of the abdomen was used as the screening method due to high sensitivity rate for detection of the stone and low false positive rate. The examination included general examination of the abdomen with more con-

centrate on the gall bladder in supine and left lateral decubitus position. For female, ultrasonography of the lower abdomen were included. The collected data included age, sex, weight, height, number of parity, previous illness and associated diseases, dietary and weight status. The ultrasonographic data included presentation of gall stones or history of cholecystectomy due to gall stones and general pathology in the abdomen. All the collected data were analyzed for prevalence rate and risk factors by Chi-square test.

## RESULT

**TABLE 1** Prevalence rate of gall stone by sex.

Sex	Number		Gall stone found	
	%	N	%	N
Male	16.0	(64)	1.6	( 1)
Female	84.0	(336)	5.1	(17)
Total	100.0	(400)	4.5	(18)

$$\chi^2 = 1.64 \quad p = .6486$$

This table shows that total prevalence rate of gall stones in this group is 4.5%. There is no significant difference between prevalence rate in male or female but there is high tendency of gall stone in female sex than male.

**TABLE 2** Prevalence of gall stones by age.

Age(year)	Normal		Gall stone	
	%	N	%	N
20-29	98.2	(55)	1.8	( 1)
30-39	98.0	(194)	2.0	( 4)
40-49	93.5	(100)	6.5	( 7)
50 Up	84.6	( 33)	15.4	( 6)

$$\chi^2 = 22.58 \quad p = .0072$$

This table shows significant increased prevalence rate in aging. The prevalence rate is 6.5% in the group between age 40-49 years while the rate in the group of age 50 years up is 15.4%.

**TABLE 3 Prevalence rate of gall stones by weight status**

<b>Weight status</b>	<b>Normal</b>		<b>Gall stone</b>	
	<b>%</b>	<b>N</b>	<b>%</b>	<b>N</b>
<b>Normal</b>	94.6	(297)	5.4	(17)
<b>Increased</b>	98.6	( 68)	1.4	(1)
<b>Decreased</b>	100.0	(52)	-	(0)

$$X = 4.87 \quad p = .5606$$

This table shows that weight status is not a significant risk factor for gall stone prevalence rate.

**TABLE 4 Prevalence rate of gall stones and associated diseases.**

<b>Associated Disease</b>	<b>Normal</b>		<b>Gall stone</b>	
	<b>%</b>	<b>N</b>	<b>%</b>	<b>N</b>
<b>Non</b>	96.2	(355)	3.8	(14)
<b>DM</b>	100.0	( 5)	-	( 0)
<b>Hyperlipidemia</b>	85.0	(17)	15.0	( 3)
<b>Hemolytic anemia</b>	83.3	(15)	16.7	( 1)

$$X = 12.05 \quad p = .2104$$

This table shows no significant correlation between associated diseases and prevalence rate of gall stones, however, high prevalence rate is noticed in hyperlipidemia and hemolytic anemia, 15% and 16.7% respectively.



**TABLE 5 Prevalence rate of gall stone by number of parity.**

No of parity	Normal		Gall stone	
	%	N	%	N
0	98.0	(101)	(2.0)	2
1	95.0	( 57)	(5.0)	3
2	94.2	( 97)	(5.8)	6
3	95.3	(41)	(4.7)	2
4	85.0	(17)	(15)	3
5	83.3	(5)	(16.7)	1

$$X = 31.89 \quad p = .0226$$

This table shows significant increase of prevalence rate in multiparities, the prevalence rate is 15% and 16.7 % in the group of 4 and 5 parities respectively.

**TABLE 6 Prevalence rate of gall stone by obesity.**

	Normal		Gall stone	
	%	N	%	N
Normal weight	97.0	259	3.0	8
Obesity	92.5	123	7.5	10

$$X = 5.80 \quad p = .1218$$

This table shows that there is no significant correlation between gall stone prevalence rate and obesity.

**TABLE 7 Other diseases that incidentally found by ultrasonographic examination.**

Disease	
Cholesterol polyps of gall bladder	5
Absent of R.kidney	1
Chronic pyelonephritis	3
Renal stone	2
Ovarian cyst	5
Myoma uteri	4
Endometriosis	3

## DISCUSSION

Gall stone is one of common diseases. Studies of gall stone prevalence rates are difficult to perform and the results must be viewed in context of the population studied as well as the methods used to select and examine the population. The result for one population can not be applied to the others, particularly if the groups are differ in race, ethnicity or dietary habits. Many earlier prevalence reports used necropsy data which is useful for comparing prevalence rates between countries or ethnic groups but may not reflect the true prevalence<sup>8</sup> Ultrasonography is a sensitive screening method for detection of gall stone. Many studies report 9.4-11 % prevalence rate of total population, the rate was 6.7 - 9.4 % in male and 9.4 - 23.2 % in female. The rate is increased with aging. The highest prevalence rate is in Pima Indian, a report from USA which is as high as 48.6%.<sup>3,8</sup> There are few reports of prevalence rate from Asian countries. The prevalence of gall stone in hill tribes people in Northern part of Thailand, studied by the investigators from Nippon Medical School and Faculty of Medicine, Chiangmai University, is only 2.6%.<sup>4</sup> The rate is very low compared to the

Western studies. The prevalence rate in Saraburi hospital personnel is 4.5%, twice the rate of hill tribe people in the Northern part of Thailand. However this rate is still lower than the Western countries. A report from Denmark<sup>9</sup> described prevalence rate for males age 30,40,50,60 year to be 1.8%, 1.5%, 6.7% and 12.9% respectively, and for females age 30,40,50,60 years to be 4.8%, 6.1%, 14.4% and 22.4% respectively. This report is rather closed to the rate in Saraburi hospital personnel.

The risk factors that increase the prevalence rate of gall stone in this study are aging and multiparities which are the same as many reports.<sup>3,5</sup> Schuster<sup>5</sup> mentioned that age is the most predictive factor of gall stone. In this study although gall stone is found more in female and obese groups, it is not significant statistically. Also associated diseases such as DM, hypelipidemia and hemolytic anemia are not the risk factor for gall stone. However stone prevalence is rather high in hyperlipidemia and hemolytic anemia groups. Thus 4F hypothesis should be reduced to 2F which are Forty and Fertile by this study.

Other diseases that were incidentally found by Ultrasound study include 5 gall bladder polyps, 3 chronic pyelonephritis, 2 renal stones, 1 agenesis of



R.kidney. Gynecological problems are also common, 5 ovarian cyst, 4 myoma uteri and 3 endometriosis. This reflect that the hospital personnel are neglected for yearly physical examination.

### CONCLUSION

The prevalence rate of gall stone in Saraburi hospital personnel is 4.5% (18 in 400 cases) The rate in male is 1.6 % and the rate in female is 5.1%. Risk factor of gall stone is aging and multiparities. Female sex and obesity are not significant risk factor by this study.

### REFERENCES

1. Cooperberg PL, Gibney RG. Imaging of the gall bladder. *Radiology* 1987;163:605-613.
2. Valderama R, Bru C, Bianchi L, Teres J. *AJR* 1994;163:1535. (letter)
3. Bates T, Harrison M, Lowe D, Lawson C, Padlay N. Longitudinal study of gall stone prevalence at necropsy. *Gut* 1992;33(10): 103-7.
4. Prathnadi P, Sundu T, Pucharapimol S, Suprasert S, Suchamong P, Varit C. Incidence of gall stone in hilltribes people in norhtern part of Thailand (preliminary report using ultrasonography) *Medical journal of Chiangmai hospital* 1987;26(3):186.
5. Schuster JJ, Raptopoulos V, Baker SP. Increased prevalence of cholelithiasis in patients with abdominal aortic aneurysm: Sonographic evaluation. *AJR* 1988;152:509-511.
6. Gelfan DW, Wolfman NT, Ott DJ, Watson NE, Chen Y M, Dale WJ. Oral cholecystography vs gall bladder sonography : A prospective, blinded reappraisal. *AJR* 1988;151:69-72.
7. Yamane T. *Statistics:An introductory analysis*. Tokyo: Harper international ed. 1973.
8. Buckus *Gastroenterology* 5th ed. Philadelphia: W.B. Saunders, 1995;2674-2729.
9. Jorgensen T. Prevalence of gall stones in a Danish population. *Am J Epidemiol* 1987;126:912-921.

## HAND-MADE BODY LEAD APRON

Atchara SANGCHAI B.A. (Political Science), Cert of Medical Radiography  
Patchrin PEKANAN M.D., Preecha TOSKULKAO B.Ed (Science),  
Cert of Medical Radiography

### ABSTRACT

A hand-made body lead apron was successfully done by using the lead sheets in the used dental films. The x-ray protections was perfect. The total cost was much cheaper than the commercial one. However, its weight was higher due to the thickness of the total lead used. The process in making this apron was simple and should be promoted to be used in our country.

### INTRODUCTION

Radiation protection to the patients and the personnels working in the department of Radiology is very important. Ignoring the radiation protection would bring hazard to both the patients and the personnels. In the old days when x-ray was used in the medicine in the year 1922, many involved personnels were dead from cancer,<sup>1,2</sup> leukemia<sup>3</sup> and some had short lifespan, decreased length of stay for 6 years.<sup>4,5</sup> They might be infertile within one year if they received the x-ray dose up to 250 rems (2.5 Sv).<sup>6</sup> Owing to these hazards, the international commission on radiological protection (ICRP)<sup>7</sup> proposed the following general principles: (a) No practice involving exposures to radiation should be adopted unless it produces sufficient benefit to the exposed individuals or to society to offset the radiation detriment it causes (b). In relation to any particular source within a practice, the magnitude of individual doses, the number of people exposed and the likelihood of incurring exposures where these are not certain to be received should all be kept as low as reasonably achievable, economic and social factors being taken into account. This procedure should be constrained by restrictions on the doses to individuals, so as to limit the inequality likely to result from the inherent economic and social judgements (c). The

exposure of individuals resulting from the combination of all the relevant practices should be subject to dose limits, or to some control of risk in the case of potential exposures. These are aimed at ensuring that no individual is exposed to radiation risks that are judged to be unacceptable from these practices in any normal circumstances. Not all sources are susceptible to control by action at the source and it is necessary to specify the sources to be included as relevant before selecting a dose limit.

For the optimisation of protection (principle c), the involved personnels wear the lead apron to protect the internal body organs. Since the manufactured lead aprons are all imported and are expensive, an attempt to make our own lead apron was done.

### MATERIAL AND METHODS

The industrial made body lead aprons were made from the mixture of lead and rubber which are expensive (6500 - 10000 Baht per unit). In order to balance the budget of the division, we consider using the throw-away material for the x-ray protection. The lead sheet for scattering-ray protection in the dental films were collected after the films had been exposed. The dental films were composed of the jacket, two pieces of x-ray films



with paper covering and the lead sheet. We used the lead sheets, size 3.1 X 4.1 cm. in the periapical films which were the most frequently used size. Each piece of the lead sheet was 0.07 mm thick (Fig.1).

There were several rows of tiny projections on each end of the lead sheets. They were made flat by hand, using bottles or cans. The thickness of one body lead apron was equal to the thickness of 9 pieces of lead sheets. There were three sets of lead sheets, each set was composed of three sheets of lead covered by a piece of thin cloth. The purpose of making the apron this way was to seal the holes caused by the sewed-needles. The size of the apron was 62 X 100 cm. The total lead sheets used were 5435 sheets (Fig. 2). Finally, the apron was covered by the artificial leather as in figure 3., ready for use (Fig. 4). The total cost for the material used for this apron was about 2000 Bahts. The weight of our apron was 6.0 kilograms. Total thickness of lead is 0.63 mm.

## RESULTS

Six pieces of the Kodak ultraspeed periapical dental x-ray films were attached to the inside of the front part of the lead apron. The lead apron was routinely used in the fluoroscopic DSI unit for 6 weeks. The attached films were detached from the apron one film per one week.

Then the lead apron was hung 1 meter away from the x-ray tube, in the general unit. Six similar dental x-ray films were attached to the inside and six films to the outside of the front part of the lead apron. Exposure was allowed for 6 weeks; for each week, one film from the inside and one film from the outside part of the apron was removed. The identical performance was applied to the manufactured lead apron routinely used in that room.

The processed films that were previously attached to the lead aprons were measured for densities by the densitometer. The results were

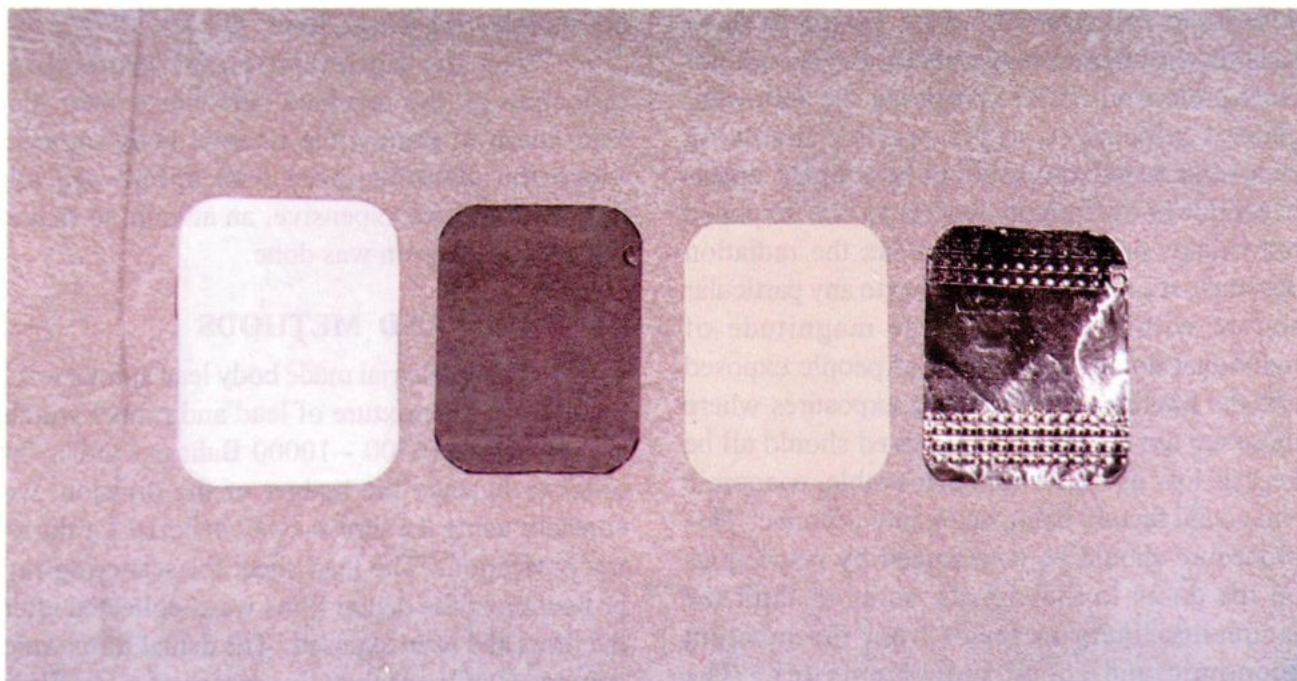


**Fig. 1** Components of the dental films: jacket, film, film and lead sheet



shown by the graphic drawing (Fig.5). From this experiment, the study proved that this hand-made lead apron could protect the scattered radiation as safe as the manufactured one.



Fig. 2 Lead sheets sewed on the thin piece of cloth

## DISCUSSION

There are several items that provide protection for associated personnel during a fluoroscopic/radiographic imaging procedure. The first and foremost is the lead apron worn by all individuals who must work in the room when the x-ray tube is operated. Lead equivalent thicknesses from 0.25 mm to 0.5 mm are typical. Often, the lead is in the form of a rubber material to provide flexibility and handling ease. Aprons protect the torso of the body and are available in fronto or wrap-around fitting designs, the latter being important when the back is exposed to the scattered radiation a considerable portion of the time. Greater than 90% of the incident scattered radiation is attenuated by the 0.25 mm thickness at standard x-ray energies (less than 100 keV). Thickness of 0.35 and 0.50 mm lead in an apron give greater protection (up to 95-99% attenuation), but weigh 50 to 100% more than the minimal 0.25 mm thickness. For long fluoroscopic procedures, the weight of the apron often becomes a limiting



Fig. 3 The appeared lead apron after being covered with the imitated leather



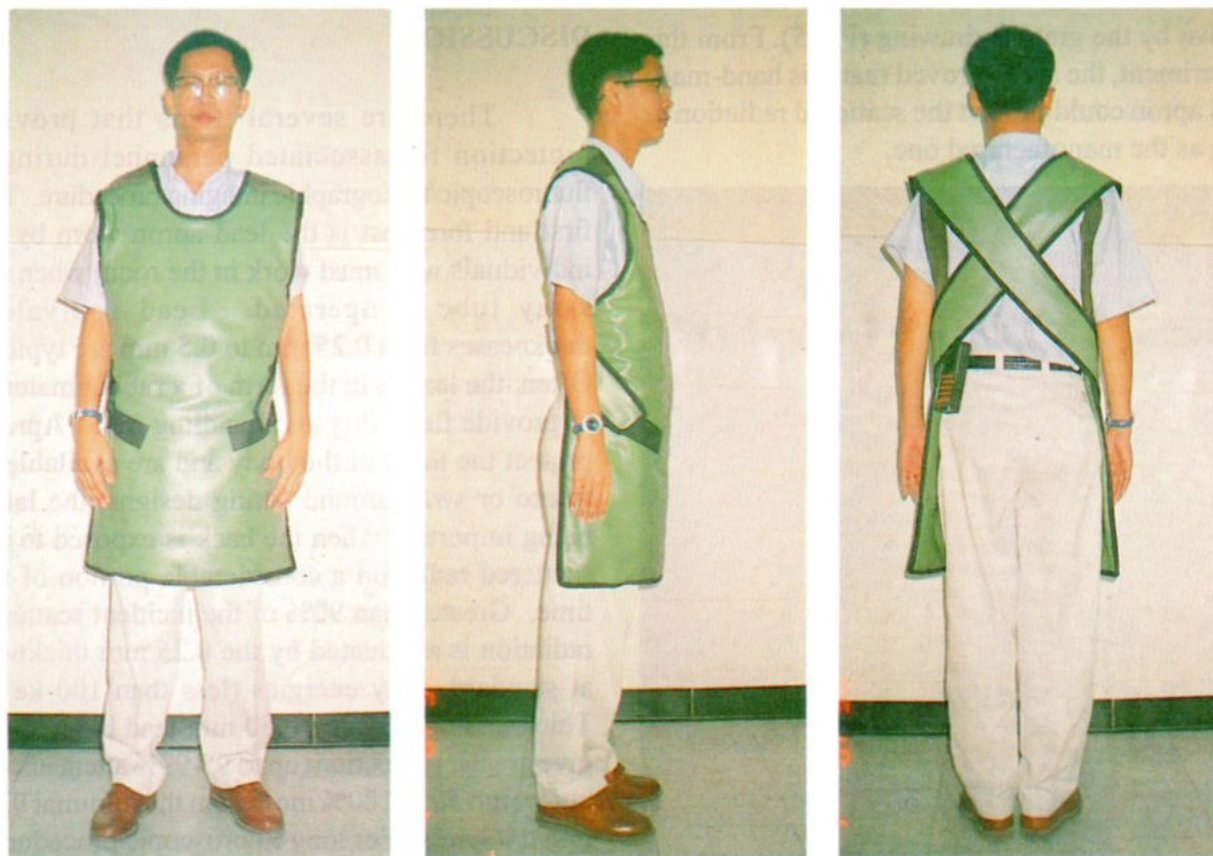


**Fig. 4** The hand-made body lead apron on the real technician.

factor in the ability of the radiologist and the attending staff to complete the case without substitutions. The areas not covered by the apron include the arms, lower legs, the head and neck, and the back (except for wrap-around type aprons).

The body areas not protected by the apron include the thyroid and the eyes. Accordingly, there are thyroid shields and leaded glasses that can be worn by the personnel in the room. The thyroid shield wraps around the neck to provide similar shielding as the lead apron does. Leaded glasses attenuate the incident x-rays to a lesser extent, typically 30-70 %, depending on the content (weight) of the lead. Normal eye glasses provide limited protection, typically much less than 20% attenuation. Whenever the hands must be in the primary beam, leaded gloves made of 0.5 mm thick lead (or greater) should be worn.

The lead aprons utilized in diagnostic radiology are of limited value in nuclear medicine

because, in contrast to their effectiveness in reducing exposure from low energy scattered x-rays, they do not attenuate enough of the medium energy photons emitted by Tc-99m (140 keV) to be practical.<sup>8</sup>

Film are optically and x-ray sensitive. The film densitometer measures the optical density of a selected film area by comparing the light intensity without the film in place to the light intensity with the film in place, and taking of the log of the ratio. The optical density (OD) of film is measured at a given point and describes the amount of light that gets through the film base and developed emulsion. If the film transmits a certain fraction ( $T_1$ , the transmittance) of the light shone upon it, then the OD will be:  $OD = -\text{Log}(T) = \text{Log}(1/T)$ . A densitometer is used to measure OD. A characteristic curve for the screen-film system can also be produced by exposing the film in a cassette with screens by

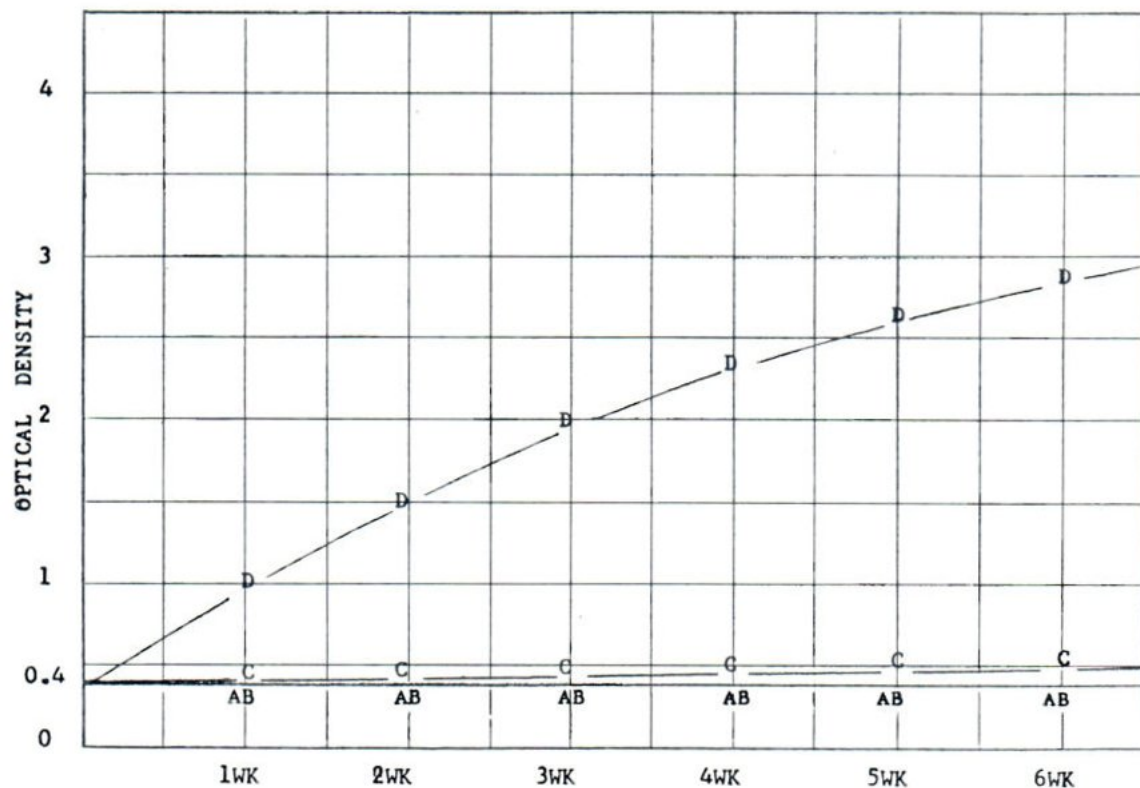


**Fig. 5** Optical density of the films attached to the lead aprons  
 A = control  
 B = films that were attached at the innerside of the hand-made lead apron in the fluoroscopic and general rooms  
 C = films that were attached at the manufactured lead apron (0.5 mm thick) in general room  
 D = films that were attached in front of the aprons in general room

using x-ray radiation. In principle, the characteristic curves for light exposure will be quite similar. X-ray film typically used in radiology has a slight tint to the mylar base, so that unexposed film has an OD of about 0.13 after having been developed. Heavily exposed film can yield OD of about 3.0 to 3.5 in radiography.

The weight of our lead apron is heavier than the manufactured apron of the same design which weigh 3.2 - 5.5 kg. However, the thickness of our apron is more than 0.5 mm. An experiment will be performed in making another apron to reduce the weight by reducing the thickness of the lead sheets previously used but still effective for x-ray protection.



**REFERENCES**

1. Stone RS. Common sense in radiation protection applied to clinical practice. *Am J Roentgenol* 1957;78:993-9.
2. Quimby EH, Pool J. Protection in radiology. *Radiology* 1942;41:272-81.
3. March HC. Leukemia in radiologist. *Radiology* 1944;43:275
4. Warrin S. Longevity and causes of death from irradiation in physicians. *JAMA* 956;162:464-8.
5. Braestrup CB. Past and present radiation protection exposure to radiologists from the point of view of life expectancy. *Am J Roentgenol* 1957;78:983-92.
6. Meschan I. An atlas of anatomy basis to radiology. Philadelphia: W.B. Saunder company, 1975:24-35.
7. International Commission on Radiological Protection; recommendation of ICRP. New York: Pergamon Press, 1993.8. Bushberg JT, Seibert JA, Leidholdt EMJr, Boone JM. The essential physics of medical imaging. Baltimore: Williams & Wilkins, 1994:613-5.
9. Bushberg JT, Seiber JA, Leidholdt EMJr, Boone JM. The essential physics of medical imaging. Baltimore: Williams & Wilkins, 1994:148-53.
10. Bushberg JT, Seiber JA, Leidholdt EMJr, Boone JM. The essential physics of medical imaging. Baltimore: Williams & Wilkins, 1994:421.

## "HEPERECHOIC DOTS" AND "SMALL FAT DENSITIES" US AND CT SIGNS OF XANTHOGRANULOMATOUS CHOLECYSTITIS: A CASE REPORT

Darunee BOONJUNWETWAT, M.D.

Onrudi HOJAN, M.D.

### ABSTRACT

We reported the US and CT signs of a case proved to be xanthogranulomatous cholecystitis. Even one case was found, but the imaging features were characteristic correlating with the histopathology. If the preoperative diagnosis or awareness of the disease could be made, the proper planning for treatment would be gained. The US showed mark thickening of the gallbladder wall containing multiple fix hyperechoic dots without shadowing. Increased vascularity was demonstrated by color doppler study. The CT shows a soft tissue mass at the gallbladder bed having multiple small fat densities, associated with small calcification or stone.

### INTRODUCTION

Xanthogranulomatous cholecystitis (XGC) is a focal or diffuse destructive inflammatory process of the gall bladder<sup>1</sup>. It is an uncommon form of cholecystitis which is being recognized with increasing frequency<sup>2</sup>. XGC occasionally may be confused with a malignant process<sup>3</sup>. We report a case of XGC with suggestive findings that are found in sonography and computerized tomographic imaging.

Laboratory datas are listed as below :

CBC : WBC 7700 u/L

Neutrophiles 77%

Lymphocytes 23%

SGOT : 81 u/L

SGPT : 80 u/L

Alkaline phosphatase : 551 u/L

Alpha feto protein : 1.24

CEA : 2.9

HBs Ag : positive

Hemoculture : positive for Salmonella A

### CASE REPORT

A 39-year-old man presented with fever for 4 days and 2 times of diarrhea before admission. On physical examination only hepatomegaly was found.

The laboratory findings were consistent with his diagnosis of salmonellosis A septicemia. The patient had a previous check up by ultrasound 3 months before admission showing a markedly thick walled gallbladder, with multiple fixed hyperechoic spots (Fig.1). A repeated ultrasound was



performed using 3.5 MHZ sector probe. The findings revealed a low echoic mass at the gallbladder area, about 6x6 cm<sup>2</sup> in size, without visualized gallbladder lumen. The mass contained large amount of fixed hyperechoic dots without posterior shadowing. (Fig.2), as well as increased vascularity by color doppler study. (Fig.3) CT scan showed a soft tissue mass at the gallbladder fossa with multiple small areas of fat densities.(Fig.4A) A small calcification was seen at the mass adjacent to the pancreatic head.(Fig.4B)

The diagnosis of suspected gallbladder carcinoma was made. At operation, the gallbladder was found to have inflamed thick wall, with adhesion to the hepatic flexure of colon and the first part of duodenum. Extracholecystic stone was found 5 mm. in size, considered to have a previous perforation. The patient was undergone a total cholecystectomy. The pathological diagnosis turned out to be a chronic cholecystitis with xanthogranulomatous reaction. Microscopic examination revealed fibrotic gallbladder and inflammatory cell infiltration of the wall. Deep penetration of the surface epithelium into the muscular layer forming sinuses in which inspissated bile was found. Many foam cells and chronic inflammatory cells were collected focally.

## DISCUSSION

XGC is a rare condition<sup>4-5</sup> associated with chronic recurrent inflammation of the gallbladder due to gall stone<sup>4</sup>. It is characterized histopathologically by lipid-laden histiocytes and multinucleated giant cells infiltrating the gallbladder wall<sup>5</sup>. Increasing fibrosis is noted at a late stage<sup>1</sup>. It is a benign process but may mimic gall bladder malignancy according to the slow insidious onset and its appearance on imaging studies<sup>3-10</sup>.

XGC was first described in 1970 by Christensen and Ishak<sup>11-12</sup> as "fibroxanthogranulomatous inflammation". Since then over 60 cases have been described under a variety of synonyms, including "ceroid or ceroid-like histiocyte granu-

loma of the gallbladder", and "biliary granuloma cholecystitis"<sup>12</sup>. But in the view of Goodman and Ishak<sup>12-13</sup>, the best name for this condition is xanthogranulomatous cholecystitis as this emphasises its inflammatory nature and its conceptual similarity to the renal condition, xanthogranulomatous pyelonephritis<sup>12</sup>.

Sonography of xanthogranulomatous cholecystitis characteristically appear as cholelithiasis and nodular or diffuse thickening of the gallbladder wall<sup>3,12</sup> which may misinterpreted as tumor or intramural abscess<sup>14</sup>.

On computed tomographic imaging; irregular thickening of the gallbladder wall is the most common abnormality in addition to gall stone. However, a mass may be presented in the gallbladder fossa. No evidence of metastases or biliary dilatation will be seen<sup>4</sup>.

Radiologically, XGC is extremely difficult to be differentiated from gallbladder cancer<sup>3</sup>.

In our case, sonography showed an enlarged gallbladder with thick wall as others having described. There are multiple internal hyperechoic dots without posterior shadowing, these may represent lipid-laden component histologically. Color doppler helps to confirm the presence of inflammation by demonstrating the increased vascularity. As well as CT scan revealed multiple small areas of fat densities in the thick gallbladder wall. We would like to present these US and CT signs to establish the diagnosis of xanthogranulomatous cholecystitis. Cholecystectomy is the treatment of choice for the XGC. In case of severe inflammatory reaction and fibrosis within the gallbladder, a subtotal cholecystectomy is required because it is unsafe to do conventional cholecystectomy<sup>7</sup>.

The complications of XGC are biliary fistula, perforated gallbladder with or without abscess formation<sup>1,6</sup>, adhesion and high rate of postoperative infection<sup>12</sup>.

The correct diagnosis of XGC is important for several reasons, the first and foremost is due to the high frequency of complications, but not the least is due to the condition may mimic preoperatively to the suspicious of malignancy<sup>1</sup>.



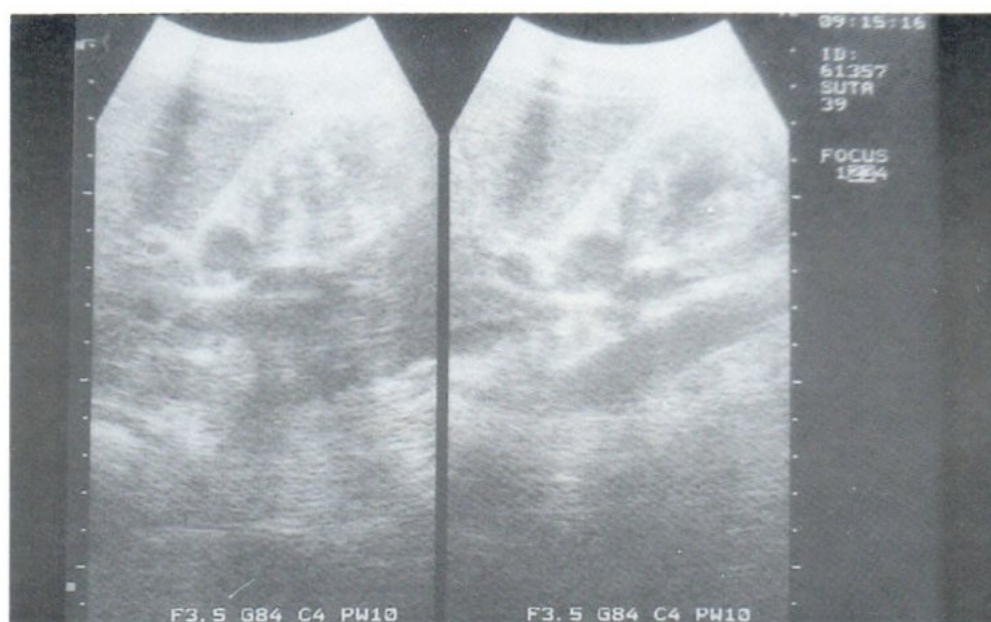


**Fig. 1** US of gallbladder showing diffuse thickening of gallbladder wall with multiple fix hyperechoic dots.

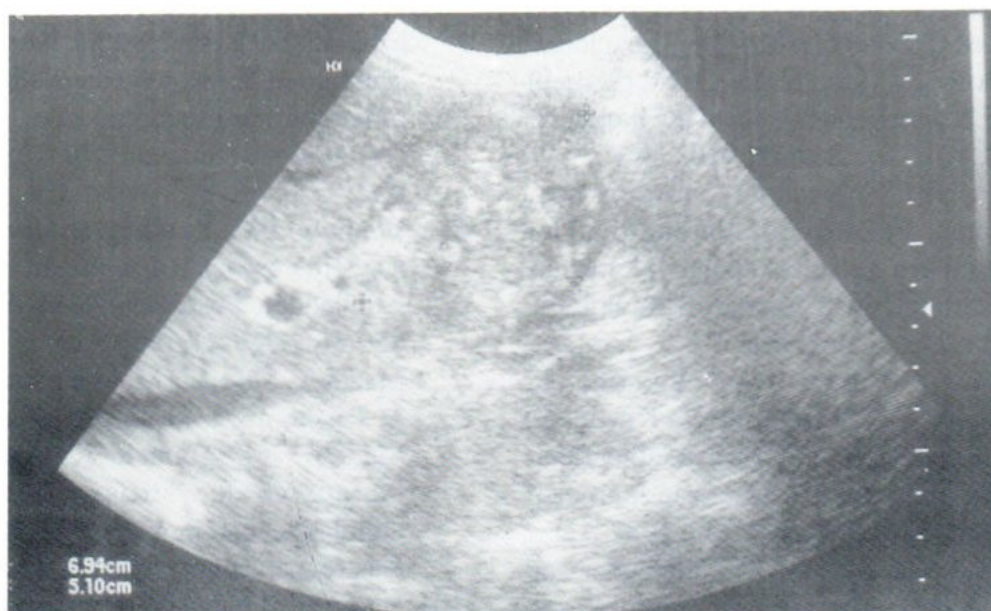


**Fig. 2** Follow up US 3 months later showing progressive thickening of gallbladder wall with lumen obliteration, containing large amount of hyperechoic dots without posterior shadowing.





**Fig. 3** Color doppler study showing increased vascularity at the gallbladder area.

## REFERENCE

1. Ladefoged C, Lorentzen M. Xanthogranulomatous cholecystitis. A clinicopathological study of 20 cases and review of the literature. *APMIS*. 101(11) : 869-75, 1993 Nov
2. Houston JP, Sampson MA, Collins MC. Ultrasound diagnosis of the gallbladder perforation in a case of xanthogranulomatous cholecystitis. *British Journal of Radiology*. 62(735) : 273-4, 1989 Mar
3. Hanada K, Nakata H, Nakayama T, Tsukamoto Y, Terashima H, Kurod Y, Okuma R. radiologic findings in xanthogranulomatous cholecystitis. *American Journal of Roentgenology*. 148(4) 727-30, 1987 Apr
4. Thomas E. Herbener. The gallbladder and biliary tract, Computer tomography and Magnetic resonance imaging of the whole body, 3rd edition 1994 Volume 2 : 987
5. Brooke Jeffray, JR. Inflammatory and nonneoplastic diseases of the llbladder, Margulis and Burhenne's Alimentary tract radiology, 5th edition 1994 Volume 2 : 1289
6. Houston JP, Collins MC, Cameron I, Reed MW, Parsons MA, Roberts KM. Xanthogranulomatous cholecystitis. *British Journal of Surgery*. 81(7) : 1030-2, 1994 Jul
7. Howard TJ, Bennion RS, Thompson JE Jr. Xanthgranulomatous cholecystitis : a chronic inflammatory pseudotumor of the gallbladder. *American Surgeon*. 57(12) : 821-4, 1991 Dec
8. Benhow EW. Xanthogranulomatous cholecystitis associated with carcinoma of the gallbladder. *Postgraduate Medical Journal*. 65(766) : 528-31, 1989 Aug
9. Maeda T, Shimada M, Matsumata T, Adachi E, Taketomi A, Tashiro Y, Tsuneyoshi M, Sueishi K, Sugimachi K. Xanthogranulomatous cholecystitis masquerading as gallbladder carcinoma. *American Jorunal of Gastroenterology*. 89(4) : 628-30, 1994 Apr
10. Dao AH, Wong SW, Adkins RB Jr. Xanthogranulomatous cholecystitis. A clinical and pathologic study of twelve cases. *American Surgeon*. 55(1) : 32-5, 1989 Jan
11. Christensen AH, Ishak KG. Benign tumors and pseudotumors of the gall bladder. *Archives of patho-logy* 1970; 90 : 423-32
12. Roberts KM, Parsons MA. Xanthogranulomatous cholecystitis :clinicopathological study of 13 cases. *Journal of Clinical pathology*. 40(4) : 412-7, 1987 Apr



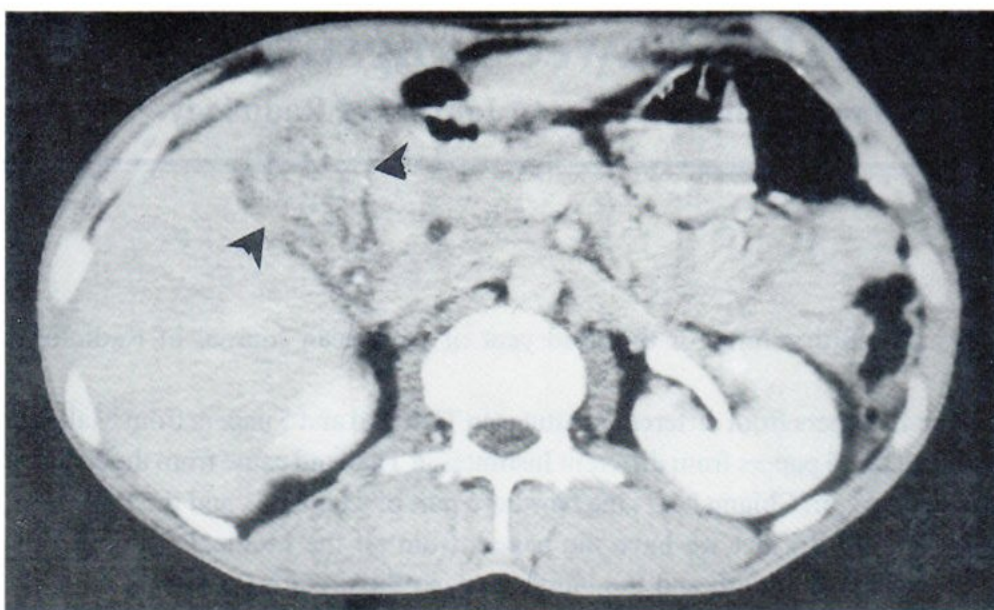


**Fig. 4A** Axial CT scan showed soft tissue mass (arrow heads) at the gallbladder fossa having multiple small areas of fat density.

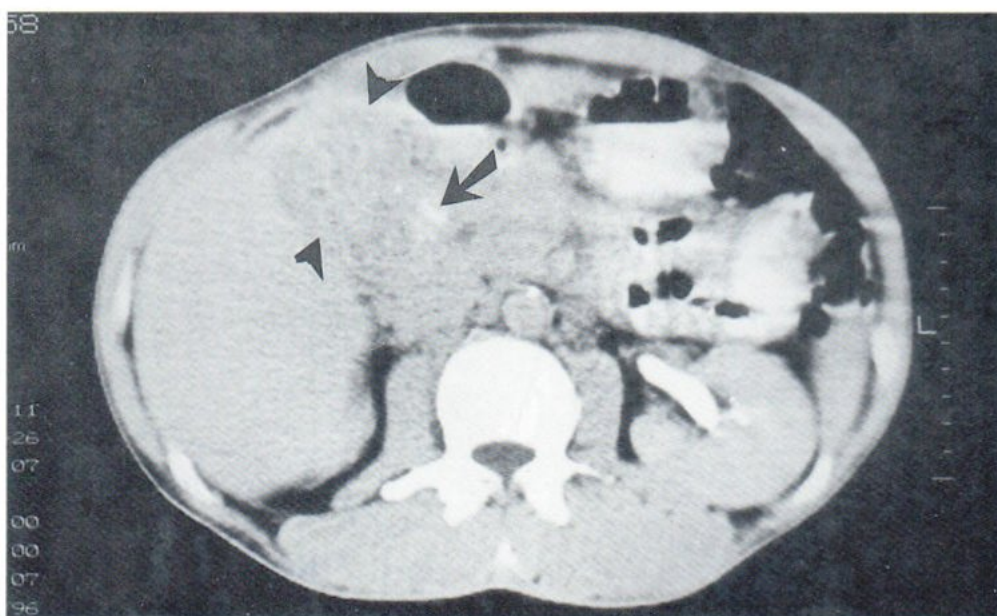


**Fig. 4B** Axial CT scan showed a calcification (arrow) at the mass of gallbladder. (arrow heads)

13. Goodman ZO, Ishak KG. Xanthogranulomatous cholecystitis. *Am J Surg Pathol* 1981; 5 : 653-9
14. Benbow EW. Xanthogranulomatous Cholecystitis. *British Journal of Surgery*. 77(3) : 255-6, 1990 Mar



**Message from**  
**Prof. Dr. Kawee Tungsubutra**  
**Editor-in-Chief, The Asean Journal of Radiology.**

---

This is the third volume or the third year of the Asean Journal of Radiology.  
(Asean J.R.)

We have 15 papers from different Institutes in Thailand and 5 papers from Malaysia and Singapore. The 15 papers from different Institutes in Thailand came from the Medical Schools in Bangkok, in Chiang Mai, the Northern part of Thailand, and the Provincial Hospital in Saraburi. In fact we have the papers from all the Medical School in the Central, the North, the South and the North-East, in the previous Volumes (I & II). Only papers from Indonesia and Philippines that we have never received. We hope, we will have some papers from the two member countries in the near future.



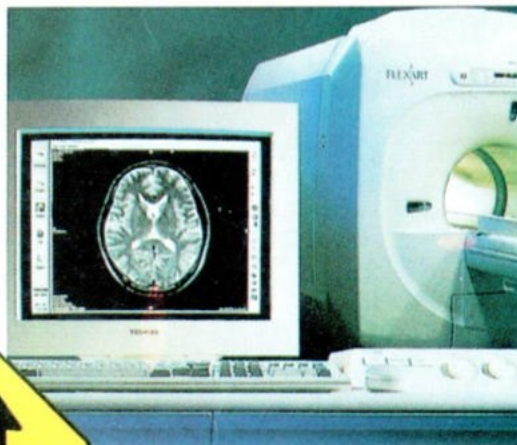
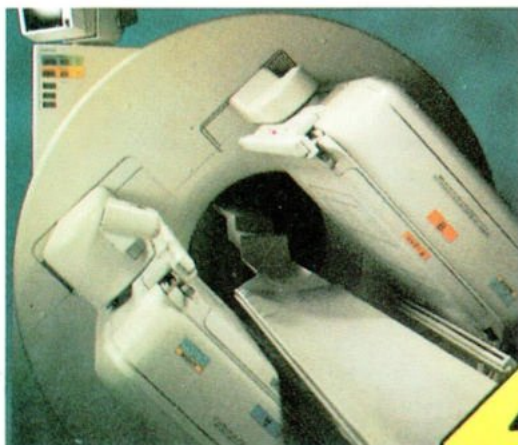
**Kawee Tungsubutra**  
**January 1, 1997**

**DESTINATION:  
A NEW CENTURY  
OF INNOVATION**

In Touch with Tomorrow

**TOSHIBA**

GLOBAL IMAGING ■ MEDICAL SYSTEMS



**B**ecause we listen carefully to our customers, Toshiba is always focused on providing the medical imaging products that can meet their clinical financial needs.



**CMC BIOTECH CO.,LTD.**

1433 Soi 3/3 Muban Town-in-Town, Ladphrao 94 Road, Bangkok 10310

Tel. 530-4995-6, 559-3261-2, 559-3524-5 Fax: (662) 539-6903

**Southern Branch**

306 Prachayindee Road, Khorhong Haadyai Songkhla 90110 Tel. (074) 356259,

Fax: (074) 364-004 Handphone 01-9359703 Pagephone 151, 152 call 341790

**North Eastern Branch**

301/155 Muban Khon Kaen Villa, Mittrapab Road, Amphur Muang, Khon Kaen 40000

Tel. (043) 246210, 244729 Handphone 01-9283082 Pagephone 151, 152 call 341787



